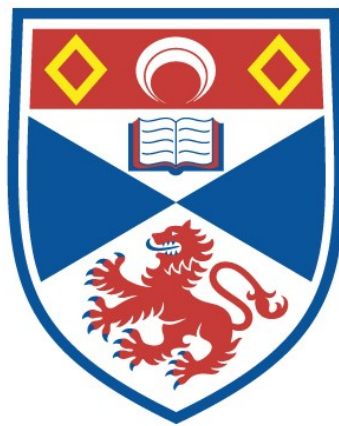


THE ANAEROBIC FUMARATE REDUCTASE OF
'ESCHERICHIA COLI': A STUDY OF ITS PROSTHETIC
GROUPS

David Simpkin

A Thesis Submitted for the Degree of PhD
at the
University of St Andrews



1986

Full metadata for this item is available in
St Andrews Research Repository
at:

<http://research-repository.st-andrews.ac.uk/>

Please use this identifier to cite or link to this item:

<http://hdl.handle.net/10023/14389>

This item is protected by original copyright

The Anaerobic Fumarate Reductase of Escherichia coli:

A study of its Prosthetic Groups

by

David Simpkin

University of St. Andrews

Department of Biochemistry and Microbiology

North Street

ST. ANDREWS

Fife.



ProQuest Number: 10166363

All rights reserved

INFORMATION TO ALL USERS

The quality of this reproduction is dependent upon the quality of the copy submitted.

In the unlikely event that the author did not send a complete manuscript and there are missing pages, these will be noted. Also, if material had to be removed, a note will indicate the deletion.



ProQuest 10166363

Published by ProQuest LLC (2017). Copyright of the Dissertation is held by the Author.

All rights reserved.

This work is protected against unauthorized copying under Title 17, United States Code
Microform Edition © ProQuest LLC.

ProQuest LLC.
789 East Eisenhower Parkway
P.O. Box 1346
Ann Arbor, MI 48106 – 1346

TH A 4 11

for Lesley

DECLARATION

I David Simpkin hereby certify that this thesis which is approximately 52,000 words in length has been written by me, that it is the record of work carried out by me, and that it has not been submitted in a previous application for a higher degree.

date.....2/9/85..... signature of candidate.....

I was admitted as a research student under Ordinance No. 12 in October 1982, and as a candidate for the degree of Ph.D. in February 1983; the higher study for which this is a record, was carried out in the University of St. Andrews between October 1982 and September 1985.

date.....2/9/85..... signature of candidate.....

CERTIFICATE

I hereby certify that the candidate has fulfilled the conditions of the Resolution and Regulations appropriate to the degree of Doctor of Philosophy of the Universty of St. Andrews and that he is qualified to submit this thesis in applicaton for that degree.

date. 2/1/85..... signiture of supervisor

Copyright Declaration

In submitting this thesis to the University of St. Andrews I understand that I am giving permission for it to be made available for use in accordance with the regulations of the University Library for the time being in force, subject to any copyright vested in the work not being affected thereby. I also understand that the title and abstract will be published, and that a copy of the work may be made and supplied to any bona fide library or research worker.

Academic Record

I graduated from the University of Hull in July 1982 with an upper second class (Honours) special degree in Biochemistry. I commenced my studies in St Andrews, for a Ph.D. in October of the same year.

Acknowledgements

I would like to thank my supervisor Dr W.J. Ingledew for his help and guidance throughout my period of study in St. Andrews. Thanks are also due to Dr C.A. Lewis for her helpful advice and discussions, to Mr S.D. Finlayson for help and advice on practical matters and to Mr G. Bruce and Mr A. Houston for technical assistance. I would also like to thank Dr T. Ohnishi for allowing me to visit her laboratory and for her invaluable discussions. Last, but by no means least, I must thank Lesley for her support and understanding, and also for doing the photocopying.

ABSTRACT

The prosthetic groups of the respiratory fumarate reductase from Escherichia coli have been studied by electron paramagnetic resonance. The iron-sulphur clusters of this enzyme were characterised in membranes from a strain of E. coli with amplified expression of the fumarate reductase. Two ferredoxin centres, paramagnetic in the reduced state (FR1 & FR2, E_m -50mV & -280mV) were shown to be present at the same concentration as the flavin, together with a centre paramagnetic in the oxidised state (FR3, E_m -30mV), present at the same concentration. Another ferredoxin signal was observed in reduced membranes at 1/10th the concentration of the other centres.

The relaxation processes of the iron-sulphur centres were characterised and shown to be similar to those reported for other iron-sulphur centres. These relaxation processes changed when more than one centre was paramagnetic, indicating interaction between the centres, which were characterised between FR1 & FR2, and FR1 & FR3, by the observed changes in e.p.r. properties. Estimates of the distances between centres were made from these observed changes.

The orientation of the g-tensors of the iron-sulphur centres was studied in membrane multilayers, both from a wild-type strain and a strain with amplified expression of the enzyme. The iron-sulphur clusters were shown to have distinct orientations in both cases, with the amplified strain producing crystalline multilayers. The interactions between the iron-sulphur centres were shown to have an angular dependence and thus to be magnetic dipole-dipole interactions.

The location of the iron-sulphur centres was studied using the exogenous paramagnetic probe dysprosium(III), and they were all shown to be on the cytoplasmic aspect of the cell membrane. The catalytic site of fumarate reduction was also located as cytoplasmic, by the use of mutant strains of *E. coli*, and inhibitors of the dicarboxylic acid porter. The iron-sulphur centres were shown to be located deep within the catalytic subunits of the enzyme.

The flavin moiety of fumarate reductase was characterised in the isolated enzyme by e.p.r.. The semiquinone form of the flavin was shown to be stable in the physiological pH range and to have an E_{m7} of -12mV ($n = 2$). Interaction between the semiquinone and FR1 was shown and characterised.

Abbreviations

- ATP - adenosine 5' triphosphate
- DCPIP - 2,6 dichlorophenol indophenol
- DMSO - dimethyl sulphoxide
- EDTA - ethylene diamine tetraacetic acid (disodium salt)
- E.p.r. - electron paramagnetic resonance
- ETP - electron transport particles
- FAD - flavin adenine dinucleotide
- FMN - riboflavin monophosphate
- PMS - N-methyl phenazonium methosulphate
- SDS - sodium dodecyl (lauryl) sulphate
- TES - (N-tris[Hydroxymethyl]methyl-2-aminoethanesulphonic acid)
- TMAO - trimethylamine oxide
- TMPD - Tetramethyl-p- Phenalenediamine
- Tris - Tris(hydroxymethyl)aminomethane

CONTENTS

Declaration	1
Certificate	ii
Copyright Declaration	iii
Academic Record	iv
Acknowledgements	v
Abstract	vi
Abbreviations	viii
Contents	ix
List of Figures and Tables	xiv
1. General Introduction	1
1.1. Respiration in <i>E. coli</i>	2
1.1.1. Overview of <i>E. coli</i> Electron-Transport Chains	4
1.2. Electron Transport to Oxygen	5
1.3. Anaerobic Electron Transport	8
1.3.1. Electron Transport to Nitrate	9
1.3.2. Electron Transport to Nitrite	11
1.3.3. DMSO / TMAO Supported Electron Transport	14
1.3.4. Electron Transport to Fumarate	15
1.4. Uniqueness of Fumarate Reductase	17
1.4.1. Structure of Fumarate Reductase	17
1.4.2. The Membrane Organisation of Fumarate Reductase	19
1.4.3. Fumarate Reductase from Other Organisms	23
1.4.4. Succinate dehydrogenase	24
1.5. The Study of Iron-Sulphur Centres by e.p.r.	28

1.5.1. Types of Iron-Suphur Centre	31
1.5.2. Cluster-Cluster and Cluster-Spin Interactions	32
1.6. Objectives of this Research	34
2. Materials and Methods	37
2.1. Organisms	38
2.2. Growth Media and Growth Cultures	38
2.3. Preparation of Membrane Particles	41
2.4. Purification of Fumarate Reductase	42
2.5. Enzyme Activities	43
2.5.1. Fumarate Reductase	43
2.5.2. Oxidase Activities	44
2.5.3. Succinate Dehydrogenase	44
2.6. Empirical Determinations	45
2.6.1. Acid Non-Extractable Flavin	45
2.6.2. Non-Haem Iron	47
2.6.3. Acid-Labile Sulphur	49
2.6.4. Protein Estimations	49
2.7. Sample Preparation for e.p.r.	49
2.7.1. Oriented Multilayers	52
2.7.2. Redox Titrations	53
2.8. E.p.r. Spectroscopy	54
2.9. Fluorimetry	58
2.10. Computation	59
2.10.1. Redox Data	59
2.10.2. E.p.r. Simulations	59

3. Characterisation of the Membrane Bound Fumarate Reductase	61
3.1. Introduction	62
3.2. Results and Discussion	63
3.2.1. Initial Characterisation of the Fumarate Reductase	63
3.2.2. Studies with <u>dct</u> Mutants	67
3.2.3. Studies with Inhibitors	70
3.2.4. Discussion of the Catalytic Site's Location	74
3.2.5. Studies on the Nature of the Catalytic Site	76
3.3. Conclusions	82
4. Characterisation of the Iron-Sulphur Centres	83
4.1. Introduction	84
4.2. Results and Discussion	85
4.2.1. Comparison of membranes from EMG2 and JRG1031	85
4.2.2. The E.P.R. Spectra of JRG1031 Membranes	88
4.2.3. Redox Titrations of the Ferredoxin Signal	99
4.2.4. Redox Titrations of the HiPIP Signal	104
4.2.5. Interactions and the E.P.R. Spectral Characteristics	107
4.2.6. Relaxation of the Ferredoxin Signals	115
4.3. Conclusions	119
5. Intrinsic Spin-Lattice Relaxation of the Iron-Sulphur Centres and the Effects of Dysprosium(III)	124
5.1. Introduction	125
5.2. Results and Discussion	127
5.2.1. The Relaxation Processes of the Ferredoxin	

Centres	127
5.2.2. The Relaxation Processes of the HiPIP Centre	135
5.2.3. Membrane-Bound Interactions with Dysprosium	141
5.2.4. Dysprosium Studies on the Isolated Enzyme	155
5.2.5. Conclusion	158
6. Characterisation of the Flavin Moiety	161
6.1. Introduction	162
6.2. Results and Discussion	164
6.2.1. Initial Characterisation	164
6.2.2. Thermodynamic Characterisation	173
6.2.3. Spatial Relationship	182
6.3. Conclusions	188
7. Studies on the Orientation of the Iron-Sulphur Centres	189
7.1. Introduction	190
7.2. Results and Discussion	192
7.2.1. Signals Observed from Succinate Reduced Multilayers	192
7.2.2. Signals from Dithionite Reduced Multilayers	202
7.2.3. Signals Observed from Oxidised Multilayers	207
7.2.4. Studies on a Non-Amplified Strain of <i>E. coli</i>	210
7.2.5. Studies on the Crystal Membranes	215
7.3. Conclusions	220
8. Spatial Relationships of the Iron-Sulphur Centres	222
8.1. Introduction	223
8.2. Results and Discussion	224
8.2.1. Interaction Between the Ferredoxin Centres	224

8.2.2. Interaction Between FR1 and FR3 (HiPIP)	237
8.2.3. Contributions of Exchange and Dipolar Coupling	241
8.2.4. Estimates of the Inter-Spin Distances	244
8.2.5. Oriented Multilayer Studies	250
8.3. Conclusions	263
9. General Conclusions	267
9.1. The Prosthetic Groups of Fumarate Reductase	268
9.2. Membrane Location of the Catalytic Site and the Prosthetic Groups	272
9.3. Orientation and Spatial Relationships of the Prosthetic Groups	274
9.4. Future Developments	277
Bibliography	280

List of Figures and Tables

Chapter 1

Figure 1.1 Electron Transport to Oxygen	7
Figure 1.2 Anaerobic Electron Transport	12
Figure 1.3 Model for the Membrane Structure of Fumarate Reductase	22
Figure 1.4 Types of Iron-Sulphur Centre	30

Chapter 2

Table 2.1 Characteristics of the Bacterial Strains	39
Figure 2.1 Standard Curve; Flavin Determination	46
Figure 2.2 Standard Curve; Iron Determination	48
Figure 2.3 Standard Curve; Sulphide Determination	50
Figure 2.4 Standard Curve; Protein Determination	51
Figure 2.5 Standard Curve; Thermocouple EMF	56
Figure 2.6 Temperature Difference of the e.p.r. Cavity	57

Chapter 3

Table 3.1 Fumarate Reductase Activities from Whole Cells and Membrane Particles of the <i>E. coli</i> K12 strains	68
Table 3.2 Fumarate Reducase Activities in the Presence of Added Dicarboxylic Acids	71
Table 3.3 Rates of Reaction with Alternative Substrates	79
Figure 3.1 pH Dependence of Enzyme Activities	64
Figure 3.2 Determination of K_m and V_{max}	66
Figure 3.3 Alternative Substrates for Fumarate Reductase	77

Chapter 4

Table 4.1 Partial Reactions of Respiratory Chains in ETP's	87
Table 4.2 Quantitation of the Iron-Sulphur Centres in Membranes from <i>E. coli</i> Strains EMG2 and JRG1031	96
Figure 4.1 (a) E.p.r. Spectra of Oxidised Membranes	89
Figure 4.1 (b) Simulation of the HiPIP Spectra	90
Figure 4.2 (a) E.p.r. Spectra from Succinate Reduced Membranes	92
Figure 4.2 (b) E.p.r. Spectra from Dithionite Reduced Membranes	93
Figure 4.2 (c) Simulations of the Ferredoxin Spectra	94
Figure 4.3 E.p.r. Spectrum of the Broad Ferredoxin	98
Figure 4.4 Potentiometric Titration of the Ferredoxin Signal, pH7.0	100
Figure 4.5 Nernst Plots of e.p.r. Signals, pH7.0	101
Figure 4.6 Potentiometric Titrations, Ferredoxin Signal	103
Figure 4.7 Potentiometric Titration of the HiPIP Signal	105
Figure 4.8 Temperature Dependence of e.p.r. Signals	108
Figure 4.9 Power Saturation Profiles, Ferredoxin Signals	109
Figure 4.10 Temperature Dependence of e.p.r. Signals from Samples Poised at Various Potentials	111
Figure 4.11 Variation of P1/2 with Redox Potential	114
Figure 4.12 Saturation of the Broad Signal	117
Figure 4.13 Temperature Dependence of the Spin Concentration for the Ferredoxin Signal	118

Chapter 5

Table 5.1 Distance Measurements from the Effects of Dy ³⁺ on the Intrinsic e.p.r. Properties of the Iron-Sulphur
--

Centres	149
Table 5.2 Distance Measurements from Isolated Fumarate Reductase	154
Figure 5.1 Temperature Dependence of P1/2 for the Ferredoxin Signals from Succinate and Dithionite Reduced Membranes	128
Figure 5.2 Temperature Dependence of Line widths for Succinate and Dithionite Reduced Membranes	130
Figure 5.3 Variation of Intensity with Temperature for Succinate Reduced Membranes	133
Figure 5.4 Temperature Dependence of P1/2 for the HiPIP Signal	136
Figure 5.5 Temperature Dependence of Linewidth for HiPIP	137
Figure 5.6 Temperature Dependence of Intensity for HiPIP	138
Figure 5.7 Temperature Dependence of Linewidth for Membranes Poised at -70mV	140
Figure 5.8 Effect of Dy-EDTA on Power Saturation of FR1	142
Figure 5.9 E.p.r. Spectra of Succinate Reduced Membranes in the Presence of Dy-EDTA	144
Figure 5.10 E.p.r. Spectra of Oxidised Membranes in the Presence of Dy-EDTA	145
Figure 5.11 Variation of P1/2 with Dy-EDTA Concentration	146
Figure 5.12 Variation of $\delta P1/2$ with Temperature for the Three Redox states	147
Figure 5.13 Temperature dependence of Linewidth in the Presence of 5mM Dy-EDTA	151
Figure 5.14 Variation of Linewidth with Dy-EDTA Concentration	152
 <u>Chapter 6</u>	
Table 6.1 Saturation Parameter (P1/2) for the Flavin Free Radical	184

Figure 6.1 Redox Titration of the Free Radical Signal; JRG1031 Membranes	165
Figure 6.2 E.p.r. Spectra of the Free Radical Signals	166
Figure 6.3 Redox Titration of the Free Radical Signal; Isolated Enzyme	168
Figure 6.4 Power Profiles of the Free Radical, 145K	170
Figure 6.5 Redox Titration pH7.0 of Free Radical Adjusted for Interaction with FR1	171
Figure 6.6 pH Dependence of E_m	175
Figure 6.7 pH Dependence of Maximum Free Radical Concentration	176
Figure 6.8 pH Dependence of E_m (I) and E_m (II)	178
Figure 6.9 Power Profiles of the Flavin Free Radical, 180K	182
 <u>Chapter 7</u>	
Figure 7.1 E.p.r. Spectra of Succinate Reduced Oriented Multilayers	193
Figure 7.2 Angular Dependence of e.p.r. Signal Amplitude from Succinate Reduced Multilayers	195
Figure 7.3 Computer Simulations of e.p.r Spectra of Centre FR1	197
Figure 7.4 Angular Dependence of e.p.r. Simulations	198
Figure 7.5 Model for a Chromophore with Rhombic Symmetry, within Oriented Multilayers	200
Figure 7.6 Model for a Chromophore with Rhombic Symmetry, within Crystalline Multilayers	201
Figure 7.7 E.p.r. Spectra of Dithionite Reduced Oriented Multilayers	203
Figure 7.8 Angular Dependence of e.p.r. Signals from Dithionite Reduced Multilayers	204

Figure 7.9 E.p.r. Spectra of Oxidised Oriented Multilayers	208
Figure 7.10 Angular Dependence of e.p.r. Signal Amplitude from Oxidised Multilayers	209
Figure 7.11 Angular Dependence of e.p.r. Signals of Succinate Reduced Multilayers from a Wild-type Strain of <i>E. coli</i>	212
Figure 7.12 Angular Dependence of e.p.r. signals of Oxidised Multilayers from a Wild-type Strain of <i>E. coli</i>	213
Figure 7.13 Angular Dependence of e.p.r. Signals of Succinate Reduced Multilayers Cut at Right Angles	216
Figure 7.14 Angular Dependence of e.p.r. Signals from Oxidised Multilayers Cut at Right Angles	217
Figure 7.15 Models for the Angular Dependence of e.p.r. Signals	219
 <u>Chapter 8</u>	
Figure 8.1 E.p.r. Difference Spectrum	226
Figure 8.2 (a) Low Temperature e.p.r. Spectra Ferredoxin Signals	227
Figure 8.2 (b) Low Temperature Spectrum Dithionite Reduced Membranes	228
Figure 8.3 Power Saturation Profiles, Ferredoxin Signals	230
Figure 8.4 Power Saturation Profiles of FR1 and FR2 at 4.5K	232
Figure 8.5 E.p.r. Half-Field Signals	234
Figure 8.6 Potentiometric Titration of the Half-Field Signals	235
Figure 8.7 E.p.r. Spectrum of Membranes Poised at -70mV	239
Figure 8.8 Power Saturation Profiles, Ferredoxin Signal	240
Figure 8.9 Variation of the Inter-Spin Distance with θ_R , for FR1 + FR2	247
Figure 8.10 Variation of the Inter-Spin Distance with θ_R , for FR1 + FR3	249

Figure 8.11 Angular Dependence of $\delta P_{1/2}$ for FR1 + FR2	251
Figure 8.12 Angular Dependence of Linewidth for FR1 + FR2	252
Figure 8.13 Angular Dependence of $\delta P_{1/2}$ for FR1 + FR3	254
Figure 8.14 Angular Dependence of linewidth for FR1 + FR3	255
Figure 8.15 Angular Dependence of FR3 Linewidth	256
Figure 8.16 Variation of the Angular Function	257
Figure 8.17 Angular Dependency of $\delta P_{1/2}$ (gz) of FR1 + FR2	260
Figure 8.18 Angular Dependence of $\delta P_{1/2}$ (gz) of FR1 + FR3	261
Figure 8.19 Model for the Interaction of Two Rhombic Spins	262
Figure 8.20 Model for the Interaction of the Iron-Sulphur Centres of Fumarate Reductase	264

CHAPTER ONE

General Introduction

1.1 Respiration in E. coli

Escherichia coli, a facultative anaerobic bacterium from the human gut, has been studied extensively in the laboratory environment, because of the ease with which it adapts to growth on a variety of culture media. Under these differing growth conditions E. coli can synthesise varying electron-transport chain components dependent upon the growth phase, terminal electron acceptor, the carbon source and the strain of E. coli. E. coli derives its energy for growth either by fermentation via glycolysis or from oxidative phosphorylation to oxygen or a number of alternative electron acceptors (Haddock & Jones 1977, Haddock 1980, Ingledew & Poole 1984).

The formation of adenosine 5' triphosphate (ATP) by E. coli can be considered to occur by two general methods, either by substrate level phosphorylation from growth on fermentable carbon sources or by oxidative phosphorylation. In the latter case ATP synthesis is coupled to electron transport reactions, from a variety of non-fermentable carbon sources, to a number of terminal electron acceptors. The oxidation-reduction (redox) enzymes which catalyse oxidative phosphorylation are membrane bound, and have been shown to be asymmetrically distributed in the cytoplasmic membranes of bacteria (Haddock & Jones 1977, Haddock 1980). The three most widely accepted models of energy coupling of electron transport to ATP synthesis are: the chemical theory, the chemiosmotic theory

and the conformational theory, all of which have been widely reviewed by many workers (Baltscheffsky & Baltscheffsky 1974, Boyer 1974, Green 1974, Greville 1969, Harold 1972 & 1977, Haddock & Jones 1977, Slater 1974). It is fair to say that the chemiosmotic theory (Mitchell 1966 & 1968) has received most support, as this theory presents a model to link various energy-dependent functions in bacteria, mitochondria, chloroplasts, muscle cells and nerve cells.

Haddock & Jones (1977) reviewed the application of the chemiosmotic theory to E. coli and outlined the major criteria, namely asymmetric distribution of the redox enzymes catalysing oxidative phosphorylation and the production of a proton-motive force (Δp) across a closed membrane system. The proton-motive force can consist of a membrane potential ($\Delta \psi$) and a pH gradient (ΔpH), though both do not need to be present simultaneously. The mechanism of proton translocation is unknown at present. There are two possible mechanisms by which this may occur: the loop mechanism proposed by Mitchell (1966), whereby the protons are translocated as a consequence of the position and organisation of the redox components, or the conformational pumping of proton by the respiratory complex. The production of Δp by E. coli can occur via a range of electron-transport chains dependent upon the conditions of growth. The individual redox enzymes vary in the different electron-transport chains, as their expression may be induced or repressed by the electron donors and acceptors available to the bacteria (Haddock & Jones 1977,

Ingledew & Poole 1984), offering a wide variety of experimental systems to study this important problem, which is fundamental to biochemistry.

1.1.1 Overview of E. coli Electron-Transport Chains

There are significant differences in the protein content of E. coli during aerobic growth from those during anaerobic growth (Smith & Neidhardt 1983 a & b) which indicate the changes in redox carriers that occur for growth on different terminal electron acceptors. The most striking change, other than the terminal enzymes of the respiratory chains, is the cytochrome content of the cells (Pundek & Bragg 1976, Reid & Ingledew 1979, Shipp 1972, Ingledew & Poole 1984). The number and type of the cytochromes varies with the growth conditions. The quinone present in the membranes of E. coli as an intermediate electron acceptor, also alters in changing from aerobic to anaerobic growth conditions. In aerobically grown cells ubiquinone-8 predominates, whereas menaquinone-8 (vitamin K) predominates in anaerobically grown cells (Jones & Garland 1982, Haddock & Jones 1977, Ingledew & Poole 1984). The electron donors to the electron-transport chains also change with the growth conditions for E. coli. The major electron donors are the dehydrogenases which are dependent on the carbon source present, though some dehydrogenases can exist in more than one form, depending on the growth conditions (c.f. L-glycerol-3-phosphate dehydrogenase,

Ingledew & Poole 1984). Some of the dehydrogenases have been suggested to be specific for the quinone moieties (Wallace & Young 1977, Jones & Garland 1982) to which they donate electrons. The dehydrogenases can contain redox centres such as flavin, iron-sulphur centres and molybdenum centres, as well as cytochromes to transfer their electrons.

1.2 Electron Transport to Oxygen

E. coli has two terminal oxidases that transfer electrons to molecular oxygen. Cytochrome o (a b-type cytochrome) that is induced under conditions of vigorous aeration and cytochrome d (cytochrome a₂) which is synthesised under conditions of limiting oxygen tension (Poole 1982, 1983). Together with the terminal oxidases, other cytochromes that are specific to the electron-transport chains under these conditions are synthesised (Poole 1982, 1983, Pundek & Bragg 1976, Reid & Ingledew 1979, Ingledew & Poole 1984).

Cytochrome o is usually shown to be present in E. coli by its binding of carbon monoxide (CO), which gives rise to its characteristic difference spectrum (reduced + CO minus reduced). A mid-point potential of +250 mV has been determined for cytochrome o (Reid & Ingledew 1979). The electron-transport chain to cytochrome o has not been clearly defined, though it is known that two b-type cytochromes (b_{562/556} (split band) and b₅₅₆) together with ubiquinone,

are involved. Downie & Cox (1978) proposed that electrons were passed from NADH dehydrogenase to ubiquinone and then to cytochrome b_{562} , before being passed to cytochrome b_{556} , which also acts as an electron acceptor from other dehydrogenases (fig.1.1). Electrons are then passed via ubiquinone to cytochrome ρ . Alternatively, Kita and Anraku (1981) proposed that all the dehydrogenases passed their electrons to the quinone pool before passing to cytochrome b_{556} and then to cytochrome b_{562} via ubiquinone again, and finally to cytochrome ρ (Fig.1.1). The majority of experimental data to date favours the second (more recent) scheme because of the mid-point potentials and the fact that cytochrome ρ co-purifies with cytochrome b_{562} (probably $b_{562/556}$).

Under conditions of limiting oxygen cytochrome d supplements cytochrome ρ as the terminal oxidase of *E. coli*, as well as being the oxidase synthesised under a variety of other growth conditions (Pundek & Bragg 1976, Reid & Ingledew 1979, Shipp 1972, Ingledew & Poole 1984). The electron-transport chain to cytochrome d is hardly any less complex than that to cytochrome ρ . 'Cytochrome a_1 ' is also induced, together with cytochrome d and was long assumed to act as an oxidase in *E. coli*. However Reid and Ingledew (1979) showed that 'cytochrome a_1 ' did not bind CO and thus its role as a terminal oxidase was put in doubt. The electron-transport chain to cytochrome d also contains cytochrome b_{558} (distinct from cytochrome ρ) as well as cytochromes b_{562} and b_{556} . The electrons under conditions of

Electron-Transport to Oxygen

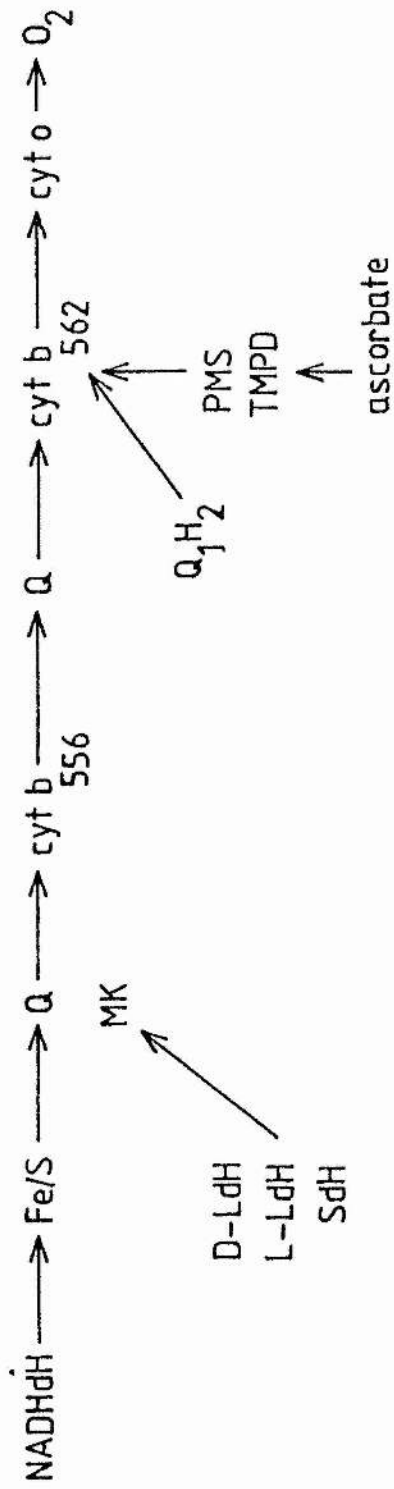


Figure 1.1

Electron transport to oxygen

The two proposed schemes for electron transport from NADH dehydrogenase to molecular oxygen, via cytochrome α , are shown. The top scheme denotes the sequence of redox carriers proposed by Downie & Cox (1978) and also includes the scheme for electron transport to molecular oxygen via cytochrome α .

The lower scheme denotes that proposed by Kita & Anraku (1981) for electron transport to molecular oxygen, from NADH dehydrogenase, via cytochrome α . The position of interaction of the other dehydrogenases is also shown.

Abbreviations: NADH & NADHdH, NADH dehydrogenase; D-LdH, D-lactate dehydrogenase; L-LdH, L-lactate dehydrogenase; SdH, succinate dehydrogenase; Q, ubiquinone; MK, menaquinone; cyt, cytochrome; PMS, phenazine methosulphate; TMPD, tetramethyl-p-phenalinediamine; Fe/S & Fe, iron-sulphur centres.

limiting oxygen pass to cytochrome b_{558} and then to cytochrome d instead of directly to cytochrome a (Fig.1.1). Evidence is not available at the present time concerning the membrane location of the b -type cytochromes, though it is generally assumed that the two oxidases are located on the periplasmic aspect of the *E. coli* membrane. The electron-transport chains induced aerobically in *E. coli* are therefore fairly complex, involving at least six redox enzymes in each case.

1.3 Anaerobic Electron Transport

E. coli is a facultative anaerobe and as such is capable of anaerobic growth on a number of carbon sources together with alternative electron acceptors. Electron transport to nitrate, nitrite, fumarate, dimethylsulphoxide and trimethylammonium oxide have all been determined in *E. coli*, each with its own distinct electron-transport chain (Haddock & Jones 1977, Haddock 1980, Kroger 1978, Ingledew & Poole 1984). The best characterised and most extensively studied has been the electron-transport chain that terminates with nitrate reductase.

1.3.1 Electron Transport to Nitrate

The electron-transport chain induced under anaerobic conditions in the presence of nitrate is simple, consisting of dehydrogenase, quinone and reductase enzymes. However, the dehydrogenases and reductase are themselves complex molecules containing several redox centres each (cytochromes, iron-sulphur centres and molybdenum centres), through which they achieve electron-transport and proton-translocation. E. coli can utilise nitrate as a terminal electron acceptor by means of the enzyme nitrate reductase, which is induced in the presence of nitrate and molybdenum, but which is repressed in the presence of oxygen (Haddock & Jones 1977). Growth can occur on a variety of non-fermentable substrates such as D-lactate (Haddock & Jones 1977, Ingledew & Poole 1984). In E. coli nitrate is reduced to nitrite in a two electron reduction which also involves the consumption of two protons. The reaction has a mid-point potential of +420 mV at pH 7.0, which gives a ΔG° for nitrate reduction from NADH of ≈ -39 Cal/mol (Ingledew & Poole 1984). This provides a large enough G° for the production of more than 1 ATP/2e⁻. H⁺/2e⁻ ratios of 4 for oxidation of malate and 2 for oxidation of succinate, glycerol and D-lactate were found. An H⁺/2e⁻ ratio of >2 was also found for formate reduction, but this case was more complex because of the production of CO₂ and H⁺ movement linked to formate uptake (Garland et al. 1975), which will affect the measured proton translocation.

Nitrate reductase contains both molybdenum (bound to pterin, Johnson 1980) and iron-sulphur centres in the catalytic subunits (α & β), together with a b -type cytochrome in a third subunit (γ). This b -type cytochrome (b_{556}^{NR}) is specifically induced under these growth conditions. If potassium selenite is also included in the medium, high levels of a membrane bound formate dehydrogenase are also induced (c.f. Ingledew & Poole 1984 for review). The minimum stoichiometry required for activity (quinone dependent) is 1, 1, 2 subunits. Electron paramagnetic resonance (e.p.r.) studies have shown at least three iron-sulphur centres: a high potential Fe-S type and at least two ferredoxin type centres, in addition to a molybdenum (V) signal. The redox behaviour of some of these centres has been characterised but the position and sequence of the centres is not known. The location of the catalytic site of nitrate reductase has been found to be cytoplasmic (Ingledew *et al.* 1978, Jones *et al.* 1978a & b), although the enzyme itself is transmembraneous, the γ subunit being located near the periplasmic aspect of the cell membrane (Boxer & Clegg 1975). This has important considerations for the proposed model of nitrate reductase based oxidative phosphorylation, because of the consumption of protons by the terminal reaction and the requirement for a transport system to bring nitrate into the cells. The location of the subunits has been investigated by labelling studies and confirmed by the use of antibodies (Boxer & Clegg 1976, Graham & Boxer 1978, Graham *et al.* 1981, Graham & Boxer

1980a & b, MacGregor & Christopher 1978).

The formate dehydrogenase has been shown to contain a molybdenum centre and a HiPIP-type iron-sulphur centre by e.p.r. spectroscopy, and to be associated with a b-type cytochrome of low potential (Ruiz-Herrera & De Moss 1969, Hackett & Bragg 1983a & b). Other cytochromes (b,d & 'a₁') are also induced under these conditions, but these are not thought to participate in electron-transport from formate to nitrate. The accepted pathway (Fig.1.2) for electron flow to nitrate reductase, from formate dehydrogenase and other dehydrogenases, is via the quinone pool. Formate dehydrogenase translocates $2H^+/2e^-$ in addition to those translocated by the quinone pool ($2H^+/2e^-$).

1.3.2 Electron Transport to Nitrite

E. coli can rapidly reduce nitrite to ammonia under anaerobic conditions. The six electron reduction has a mean mid-point potential of +275 mV at pH 7.0, giving ΔG° of -27.4 Cal/mol (Ingledeu & Poole 1984) for reduction of nitrite from NADH. There are three separate pathways by which this occurs: NADPH:sulphite reductase, a soluble enzyme which also has appreciable nitrite reductase activity; a soluble NADH:nitrite reductase, and a respiratory nitrite reductase. The latter is partially membrane dependent and linked to a respiratory chain (Ingledeu & Poole 1984). The major

Anaerobic Electron-Transport Chains

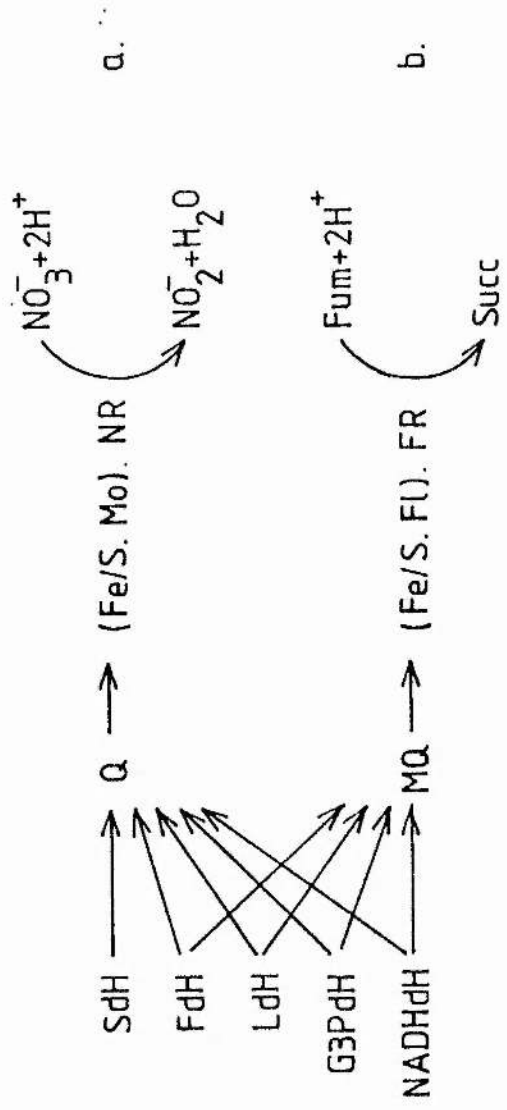


Figure 1.2

Anaerobic Electron Transport Chains

Electron transport to the two best characterised, alternative electron acceptors, nitrate and fumarate are shown. Scheme a, denotes electron transport from the various dehydrogenases to nitrate reductase. Scheme b, denotes electron transport to fumarate from the dehydrogenases.

Abbreviations: SdH, succinate dehydrogenase; FdH, formate dehydrogenase; LdH, L-lactate dehydrogenase; G3PdH, L-glycerol-3-phosphate dehydrogenase; NADHdH, NADH dehydrogenase; Q, ubiquinone; MQ, menaquinone; Fe/S, iron-sulphur centres; Mo, molybdenum centres; Fl., flavin moiety (8-alpha-[N(3)-histidyl]-FAD); N.R., nitrate reductase; F.R., fumarate reductase; fum, fumarate; succ, succinate. The chemical formulae have their usual meanings.

dehydrogenases found to donate electrons to this respiratory chain, are the formate and lactate dehydrogenases (Abou-Jaoude *et al.* 1979a & b), and either ubiquinone or menaquinone can be utilised by the system. A low potential α -type cytochrome (α_{552}) is also induced by growth on nitrite and has been inferred to be associated with the nitrite reductase (Fujita & Sato 1966b, 1967). It has been shown to be rapidly oxidised by nitrite (Gray *et al.* 1963) and to reduce this to ammonia (Liu *et al.* 1981). A periplasmic location for this cytochrome has been found (Fujita & Sato 1966a & b, 1967). The membrane bound nitrite reductase of *E. coli* has not been well characterised and its structure, membrane location and prosthetic groups, other than the α -type cytochrome, are not known. Presumably electrons are donated from the quinone pool to cytochrome α_{552} and then to the prosthetic groups of nitrite reductase. It has been demonstrated by Motteram *et al.* (1981) that electron-transport from formate to nitrite can support a membrane potential ($\Delta\psi$) of upto 150 mV though ΔpH and thus Δp was not measured.

1.3.3 DMSO / TMAO Supported Electron Transport

Trimethylamine N-oxide (TMAO) is reduced by E. coli to trimethylamine under anaerobic conditions. TMAO can support the growth of E. coli with glucose and formate as carbon sources and also on hydrogen. TMAO reductase is a membrane bound enzyme which accepts electrons via quinone from NADH, NADPH and formate. Both b-type and q-type cytochromes are also involved in electron transport (Ingledeu & Poole 1984). TMAO reductase activity is dependent on the same molybdenum cofactor as nitrite reductase, but the structure and membrane location of the enzyme is not known. However TMAO reductase has been shown to be coupled to proton translocation (Takagi et al. 1981) with $H^+/2e^-$ ratio of 3 to 4 and the generation of a membrane potential.

Dimethylsulphoxide (DMSO) is reduced by E. coli to dimethylsulphide and can support anaerobic growth (Paterson & Ingledeu unpublished results). Growth of E. coli on DMSO plus glycerol as carbon source induces cytochromes d, 'a₁', two b-type cytochromes (b₅₅₅ & b₅₅₈) and a q-type cytochrome (Ingledeu & Poole 1984). Very little is known about this electron-transport chain but it is thought to be similar to that involved in electron transport to TMAO.

1.3.4 Electron Transport to Fumarate

E. coli, like many other bacteria, can utilise fumarate as an alternative electron acceptor, to support growth on non-fermentable carbon sources such as glycerol. Fumarate is reduced to succinate by fumarate reductase (E.C.1.3.99.1) in the terminal reaction of electron transport. In E. coli the electron-transport chain to fumarate is one of the simplest known (Fig.1.2). Fumarate reductase receives electrons from menaquinone which receives them in turn from the dehydrogenases. The major dehydrogenases in electron-transport to fumarate from growth on glycerol are lactate, glycerol-3-phosphate, NADH and formate dehydrogenase (Ingledeu 1983). Cytochromes d, 'a₁' and at least two b-type cytochromes are induced during anaerobic growth in the presence of fumarate (Reid & Ingledeu 1979).

The fumarate / succinate couple has a mid-point potential of +30 mV at pH 7.0 for the two electron reaction. For reduction of fumarate from NADH the G° is -16.1 Cal/mol. Brice et al. (1974) and Gutowski & Rosenberg (1976, 1977) demonstrated that proton translocation occurred during fumarate dependent respiration in E. coli, from endogenous substrates with an $H^+/2e^-$ ratio ≈ 1 . Miki & Lin (1973, 1975) later measured stoichiometries of 2 for proton translocation coupled to glycerol-3-phosphate oxidation by fumarate. The matter is more complex in using pulses of fumarate to measure the proton translocation, because of anomalies in the stoichiometry. The

product of fumarate reduction, succinate is a competitive inhibitor of fumarate reductase (Hirsch *et al.* 1963) and the dicarboxylic acid porter (Kay & Kornberg 1971), leading to an underestimate of the stoichiometry. The porter for fumarate is a proton symporter (Gutowski & Rosenberg 1977), which leads to a further underestimate of the stoichiometry. A ΔpH was produced by respiration from either NADH or formate to fumarate (Haddock & Kendall-Tobias 1975) though not from lactate, and was variable in respiration from glycerol-3-phosphate. Hellingwerf *et al.* (1981) measured the Δp from fumarate supported respiration as $\sim +105$ mV which is surprisingly low, however there was no significant ΔpH in whole cells, so this may reflect only $\Delta\psi$. The ΔpH may have been collapsed by the action of the proton symporter in the uptake of fumarate (Ingledeu & Poole 1984). Miki & Lin (1975) have reported an ATP/fumarate ratio of 0.1, from electron transport to fumarate from glycerol-3-phosphate, which is very low, although they qualify this by stating that their membrane preparations were not wholly sealed and hence an underestimate would be expected.

Solute transport linked to fumarate reduction has also been reported (Konings & Kaback 1973, Miki & Lin 1975). Lactose and some amino acid were taken up by membrane vesicles (right-side out), in an energy dependent process driven by fumarate reduction, linked electron transport to glycerol-3-phosphate oxidation.

1.4 Uniqueness of Fumarate Reductase

Fumarate reductase is one of the class of succinate-fumarate oxidoreductases that catalyse the interconversion of succinate to fumarate plus hydrogen (reducing equivalents) and vice versa. E. coli can synthesise two enzymes of this class, fumarate reductase and succinate dehydrogenase. The two enzymes have striking structural similarities but are under separate genetic control. Succinate dehydrogenase is induced aerobically and repressed anaerobically, whereas fumarate reductase is induced anaerobically in the presence of fumarate and repressed by oxygen and nitrate (Hirsch et al. 1963, Spencer & Guest 1973). Although both enzymes show both succinate dehydrogenase and fumarate reductase activity, the K_m and V_{max} values are such that each favours its own reaction (Hirsch et al. 1963, Spencer & Guest 1973, Dickie & Weiner 1979). The induction / repression of each enzyme is such that both are not active under the same growth conditions.

1.4.1 Structure of Fumarate Reductase

The E. coli fumarate reductase was first isolated by Dickie & Weiner (1979) in a two subunit form. Polypeptides of M_r 70 000 and 24 000 in a molecular ratio of 1:1 were found. Later studies (Lemire et al. 1982) showed that two other peptides of M_r 15 000 and 14 000 were also present in a 1:1

ratio with the other two peptides. Strains of *E. coli* with amplified expression have been constructed (Cole & Guest 1979a & b) and a soluble fumarate reductase has been observed in these strains. This enzyme was in the two subunit form and was similar to that isolated by Dickie & Weiner. This soluble fumarate reductase is more labile than the four subunit form, the two anchor polypeptides conferring some degree of stability on the enzyme and being necessary for membrane binding of the enzyme. The membranes in the fumarate reductase amplified strains of *E. coli* are said to be saturated with the enzyme, as the soluble form accumulates in the cytoplasm.

The fumarate reductase genes are arranged as a distinct operon consisting of a promoter-operator region, four cistrons (*frd A,B,C,D*) and a transcriptional terminator. This operon maps close to the β -lactamase gene (*Amp C*), enabling amplified expression to be maintained by aerobic growth in the presence of ampicillin (Cole & Guest 1979a & b). The complete DNA sequence of the catalytic cistrons has been determined and used to predict the primary structure of the subunits (Weiner *et al.* 1984a for review). The flavin containing subunit, the product of *frdA*, consists of 602 amino acids (M_r 66 052) and has a nine residue sequence identical to the FAD binding site of bovine-heart succinate dehydrogenase. The iron-sulphur subunit has 244 amino acid residues giving an M_r of 27 082.

The non-haem iron and acid-labile sulphur content of the purified enzyme have been measured at 4 to 5 mol each / mol enzyme (Cole *et al.* 1982). From the primary structure of the iron-sulphur subunit it has been suggested that this subunit may contain either two binuclear ([2Fe-2S]) ferredoxin centres (Cole *et al.* 1982), or a single tetranuclear ([4Fe-4S]) ferredoxin centre (Weiner *et al.* 1984a). This polypeptide chain contains 11 cysteine residues, 10 of which are conserved in the *E. coli* succinate dehydrogenase (Guest *et al.* 1984). The flavoprotein subunit also contains 10 cysteine residues but these are scattered through the peptide and are not in distinct clusters. It is possible that this subunit may also contain an iron-sulphur centre(s) (Ingledeew & Poole 1984).

1.4.2 The Membrane Organisation of Fumarate Reductase

The catalytic portion of the *E. coli* fumarate reductase has been assigned to the cytoplasmic aspect of the cytoplasmic membrane. The evidence for this is as follows: the two subunit form of the enzyme accumulates in the cytoplasm when the membranes are saturated with fumarate reductase (Cole & Guest 1979b). Secondly, membrane-impermeable dyes cannot be rapidly oxidised in whole cells by utilising fumarate, whereas they can be oxidised in broken cells (Jones & Garland 1977). Membrane-permeable dyes can be oxidised rapidly in both whole and broken cells, indicating that the dyes feed electrons

and/or protons to fumarate reductase or another electron-transport component located on the cytoplasmic aspect of the membrane. Thirdly, Van der Plaas *et al.* (1983) used crossed-immunoelectrophoretic and immunoabsorption techniques to show that at least part of the fumarate reductase was located on the cytoplasmic aspect of the cell membrane. They did not detect any antigenic determinants of fumarate reductase located on the periplasmic aspect of the cell membrane.

Recently, Weiner and coworkers (Lemire *et al.* 1983, Weiner *et al.* 1984a & b) have determined the membrane structure of fumarate reductase from electron microscope studies. They have pictured 4 nm 'knobs' on negatively stained everted membrane particles. They assigned these to fumarate reductase because after removal of the enzyme activity by urea treatment, a reconstituted activity and structure was observed after incubation of the stripped membranes with the two subunit form of the enzyme. Chymotrypsin treatment removed only the 69 kdalton subunit (flavoprotein subunit) revealing a 1 nm diameter knob which was assumed to be the iron-sulphur subunit. Weiner *et al.* (1984a) have also suggested a membrane intrinsic structure for the two anchor polypeptides by comparison to other proteins with similar structural features and hydrophobicity (fig.1.3). The two anchor polypeptides appear to anchor the catalytic portion of fumarate reductase to the membrane (fig.1.3). The structure shown by Weiner *et al.* (1984a) may

indicate a transmembraneous structure for these two polypeptides. The excess fumarate reductase in strains of E. coli with amplified expression of the enzyme has been shown to be accommodated into novel membraneous structures produced by these strains (Weiner et al. 1984a, Elmes & Weiner 1985; Lemire et al. 1983).

The membrane location of the catalytic portion implies that the site of the terminal reaction, of the fumarate supported electron transport, is on the cytoplasmic aspect of the cell membrane. However, the possibility of a periplasmic reaction site cannot be excluded if the two anchor polypeptides are transmembraneous. The consequences of a cytoplasmic reaction site are; the requirement for a dicarboxylic acid porter, to transport fumarate into the cell, as shown by Kay & Kornberg (1971) and also the consequences of this on proton translocation driven by fumarate dependent electron transport.

A Model for the Structure of Fumarate Reductase

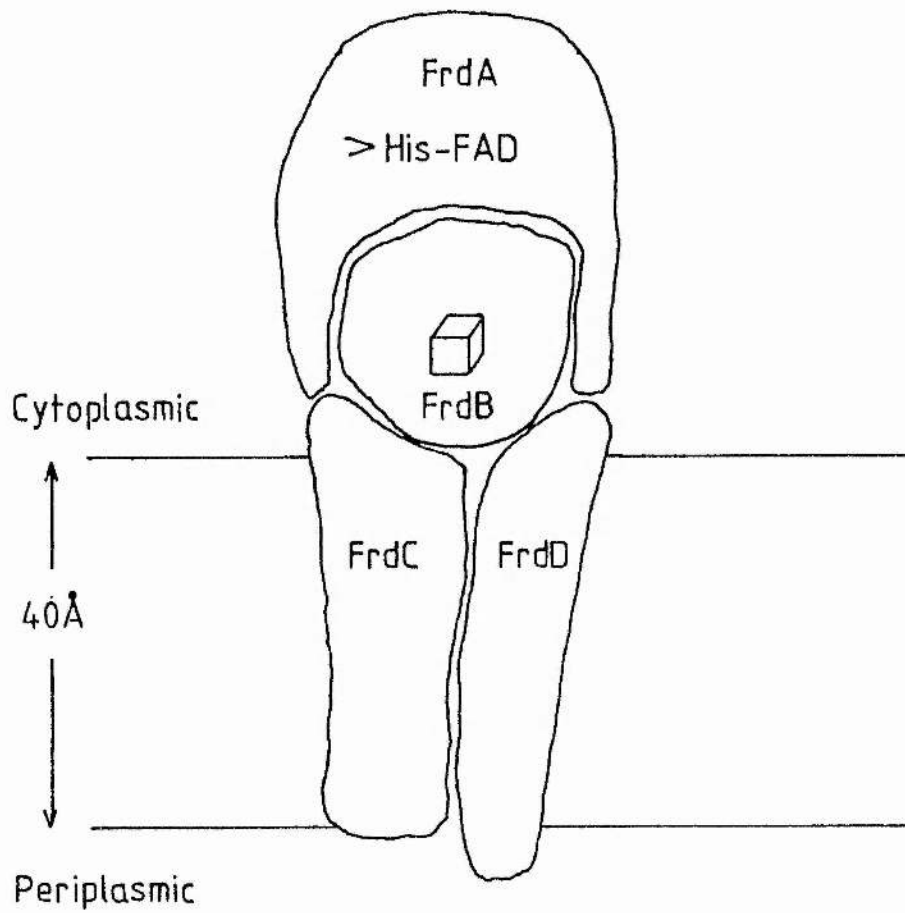


Figure 1.3

Model for the Membrane Structure of Fumarate Reductase

The model proposed by Weiner et al. (1984), for the structure of fumarate reductase bound to the E. coli membranes, is shown. The two catalytic subunits (frdA & B) are membrane extrinsic on the cytoplasmic aspect of the the membrane. The two anchor polypeptides are shown to be transmembraneous as proposed by Weiner et al. (1984). The location of the flavin and the 'tetranuclear' centre (HiPIP) are those proposed by Weiner et al. (1984), based on the nucleotide sequence of the frdA & B codons.

1.4.3 Fumarate Reductases from other Organisms

The ability to use fumarate as an alternative electron acceptor, for electron transport driven respiration, is a wide spread ability among chemiotrophic anaerobic bacteria. Most of the enterobacteria, as well as many of the rumen bacteria, have the ability to utilise fumarate and derive ATP from its reduction (c.f Kroger 1978 for review). Klebsiella pneumonia has been shown to extrude protons on the addition of fumarate with a stoichiometry similar to that of E. coli (Kroger 1978). Wolinella (Vibrio) succinogenes is the most widely studied organism, as well as E. coli, which utilises fumarate respiration. The electron-transport chain from formate to fumarate has been well characterised in this organism (Kroger 1978), and as for other organisms grown under these conditions, the membranes were shown to contain b-type cytochromes. Menaquinone or desmethylmenaquinone has been shown to be necessary for active electron transport in several bacteria (Kroger 1978). The fumarate reductase from W. succinogenes has been purified (Unden et al. 1980) and shown to consist of two peptides of M_r 79 000 and 31 000, though some of the enzyme co-purified with a b-type cytochrome. The peptides were shown to be present in a 1:1 ratio and the b-type cytochrome was later shown to be required in a 2:1 ratio with these peptides for full activity (Unden & Kroger 1982). The 79 000 dalton peptide binds 1 mol of FAD / mol enzyme and it contains non-haem iron and acid-labile sulphur, as does the smaller polypeptide. The non-haem iron

and acid-labile sulphur were assigned to one $[4\text{Fe-4S}]^{3+(2+,1+)}$ iron-sulphur centre and one $[2\text{Fe-2S}]^{2+(2+,1+)}$ iron-sulphur centre by e.p.r. spectroscopy (Albracht *et al.* 1981). The $[4\text{Fe-4S}]$ cluster was located in the 79 000 dalton subunit and the $[2\text{Fe-2S}]$ centre was located in the 31 000 dalton subunit. The enzyme was shown to contain two b -type cytochromes (spectrally similar) with different mid-point potentials of -20 mV and -200 mV. Mid-point potentials of the iron-sulphur centres were measured at -59 mV ($[2\text{Fe-2S}]$) and -24 mV ($[4\text{Fe-4S}]$) though values 30 to 100 mV more negative were obtained using mediator dyes as opposed to the succinate/fumarate couple (Uden *et al.* 1984). This electron-transport chain has been shown to function in reconstituted liposomes (Uden & Kroger 1982) and must be taken to represent the whole of this simple electron-transport chain.

1.4.4 Succinate dehydrogenase

E. coli possesses two genetically distinct, membrane-bound succinate-fumarate oxidoreductases, that catalyse the interconversion of fumarate and succinate (Hirsch *et al.* 1963, Spencer & Guest 1973). Succinate dehydrogenase is induced in E. coli by aerobic growth on non-fermentable substrates (Ruiz-Herrera & Garcia 1972), and oxidises succinate to fumarate, donating electrons to an electron-transport chain. It is repressed by anaerobiosis

(Spencer & Guest 1973), other than by growth on nitrate (Ingledeu & Poole 1984). The enzyme is structurally very similar to fumarate reductase (Ingledeu & Poole 1984, Beinert & Albracht 1982), containing two catalytic subunits and two anchor polypeptides (Condon & Owen 1982a & b, Owen & Condon 1982). The flavoprotein polypeptide contains the same covalently bound FAD moiety as fumarate reductase as well as non-haem iron and acid-labile sulphur. The iron-sulphur subunit also contains these cofactors.

Most of the e.p.r. studies to date have been performed on the bovine-heart succinate dehydrogenase and have shown the presence of at least two iron-sulphur clusters in this enzyme: a HiPIP-type centre and a binuclear ferredoxin centre (Ohnishi *et al.* 1976a & b). The presence of a second binuclear ferredoxin centre has been shown to be dependent upon the enzyme preparation (c.f. Beinert & Albracht 1982 for review), as is the presence of the HiPIP centre. Quantitation of the spin intensity of the e.p.r. signal has shown an increase from 0.9 spins / flavin, when reduced with succinate, to 1.4 spins / flavin upon reduction by dithionite. The second centre was postulated to be more rapidly relaxing than that reducible by succinate, so its full spin intensity could not be determined because of extreme lifetime broadening of the spectra (c.f. Ohnishi 1979 for review). The two ferredoxin centres (S1 & S2) have been shown to be spin coupled with the relief of saturation of centre S1 spins by the more rapidly relaxing S2 cluster (Ohnishi *et al.* 1976a, Salerno *et al.*

1979b, Ohnishi 1979). The HiPIP centre has also been shown to interact with a spin coupled ubiquinone pair and to be the site of interaction of the enzyme with the electron-transport chain (Ingledeu *et al.* 1976, Salerno & Ohnishi 1980). The HiPIP centre has recently been shown to be a three iron cluster ([3Fe-3S]) by low temperature magnetic circular dichroism spectroscopy (MCD), also the presence of a [4Fe-4S] has been shown (Johnson *et al.* 1985) but spin quantitation of this centre gave values of approximately 1/10 of those for S1 (T. Ohnishi personal communication). It has been postulated that this centre could be responsible for the effects seen on S1 at low redox potentials as it also has a low mid-point potential.

Cammack *et al.* (1984) and Condon *et al.* (1985) have recently shown that the succinate dehydrogenase from *E. coli* is very similar to that from bovine-heart mitochondria. They have reported signals from all three e.p.r. detectable centres (S1, S2 & S3) together with their mid-point potentials; S1, 10 mV; S2, -175 mV; S3, 65 mV. Centres S1 & S3 are very similar to those from bovine-heart succinate dehydrogenase, though S2 has a higher potential (-400 mV in bovine-heart enzyme). A *b*-type cytochrome was also reported to be present in the enzyme preparation although no quantitations for this and the iron-sulphur centres were presented. This may however indicate a similarity to the fumarate reductase from *W. succinogenes* which contains two *b*-type cytochromes. The molecular weights of the four enzyme

subunits were also reported giving M_r of 71 000 (flavoprotein), 26 000 (iron-sulphur polypeptide), 17 000 and 15 000 (anchor polypeptides). The succinate dehydrogenase from E. coli has thus been shown to be structurally very similar to that of bovine-heart mitochondria and the fumarate reductase from E. coli.

Guest et al. (1984) have shown that the two enzymes from E. coli have a large degree of homology, by comparing the sequences of the genes encoding the two enzymes. The iron-sulphur subunits have 10 of 11 cysteine residues conserved in three clusters, though some contain only three residues and thus will require either cysteines from elsewhere or nitrogens as ligands to form active iron-sulphur clusters. The FAD binding site is strongly conserved in the flavoprotein subunit, but the cysteine residues are not, only 1 from 10 (frd) or 11 (sdh) being retained, which may be the active site cysteine. This would seem to indicate that all three iron-sulphur clusters are in the iron-sulphur subunit rather than in both it and the flavoprotein subunit. The anchor polypeptides also show a degree of homology in their hydrophobicity and both may contain regions of α -helices to anchor the enzymes to the membranes. These regions may also act as proton and/or electron channels (Guest et al. 1984, Weiner et al. 1984a).

1.5 The Study of Iron-sulphur centres by e.p.r.

Electron paramagnetic resonance is a technique which enables the study of those redox centres that contain unpaired electrons and are thus paramagnetic. Different redox centres give their own characteristic e.p.r. spectra, dependent upon the environment of the electron. Cytochromes, flavins, quinones and iron-sulphur centres can all be detected in a paramagnetic state; free radicals in the case of flavins and quinones and specific valence states of the iron in cytochromes and iron sulphur centres. Cytochromes can also be studied by e.p.r. by spin-labelling the haem moiety with nitric oxide (NO) to obtain a paramagnetic species.

Iron-sulphur centres were first shown to be present in plants with the isolation of soluble plant ferredoxins which contained non-haem iron and acid-labile sulphur (Davenport et al. 1952, Arnon et al. 1957, San Pietro & Lang 1958). Palmer and coworkers (Palmer & Sands 1966, Palmer et al. 1966) showed that e.p.r. spectroscopy at low temperatures gave similar spectra from these and other proteins containing non-haem iron and acid-labile sulphur ($g_{av} = 1.94$). The unification of the field of iron-sulphur proteins by their e.p.r. signals was a major step forward in the study of these electron-transport proteins. These proteins were all found to contain two or more iron atoms (in multiples of two). A model for the structure of 2-iron centres was proposed by Gibson et al. (1966), in which the iron atoms are bonded to four sulphur


atoms (2 cysteine and 2 acid-labile sulphurs) in tetrahedral arrays, with the two acid-labile sulphur atoms being shared by both iron atoms (Fig.1.4). In the oxidised state both iron atoms are high-spin ferric (Fe (III)), and the cluster is diamagnetic and in the reduced state one iron atom becomes ferrous (Fe (II)) and the cluster is thus paramagnetic with a net spin of $1/2$. Later a model was proposed for the 4-iron centres in which the unpaired electrons could be present in either the reduced or oxidised form, ($1+$ or $3+$ states). A cubic structure was proposed (fig.1.4) with the iron atoms linked by acid-labile sulphurs and each liganded to a cysteine residue of the protein. The e.p.r. spectrum produced is characteristic of the two type of iron-sulphur centre, though the lack of information at present prevents interpretation of the e.p.r. spectra in terms of the structure of these centres.

Where more than one iron atom is involved in the cluster there is spin coupling between the iron atoms (Palmer 1973), and the net spin for the centre determines whether it is e.p.r. detectable. Odd spins only are e.p.r. detectable i.e. with net spins of $1/2$, $3/2$, $5/2$ etc.. The spin coupling between the high-spin iron atoms is characterised by the antiferromagnetic exchange coupling constant (J).

Figure 1.4

Types of Iron-Sulphur Centre

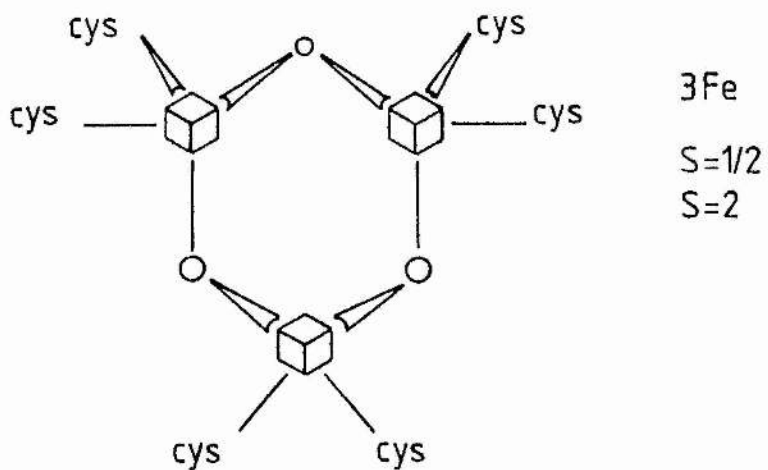
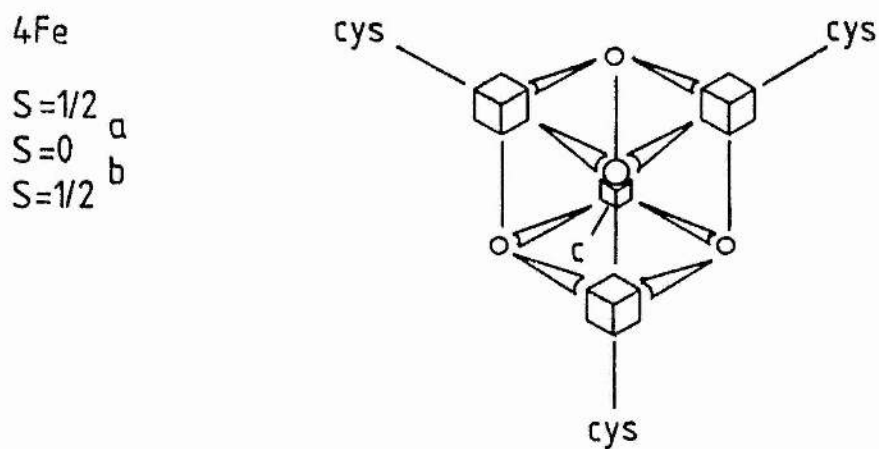
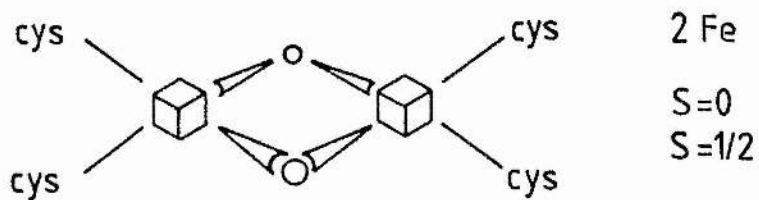
The proposed structures for the smaller iron-sulphur centres are shown. The binuclear ferredoxin cluster (top) with its spin states, after the model of Gibson *et al.* (1966), is shown. The gz axis lies through the iron atoms and the gx axis lies through the sulphur atoms. The tetranuclear cluster (centre) is shown with the possible spin states for this cluster; a) denotes the spin states for HiPIP-type centres and b) denotes the spin states for ferredoxin-type centres. The lack of knowledge concerning the relationship between e.p.r. properties and structure, precludes the assignment of g-axes to any given direction. The trinuclear cluster (bottom) is depicted as the [3Fe-3S] type and is shown with its possible spin states. Again g-axes cannot be assigned to this centre at the present time.

() - iron atoms

(O) - sulphur atoms

cys - cysteine residues.

Iron-Sulphur Clusters



1.5.1 Types of Iron-Sulphur Centres

Iron-sulphur centres containing 1,4 and 8 iron atoms have been characterised as well as the two iron ferredoxins, and all have been shown to have the same tetrahedral symmetry about the iron atoms. It has been proposed that the more complex centres are composed of units made-up from the simpler centres (Fig.1.4). Recently 3 iron centres have been reported from aconitase and two ferredoxins (Emptage *et al.* 1980, Kent *et al.* 1982a) which appear to be paramagnetic in the oxidised state. Iron-sulphur centres of this type have been postulated for a number of the more difficult to classify centres in the light of this recent discovery. Among these is the HiPIP centre from succinate dehydrogenase, which has been shown to be of this type by magnetic circular dichroism (Johnson *et al.* 1985).

As well as the well classified functions of iron-sulphur centres as electron-transferring redox centres, that participate in respiration, there is growing evidence for other functions for these clusters. Some centres have been found to function as oxygenases (Subramanian *et al.* 1979) and others to function as allosteric regulators (Buchanan *et al.* 1979) for the activity of other enzymes. Thus iron-sulphur centres may not be confined only to the role of electron transport but may play a wider role in the metabolism of the cell in general, as does the haem moiety for instance.

1.5.2 Cluster-Cluster and Cluster-Spin Interactions

Where more than one iron-sulphur centre or other paramagnetic species is present in a molecule, then cluster-cluster interactions can occur if both of the species are paramagnetic and the distance between the centres is not too great (Mathews et al. 1974). This interaction is manifest by a change in the intrinsic e.p.r. properties of the two species. The interactions may take the form of magnetic dipole-dipole interactions or exchange / superexchange interactions, but usually a mixture of both is encountered (Mathews et al. 1974). The resultant e.p.r. behaviour is observed as spin relaxation, as determined by relief from microwave power saturation (Ohnishi 1979, Rupp et al. 1978), splitting or broadening of resonances, as in hyperfine interactions (Lowe et al. 1972) and by triplet e.p.r. resonances (Steenkamp et al. 1978), visualised as 'half-field' resonances ($\Delta m_S = 2$). In the absence of a large exchange component, distances between the centres can be estimated which can give a useful assessment of possible electron-transfer pathways (Salerno et al. 1979b, Ohnishi et al. 1982). Where exchange interactions occur, the feasibility of electron-transfer is shown by the nature of the interaction. Magnetic interactions with iron-sulphur centres are not limited to those between iron-sulphur centres alone but can occur with other species such as flavin (Ohnishi et al. 1981), semiquinone (Ruzicka et al. 1975) and molybdenum (Lowe et al. 1972).

Spatial relationships between the centres and their location within membranes (sidedness), can be ascertained by the use of paramagnetic probes (c.f. Ohnishi 1979 for review) such as Gd(III), Ni(II) and Dy(III) ions. These probes are inert, membrane impermeable and by their large magnetic dipole cause spin-spin interactions, so can thus be used to estimate distances of the redox centre from the membrane or protein surface. These distances have to be taken as estimates only, as there can be the possibility of large errors attached to them, which arise from the assumptions made that the interactions are largely dipolar in nature. The mechanism of interaction is not usually known. However, in the absence of data on the structure of these redox proteins, they can provide useful information about the possible pathways of electron-transfer and redox mechanisms, and serve as a guide to further structural determinations.

A further development in this area is the production of oriented multilayers from the biological structure under consideration e.g. mitochondrial and bacterial membranes. The orientation of the g-tensors of the paramagnet can be deduced by the dependence of the e.p.r. signal on the direction of the magnetic field, with respect to the orientation of the multilayers. This has been done successfully for haem and iron-sulphur proteins in mitochondria (Ericinska *et al.* 1978a & b, Salerno *et al.* 1979a) and for a ubisemiquinone pair from the bovine-heart

succinate dehydrogenase complex (Ohnishi 1979, Salerno et al. 1977, 1979a).

At present the structure of only a few iron-sulphur proteins has been determined (c.f. Adman 1979 for review), so the relationship between structure and function is not well defined. For instance, the difference in structure of [4Fe-4S] centres that makes some the HiPIP-type (3+) and others the ferredoxin type (1+) is not fully understood, but the role of hydrogen bonds between sulphur atoms of the centres and nitrogens of the amino-acid side-chains, has been proposed as a cause of the differing redox behaviour (Adman 1979). Information on the mechanism of electron-transfer reactions involving iron-sulphur proteins is still also very limited (Beinert 1982), though some rapid electron-transfer mechanisms have been observed.

1.6 Objectives of this Research

The objective of this research has been to study the fumarate reductase from E. coli, looking particularly at its prosthetic groups using the techniques of e.p.r. (iron-sulphur centres and flavin) and fluorescence (flavin only). The enzyme succinate dehydrogenase, a member of the same class of enzymes (succinate : fumarate oxidoreductase E.C.1.3.99.1) was used as a model for two reasons. Firstly, this enzyme has been extensively studied by e.p.r.

(bovine-heart mitochondrial enzyme) and could provide guide lines for subjective research. Secondly, as a member of the same class of enzymes, succinate dehydrogenase catalyses the same reaction, albeit in reverse, so comparison of the two enzymes may yield insights into the differing abilities of the two enzymes to catalyse these reverse reactions. Information concerning their differing roles as electron-transfer proteins, with respect to their separate electron-transport chains, may also be gained from a comparison of differences in their redox behaviour.

Most of the e.p.r. was performed on a strain of E. coli that contains amplified expression of the fumarate reductase. This enabled the enzyme to be studied in situ on the cytoplasmic membrane. Succinate dehydrogenase has been the source of some controversy concerning the number of its binuclear iron-sulphur centres (c.f. Albracht 1980 for review). The number and detectability of the second (low potential) ferredoxin seems to be dependent on the enzyme preparation of succinate dehydrogenase. In studying the fumarate reductase in the membrane bound form, it was hoped to overcome any anomalies that may arise in purifying the enzyme and so gain a clear picture of the number and type of iron-sulphur centres present in this enzyme. The flavin moiety was also studied as this is the site of interaction with the substrate (fumarate/succinate). Changes in the properties of this prosthetic group may provide information on the differing reactivities of the two enzymes towards fumarate

and succinate.

CHAPTER TWO

Materials and Methods

2.1 Organisms

The Escherichia coli strains used in this research are shown in Table 2.1, together with their genetic characteristics. Strain JRG1031 was used primarily for the e.p.r. spectroscopy with EMG2 as a control strain. All strains were kept as stock cultures on nutrient agar slopes. JRG1031 had 800 $\mu\text{g/ml}$ of ampicillin added to retain the expression of the β -lactamase dependent plasmid.

2.2 Growth Media and Growth of Cultures

Growth of batch cultures was either on glycerol/fumarate medium similar to that of Spencer & Guest (1973), or on nutrient broth. The glycerol/fumarate medium contained the following:

potassium phosphate (mono basic) 3.0 g/l, potassium phosphate (dibasic) 12.0 g/l, ammonium sulphate 2.0 g/l, fumaric acid 5.8 g/l, potassium hydroxide 5.3 g/l, acid hydrolysed casein 1.0 g/l, glycerol 5 ml/l, trace metals 1 ml/l 50mM ammonium molybdate / potassium biselenite 1 ml/l, pH 7.2.

The nutrient broth contained the following:

potassium phosphate (mono-basic) 3.0 g/l, potassium phosphate (dibasic) 12.0 g/l, yeast extract 5.0 g/l, peptone 10.0 g/l, pH 7.2.

Table 2.1.

Characteristics of Bacterial Strains

<u>Strain</u>	<u>Characteristic</u>	<u>Source</u>
EMG2	Prototroph	M. Peacey, Edinburgh
JRG1031	Spontaneous mutant of JRG997 <u>ilv</u> , <u>metB</u> , <u>ampA1</u> , <u>ampC</u> ⁺ , <u>frd</u> ⁺ , <u>sdh</u> ⁺ , tolerates ampicillin to 800 µg/ml	J.R. Guest, Sheffield
CBT38	<u>levB6</u> , <u>lacY1</u> , <u>detB3</u> , <u>bioA2</u> , <u>rpsL129</u> , <u>thi-1</u> , <u>l</u> ⁻	E. coli Genetic Stock Centre, Yale
CBT312	<u>sdh-2</u> , <u>rpsL129</u> , <u>detA2</u> , <u>thi-1</u>	University School
CBT313	<u>sdh-2</u> , <u>rpsL129</u> , <u>detA4</u> , <u>thi-1</u>	of Medicine, New
CBT315	<u>sdh-2</u> , <u>rpsL129</u> , <u>detA5</u> , <u>thi-1</u>	Haven, Conn. 06510, U.S.A.

Abbreviations. The genetic nomenclature conforms to the recommendation of Demerec *et al.* (1968). The structural genes are abbreviated as follows: frd, fumarate reductase; sdh, succinate dehydrogenase, and det, dicarboxylic acid transporter.

Growth for e.p.r. spectroscopy was in batch cultures of 201 of the glycerol/fumarate medium. 200ml of nutrient broth (plus 800 $\mu\text{g/ml}$ of ampicillin for JRG1031) was inoculated by loop-transfer from a culture of the bacterial strain on a nutrient agar plate. This culture was then grown aerobically for 18hrs at 37°C before being used as an inocula for the batch culture. The batch cultures were grown in stoppered vessels, with gentle stirring at 37°C for 18hrs. Cells were harvested by continuous-flow centrifugation at 18 000 r.p.m., using an M.S.E. continuous-flow rotor running in an M.S.E. Highspeed 18 centrifuge, with a flow rate of approximately 250 ml/min. The cells were washed twice by resuspension in potassium phosphate buffer (20mM, pH 7.2) and centrifugation at 9 000g for 20min, at 4°C . The cell paste was frozen in liquid N_2 and stored at -30°C until required, unless fresh whole cells were required, when the cell paste was used immediately for experimentation.

Fresh cells for the enzyme assays were grown, at 37°C , either on the glycerol/fumarate medium or on nutrient broth containing glucose (0.5% w/v), in 500ml bottles filled to the neck. Inocula (5ml) were of cells grown anaerobically on nutrient broth, at 37°C for 18hrs. The cells for the assays were harvested by centrifugation (9 000g for 20min) using a G.S.A. rotor of a Sorval R.C.3B Superspeed centrifuge, after 18hrs growth. They were washed twice by resuspension in

potassium phosphate buffer (20mM, pH 7.2) and centrifugation as described above.

2.3 Preparation of Membrane Particles

Membrane particles (electron transport particles, ETPs) were prepared by French Pressure Cell treatment of the E. coli. Cells were thawed and resuspended by homogenisation in TES buffer (20mM, pH 7.2) containing EDTA (5mM), to a concentration of approximately 0.1g cells/ml. DNase I (20 μ g/ml, Sigma Chem. Co., P.O.Box 14508, St. Louis, Mo 63178) was added and the suspension was subjected to two passages through a French Pressure Cell (American Instrument Co., Silver Spring Maryland 20910), at approximately 120MPa. Unbroken cells and cell debris were removed by centrifugation at 9 000g for 15min, at 4°C. The supernatant was decanted and subjected to centrifugation at 124 000g for 1.5hrs, at 4°C in the 8 x 50ml rotor of an M.S.E. PrepSpin 50 ultracentrifuge. The pellet was washed once by resuspension in the same buffer and centrifugation as described above. The membranes were resuspended to a final concentration of approximately 100mg/ml in the same buffer and frozen in and stored under liquid N₂ until required.

2.4 Purification of Fumarate Reductase

The two subunit form of fumarate reductase was purified by Triton X100 (Sigma) extraction and chromatography on phenyl-sepharose (Pharmacia Fine Chemicals, Uppsala, Sweden) as described by Dickie & Weiner (1979), with the inclusion of sodium succinate (15mM) in the column elutant. The peak of enzyme activity from the phenyl-sepharose column was concentrated approximately 20-fold by ultrafiltration with an XM100 membrane (Amicon Corp., Boston, Mass.). To remove the sodium cholate from this fraction it was applied to a column of Sephacryl S-200 (Pharmacia), equilibrated with Tris-phosphate buffer (50mM, pH7.0) containing dithiothreitol (0.2mM) and sodium succinate (15mM), and eluted with the same. The peak of fumarate reductase activity was concentrated approximately 20-fold, as described, to yield the fraction used for experimentation (typically 0.15mM, 2.0ml). This fraction was frozen in and stored under liquid N₂ until required.

2.5 Enzyme Activities

2.5.1 Fumarate Reductase

Fumarate reductase activity was measured spectroscopically at 30°C by following the reoxidation of reduced benzyl viologen (molar extinction coefficient, $7.78 \times 10^3 \text{ cm}^{-1}$), using the method of Spencer & Guest (1973) modified as follows: benzyl viologen (120 μM) was reduced by titration with a freshly prepared solution of sodium dithionite, to give an absorbance at 550nm of 0.8 to 0.9. Fumarate (final concentration up to 15mM) of other substrates and inhibitors were added and the rate of basal oxidation was followed for 5 minutes before the reaction was initiated by the addition of cells or ETP. The buffer was potassium phosphate (50mM, pH 7.5), which had been de-oxygenated by bubbling with O_2 free N_2 (British Oxygen Co.). Stoppered cuvettes with a light-path of 1cm were used, the stopper had a fine hole drilled through it to facilitate the addition of samples using a micro-syringe. The reaction volume was 3.25ml. Two mol. of benzyl viologen react per mol. of fumarate reduced.

2.5.2 Oxidase Activities

Substrate dependent oxidase activities were measured at 30°C using a Clark-type oxygen electrode (Rank Bros., Bottisham, Cambridge, U.K.). The buffer used was potassium phosphate (50mM, pH 7.5), all substrates were 5mM (final concentration) and the cells or ETP were approximately 0.25mg protein/ml (final concentration in 3ml reaction volume). The cells or ETP were incubated in the electrode for 5 minutes, to measure the basal oxidation, before addition of the substrate.

2.5.3 Succinate dehydrogenase

Succinate dehydrogenase activity was measured essentially as described by Spencer & Guest (1973), following the reduction of 2,6 dichlorophenol indophenol (molar extinction coefficient $21 \times 10^3 \text{ cm}^{-1}$), spectroscopically at 600nm. The buffer used was potassium phosphate (50mM, pH 7.5), bubbled with O_2 free N_2 to remove the oxygen and the reaction volume was 3.25ml. The reaction mixture in stoppered cuvettes contained: potassium cyanide (1mM, neutralised with HCl); DCPIP (0.2mg); PMS (2mg); sodium succinate (up to 15mM) and either cells or ETP (approximately 0.25mg protein/ml). The basal rate of oxidation was followed for 5 minutes before initiating the reaction by addition of the sodium succinate.

2.6 Empirical Determinations

2.6.1 Acid non-extractable Flavin

The acid non-extractable content of ETP and the purified enzyme was measured spectroscopically using the method of Wilson & King (1964), correcting for acid extractable flavin contamination. A molar extinction coefficient (450nm) of $10.3 \times 10^3 \text{ cm}^{-1}$ was used for FAD. The change in absorbance at 450nm was computed as shown by Wilson & King (1964):

$$(A_{450}^{\text{ox}} - A_{450}^{\text{red}}) - (A_{530}^{\text{ox}} - A_{530}^{\text{red}})$$

The fluorescence of hydrolised samples and FMN standards (fig.2.1) was measured with excitation wavelength of 450nm and emission wavelength of 520nm. The excitation slitwidth was 5nm and the emission slitwidth was 10nm. The total acid extractable flavin was determined from the following equation:

$$\text{Conc. acid extractable flavin} = (\text{equivalent conc. FMN, pH 3.2}) - (\text{equivalent conc. FMN, pH 7.4})$$

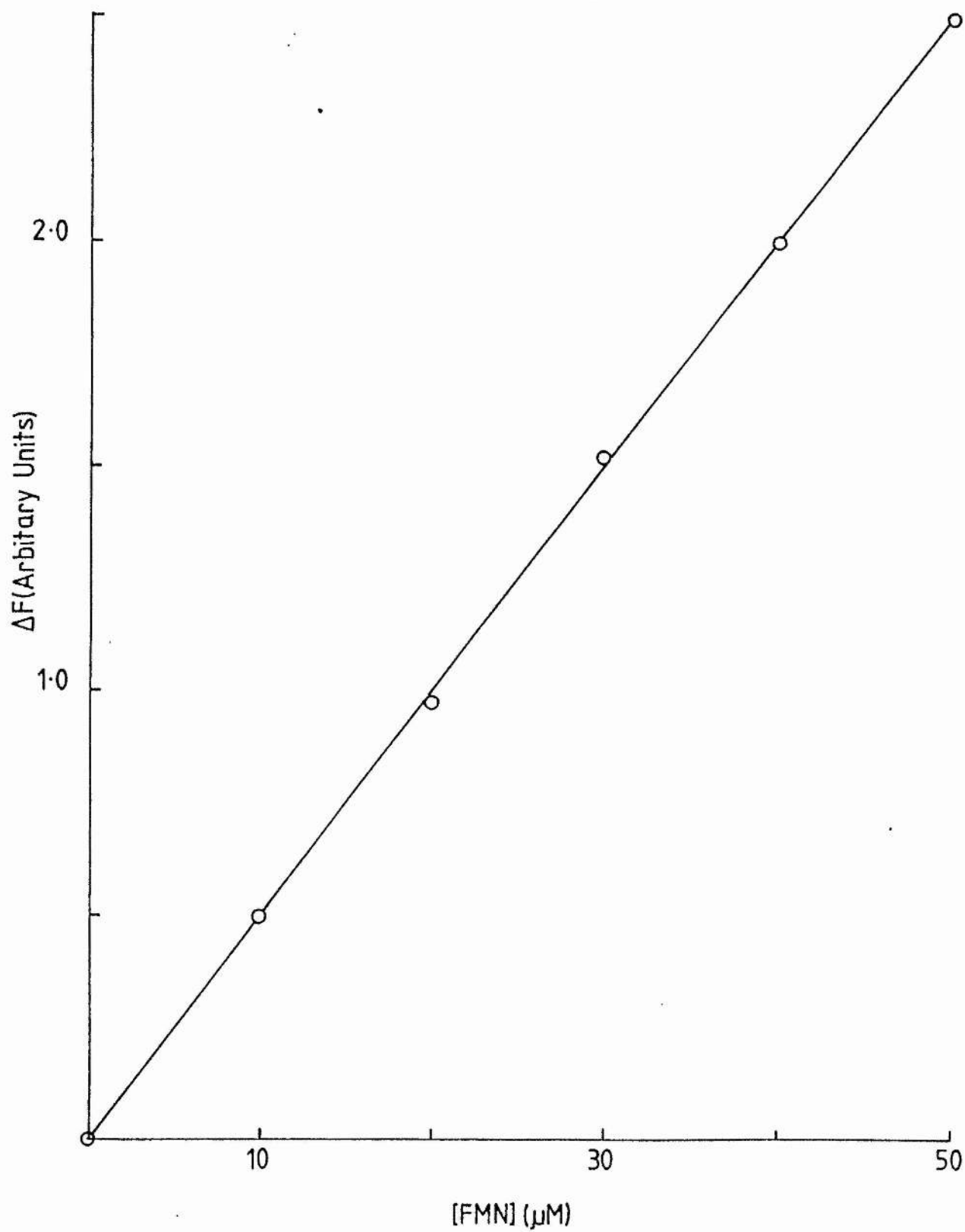
The acid non-extractable flavin of the sample was obtained using the following equation:

Figure 2.1

Standard Curve; Flavin Determination

The change in fluorescence intensity (pH3.2 - pH7.4, oxidised minus reduced for both pHs), at 520nm, is shown versus the concentration of the FMN standards. The equivalent concentration of the standard was taken to be the total concentration of flavin. This value was then corrected for contamination by acid-extractable flavin, as described in the text. A fresh standard curve was constructed for each set of assays.

Standard Curve, Flavin Determination



Acid non-extractable flavin = (flavin determined spectrophotometrically) - (flavin determined fluorimetrically)

where the total flavin minus the acid extractable flavin (contaminant) gave the true value for the acid non-extractable flavin of the sample.

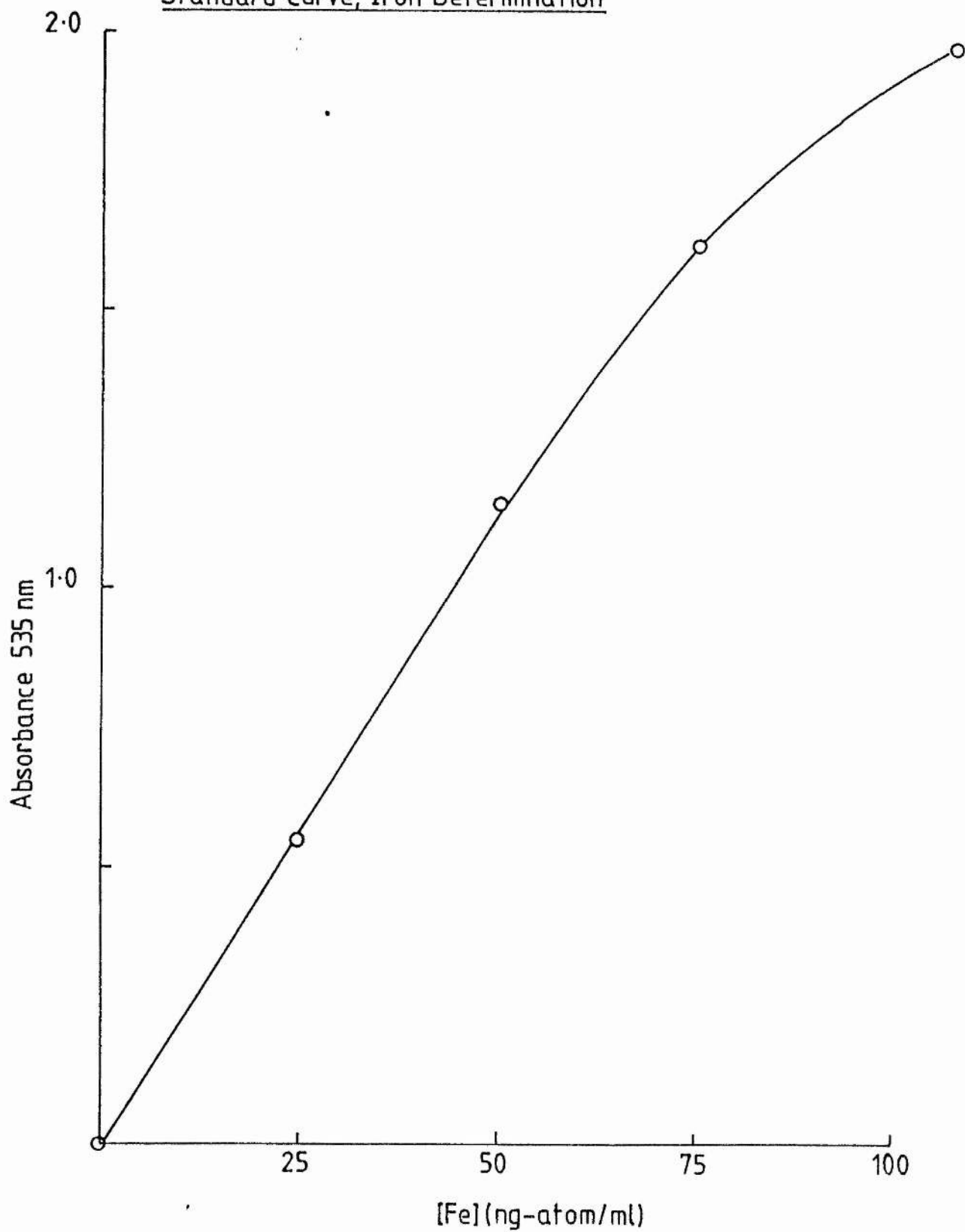
2.6.2 Non-Haem Iron

The non-haem iron content of the ETP was measured, spectroscopically by the method of King *et al.* (1964). Iron(II) sulphate was used to construct a standard curve (fig.2.2). All glassware used was washed with HCl (2M) and distilled water passed through a deioniser. All reagents were prepared using deionised, distilled water and care was taken to exclude dust and other contaminants from all apparatus. The same set of apparatus was used for each set of determinations as this was considered less likely to contain any contamination, having been through the cleaning procedure.

Figure 2.2Standard Curve; Iron Determination

The method of King *et al.* (1964) was used for the determination of non-haem iron. The standard curve for absorbance at 535nm versus the concentration of iron (ng atom/ml) is shown for the iron (II) sulphate standards. The iron concentration was estimated directly from the curve, then corrected for any dilution factors. A fresh standard curve was constructed for each set of assays.

Standard Curve, Iron Determination



2.6.3 Acid-Labile Sulphur

Acid-labile sulphur was determined by the method of Rabinowitz (1978), using sodium sulphide to construct a standard curve (fig.2.3). Care was taken to minimise the loss of H_2S produced during the assay and fresh standards were run with each set of determinations.

2.6.4 Protein Estimations

Protein determinations were performed using the method of Lowry et al. (1951). The method was modified by the inclusion of sodium dodecyl sulphate (SDS, 1%, final concentration) in the reagents and blanks, to ensure the solubilisation of the membrane proteins. The reagents and blanks were kept at a temperature of $40^{\circ}C$ throughout the assay. Bovine serum albumin (BSA) was used as a standard (fig.2.4), and a fresh standard curve was constructed for each set of assays.

2.7 Sample Preparation for e.p.r.

Samples for e.p.r. spectroscopy were placed in quartz e.p.r. tubes with an internal diameter of approximately 3mm. The samples were either reduced or oxidised in the e.p.r. tubes, before freezing in a mixture of methylcyclohexane and isopentane (1 : 4), cooled to $-80^{\circ}C$ with a liquid N_2 cold

Figure 2.3**Standard Curve: Sulphide Determination**

The method of Rabinowitz (1978) was used for the determination of acid-labile sulphur. The standard curve shows absorbance 670nm versus the concentration of sodium sulphide standards. The standards were diluted from a stock solution of sodium sulphide, which had been standardised using thiosulphate titrations. The concentration of acid-labile sulphur was estimated directly from the curve and adjusted for any dilution factor. A fresh standard curve was constructed for each set of assays.

Standard Curve, Sulphide Determination

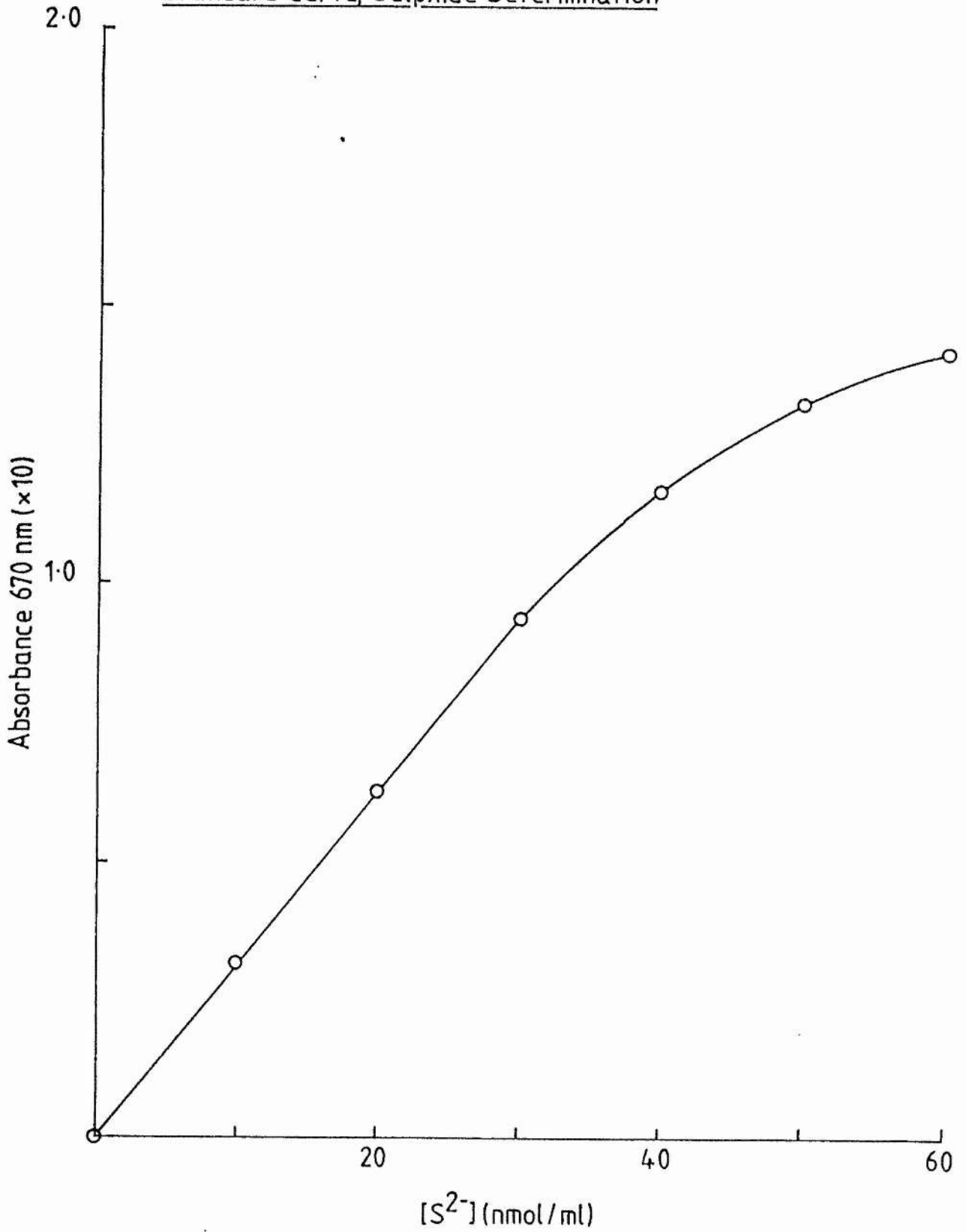
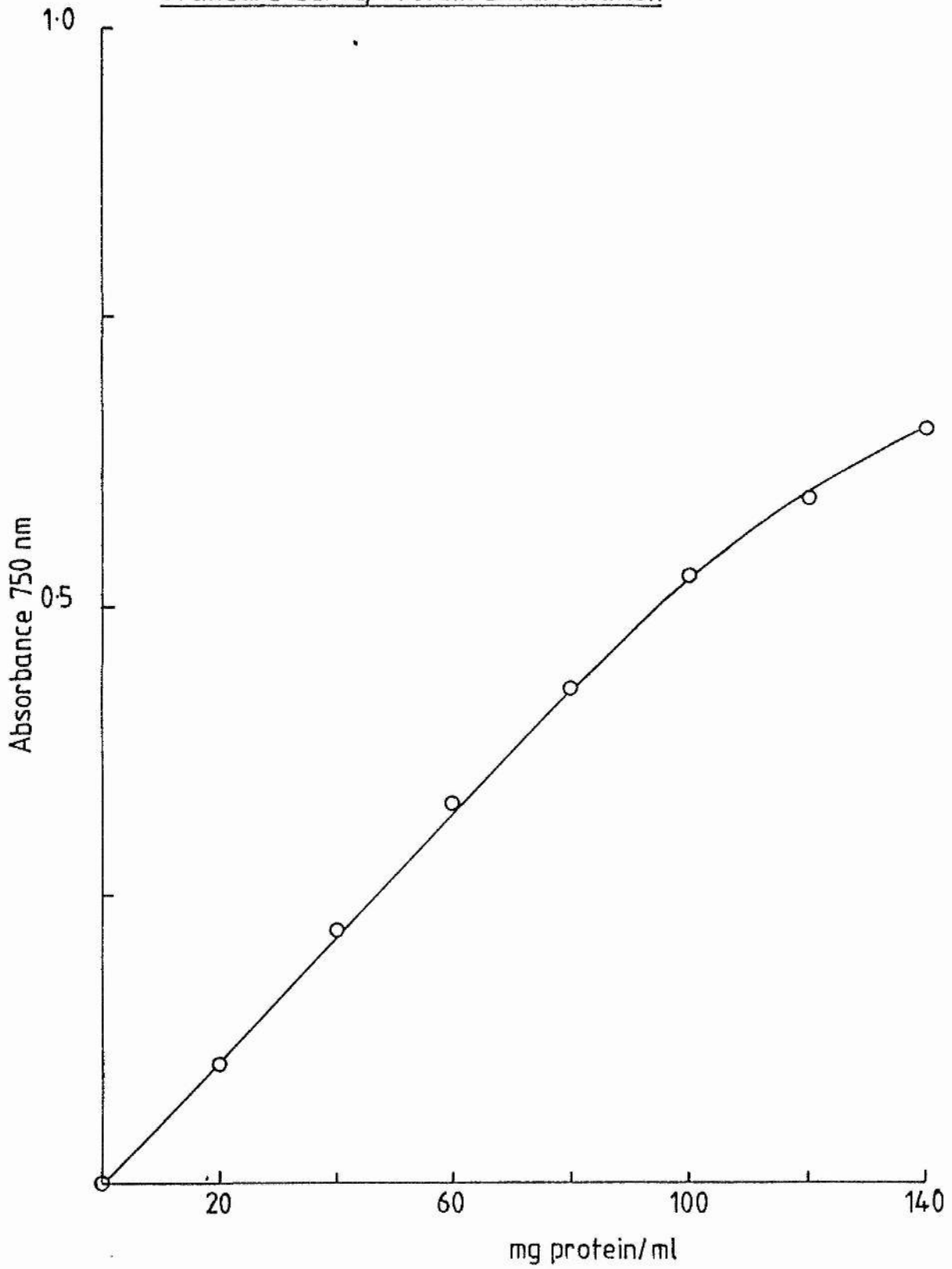


Figure 2.4

Standard Curve; Protein Determination

The method of Lowry *et al.* (1951), modified as described in the text, was used for the determination of the total protein concentration. The standard curve shows absorbance at 750nm versus the concentration of the BSA standards. The protein concentration of the samples was estimated directly from the curve and then corrected for any dilution factors. A fresh standard curve was constructed with each set of assays.

Standard Curve, Protein Determination



finger. Oxidised samples were prepared by incubation of the sample at room temperature for 5 minutes after the addition of H_2O_2 (0.05%, 5 μ l). Succinate or dithionite reduced samples were prepared by incubation at room temperature after the addition of solid sodium succinate or solid sodium dithionite, for 15 minutes (succinate) or 5 minutes (dithionite). Samples were stored frozen in liquid N_2 until e.p.r. spectra could be obtained.

For dysprosium studies ETP or fresh whole cells were incubated with the dysprosium in Eppendorf tubes for 5 minutes, before transference to the e.p.r. tubes and either being reduced or oxidised. A stock solution of dysprosium (III) chloride (60mM; Koch-Light Labs Ltd., Coinbrook, Bucks., U.K.) chelated with EDTA (120mM) was diluted in the sample suspension to the required concentration. Lanthanum-EDTA was used as a non-paramagnetic control.

2.7.1 Oriented Multilayers

Oriented multilayers were prepared essentially as described by Blum *et al.* (1980). Membranes were thawed and diluted to approximately 10mg protein/ml in TES buffer (2mM, pH 7.2), containing EDTA (0.5mM). The membranes were centrifuged onto the Mylar sheets coated with collodion (nitrocellulose) and supported, flat in specially adapted

centrifuge tubes. Controlled dehydration of the membranes was then elicited in the presence of a humidity buffer, damp ammonium sulphate. Oxidised multilayers were prepared by dehydration in the presence of air. For multilayers required to be reduced, sodium succinate (15mM) was added to the dilution buffer and the dehydration of the membranes was performed under a partial atmosphere of hydrogen (80% N₂, 10% H₂, 10% CO₂). This produced multilayers that were partially reduced (both FR1 and HiPIP were partially present as shown by e.p.r. spectroscopy). Further reduction was achieved by incubation of the multilayers, in the e.p.r. tubes, with either sodium succinate (1M, 10 μ l) or sodium dithionite (1M, titrated to pH 7.0 with KOH, 10 μ l). The multilayer sheets produced from the dehydration were cut into strips (approximately 2.5mm wide) and two of these were placed in each e.p.r. tube, containing glycerol (50% v/v). The samples were then further reduced if this was required. The samples were frozen in the freezing mixture and stored under liquid N₂ until the e.p.r. spectra could be obtained.

2.7.2 Redox Titrations

Potentiometric redox titrations were performed as described by Dutton (1978). The following redox mediators were added at a concentration of 50 μ M: methyl viologen, benzyl viologen, safranin T, phenosafranin, indigo disulphonate, resorufine, duroquinone, 1,4 naphthoquinone, 1,2 naphthoquinone

and 1,2 naphthoquinone-4-sulphonic acid. For redox titrations of the flavin moiety of fumarate reductase, redox dyes that undergo redox changes close to $n = 2$ were used to minimise interference from semiquinone radicals at $g = 2.00$. The following redox mediators were used for these titrations: 1,4 naphthoquinone, duroquinone, indigo disulphonate, indigo tetrasulphonate, 2-hydroxy 1,4 naphthoquinone, phenosafranine and safranin T, all at concentrations of 50 μ M. The redox titration vessel was purchased from the University of Pennsylvania glass workshop; a combination platinum-calomel reference electrode (Russell pH, Auchtermuchty, Fife, U.K.) was used to measure the ambient electrode potential. The vessel was continuously flushed with O_2 free N_2 (British Oxygen Co.) which had been passed through a Nil-Ox apparatus (Jencons Scientific, Mark Rd., Hemel Hempstead, U.K.), to remove any residual O_2 . Samples were transferred anaerobically to e.p.r. tubes and frozen in the freezing mixture, before being stored in liquid N_2 .

2.8 E.p.r. Spectroscopy

E.p.r. spectra were recorded using a Bruker 200D electron spin resonance spectrometer (Bruker Analytische Messtechnik gmbH., Silberstreifen, D-7512 Rheinstetten 4, West Germany), fitted with an Oxford Instruments ESR-9 variable temperature cryostat (Oxford Instruments, Oxford, U.K.). Temperature control of the e.p.r. cavity was achieved either by a liquid

He transfer line (Oxford Instruments) or by a liquid N₂ transfer line (built in the Biochemistry workshop, St. Andrews). The flow rate through the transfer lines and the cavity temperature was measured and controlled by an Oxford Instruments DCT2 temperature control. The sample temperature was checked and calibrated using a thermocouple (chromel-gold at 0.07% iron). Fig.2.5 shows the EMF versus temperature for the thermocouple. The sample temperature was found to be constant over the first 10mm from the cavity base (fig.2.6). The DCT2 temperature controller was also shown to give an accurate read-out of the sample temperature in this region. The temperature increased above this reading as the distance from the cavity base became greater than 10mm, though this effect was dependent on the flow-rate employed (fig.2.6). This effect was observed for both transfer lines.

The e.p.r. spectrometer was interfaced to a Comart Communicator CP100 microcomputer (Comart Ltd., Little End Rd., Eaton Socon, St. Neots, Cambridge, U.K.), which was used to digitise and store the e.p.r. spectra. Manipulations of the e.p.r. spectra were also performed using this microcomputer (see Computation). The Comart Communicator was itself on-line to the University of St. Andrews VAX 11/780s (Digital Equipment Corp.), and the graphics packages of this computer were utilised for spectral output.

Figure 2.5

Standard Curve; Thermocouple EMF

The standard curve shows the change in EMF (V) with temperature for the Cromel-gold thermocouple used to check the calibration of the DCT2 temperature controller and the sample temperature. The temperature of the thermocouple in the e.p.r. cavity was then estimated directly from this curve.

Standard Curve, Thermocouple EMF

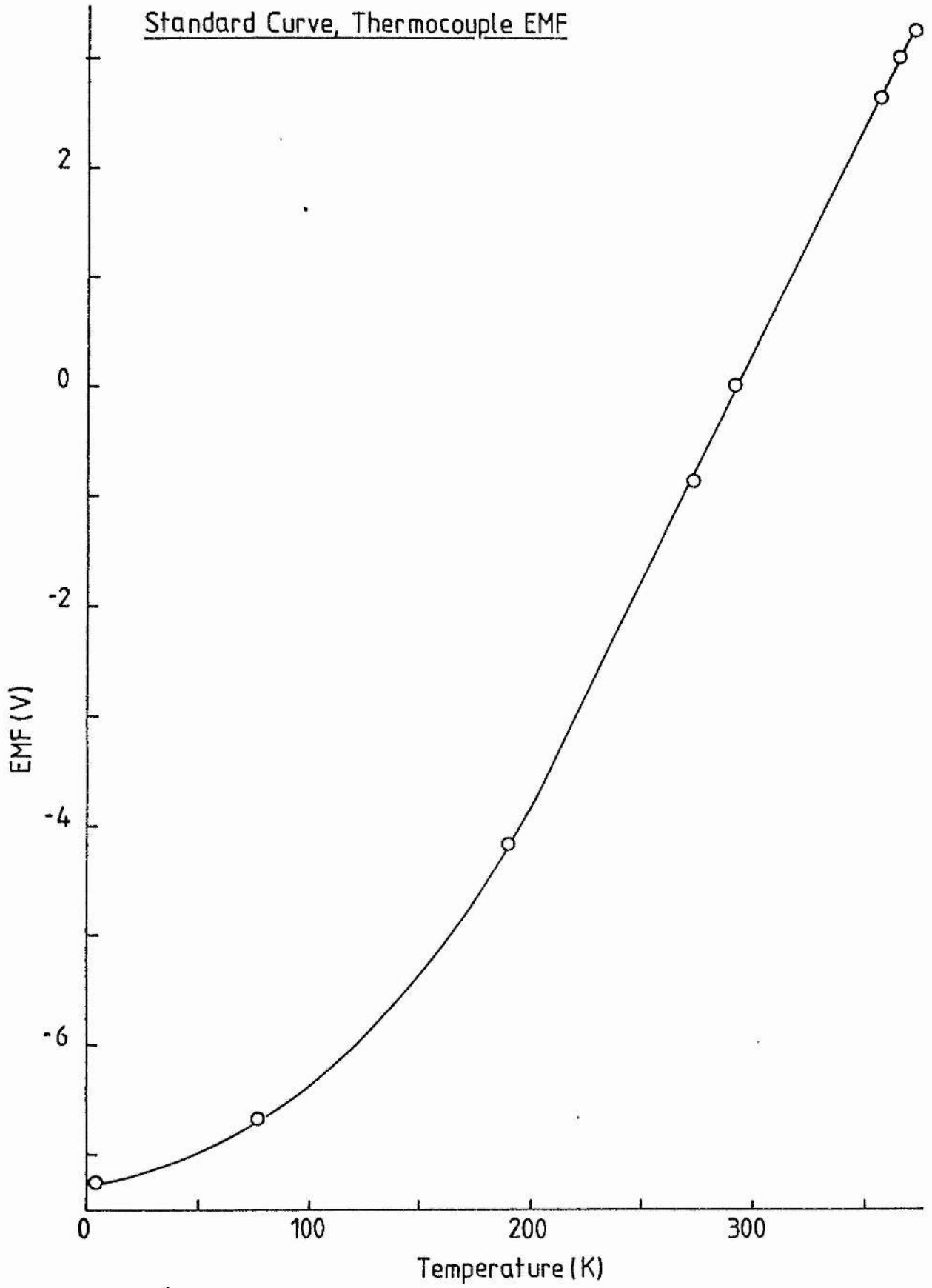
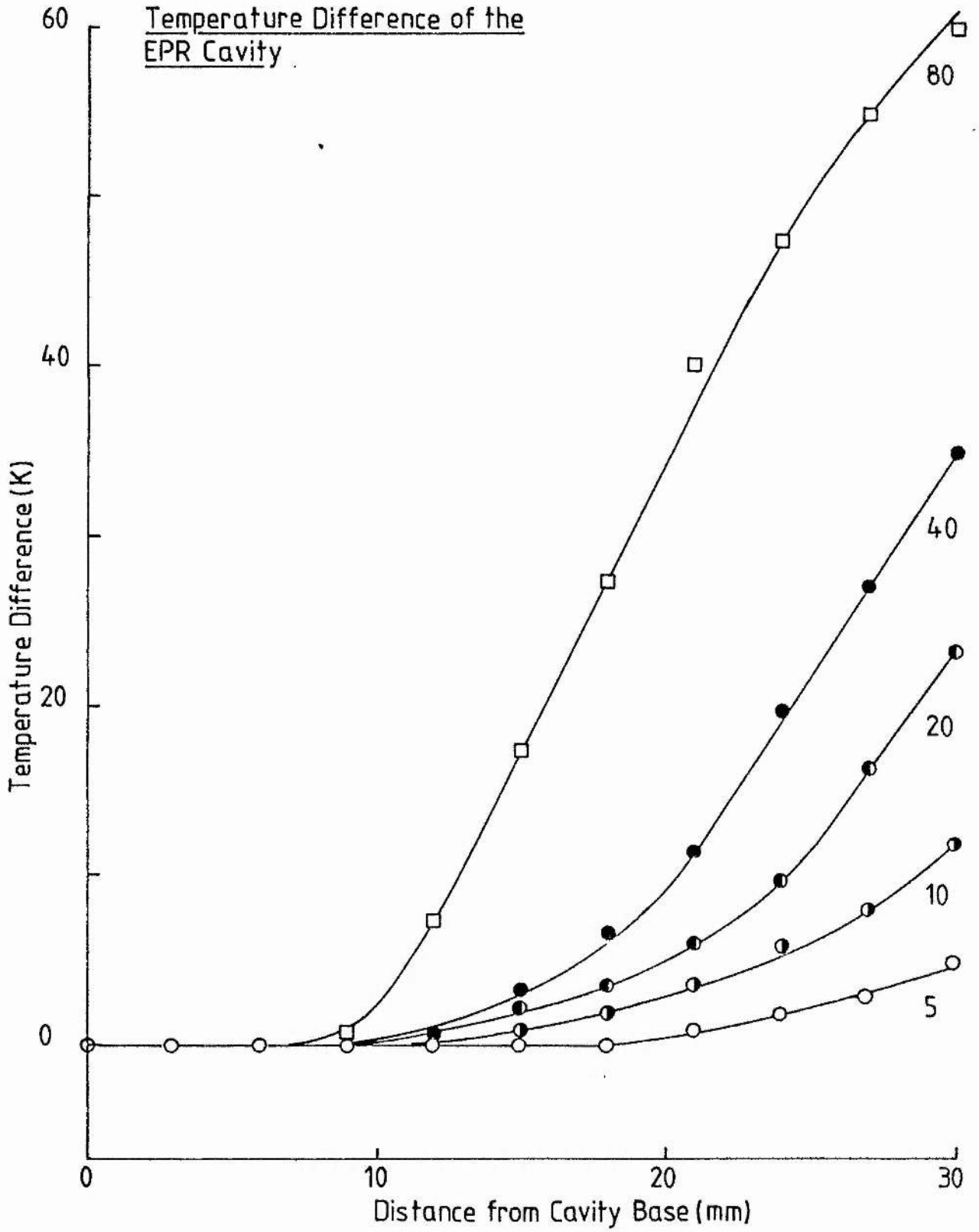


Figure 2.6

Temperature Difference of the e.p.r. Cavity

The temperature of the sample in the e.p.r. cavity was measured using the thermocouple (fig.2.5). The curve shows deviation of temperature from that output on the Oxford DCT2 temperature monitor. The distance from the sample base was taken as the distance of the thermocouple from the base of an e.p.r. tube; the thermocouple rested on a solid support. A range of temperature settings is shown, indicated to the right of the curves, for the DCT2 temperature controller. (O), are points obtained with the liquid He transfer line and (□) points are points obtained with the liquid N₂ transfer-line.

Temperature Difference of the EPR Cavity



2.9 Fluorimetry

Fluorimetry was performed using an Aminco-Bowman J4-8960E scanning spectrofluorimeter (American Instrument Co.) linked to a Gould Bryans 50 000 x-y recorder (Gould Bryans, Willow Lane, Mitcham, Surrey, U.K.). Matched optical quartz fluorimetry cuvettes were used throughout for all experiments.

Redox titrations by fluorimetry were performed in an anaerobic cuvette fitted with a combination platinum-calomel electrode (Russell pH) and sample ports. The cuvette was flushed continuously with O_2 free N_2 (British Oxygen Co.), which had been passed through a Nil-Ox scrubber (Jencons Scientific). The following redox mediator dyes were added to a final concentration of 2.5 M: benzyl viologen, methyl viologen, phenosafranine, indigo disulphonate, resorufin, duroquinone, 1,4 naphthoquinone, 1,2 naphthoquinone and 1,2 naphthoquinone-4-sulphonic acid. These were found to have minimal interference over the redox range employed. The redox titration was performed essentially as described by Dutton (1978) and the sample allowed to equilibrate. The stirrer was switched off briefly, once the sample was equilibrated, to minimise interference from turbulence, and the fluorescence intensity of the sample was determined. The redox titration was analysed as described in Computation.

2.10 Computation

2.10.1 Redox Data

The redox titration data was analysed using a program developed by A.R. Crofts, Chemistry Department, University of Illinois at Urbana. The program gave best-fit data to the experimental points and produced Nernst plot data for the specified n-value.

2.10.2 E.p.r. Simulations

Simulation of e.p.r. powder spectra was performed using a program developed by G. Reed and H. Blum, Department of Biochemistry and Biophysics, University of Pennsylvania, Philadelphia. The three major g-values and the linewidths of each tensor (half-width at half-height) had to be specified. Graphical output of spectra was produced using Ghost subroutines on the VAX 11/780 and output on a Tektronix T4662 plotter.

Double integration of simulations and of experimental spectra was performed on the Comart Communicator, using a program developed by P.J. Robinson, Computing Laboratory, St. Andrews University, St. Andrews, U.K.

The angular dependence of e.p.r. spectra was simulated using a program developed by H. Blum, J.C. Salerno and J.S. Leigh, Department of Biochemistry and Biophysics, University of Pennsylvania, Philadelphia (Blum *et al.* 1978b). The program gave graphical output of e.p.r. spectra produced at various angles of the magnetic field to the membrane normal. The mosaic spread (disorder) of the multilayers could be estimated from comparison of the simulated and the experimental spectra.

CHAPTER THREE

Characterisation of the Membrane Bound Respiratory Fumarate Reductase
and Location of its Catalytic Site.

3.1 Introduction

Escherichia coli grows anaerobically on several non-fermentable substrates when fumarate is provided as an electron acceptor. The respiratory chain developed under these growth conditions is terminated by a membrane-bound fumarate reductase (EC 1.3.99.1). It is important to determine whether fumarate is reduced in the cytoplasm or in the periplasm, so that the inter-relationship between the organisation of the respiratory chain and its proton-translocating ability can be understood.

Direct evidence that the fumarate reductase enzyme complex is at least in part located on the cytoplasmic side of the membrane has been presented by a number of workers using immunological and electron microscopic methods (Van der Plaas *et al.*, 1983; Lemire *et al.*, 1983). However, the location of the catalytic site of a membrane-bound enzyme need not be the same as that of the bulk of the enzyme protein, as detected by non-enzymic means. In this chapter the membrane bound enzyme is characterised by its enzymic reactions and the location of its catalytic site determined. By studying the rates of reaction of fumarate reduction in whole cells and membrane particles the requirement for the uptake of fumarate into the cell, prior to its reduction can be determined. Inhibitors of the dicarboxylic acid porter and mutant strains of E. coli, lacking this porter were used to influence the uptake of fumarate. In cells that require the uptake of fumarate prior

to its reduction, an indirect inhibition of the fumarate reduction will be achieved by blocking the fumarate entry. In mutant strains of *E. coli* lacking the dicarboxylic acid porter, no fumarate reduction should be discernible in whole cells, if the dicarboxylic acid porter is the only means of fumarate entry into the cell.

3.2 Results and Discussion

3.2.1 Initial characterisation of the fumarate reductase

As the major part of the research reported herein was performed on the membrane bound enzyme, from a strain of *E. coli* with amplified expression of the enzyme, an initial study was performed to characterise the enzyme on the membranes from this strain. The fumarate reductase induced anaerobically, in *E. coli*, is known to exhibit significant succinate dehydrogenase activity (Hirsch *et al.* 1964, Spencer & Guest 1973, Dickie & Weiner 1979), so this initial study was performed to measure the relative activities of the two reactions. Fig.3.1 shows the pH dependence of the two reactions. Both the fumarate reductase activity and the succinate dehydrogenase activity were seen to show maximal activity at pH 7.5. This pH was thus used for the assay of these activities in subsequent experiments.

pH Dependence of Enzyme Activities

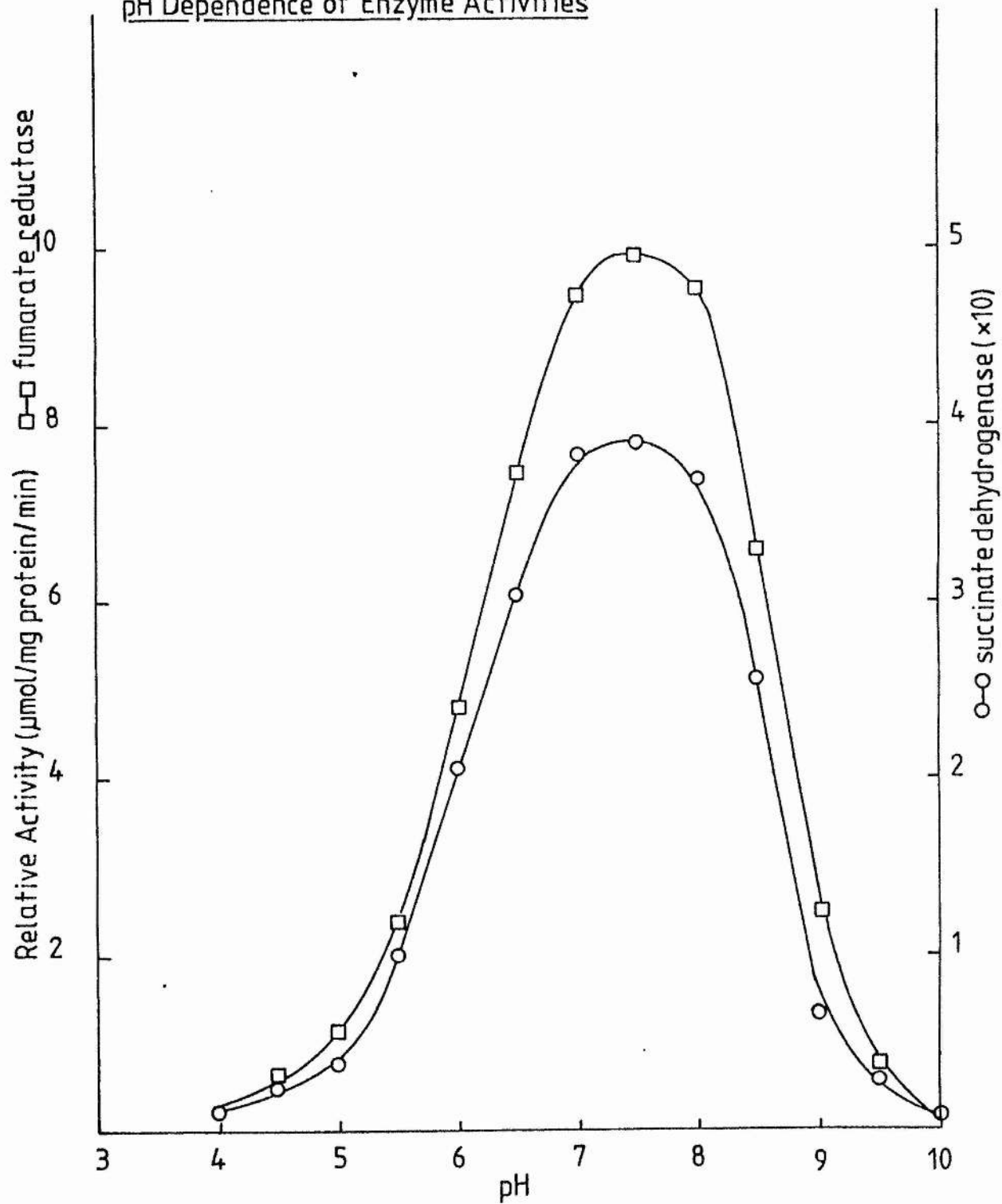


Figure 3.1

pH dependence of enzyme activities

The fumarate reductase and succinate dehydrogenase activities were measured spectrophotometrically, at 30°C, as described in the methods section. The initial activities are expressed as $\mu\text{mol/mg protein/min}$ and are shown plotted against the pH of the buffered solution. The activities were seen to drop off rapidly either side of the physiological pH range, with a maximum for both activities at pH 7.5

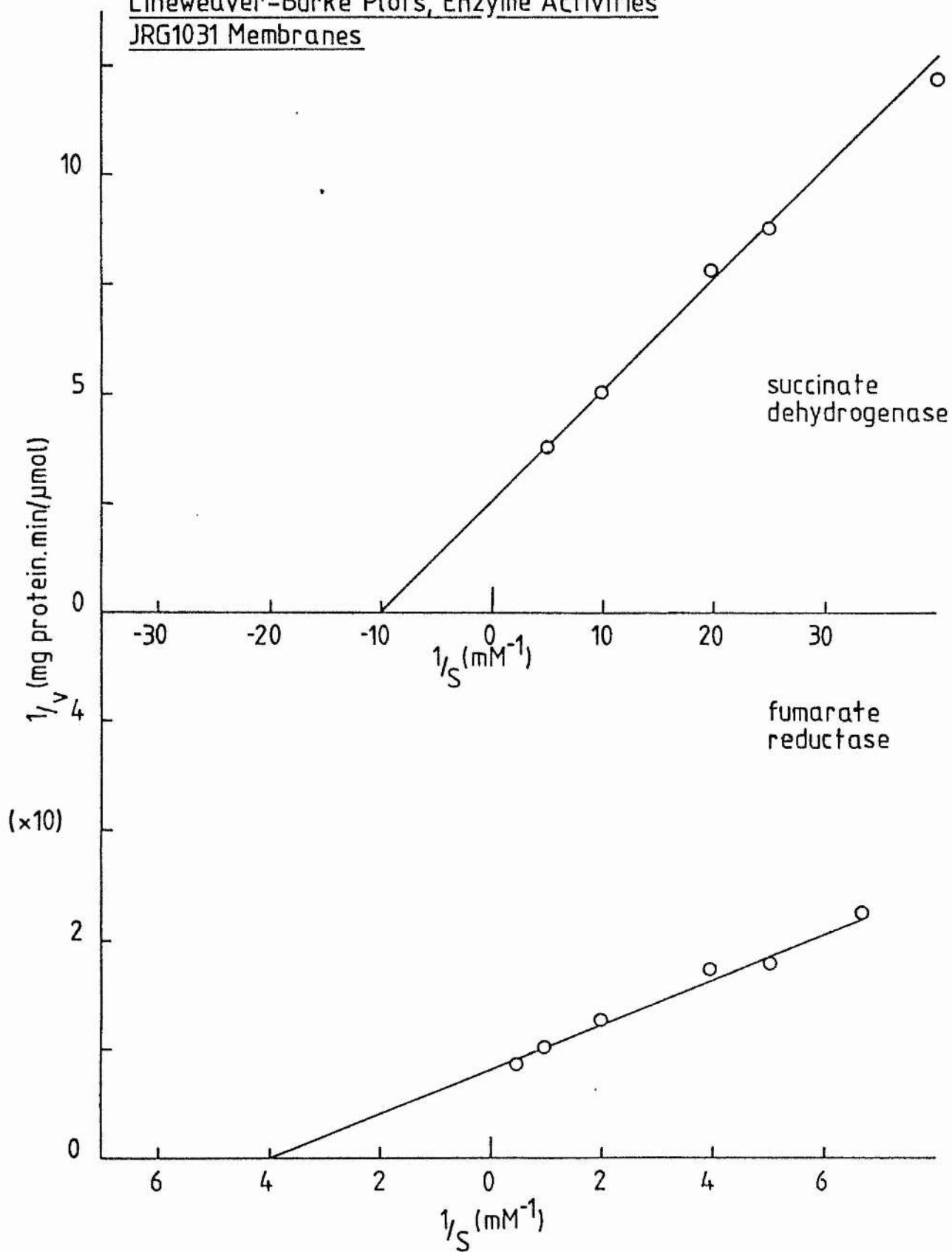
K_m and V_{max} values for the fumarate reductase and succinate dehydrogenase activities were determined graphically for both activities. This is illustrated in fig.3.2, which shows Lineweaver-Burke plots for the fumarate reductase and succinate dehydrogenase activities. Both Lineweaver-Burke and Eadie-Hofstee plots were used to determine the apparent Michaelis-Menten constants and the values for the K_m s were in good agreement from both graphical determinations. Both reactions appeared to follow simple Michaelis-Menten kinetics over the range of substrate concentrations employed. An apparent K_m of 0.25mM with a V_{max} of 12.5 mol/mg protein/min was observed for the fumarate reductase activity (benzyl viologen dependent). The succinate dehydrogenase activity (PMS-DCPIP dependent activity) was much less than the fumarate reductase activity, with an apparent K_m of 100 M and V_{max} of 0.4 mol/mg protein/min. Fumarate reductase activity was competitively inhibited by succinate, as has been described previously (Hirsch *et al.* 1963, Dickie & Weiner 1979). The membrane bound enzyme in the fumarate reductase amplified strain of *E. coli* would therefore appear to catalyse the reduction of fumarate more readily than the oxidation of succinate, as has been shown previously for other strains of *E. coli* (Hirsch *et al.* 1963, Spencer & Guest 1973, Dickie & Weiner 1979).

Figure 3.2

Determination of K_m and V_{max}

Lineweaver-Burke plots for both the fumarate reductase and succinate dehydrogenase activities are shown, to illustrate the determination of the K_m and V_{max} values. The kinetic parameters were determined from both Lineweaver-Burke plots and Eadie-Hofstee plots. The points shown are the average of three determinations at each substrate concentration. The top graph illustrates the succinate dehydrogenase activity and the bottom graph illustrates the fumarate reductase activity.

Lineweaver-Burke Plots, Enzyme Activities
JRG1031 Membranes



3.2.2 Studies with dct mutants

The majority of the fumarate reductase molecule has been shown to reside on the cytoplasmic side of the cell membrane (Van der Plaas et al. 1983, Lemire et al. 1983). This would imply that the reduction of fumarate by the cell was cytoplasmic also. Studies were therefore undertaken to investigate the site of fumarate reduction in E. coli. Fumarate reductase activities of intact cells and membrane particles were compared in order to determine any requirement for a transport process for fumarate in whole cells. Two experimental approaches were used: firstly, fumarate reductase activities in a number of E. coli strains (Table 3.1), some of which lacked the dicarboxylic acid carrier (dct mutants) were compared; and secondly, fumarate reductase activities, in the presence of inhibitors of the dicarboxylic acid carrier, were compared. The fumarate reductase activity was measured by the benzyl viologen assay, in whole cells and membrane particles. Jones & Garland (1977) have shown that reduced benzyl viologen can readily cross the cytoplasmic membrane of E. coli K12, so this assay is suitable for both membranes and whole cells. If the site of fumarate reduction is cytoplasmic, as implied by the majority of experimental evidence, then uptake of fumarate prior to its reduction would be necessary in whole cells. A blockage of this uptake would result in the loss of measurable activity in whole cells.

Table 3.1.

Fumarate reductase activities from whole cells and membrane particles
of the of E. coli K12 strains

Strain	<u>Whole Cells</u>	<u>Membrane Particles</u>	
	F.R.	F.R.	NADH. Ox.
EMG2 (wildtype)	65 ± 4	125 ± 11	60 ± 4
JRG1031 (clone)	80 ± 7	910 ± 20	165 ± 9
CBT38 (<u>det</u> ⁻)	0	20 ± 3	12 ± 1
CBT312 (<u>det</u> ⁻)	0	40 ± 6	10 ± 2
CBT313 (<u>det</u> ⁻)	0	50 ± 6	9 ± 1

All strains of *E. coli* were grown in nutrient broth because det mutants did not grow in glycerol/fumarate medium. Inverted membrane vesicles were prepared using a French pressure cell. Fumarate reductase activities are given in nmol fumarate reduced / mg protein / min (which because of the different electrical equivalencies is half of the benzyl viologen oxidation rate, it is the latter which is actually measured). The results are the mean values (± the maximum variation from the mean) of three assays each on three separate cultures. NADH oxidase activities are expressed in ng atoms O/mg protein/min.

Fumarate reductase activities in intact bacteria and membrane particles derived from dct mutant strains were compared with those of wild type. The dct mutants could not grow anaerobically on glycerol plus fumarate as an alternative electron acceptor, so all strains were grown on nutrient broth for these experiments. This mode of growth had the disadvantage of yielding lower activities for both the fumarate reductase and (where present) the dicarboxylic acid carrier. Substantial rates of fumarate reductase activity were detected in the intact cells of strains EMG2 and JRG1031, but there was no activity observed in the mutants CBT38, CBT312 and CBT313 (Table 3.1). The membrane particles of all strains had fumarate reductase activity. The fumarate reductase activity was greatest in the strain containing amplification of the frd gene (JRG1031). A comparison of the rates of fumarate reduction, by cells and membrane particles, shows that fumarate reductase activity was latent in whole cells in all strains but EMG2 (Table 3.1). In strain JRG1031, the rate of fumarate reduction in whole cells was high, but the specific activity in the membranes was ten-fold greater, presumably because a rate limitation imposed by the transport process was removed in the latter case. A K_m of 20-30 μ M has been reported for the porter (Kay & Kornberg 1971, Lo *et al.* 1972) and a V_{max} of 25nmol/mg dry wt./min (Kay & Kornberg 1971). In the dct mutants no activity was observed in intact cells, presumably because the fumarate could not enter. These

observations show the requirement for a dicarboxylic acid carrier in whole cells but not in particles, indicating that the site of fumarate reduction is cytoplasmic.

3.2.3 Studies with inhibitors

To confirm the requirement for a porter to transport fumarate into the cells, prior to its reduction, studies were performed with inhibitors of the porter. Kay & Kornberg (1971) and Lo *et al.* (1972), showed that the dicarboxylic acid porter could catalyse uptake of fumarate and succinate, and that the addition of other dicarboxylic acids competitively inhibited the uptake of these two molecules. *E. coli* strains EMG2 and JRG1031 were grown in glycerol/fumarate medium, which enables growth by fumarate respiration and induces high activities of fumarate reductase (Spencer & Guest, 1973). Maximum rates (V_{max}) and K_m values were determined from Lineweaver-Burke plots and Eadie-Hofstee plots, these values are shown in Table 3.2. In the glycerol/fumarate grown strain EMG2 there was no significant difference between these values in cells and membrane particles in the absence of an inhibitor. In strain JRG1031, a difference in the values of these parameters in cells and membranes was observed. In JRG1031 a K_m value of 0.25 mM for fumarate was observed in membranes, close to that obtained in EMG2, but a K_m value of 0.78 mM was observed for whole cells.

Table 3.2

Fumarate reductase activities in the presence of added
dicarboxylic acids

<u>Strain</u>	<u>Inhibitor</u>	<u>K_m (mM)</u>		<u>V_{max}</u>	
		<u>Cells</u>	<u>ETPs</u>	<u>Cells</u>	<u>ETPs</u>
EMG2	None	0.25±0.03	0.20±0.07	1.57±0.1	1.62±0.4
EMG2	Aspartate	0.79±0.04	0.23±0.07	1.58±0.09	1.57±0.3
EMG2	Malate	(0.71±0.07)	0.86±0.05	(1.60±0.11)	1.65±0.7
EMG2	Tartrate	0.3±0.07	0.67±0.09	1.55±0.07	1.55±0.4
JRG1031	None	0.78±0.03	0.25±0.07	12.0±0.9	12.5±0.8
JRG1031	Aspartate	2.73±0.09	0.25±0.08	11.3±0.5	12.6±0.8
JRG1031	Malate	(3.00±0.08)	0.71±0.1	(12.1±0.7)	12.5±0.7
JRG1031	Tartrate	0.79±0.04	2.22±0.2	11.9±0.9	12.4±0.4

Bacteria were grown on glycerol/fumarate medium. K_m and V_{max} values are the mean values (\pm the maximum deviation from the mean) of three separate determinations obtained from plots of rate data at eight substrate concentrations. Disodium salts of the D,L dicarboxylic acids were added (5 mM) as inhibitors. V_{max} values are expressed as μmol fumarate reduced / mg protein / min, as explained in Table 3.1.

Presumably the K_m of approximately 0.25 mM was a consequence of the rate limitation of fumarate reductase itself, so in EMG2 cells and membranes and in JRG1031 membranes, the fumarate reductase step was rate-limiting. In strain JRG1031, the fumarate reductase is amplified and appeared to cause the porter for fumarate entry to become rate limiting in whole cells. Thus the K_m of 0.78 mM reflects the kinetics imposed on the fumarate reduction by the dicarboxylic acid carrier, rather than the kinetics of the fumarate reductase, itself.

The use of aspartate, malate and tartrate as inhibitors of either the dicarboxylic acid carrier or the fumarate reductase, confirmed the need for a dicarboxylic acid carrier for fumarate reduction in intact cells (Table 3.2). Aspartate did not inhibit fumarate reduction by membrane particles, but it was effective as a competitive inhibitor in whole cells. The interpretation of these results is that aspartate is an inhibitor of the transport process, (Kay & Kornberg, 1971) but not of fumarate reductase, and hence is an inhibitor of fumarate reduction only in intact cells. Tartrate had only a marginal effect on fumarate reductase activity in whole cells, but was a competitive inhibitor of fumarate reductase activity in membrane particles. Malate inhibited in both cells and membrane preparations. In control experiments, no detectable oxidase activities were observed for aspartate, malate and tartrate in membrane preparations or cells (O_2 electrode), and only malate supported benzyl viologen oxidation, and then only

in whole cells. The rates of malate-supported benzyl viologen oxidation were 78 ± 6 nmol/mg protein/min for strain JRG1031 and 82 ± 5 nmol/mg protein/min for strain EMG2, indicating the presence of fumarase activity in whole cells. This complicates the interpretation of the data obtained with whole cells in the presence of malate (values bracketed in Table 3.2). However the K_m for fumarate was increased in the presence of malate, showing that the primary effect of malate on fumarate reduction in whole cells was to inhibit fumarate reduction at the level of the dicarboxylic acid porter. If the conversion of malate to fumarate was distorting the results (initial rates were measured) then, in the absence of any other effect, an apparent lowering of the K_m for fumarate would result. These results complement those presented by Kay & Kornberg (1971) and Lo *et al.* (1972), as the inhibition of the uptake of fumarate by the dicarboxylic acid porter is indirectly shown by measuring the fumarate reductase activity. The uptake of fumarate and succinate was shown, by these authors, to be inhibited by the addition of various other dicarboxylic acids and it is shown here that the consequence of this, for fumarate uptake, is lower rates of fumarate reduction. This confirms the location of the site of fumarate reduction to be cytoplasmic. The results presented here also indicate that the amplification of fumarate reductase in the membranes of strain JRG1031, does not appear to be accompanied by the amplification of the dicarboxylic acid porter. Thus the rate of fumarate reduction and thus growth, of this strain is limited by the kinetics of

the porter.

3.2.4 Discussion of the catalytic site's location

These studies, using dct mutants and inhibitors of the dicarboxylic acid carrier or fumarate reductase, show that in whole cells the transmembrane transport of fumarate must precede its reduction. Thus the catalytic site is on the cytoplasmic aspect of the cytoplasmic membrane. Van der Plas et al. (1983) used a crossed-immuno-electrophoretic approach to analyse the membrane proteins of E. coli grown on glycerol with fumarate as respiratory oxidant and extended their analysis to immuno-absorption studies. By comparing the antibody binding to intact (right side-out) and disrupted membrane vesicles, they calculated the relative expression of the fumarate reductase antigen at the external and internal membrane surfaces. They were able to show that the antigenic determinants of E. coli fumarate reductase were on the cytoplasmic aspect of the cell membrane. They did not however, determine the location of the catalytic site, and the absence of antigenic determinants from the periplasmic aspect of the membrane cannot be taken as conclusive proof of the absence of any part of the fumarate reductase from this side of the membrane. Lemire et al. (1983) determined the structure of fumarate reductase on inverted membrane vesicles by a combination of antibody binding studies and electron microscopy. They assigned 'knob-like' structures, observed on

the cytoplasmic side of the cell membrane, to the catalytic subunits of fumarate reductase. By removing and restoring the fumarate reductase activity to the membrane preparation, they observed the concomitant loss and restoration of the 'knobs'. The activity was removed by chymotrypsin or urea treatment and restored by incubation of the stripped membranes with a fumarate reductase preparation. This work indicates that the bulk of the fumarate reductase is membrane associated and located on the cytoplasmic aspect of the membrane, and thus implies that the catalytic site is also cytoplasmic. The possibility, however, of the major part of the enzyme being located cytoplasmically, but the substrate binding site being accessible to the periplasmic phase, cannot be ruled out on the basis of these studies. Weiner *et al.* (1984a), by comparing the sequences of the two anchor polypeptides to those of other membrane intrinsic proteins, proposed that they were transmembraneous in structure and that they may form a proton channel through the membrane, by comparison of the structure of the anchor polypeptides to those of bacteriorhodopsin, the F_o of the ATPase and the lac carrier. If this is the case then the location of the site of reduction of fumarate could not be automatically assumed to be cytoplasmic.

Jones & Garland (1977) assumed a cytoplasmic location for fumarate reductase, on the basis of the abilities of oxidation-reduction dyes to reduce fumarate in intact and broken cells, but this approach suffered from a lack of

knowledge of the site of interaction between the dyes and the respiratory chain. Gutowski & Rosenberg (1976, 1977) also argued for an internal location of the fumarate reductase catalytic site on the basis of the effect of tartrate on respiratory proton translocation supported by a pulse of fumarate. Their conclusion that the quenching of the acidification was due to tartrate inhibiting the transport process can be questioned on two points. Firstly, tartrate is a better inhibitor of fumarate reductase than of the dicarboxylic acid carrier. Secondly, tartrate would be expected to quench the measured proton translocation by entering the cell in symport with a proton, as soon as any ΔpH is established, because the dicarboxylic acid carrier is a proton symporter (Gutowski & Rosenberg, 1976).

The work presented in this chapter complements that already presented by others and directly confirms the previously implied location of the catalytic site of fumarate reductase.

3.2.5 Studies on the nature of the catalytic site.

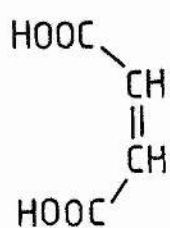
Studies to further characterise the membrane bound enzyme, in the amplified strain of *E. coli*, were performed by studying the rates of reaction of several alternative substrates for fumarate reductase (fig.3.3). All the compounds were α, β -unsaturated-carbonyl compounds and the

Figure 3.3

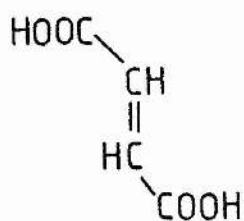
Alternative substrates for fumarate reductase

The structural formulae of the alternative substrates used in this study are shown. The structures indicate the changes in the side-groups of these molecules. The dimethylfumarate and methylcrotonate were produced by esterification of the parent carboxylic acids.

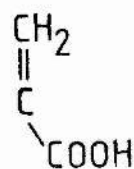
Formulae of Alternative Substrates



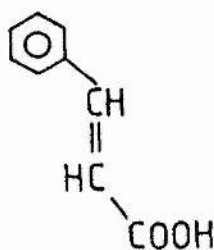
maleate



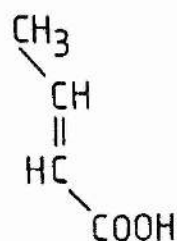
fumarate



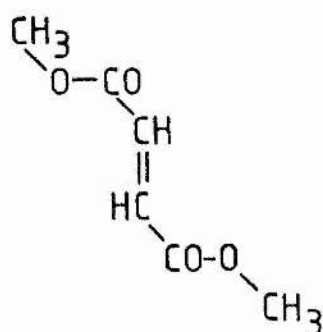
acrylate



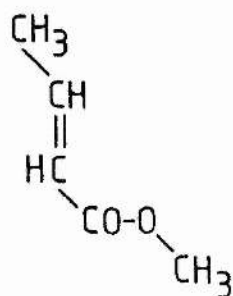
cinnamate



crotonate



methyl fumarate



methyl crotonate

rate of reduction of the double bond was measured using the benzyl viologen assay. Table 3.3 shows the rates of reaction observed for these compounds, when the initial concentration of each substrate was 5mM. Initially the stereospecificity of fumarate reductase was investigated using maleate. No reaction for this compound was observed up to an initial concentration of 20mM. Maleate is the cis isomer of 2-buten-dioate, whilst fumarate is the trans isomer of the same compound. Thus fumarate reductase of *E. coli* is stereospecific for fumarate. Maleate however, did show competitive inhibition of fumarate reduction, indicating that it may bind to the active site. An apparent K_i of 3mM was obtained for this inhibition. It can be concluded that maleate binds to the fumarate reductase in a non reactive, as a result of its cis conformation, rather than the trans conformation of fumarate.

Studies on compounds with different structures to fumarate were performed to investigate the consequences of these changes in structure. Table 3.3 shows the results from these studies. It was shown that compounds which had one of the carboxylate groups removed, were less reactive than fumarate and hence poorer substrates. The rate of reaction also decreased as the size of the replacement group increased and became more hydrophobic in nature (fig.3.3). Acrylate (R-H) reacted faster than crotonate (R-CH₃) which reacted faster than cinnamate (R-Ph), but all were reduced at a lower rate than fumarate.

Table 3.3

Rates of reaction with alternative substrates

<u>Substrate</u>	<u>Rate</u>	<u>Apparent K_i</u>
Fumarate	12.3 \pm 0.6	-
Maleate	0	3.0mM
Acrylate	9.6 \pm 0.4	8.5mM*
Crotonate	7.7 \pm 0.4	13.0mM*
Cinnamate	1.1 \pm 0.2	26.4mM*
Methyl fumarate	50 \pm 8 ($\times 10^{-3}$)	-
Methyl crotonate	10 \pm 3 ($\times 10^{-3}$)	-

Rates are expressed as μ mol/mg protein/min. The rates were measured using a final concentration of substrate of 5mM. The rates are shown as the mean values of three determinations, on three separate membrane preparations, together with the maximum variation about the mean.

* : These values can only be taken as approximations, as these substrates also show significant rates of reaction.

The necessity of the carboxylate groups was investigated by using esterified compounds as substrates for the enzyme. It was seen that these compounds gave only very low rates of reaction, Table 3.3. Methyl fumarate reacted faster than methyl crotonate, but less than fumarate and indeed, less than the other carboxylic acids. These esters lack the negative charge associated with the ionised group of the parent carboxylic acids, and are neutrally charged molecules. The carbonyl groups have a polar nature and so weak binding of these substrates to the enzyme was postulated to account for their low rates of reaction.

To account for the results obtained it was postulated that the active site of fumarate reductase must contain positively charged amino acid residues in the vicinity of the flavin moiety, to act as a substrate binding site. The sequence of amino acids around the flavin binding site has been determined by Cole (1982), from the nucleotide sequence of the *frdA* codon, which encodes for the flavoprotein subunit of fumarate reductase. This polypeptide sequence was shown to contain the same sequence of amino acids (9 residues) as that from bovine-heart succinate dehydrogenase. The sequence of amino acids around this region was shown to contain several positively charged amino acids (histidine, lysine and arginine residues) together with other amino acids with basic side groups (glutamine). The results presented here, indicate that some of these residues may form the substrate binding site for

fumarate. The requirement for the negatively charged carboxylate groups, for good rates of reaction, and the lower rates of reaction produced by introducing substrates with a less polar nature (and those with greater hydrophobicity) argue in favour of this postulate. The stereospecificity of the enzyme could also be explained by the nature of the binding of the two carboxylate groups of maleate, which may locate it in a non reactive position.

3.3 Conclusions

The fumarate reductase in the membranes from *E. coli*, strain JRG1031 has been shown to be pH dependent with the maximum rate of reaction at pH 7.5, for both fumarate reduction and succinate oxidation. The catalytic site of fumarate reduction was shown to be on the cytoplasmic side of the cell membrane, by the requirement for fumarate to be transported across the membrane prior to reduction. This located the catalytic site in agreement with the location postulated in previously published work, most notably Lemire *et al.* 1983, who showed the catalytic subunits of fumarate reductase to be located on the cytoplasmic face of the cell membrane.

Studies on the catalytic site of fumarate reductase showed the enzyme to be stereospecific for fumarate. The requirement of the negatively charged carboxylate groups, to achieve significant rates of reduction of alternative substrates, pointed to the substrate binding site containing positively charged amino acid residues.

CHAPTER FOUR

Electron Paramagnetic Resonance Characterisation of the Iron-Sulphur Centres

4.1 Introduction

The purified fumarate reductase of *E. coli* has been shown to be structurally similar to succinate dehydrogenases from a number of sources (Dickie & Weiner, 1979; Weiner & Dickie, 1979) and recent sequence determinations on the *E. coli* succinate dehydrogenase, indicate extensive sequence homologies between these two functionally distinct enzymes (Guest 1984), particularly in the cysteine residues of the iron-sulphur subunit. All succinate dehydrogenases and fumarate reductases that have been studied to date contain a co-valently linked flavin (8 α -[N(3)-histidyl]FAD), acid-labile sulphur and non-haem iron (5-8 mol. / mol. enzyme, Hederstedt & Rutberg 1981, Beinert & Albracht 1982). The non-haem iron and acid-labile sulphur are constituted as one $[4\text{Fe}-4\text{S}]^{3+}$ or $[3\text{Fe}-x\text{S}]$ centre (the term HiPIP, high potential iron-sulphur protein, is used as a generic for this centre) and either one or two ferredoxin centres usually considered as $[2\text{Fe}-2\text{S}]$ centres, but one of these may be a $[4\text{Fe}-4\text{S}]$ centre (Beinert & Albracht 1982, Dickie & Weiner 1979, Ohnishi *et al.* 1976 a & b, R. Cammack, T. Ohnishi personal communications).

In this chapter the iron-sulphur clusters from the *E. coli* fumarate reductase are resolved and then described *in situ*, using electron paramagnetic resonance. The question of whether there are one or two of the binuclear ferredoxin centres present is addressed, together with the possibility that one of these centres may be tetranuclear in nature. This

chapter presents evidence for interactions between the intrinsic centres, and discusses the relevance of the findings to the understanding of other succinate-fumarate oxido-reductases.

4.2 Results and discussion

4.2.1 Comparison of membranes from EMG2 and JRG1031

The electron transport chain developed when *E. coli* is grown on the glycerol/fumarate medium is relatively simple, consisting of specific dehydrogenases, menaquinone, and terminating in fumarate reductase. A cytochrome oxidase is also present (Ingledeew & Poole, 1984). The *E. coli* strain JRG1031 enabled the fumarate reductase to be studied in situ through the amplified expression of fumarate reductase. It is the intention, in this chapter, to report studies on fumarate reductase in situ using membranes from this *E. coli* strain. An in situ study has a number of advantages, the principal one of which is in overcoming the variability and heterogeneity which has afflicted the studies using purified preparations (for review see Beinert & Albracht, 1982). The use of membranes has the disadvantage of the presence of other iron-sulphur centres which do not belong to the fumarate

reductase. Thus, it is necessary to establish which e.p.r. detectable centres are attributable to fumarate reductase, in order to ascertain to what extent centres belonging to other enzymes may interfere with the analysis. The iron-sulphur centres developed by an *E. coli* K12 prototroph (EMG2), grown anaerobically on glycerol/fumarate medium, have been described (Ingledeu 1983) and so this earlier work can serve as a control in the present study. In this earlier study several iron-sulphur centres were described but three predominated. These three were tentatively assigned to a succinate-fumarate oxido-reductase on the basis of the predominance of fumarate reductase in the membranes, and also the similarity, in several respects, between the observed properties of the iron-sulphur centres and those reported for succinate-fumarate oxido-reductases from other sources.

Shown in Table 4.1 is a comparison of the major partial reactions of the respiratory chains of the two strains used. Table 4.2 shows a quantitation of the detected iron-sulphur centres from strains JRG1031 & EMG2. It is apparent, from Table 4.1, that the only large change in activity measured was of the fumarate reductase. This corresponds with the amplification of two e.p.r. signals (HiPIPa and ferredoxin IIa & b of Ingledeu 1983). Thus one centre, paramagnetic in the oxidised state, is amplified along with a ferredoxin-like centre reducible by succinate ($g_z = 2.03$, $g_{xy} = 1.93$) and a ferredoxin-like centre reduced by dithionite. A comparison of e.p.r. spectra of control and JRG1031 membranes, is best

Table 4.1

Partial reactions of respiratory chains in ETPs

	<u>EMG2</u>	<u>JRG1031</u>
Fumarate reductase	1.27	9.98
NADH dehydrogenase	0.62	0.68
Lactate dehydrogenase	0.08	0.42
Formate dehydrogenase	0.02	0.02
L-glyc-3P dehydrogenase [*]	0.02	0.04
Succinate dehydrogenase	0.30	0.48

Activities are expressed as $\mu\text{mol.} / \text{min.} / \text{mg protein}$

Cells were grown on glycerol / fumarate medium and ETPs were made as described in Materials and Methods.

^{*}, L-glycerol-3-phosphate dehydrogenase.

given by a comparison of the work herein with the published work on EMG2 (Ingledeu, 1983), where spectra taken over a wide range of conditions can be compared. Additional centres that are observed in the membranes from EMG2 cells are obscured in JRG1031 membranes, by overlap due to the higher levels of the three centres assigned to fumarate reductase, and the consequent use of lower gain. Thus these three resolvable species can be attributed to fumarate reductase, and the extent to which other species overlap with them spectrally is small and quantifiable.

4.2.2 The e.p.r. spectra of JRG1031 membranes

Membrane particles of JRG1031, when oxidized, exhibited at relatively low temperatures, an e.p.r. spectrum typical of either a $[4\text{Fe-4S}]^{3+}$ or $[3\text{Fe-XS}]$ iron sulphur centre. The term FR3 (fumarate reductase centre 3) is used as a generic, by analogy to centre S3 of succinate dehydrogenase, to refer to this centre. This spectrum is shown in Fig.4.1a at various temperatures. It has a narrow line-shape with $g_{y,z}$ at 2.01 and g_x at approx. 1.968 although this latter value is considerably temperature dependent. The spectral feature preceding the $g = 2.01$ lineshape was due to copper in the sample, as shown at higher temperatures where the spectrum from FR3 was no longer discernible. The spectrum at 6 K and 20mW microwave power, can be simulated using g_z at 2.01,

Figure 4.1a

E.p.r. spectra from oxidised membranes

The e.p.r. spectra obtained from H_2O_2 oxidised membranes are shown at various temperatures. The major g-values are indicated above the spectra and the temperatures are shown on the left of the spectra. The positive peak was at $g = 2.01$, but the g_y and g_x values were dependent on the temperature. The experimental conditions were: microwave power, 20mW; microwave frequency, 9.48GHz; modulation amplitude, 1.0mT; modulation frequency, 100KHz; receiver gain, 6.3×10^3 ; scan rate, 0.1mT/s at a time constant of 0.5s. Protein concentration was 103mg/ml.

E.p.r. spectra: Fumarate Reductase,
 H_2O_2 oxidised E.T.P

201

1.968
|
g-value

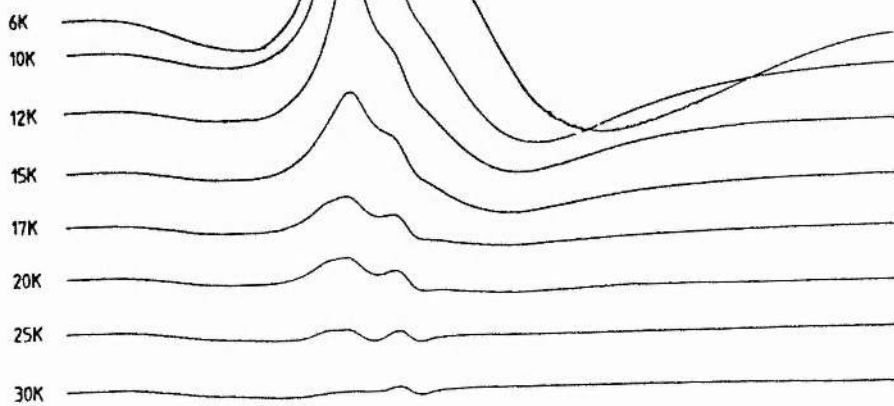
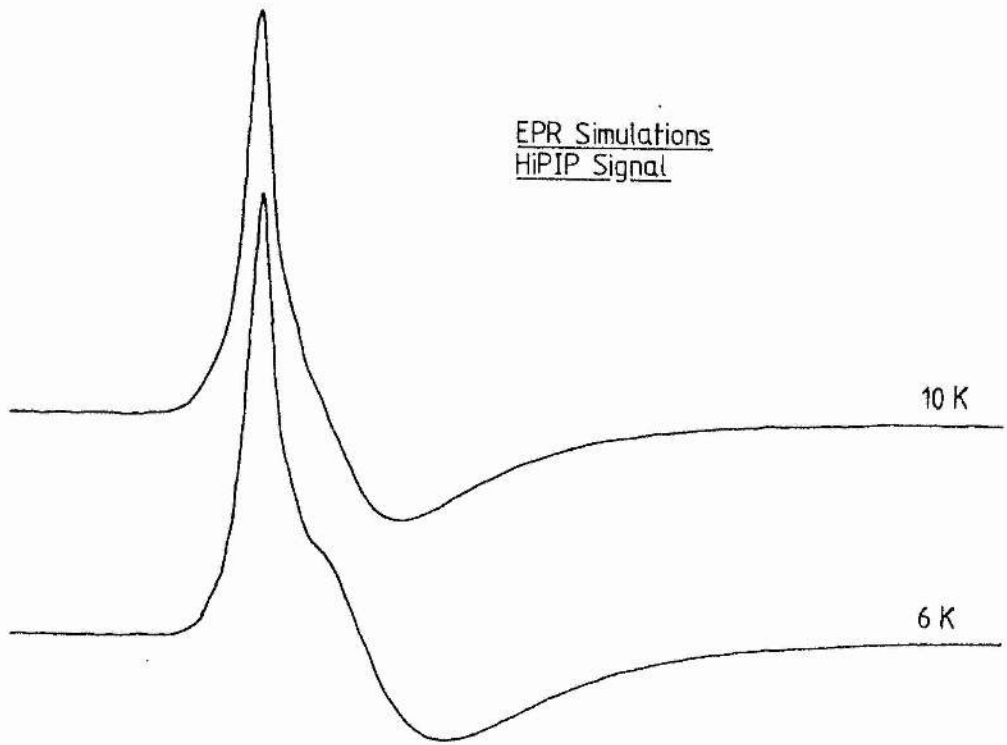


Figure 4.1b

Simulation of the HiPIP spectra

Simulations of the HiPIP spectra are shown for two temperatures, which are indicated on the right of the simulations. For the data from 6K, g-values of 2.01, 1.99 and 1.55 were employed with linewidths (half-width at half-height) of 0.70, 2.5 and 5.5mT, convoluted with a Lorentzian broadening of 0.5mT. At 10 K g-values of 2.01, 2.00 and 1.78 were employed, together with linewidths of 0.7, 2.0 and 5.0mT; Lorentzian broadening of the same magnitude as for the 6 K simulation was used.

EPR Simulations
HiPIP Signal



g_y at 1.99 and g_x at 1.55. The linewidths employed in the simulation were 0.70mT, 2.5mT, and 5.5mT respectively, (Fig.4.1b), convoluted with a Lorentzian broadening of 0.5mT. The simulation of spectra from other temperatures required differing g -values and linewidths for g_x .

In membrane particles which have been anaerobically reduced with succinate, a ferredoxin-like signal is observed with $g_z = 2.03$ and $g_{xy} = 1.93$. Fig.4.2a shows this spectrum at several temperatures. When membrane particles were reduced anaerobically with dithionite, a ferredoxin signal of similar line-shape but with apparently enhanced signal amplitude, was observed (Fig.4.2b). There is a small line-shape difference between the two reduction states, the dithionite elicited spectra being less rhombic around $g = 1.93$ than the succinate elicited spectra. This rhombicity is temperature dependent and this effect correlates with the temperature dependence of the relaxation processes (c.f. chapter 5), the difference in rhombic distortion being greater at higher temperatures. These spectra can be simulated, as shown in Fig.4.2c, and the values required for the succinate reducible ferredoxin are $g_x = 1.918$, linewidth 1.0mT, $g_y = 1.928$, linewidth 0.85mT, and $g_z = 2.03$, linewidth 0.75mT, at 12K and 20mW microwave power. For the dithionite reducible centre values of $g_x = 1.913$, linewidth 1.05mT, $g_y = 1.926$, linewidth 0.85mT and $g_z = 2.03$, linewidth 0.75mT were used, for the same temperature and microwave power.

Figure 4.2a

E.p.r. spectra from succinate reduced membranes

The e.p.r. spectra from membranes reduced anaerobically with sodium succinate are shown at various temperatures. The temperatures are indicated to the right of the the spectra and the major g-values are indicated below the spectra. The spectra show saturation of the ferredoxin signal below 30 K, as the intensity of the spectra decreases. The experimental conditions are as descibed for fig.4.1a, except the receiver gain was 5.0×10^4 . The protein concentration was 85mg/ml.

E.p.r. spectra:
Fumarate Reductase,
Succinate reduced E.T.P.

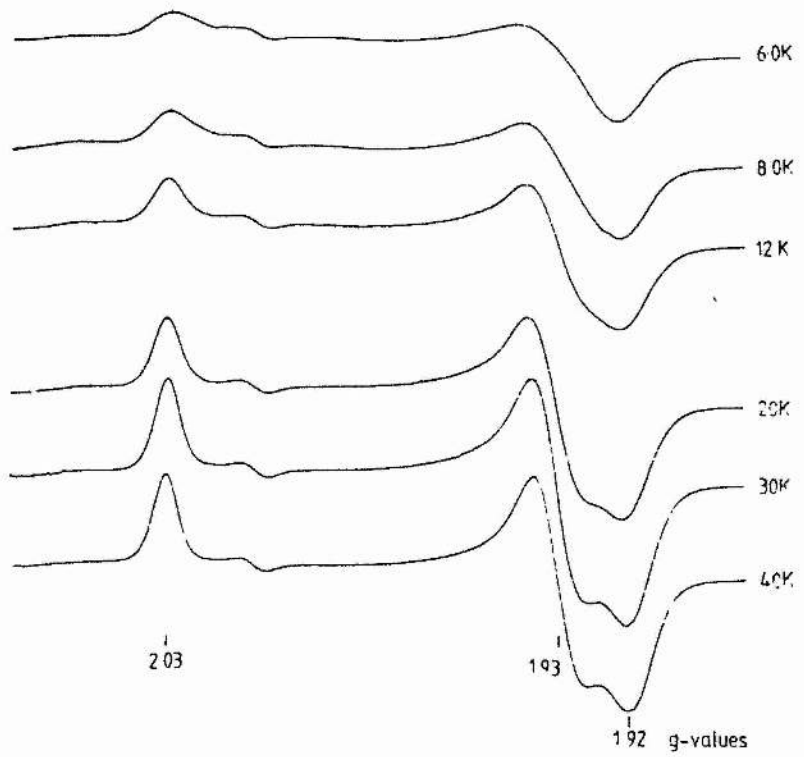


Figure 4.2b

E.p.r. spectra from dithionite reduced membranes

The e.p.r. spectra from membranes reduced anaerobically with sodium dithionite are shown at various temperatures. The temperatures are indicated to the right of the spectra and the major g-values are indicated below the spectra. The spectra have similar lineshapes to those from succinate reduced membranes, but show differing saturation, the intensity of the spectra shown increases from 28 K to 12 K. The experimental conditions were as described for fig.4.1a, except the receiver gain was 8.0×10^3 . The protein concentration was 79mg/ml.

E.p.r spectra Fumarate Reductase,
Dithionite reduced E.T.P.

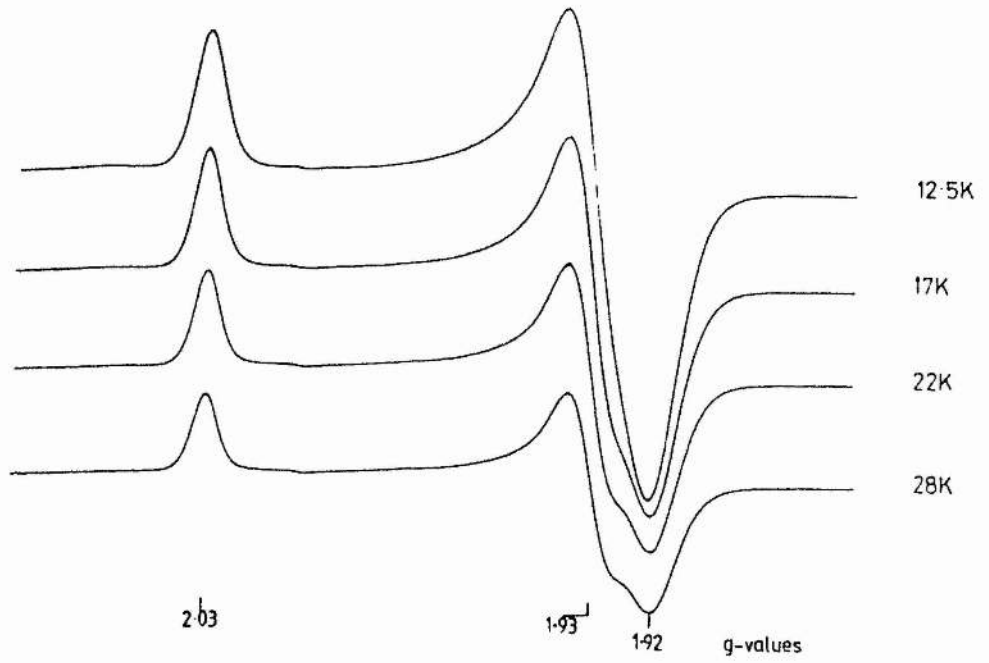
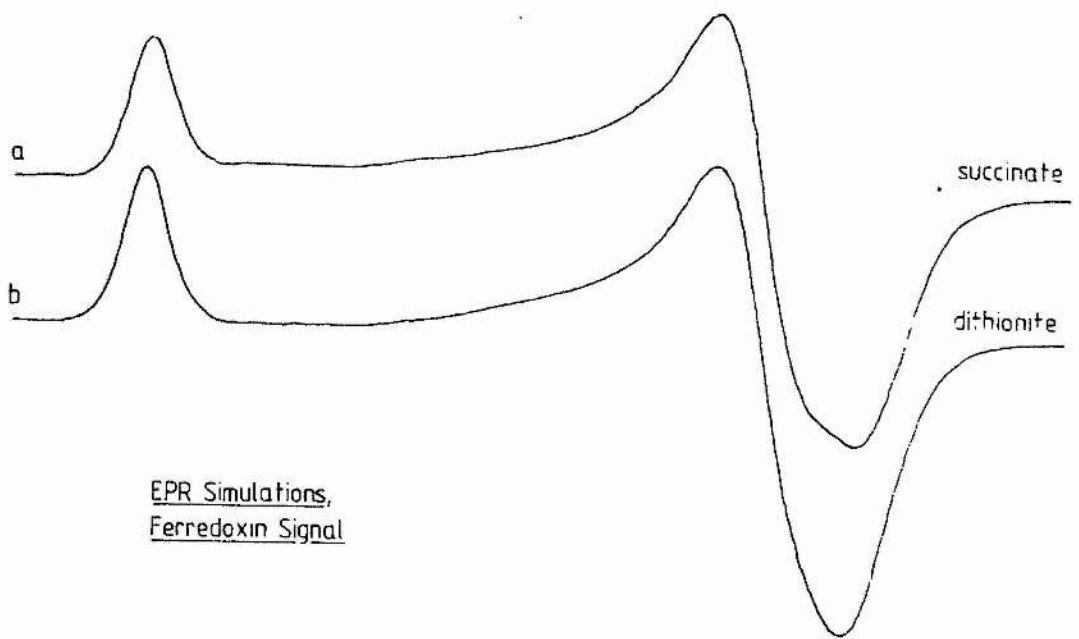


Figure 4.2c

Simulations of the ferredoxin spectra

The simulations of the ferredoxin spectra from succinate (a) and dithionite (b) reduced membranes, at 2mW microwave power and 12 K are shown. Simulation (a) was performed using g-values of 2.03, 1.928 and 1.918, together with linewidths of 0.75, 0.85 and 1.0mT. Simulation (b) was performed using g-values of 2.03, 1.926 and 1.913, together with linewidths of 0.75, 0.85 and 1.05mT.



EPR Simulations,
Ferredoxin Signal

One of the objectives of this paper is to shed light on the relationship between the e.p.r. signals observed in dithionite and succinate reduced membranes. At 50 K and 2mW microwave power, where both ferredoxin signals are unsaturated, as determined by plots of microwave power against signal height (double logarithmic plots, theoretical unsaturated slope 0.5), quantitation of the spin intensities gave values of 3.92 nmol/mg protein and 1.96 nmol/mg protein for the dithionite and succinate samples respectively (Table 4.2). Under non-saturating conditions for the HiPIP signal (15 K, 2mW), quantitation of its spin intensity gave a value of 1.94 nmol/mg protein. Copper(II)-EDTA was used as a standard for the quantitation of spin intensities. Comparison of these values with the concentration of acid non-extractable flavin, indicates that all the iron-sulphur centres of *E. coli* fumarate reductase are present at a ratio of approximately 1 : 1 to its flavin moiety (Table 4.2). Table 4.2 shows the values obtained for non-haem iron and acid-labile sulphur determinations from the membranes of strain JRG1031. Comparison of these values to those for the flavin moiety indicates approximately 6-7 atom / molecule fumarate reductase for both of these elements. Values were obtained by subtracting the EMG2 values from the JG1031 values and dividing by the spin quantitation that could be attributed to the amplification of the fumarate reductase. The acid-labile sulphur determination will be a more accurate

Table 4.2

Quantitation of the iron-sulphur centres in membranes from E. coli strains EMG2 and JRG1031

	<u>EMG2</u>	<u>JRG1031</u>
Ferredoxin 1		1.96 ± 0.08
Ferredoxin 1 + 2		3.92 ± 0.11
HIP		1.94 ± 0.09
Flavin		1.93 ± 0.10
Non-haem iron	4.3 ± 0.5	16.1 ± 1.1
Acid-labile sulphur	4.6 ± 0.7	14.9 ± 1.6

Quantitations are expressed in nmol. / mg protein and are the mean values of three determinations shown together with the variation about that mean.

Quantitations were performed by double integration of e.p.r. spectra as described in Materials and Methods. Non-haem iron and acid-labile sulphur determinations were performed as described in the text.

measurement of the iron-sulphur centres as it is specific for these centres, whilst the non-haem iron measurement could include contaminants as the enzyme is membrane bound. The estimate of non-haem iron and acid-labile sulphur per molecule of fumarate reductase can only be taken as an estimate because there will be contamination from other iron-sulphur centres but this contamination can be corrected for (as described above) because of the saturation of the membranes of this strain with fumarate reductase (approx. 20% of the protein from spin intensity measurements). Comparison of the non-haem iron and the acid-labile sulphur determinations from the two strains, indicates a close relationship between these values and the increase in fumarate reductase activity, again confirming the e.p.r. spectra to be from this enzyme. The values obtained are greater than those previously reported for this enzyme (Cole *et al.* 1982), but these latter estimations were on the isolated protein, and the isolation procedure may have been responsible for the loss of iron-sulphur clusters (the HiPIP centre from this class of enzyme is particularly labile).

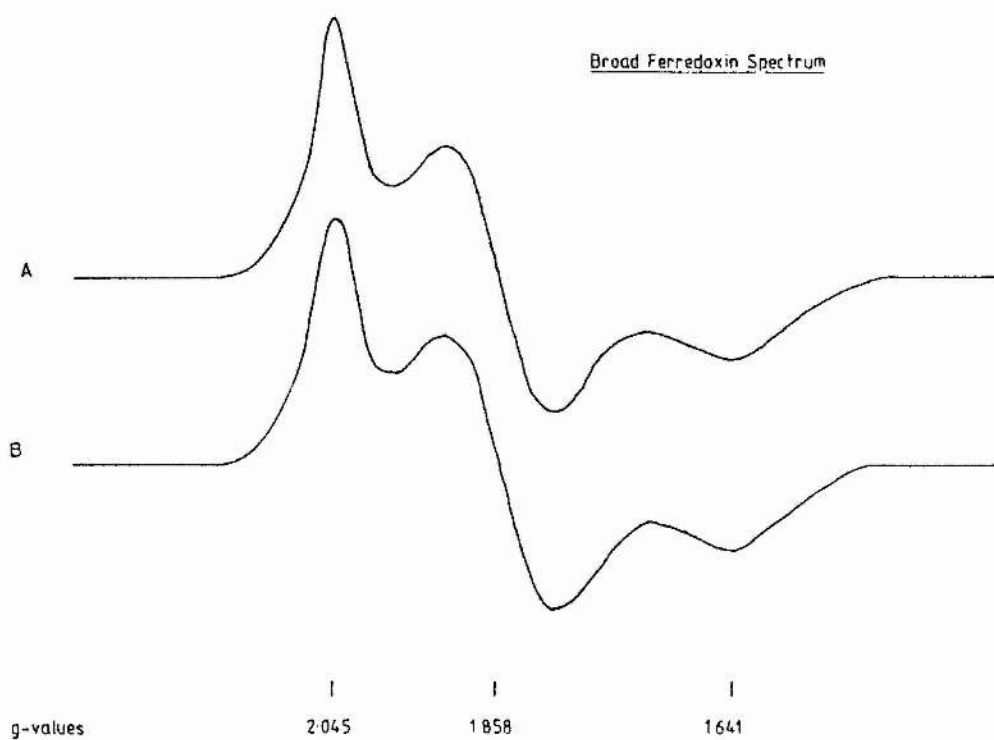
An e.p.r. signal due to a 'tetranuclear' ferredoxin centre was also observed from this enzyme when reduced with dithionite (Fig. 4.3), as has been reported from the isolated enzyme (R. Cammack, personal communication). Studies on bovine-heart mitochondrial succinate dehydrogenase have shown the presence of this type of centre, both by magnetic circular

Figure 4.3

E.p.r. spectrum of the broad ferredoxin

The e.p.r. spectrum from the broad ferredoxin signal (A) is shown together with a computer simulation of that spectrum (B). The major g-values are indicated below the spectra. The e.p.r. spectrum shown was obtained by subtracting a simulation of the dithionite reduced ferredoxin from the experimental spectra. The experimental conditions were as described for fig.4.1a except: microwave power, 20mW; receiver gain, 5.0×10^5 ; scan rate, 0.05mT/s at a time constant of 1s. The temperature was 10K and the protein concentration was 120mg/ml. The simulation (B) was performed using g-values of 2.045, 1.858 and 1.641, together with linewidths of 5.5, 7.7 and 12.5mT.

Broad Ferredoxin Spectrum



dichroism and e.p.r. spectroscopy (Johnson *et al.* 1985, T. Ohnishi personal communication). This centre in the membrane bound fumarate reductase elicits a very broad spectrum with g-values of $g_z = 2.045$, $g_y = 1.858$ and $g_x = 1.641$. The spectrum can be simulated (10K & 20mW) using these g-values and linewidths of 5.5 mT, 7.7 mT and 12.5 mT respectively. Spin quantitations were taken from the e.p.r. spectrum and the simulation, because overlap due to FR1 and FR2, in the e.p.r. spectrum may have caused errors in the quantitation. A value of 0.2 nmol/mg protein was obtained for this centre, showing it to be present at 1/10th the concentration of the other centres. The presence of this centre in bovine-heart succinate dehydrogenase has been shown to be dependent on the enzyme preparation (T. Ohnishi personal communication).

4.2.3 Redox titrations of the ferredoxin signals

Redox titrations were performed to indicate the number of components contributing to the major, 'binuclear' ferredoxin-like signal and assist in describing any interactions between centres. When spectra of redox titration samples were taken under conditions which were shown to be non-saturating (50 K and 2 mW), and signal height was plotted against the samples' ambient electrode potential, a biphasic curve resulted for the ferredoxin signal (Fig.4.4). Two distinct phases were resolved with mid-point potentials of

Figure 4.4

Potentiometric titration of the ferredoxin signal, pH 7.0

Plots of signal height (\square) and double integrated intensity (\circ) are shown plotted against the ambient electrode potential of the e.p.r. samples. The potentiometric titrations were performed as described in the text. Mid-point potentials of the two phases were approximately -50mV and -285mV . Experimental conditions were as described for fig.4.1a, except receiver gain was 8.0×10^4 ; temperature was 50 K and the protein concentration was 38mg/ml . The microwave power was 2 mW .

Redox Titration, Ferredoxin Signal 50K

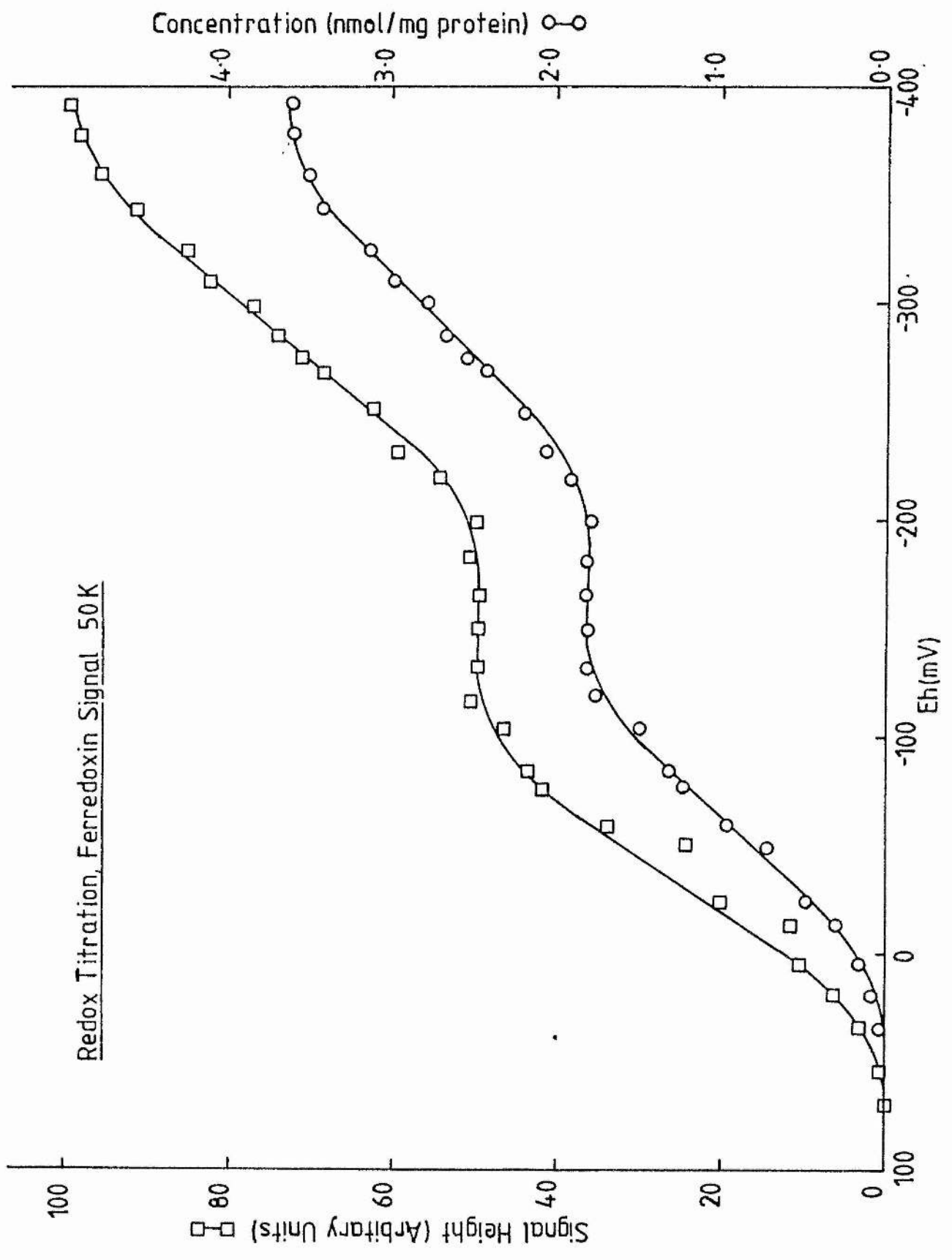
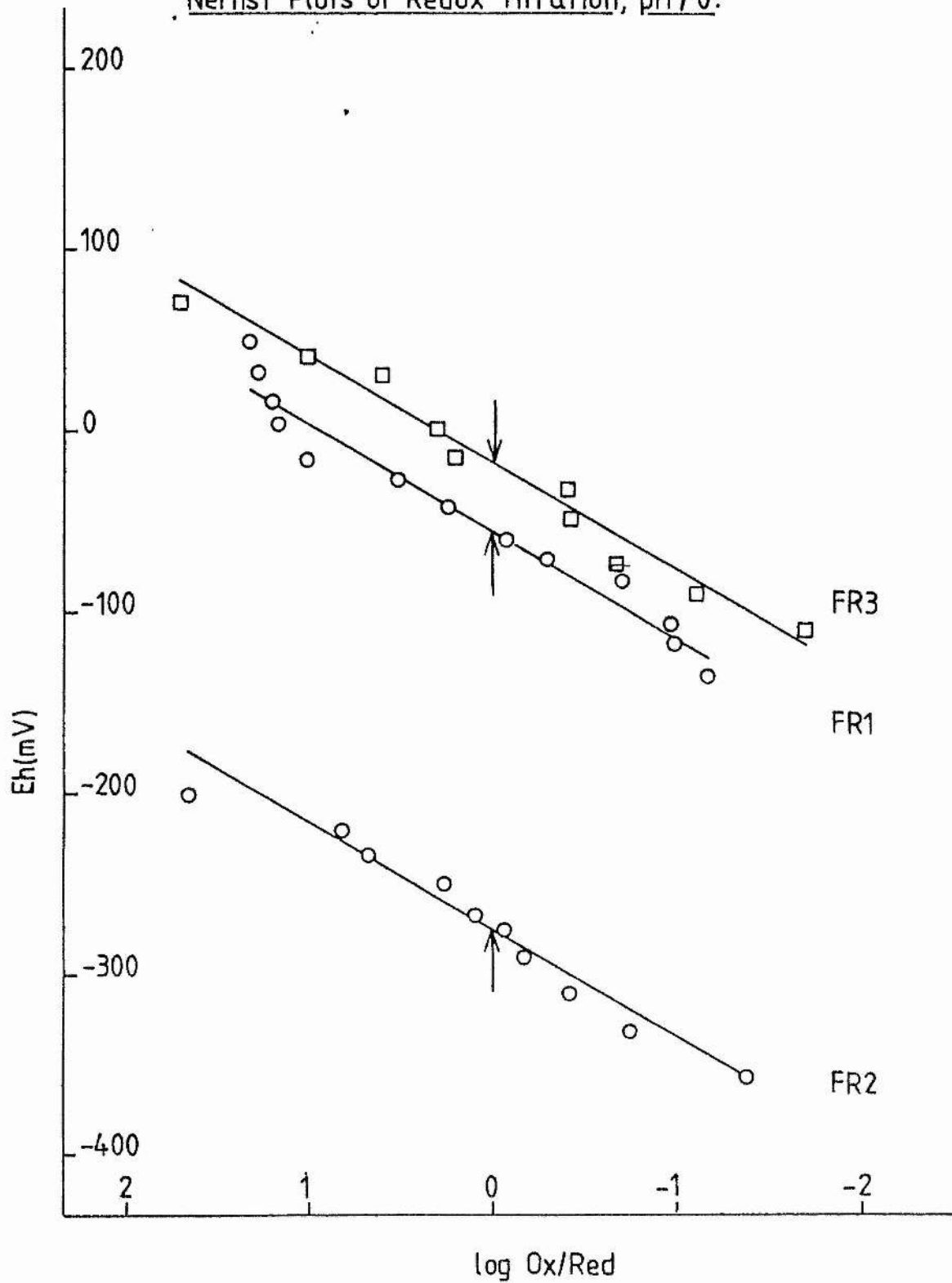


Figure 4.5

Nernst plots of the e.p.r. signals, pH 7.0

Nernst plots are shown using data points produced from computer analysis of the redox titrations as described in the text. Plots for the three major e.p.r. signals are shown: FR1, FR2 and FR3, indicated adjacent to the plots. The values of $\log \text{ox/red} = 0$ are indicated for each signal. $E_{m7.0}$ of -285mV (FR2), -55mV (FR1) and -20mV (FR3) were obtained from this plot. The values indicated in the text are the average values of three determinations.

Nernst Plots of Redox Titration, pH7.0.



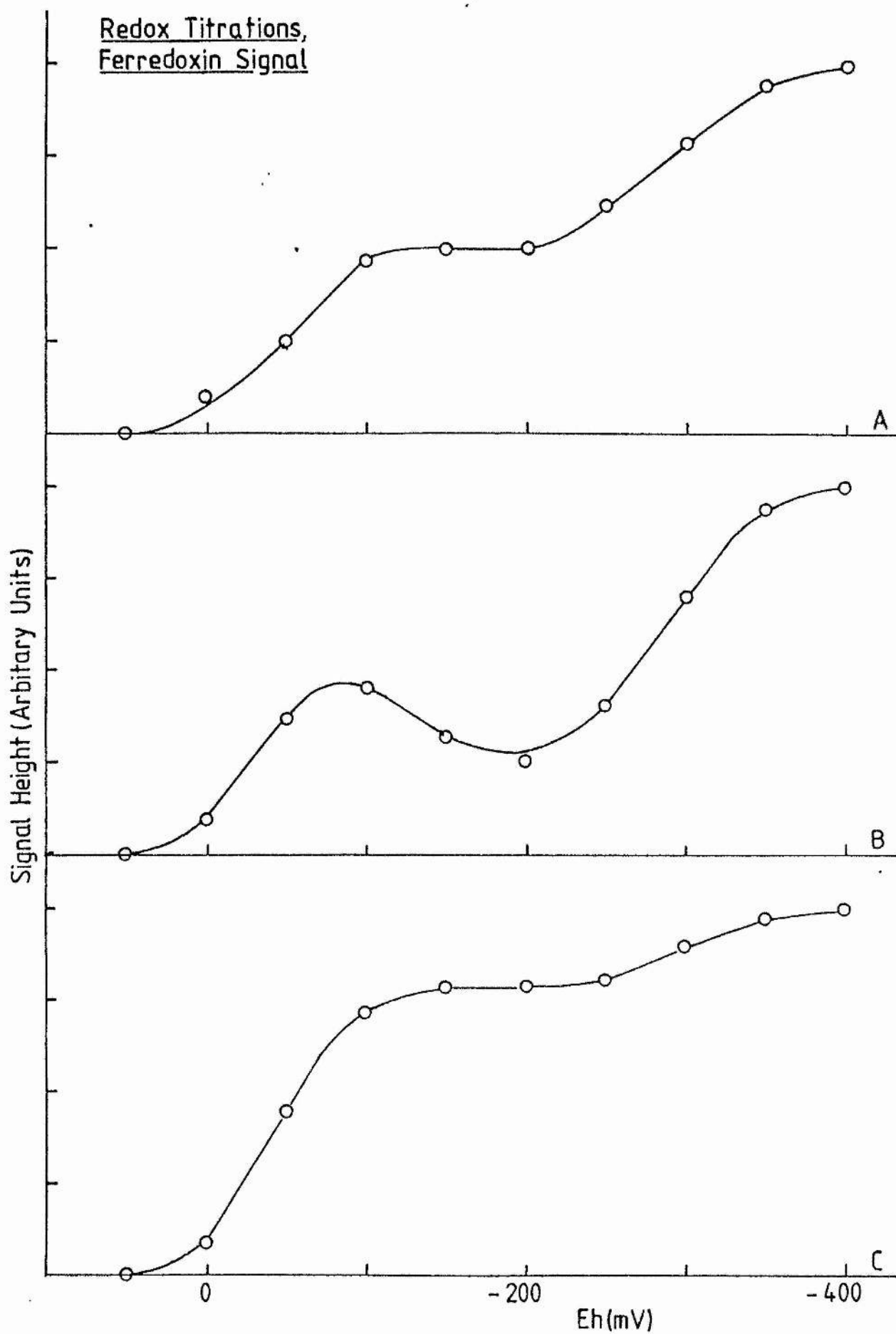
-50 ± 10 mV and -285 ± 10 mV at pH 7.0 and electrical equivalences of 1.0 as shown by Nernst plots (Fig.4.5). These values were pH-independent over the range 6.0 to 8.0 (not shown). Quantitation of the spectra (double integration, 50K and 2mW), at each electrode potential, showed that the plot of spin intensity against electrode potential was similar to the plot of signal height against electrode potential (Fig.4.4). This latter plot also confirmed that the two potentiometrically distinguishable centres were present in a 1:1 ratio. The higher potential species proved to be the succinate reducible species and is referred to as FR1 (fumarate reductase centre 1) and the lower potential species, (which is the same as the additional species reduced by dithionite) is referred to as FR2. When spectra of redox titration samples were run under conditions which cause saturation of FR1, the plots of signal height against electrode potential become more complex, as shown in Fig.4.6. On lowering the ambient electrode potential from a value at which no reduction occurs, the signal height initially increased until a potential of -70 mV was reached. Further lowering of the potential caused a decrease in signal height before it again increased at potentials below -200 mV. This effect on the titration was more pronounced with lowering of the temperature, until the region where the signal from FR1 was greatly attenuated. These changes were shown to be due to changes in the relaxation times across the electrode potential range (see later). When redox titrations were run under

Figure 4.6

Potentiometric titrations, ferredoxin signal

Redox titrations of the ferredoxin signal run under various conditions are shown. The signal height is shown plotted against the ambient electrode potential. The experimental conditions were as described for fig.4.1a, except: A), microwave power, 2mW; temperature, 50 K; receiver gain, 6.3×10^4 ; protein concentration, 35mg/ml. B), microwave power, 2mW; temperature, 12 K; receiver gain, 5.0×10^4 ; protein concentration, 35mg/ml. C), microwave power, 0.2mW; temperature, 50 K; receiver gain, 1.0×10^5 ; protein concentration, 43mg/ml.

Redox Titrations,
Ferredoxin Signal



conditions of low power and high temperature, the low-potential ferredoxin signal was not as large as under conditions described previously (Fig.4.6c). This indicated the rapid relaxation for this centre leading to loss of its e.p.r. signal under these conditions. This was also seen for the comparable centre (S2) from bovine-heart succinate dehydrogenase (Salerno et al. 1979b).

Redox titrations of the broad ferredoxin signal showed a single species and gave a mid-point potential of -260 ± 7 mV at pH 7.0 for this centre (not shown). The signal was again seen to be very broad and not as intense as those from the other iron-sulphur centres of fumarate reductase. The signals titration in the lower potential region may indicate that this centre is the cause of the interaction observed for FR1 at these low potentials.

4.2.4 Redox titrations of the HiPIP signal

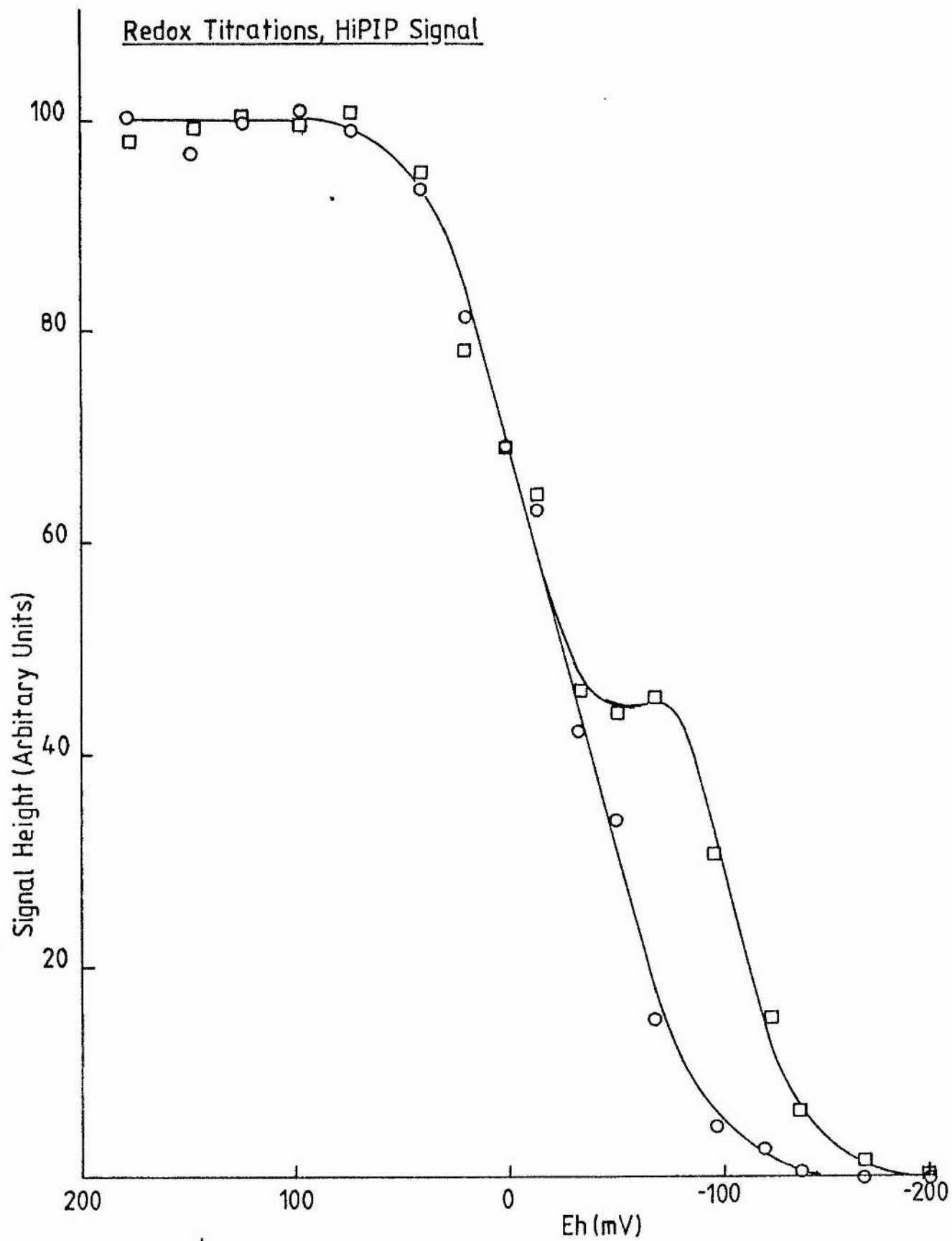
Potentiometric titration of the HiPIP centre gave a value of -30 ± 8 mV for its mid-point potential at pH 7.0, (Fig.4.5 & 4.7). This value was independent of pH over the range 6.0 to 8.0 (data not shown). The mid-point potential for this centre was lower than that reported for the similar centre in succinate dehydrogenases from mammalian, avian, and bacterial sources, including E. coli (+60 to +160 mV).

Figure 4.7

Potentiometric titration of the HiPIP signal

Redox titrations of the HiPIP signal are shown for non-saturating (O) and saturating conditions (□). The signal height is shown plotted against the ambient electrode potential of the sample. Experimental conditions were as described for fig.4.1a. The non-saturating conditions were 15 K and 2mW, the saturating conditions were 6 K and 20mW. The plots are normalised to give maximum signal height of 100%. A mid-point potential of -30mV (pH7.0) was obtained from the non-saturating plot. Protein concentration was 42mg/ml. The signal height of the HiPIP centre was corrected for interference from centre FR1.

Redox Titrations, HiPIP Signal



One possible reason for this difference is that the aforementioned respiratory systems were ubiquinone containing, whereas the current system contains menaquinone. The endogenous quinone is the most likely reductant/oxidant for the HiPIP centre (Ingledew *et al.* 1976, Salerno & Ohnishi 1980) and menaquinone has a more negative mid-point value than ubiquinone (-74 mV and +30 mV respectively at pH 7.0, Kroger, 1978). The HiPIP, in this case, functions as an oxidant of the menaquinone pool whereas in the aerobic system it functions as a reductant. One important facet of this difference in the mid-point potential of the HiPIP centre, is that it can remain substantially oxidized (and therefore paramagnetic) while the centre FR1 is substantially reduced (and therefore paramagnetic). The result of this was that interactions between HiPIP and FR1 could be studied in fumarate reductase, whereas in the other systems mentioned conditions cannot readily be obtained in which both centres were simultaneously paramagnetic. This interaction between centres FR1 and FR3 has also been reported for the isolated enzyme, as the increase in signal height of FR3 between -20mV and -70mV, under saturating conditions (Cammack *et al.* 1984).

When samples of the potentiometric titration were run under saturating conditions for the HiPIP centre (Fig.4.7.), there was again seen to be a 'hump', in the plot of signal height versus electrode potential. This 'hump' was again

centred at approx. -70 mV, indicating interaction with another redox component which titrates about this redox potential (see later).

4.2.5 Interactions and the e.p.r. spectral characteristics

Temperature profiles of the three signals (HiPIP, succinate and dithionite ferredoxins) at microwave power of 20mW, are shown in Fig.4.8. The difference in the profiles obtained for the succinate and dithionite reduced cases was notable; the succinate ferredoxin is readily saturated below 50 K, at this high power, while the dithionite reduced signal did not heavily saturate until approx. 16 K (microwave power 20 mW). The temperature profiles indicated that the succinate reducible centre, FR1, had a slower relaxation rate than when both ferredoxin centres were paramagnetic as in dithionite reduced membranes (FR1 + FR2). The HiPIP centre, in the fully oxidised sample, had a temperature profile which indicated that it had a fairly rapid relaxation time. It was, however not so rapid as the mammalian succinate dehydrogenase HiPIP, which is not readily observed above 15 K. This centre can be seen at upto 30 K. Power saturation profiles for the succinate reduced and dithionite reduced membranes are shown at different temperatures in Fig.4.9. Again it was seen that the signal from succinate reduced membranes (FR1) saturates more readily, than did the signal from dithionite reduced membranes (FR1 + FR2).

Figure 4.8

Temperature dependence of e.p.r. signals

The temperature dependence of the three major e.p.r. signals are shown by plotting the signal height against the inverse temperature. The signal height of the $g = 1.93$ signal for the dithionite reduced (O) and the succinate reduced (Δ) membranes are shown. The signal height for the $g = 2.01$ peak of the oxidised spectra is shown. The experimental conditions were as described for fig.4.1a and the protein concentration was 69mg/ml.

Temperature Dependence of
e.p.r. Signals:

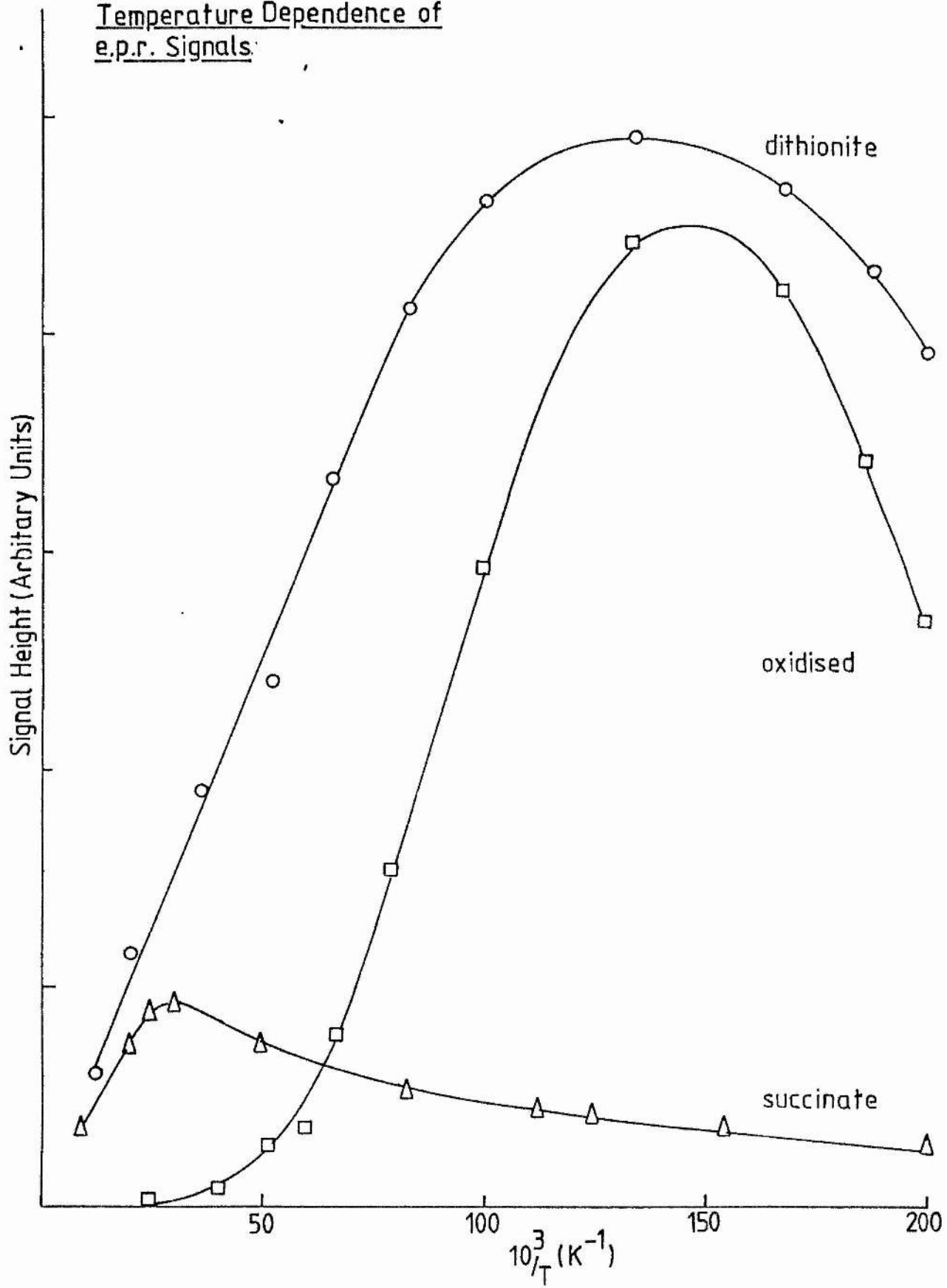
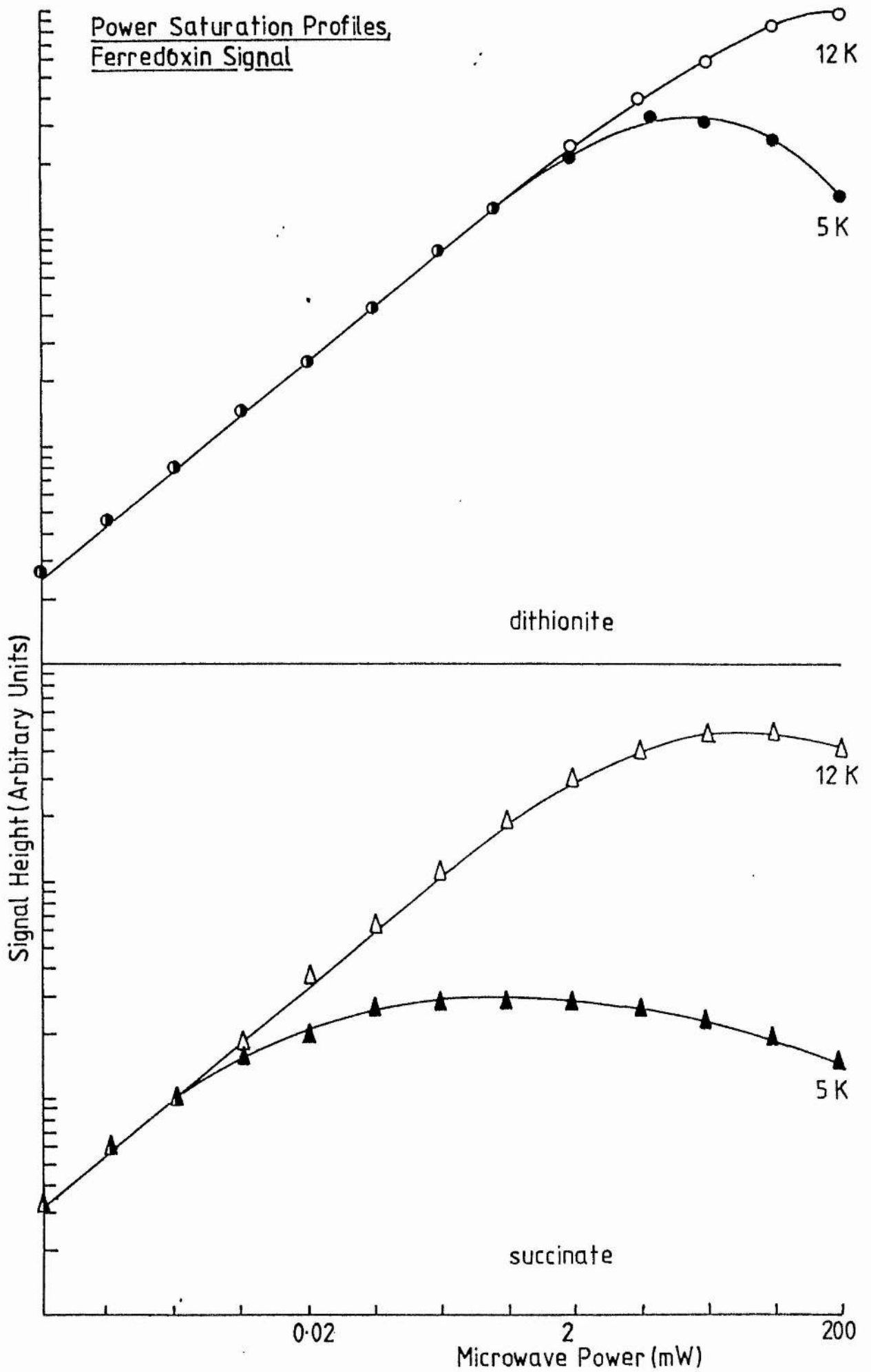


Figure 4.9

Power saturation profiles, ferredoxin signals

The power saturation profiles of the dithionite and succinate reduced ferredoxin signals are shown at two temperatures, to indicate their different saturation properties. The temperatures are indicated adjacent to the profiles. The log of signal height is shown plotted against the log of microwave power. The signal from succinate reduced membranes is seen to saturate more readily than that from dithionite reduced membranes. The experimental conditions were as described for fig.4.1a, except receiver gain was 5.0×10^4 and the protein concentration was 69mg/ml.

Power Saturation Profiles,
Ferredoxin Signal



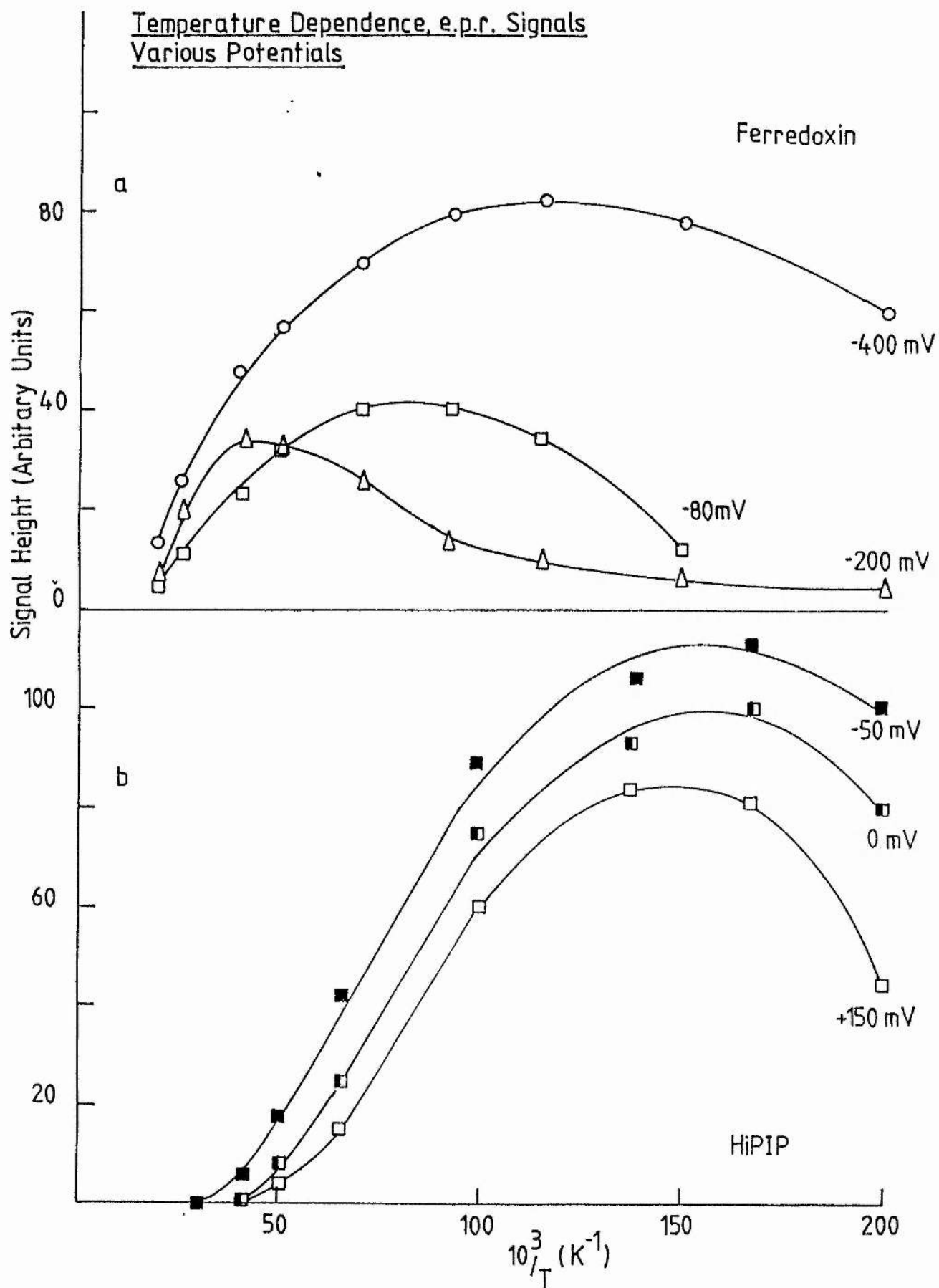
A comparison of the fully oxidised, succinate reduced, and dithionite reduced samples with samples poised at various redox potentials provides additional information (Fig.4.10a). The ferredoxin signal from a sample poised at low redox potential (< -400 mV), had approximately the same temperature profile as the dithionite reduced case. The ferredoxin signal from a sample poised at approx. -200 mV, behaved similarly to the succinate reduced sample. However, a sample poised at around -80 mV had a temperature dependence more akin to the dithionite reduced sample, i.e. it had a more rapid relaxation rate than the succinate reduced (or -200 mV poised) sample. A similar effect was seen to a lesser degree in the behaviour of the HiPIP centre (Fig.4.10b), as this species behaved similarly in the fully oxidised sample and the more positively poised redox titration samples ($> +100$ mV). However, when poised at approximately -50 mV the temperature profile, at lower temperatures, shows a greater signal height (the relaxation rate increases, Fig.4.10). Inclusion of some of FR1 gz in the signal height may contribute to the increase in signal height at these lower temperatures. These phenomena are related to changes in the saturation properties of the centre (characterised by $P_{1/2}$) and suggested an interaction between this species, which had its relaxation rate enhanced and a second species, the latter introducing a spin-lattice relaxation term (T_2). The most compelling proposal is that the HiPIP and FR1 were enhanced by interaction with each

Figure 4.10

Temperature dependence of e.p.r. signals from samples poised at various potentials

The temperature profiles of the e.p.r. signals from membranes poised at various potentials are shown. (a): the ferredoxin signal from various samples. The potential is shown adjacent to the profiles of signal height (peak to peak, $g = 1.93$) versus inverse temperature. (b): the HiPIP signal from various samples. the redox potential is shown adjacent to the profiles of the signal height (peak to baseline, $G = 2.01$) versus the inverse temperature. The experimental conditions were as described for fig.4.1a, except receiver gain was 1.0×10^5 (a) and 5.0×10^4 (b). the protein concentration was 42mg/ml.

Temperature Dependence, e.p.r. Signals
Various Potentials



other, with the introduction of a T_2 term to the other relaxation processes. It was only over the range of electrode potential in which these two centres were simultaneously paramagnetic that these effects occurred. The mid-point potential of menaquinone (-74 mV) or the possibility of the flavin titrating in this region (c.f. succinate dehydrogenase, Ohnishi *et al.* 1981), does not exclude the hypothesis that the effect on the redox titration under saturating conditions was caused by interaction with, or mediated by, one of these components. The flavin from fumarate reductase of *E. coli* had a mid-point potential ($Fl_{ox} \leftrightarrow FlH_2$ or FlH^-) of approx. -30 mV (pH 7.0, chapter 6), so this would appear to preclude this redox centre from causing the 'hump' (at -70 mV) in the FR1 redox titration. This moiety is heavily saturated under the conditions used, so it is unlikely that it could cause relaxation of another paramagnet, to the extent seen for FR1, by interaction.

Comparison of the temperature profiles of dithionite reduced, succinate reduced and the potentiometrically poised samples indicates that centre FR1 plus centre FR2 had a more rapid relaxation rate than centre FR1 on its own. When centre FR2 was paramagnetic so was centre FR1, thus if there was no interaction, centre FR1 should have contributed to the temperature and power profiles observed in low potential and dithionite reduced samples, producing a biphasic profile. This was not observed, in fact the ferredoxin species seen

behaved, in its temperature and power profiles (Fig.4.8 & 4.9) as a homogeneous species. An explanation for this observation would be that FR1 and FR2 also interact, and that this interaction resulted in both species having the same (enhanced) relaxation rate. Indeed, the relaxation rate of FR2 alone is unknown and we are unable to discern it in this present study (see chapter 5 & 8).

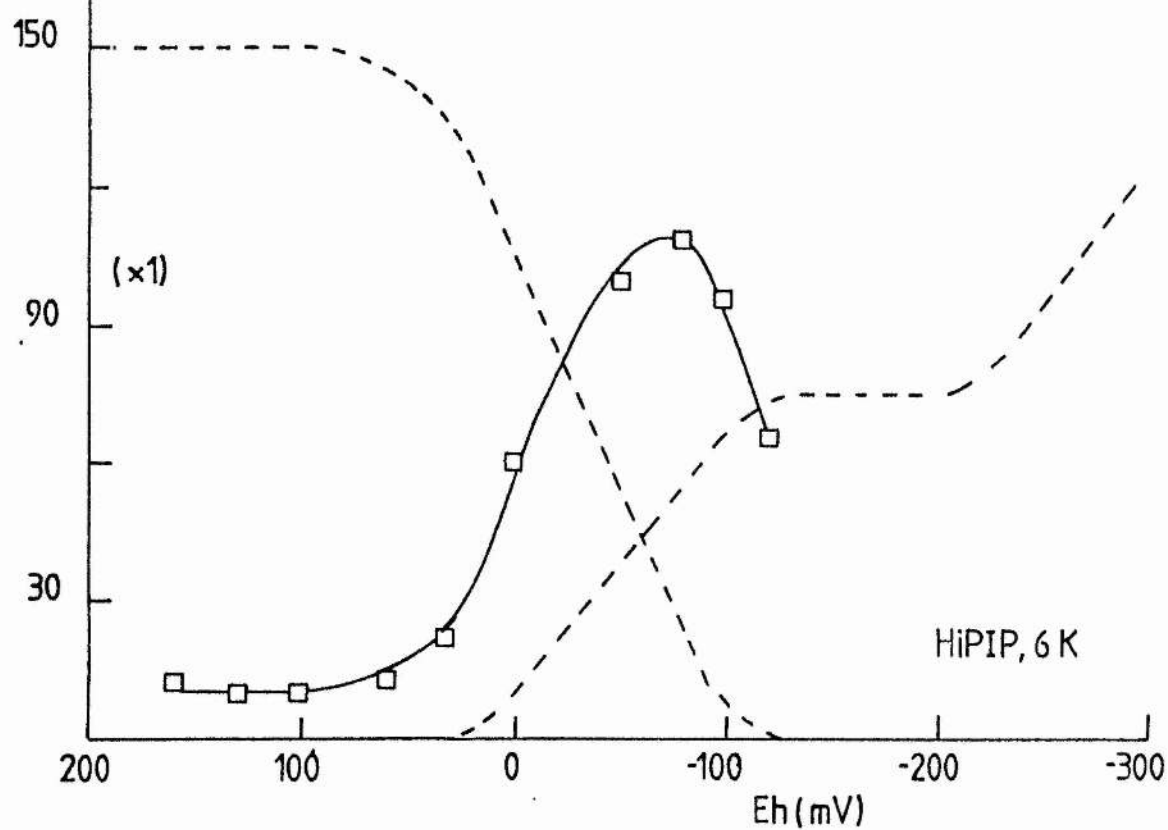
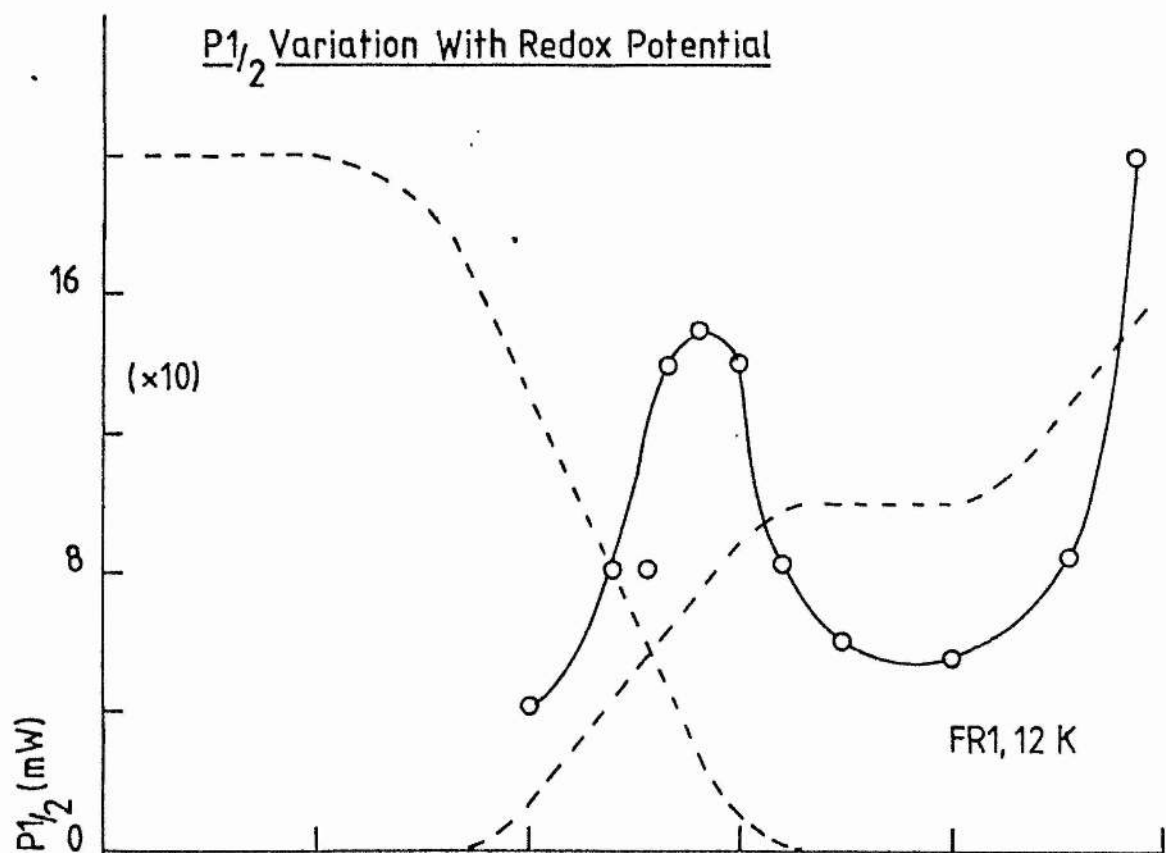
The parameter $P_{1/2}$ was measured for the ferredoxin signal and for the HiPIP signal throughout the redox potential range (Fig.4.7). $P_{1/2}$, the microwave power at which the condition $\gamma^2 T_1 T_2 H_{1/2}^2 = 1$ is met (γ is the magneto-gyric ratio and T_1 and T_2 are the spin-lattice and spin-spin relaxation times), is proportional to $H_{1/2}^2$ (the microwave magnetic field necessary to saturate a spin packet, Blum *et al.*, 1983). $P_{1/2}$ is thus proportional to $1/T_1 T_2$ and is characteristic of the relaxation processes under saturating conditions. In the absence of any spin-spin interactions $T_1 = T_2$, so a change in these parameters or the introduction of a T_2 process will be reflected as a change in $P_{1/2}$. From Fig.4.11, a correlation between the $P_{1/2}$ values, with the titrations of the centres and the 'hump' in the HiPIP and ferredoxin redox titration under saturating conditions, could be derived. This gives strong evidence for the interaction between FR1 and the HiPIP, and FR1 with FR2. The observation of small half-field signals ($\Delta m_s = 2$) should be possible for interacting species. A signal of this type was seen in dithionite reduced membranes ($g = 3.88$) and in samples poised at redox potentials, where

Figure 4.11

Variation of P1/2 with redox potential

Plots of P1/2 are shown versus the ambient electrode potential of the samples, for the ferredoxin and HiPIP signals. P1/2 was measured from power profiles and had the conditions described in the text. Top: P1/2 for the ferredoxin signal, temperature 12 K. Bottom: P1/2 for the HiPIP signal, temperature 6 K. The redox titrations of the signal heights of the ferredoxin and HiPIP signals (non-saturating conditions) are shown as the dashed lines. The experimental conditions were as described for fig.4.1a, except receiver gain was 1.0×10^5 and the protein concentration was 36mg/ml.

$P_{1/2}$ Variation With Redox Potential



both FR1 and the HiPIP were paramagnetic ($g = 3.88$ & 4.02 , chapter 8).

4.2.6 Relaxation of the ferredoxin signals

The relaxation of the broad ferredoxin centre was investigated because of its mid-point potential, which put it in the potentiometric region of FR2. A temperature profile is shown in Fig.4.12a, which indicates that this centre was also rapidly relaxing, only being detectable below 30 K. Power profiles (Fig.4.12b) also indicated the rapid relaxation of this centre. However, its low spin quantitation values would seem to exclude this centre from being an integral part of fumarate reductase, as does the non-haem iron and acid-labile sulphur determinations. The most plausible explanation for this centre, on the evidence to date, would be that it was the result of a centre conversion from the HiPIP cluster. If the HiPIP centre was of the 3Fe-type, as was the comparable centre from bovine-heart succinate dehydrogenase (Johnson *et al.* 1985), then the conversion of some of this centre to a 4Fe centre is possible, as the ease of conversion of 3Fe to 4 Fe centres has been shown (Kent *et al.* 1982, Thomson *et al.* 1981).

The behaviour of FR2 was further investigated by determining the spin quantitation of FR1 and FR2 over a range of temperatures (fig.4.13). Fig.4.13 shows the temperature dependence of the spin intensity at 2 mW. FR1 shows approximately 1.0 spins/flavin at temperatures below 50 K, and above this temperature the spin intensity decreases due to lifetime broadening. FR1 + FR2 shows approximately 2.0 spins/flavin at temperatures below 30 K, but rapidly decreases to the level of FR1 alone above this temperature. This again indicates the rapid relaxation of FR2 and the loss of its e.p.r. signal at higher temperatures, as was shown in the redox data. At 80 K only FR1 spins could be detected. This behaviour was again similar to that seen for this centre in bovine-heart succinate dehydrogenase (Ohnishi 1979).

Figure 4.12

Saturation of the broad signal

a) A temperature profile of the broad ferredoxin signal is shown by a plot of signal height against inverse temperature. b) Power profiles of the broad ferredoxin signal; log signal height is shown plotted against log incident microwave power. The temperatures are indicated adjacent to the curves. Experimental conditions were as described for fig.4.1a except the microwave power was 20mW for the temperature profile and the receiver gain was 5.0×10^5 . Protein concentration was 98mg/ml.

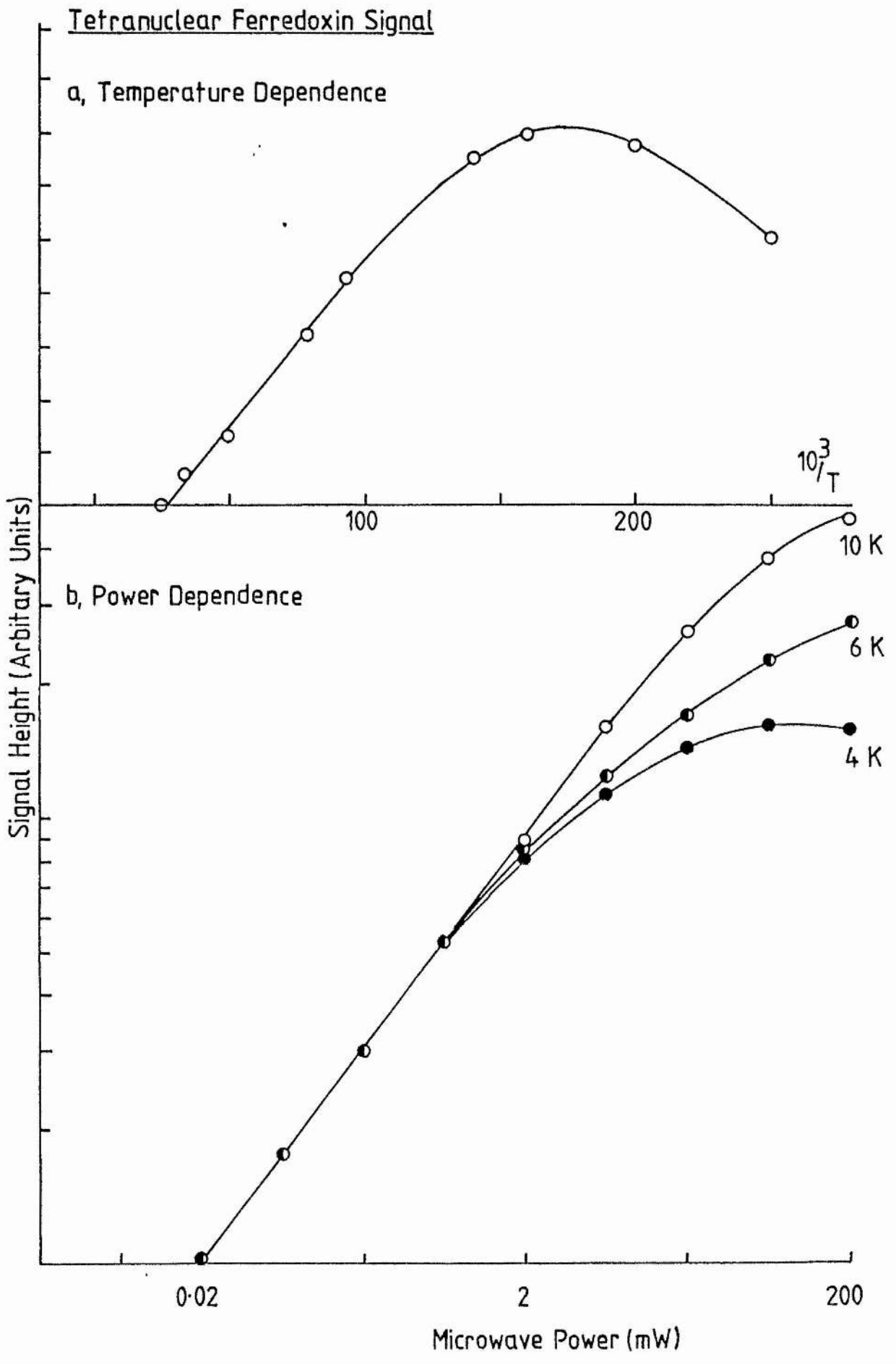
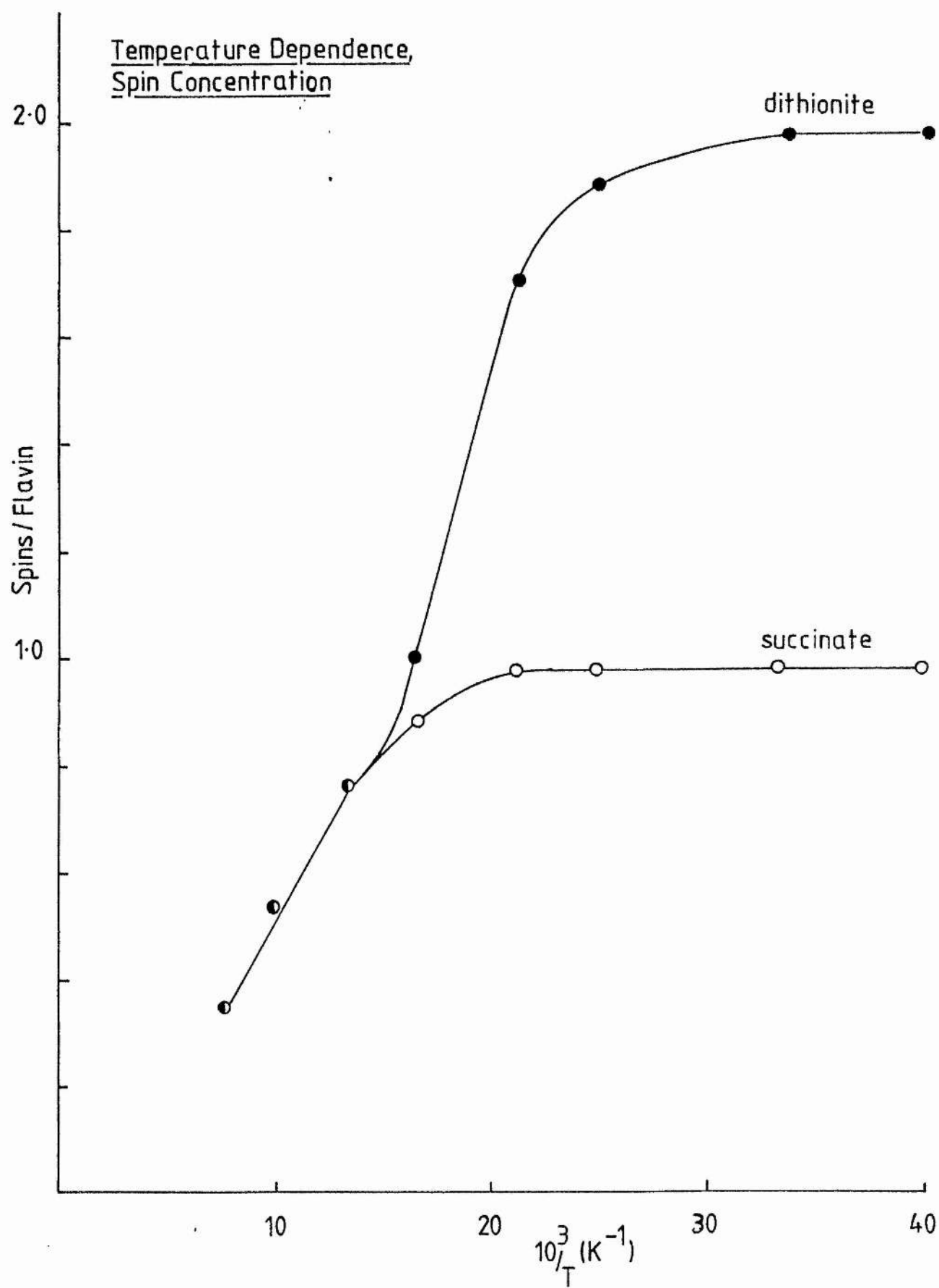


Figure 4.13

Temperature dependence of the spin concentration for the ferredoxin signal

The spin concentrations of dithionite reduced (closed symbols) and succinate reduced (open symbols) are shown plotted against the inverse temperature. Spin concentrations are expressed as spins/flavin, and were determined as described in the text. Experimental conditions were as described for fig.4.1a, except receiver gain which varied for each spin quantitation. Protein concentration was 69mg/ml. and microwave power was 2 mW.



4.3 Conclusion

The spectra obtained from samples of the JRG1031 membranes clearly showed three classes of iron-sulphur centre: a HiPIP cluster, 'binuclear' ferredoxin clusters and a 'tetranuclear' ferredoxin. Power and temperature profiles of the HiPIP signal, from oxidised membranes and samples poised at high redox potentials indicated a single homogeneous species, and this indication was strengthened by the potentiometric analysis resolving only a single component and the quantitation of the signal giving a ratio of HiPIP : flavin of 1 : 1. The ferredoxin-like signals appeared to be the result of more than one species. The combined results of the redox potentiometry, the quantitation studies on the succinate elicited spectrum and the dithionite elicited spectrum, showed that two distinct binuclear ferredoxin centres were present and in a 1 : 1 ratio. Also comparison of the iron-sulphur centre concentrations to that of the flavin, gave a 1 : 1 ratio for each of the centres of fumarate reductase. Albracht (1980), studying mitochondrial succinate dehydrogenase, suggested that the increase in signal intensity observed when some preparations of the enzyme were reduced by dithionite (c.f. succinate reduced), was an artifact produced by solubilisation of the enzyme. He suggested, that in the

isolated enzyme, the increase in signal intensity resulted from an increase in relaxation rate. This change resulted from a conformational change, which in turn resulted from the reduction of an unknown, and undetectable, component. However, this current study was performed on the membrane bound enzyme, so preparation artifacts of the type suggested by Albracht are less likely. The quantitations of the high and low potential ferredoxin signals clearly indicated the presence of two centres, although it was apparent from changes in saturation behaviour (power and temperature profiles), that the lower potential species had a more rapid relaxation rate than the high potential species. The relaxation of the high potential species was enhanced when the lower potential species became paramagnetic (reduced).

The 'tetranuclear' ferredoxin centre was shown to be present at only 1/10th the concentration of the other iron-sulphur centres and the flavin. This centre was shown to be rapidly relaxing and to have a mid-point potential (pH 7.0) of -260 mV. It is unlikely that this centre is responsible for the changes in behaviour of FR1 at low potentials, because of its low spin concentration. The tetranuclear centre would be expected to interact with only part of the FR1 population, however, at low potentials, all the FR1 population changed to a faster relaxing species, as was shown by the homogeneous saturation profiles. Thus FR1 must have been interacting with another species present at the same concentration as itself, assuming isolation of the enzyme moieties. The possibility

cannot be excluded that the 'tetranuclear' centre is not fully detectable by e.p.r., i.e. that the first excited state ($S = 3/2$) of this centre is such, that it is significantly populated under the conditions used. The HiPIP centre from bovine-heart succinate dehydrogenase has been shown to be a [3Fe-3S] centre, so it would seem likely that this centre in fumarate reductase is also of this type. The most compelling conclusion for the origin of the 'tetranuclear' ferredoxin cluster, is that it was the result of a modification of the [3Fe-3S] cluster to a [4Fe-4S] cluster upon reduction by dithionite. This had been shown to occur easily for the [3Fe-3S] cluster from aconitase (Kent *et al.* 1982) and also cluster conversion of the ferredoxins from Clostridium pasteurianum to [3Fe-3S] clusters by oxidation, has been shown (Thomson *et al.* 1981).

The succinate reducible species could be studied independently of the dithionite reducible FR2. It had a mid-point potential of -50 mV (pH 7.0) and a relatively slow spin-lattice relaxation rate. The nett relaxation rate of the centre appeared to be subject to increase by two mechanisms: interaction with the HiPIP centre, and interaction with centre FR2. Both of these interactions would introduce a spin-spin relaxation process.

Centre FR2 was present at the same concentration as centre FR1 and HiPIP, but it could not be studied in isolation, as when it is reduced, and paramagnetic, so is FR1. The centre had a mid-point potential of -285 mV. The situation was further complicated by the fact that the properties of FR1 were changed by the reduction of FR2. Temperature and power profiles of succinate and dithionite elicited spectra showed that the relaxation time of centre FR1 was enhanced on reduction of FR2. The individual profile of FR1 could not be removed from the profiles of dithionite reduced membranes to leave a sensible profile for FR2. In fact when both FR1 and FR2 were reduced, the product, although being double the concentration of FR1, behaved as a homogeneous species, as shown by its power profiles. Thus the reduction of FR2 to its paramagnetic state caused an enhancement of the relaxation time of centre FR1, to an extent that brought the overall relaxation times for the two species close together. This can perhaps best be illustrated by the observation that under conditions which heavily saturated FR1 alone, no saturation of FR2 plus FR1 was observed. It is expected that this effect was mutual to both ferredoxins with the relaxation time of FR2 being enhanced by interaction with FR1. The centres may then have had similar relaxation times in the absence of interaction.

The HiPIP centre was present in approximately equal concentrations to the two ferredoxin centres and it had a mid-point potential of -30 mV. This centre was involved in one interaction, the result of which was to enhance its relaxation rate. The evidence available points to the partner in this interaction being centre FR1.

Thus it has been shown that the fumarate reductase from *E. coli* contains three intrinsic iron-sulphur centres, as has been suggested for some of the other succinate-fumarate oxido-reductases (bovine heart succinate dehydrogenase). It has been shown that the *E. coli* fumarate reductase is unlike that from *Wolinella succinogenes* which does not contain the second ferredoxin centre, but does contain a tightly bound cytochrome *b* moiety (Albracht *et al.* 1981, Uden *et al.* 1984). Studies on the isolated fumarate reductase and succinate dehydrogenase from *E. coli*, have shown that the three major iron-sulphur clusters are all present in both of these enzymes. The redox properties of the iron-sulphur clusters, from the isolated fumarate reductase, are similar to those of the membrane bound form, whilst those of the succinate dehydrogenase have different mid-point potentials (10, -175 & 65 mV respectively, Cammack *et al.* 1984, Condon *et al.* 1985).

CHAPTER FIVE

Intrinsic Spin-lattice Relaxation of the Iron-Sulphur Centres
and the Effects of dysprosium(III).

5.1 Introduction

The iron-sulphur centres of the Escherichia coli respiratory fumarate reductase have been resolved in the previous chapter (chapter 4). In this chapter the results of investigations into the spin-lattice relaxation mechanisms of these iron-sulphur centres as affected by temperature and the rare earth ion dysprosium(III) are reported. Their membrane location with respect to sidedness and their distances from the membrane and protein surfaces were investigated and are discussed in relation to the structure of the enzyme.

Iron-sulphur centres from other sources, both binuclear and tetranuclear, have been shown to have well defined intrinsic relaxation mechanisms (Blum et al. 1979, 1981, 1983, Gayda et al. 1976, 1979, Salerno et al. 1977). Three important mechanisms have been shown to dominate: at low temperatures a T^2 temperature dependence characteristic of a phonon bottleneck process; above this region, in the intermediate temperature range, a second order Raman process becomes dominant, this is superseded by a Resonant Raman (Orbach) process at higher temperatures (Gayda et al. 1976, Blum et al., 1983). The latter process is characterised by the antiferromagnetic exchange coupling constant (J) among the high-spin iron atoms (Blum et al. 1979, 1983, Gayda et al. 1976, Salerno et al. 1977). The value of the coupling constant dictates the temperature at which this very fast relaxation phase becomes dominant and hence the temperature

range over which the centre is e.p.r. detectable.

On addition of dysprosium(III) the spin-lattice relaxation time (T_1) is enhanced by dipolar interaction between the dysprosium(III) and the iron-sulphur cluster. Recently the use of dysprosium(III) and other paramagnetic transition metal ions, as distance probes, has been developed by Hyde & Rao (Hyde & Rao 1978, Antholine et al. 1978) and Blum et al. (1981,1983) based on the earlier work of Case and co-workers (Case & Leigh 1976, Case et al. 1976). The use of dysprosium(III)-EDTA in particular has been developed because of its specific binding to carboxylate groups on the protein surface. Its rapid relaxation and large magnetic dipole result in large perturbations in the e.p.r. behaviour of the intrinsic spectra (ΔH and $P_{1/2}$ changes). These effects are quantifiable and the weighted averaged distance ($\langle r \rangle$) can be calculated either in membrane bound or isolated proteins, giving information on the position of the redox centres within the membrane or protein (Blum et al. 1981,1983, Case & Leigh 1976, Case et al. 1976a & b, Ohnishi et al. 1982).

5.2 Results & discussion

5.2.1 The e.p.r. relaxation processes of the ferredoxin centres

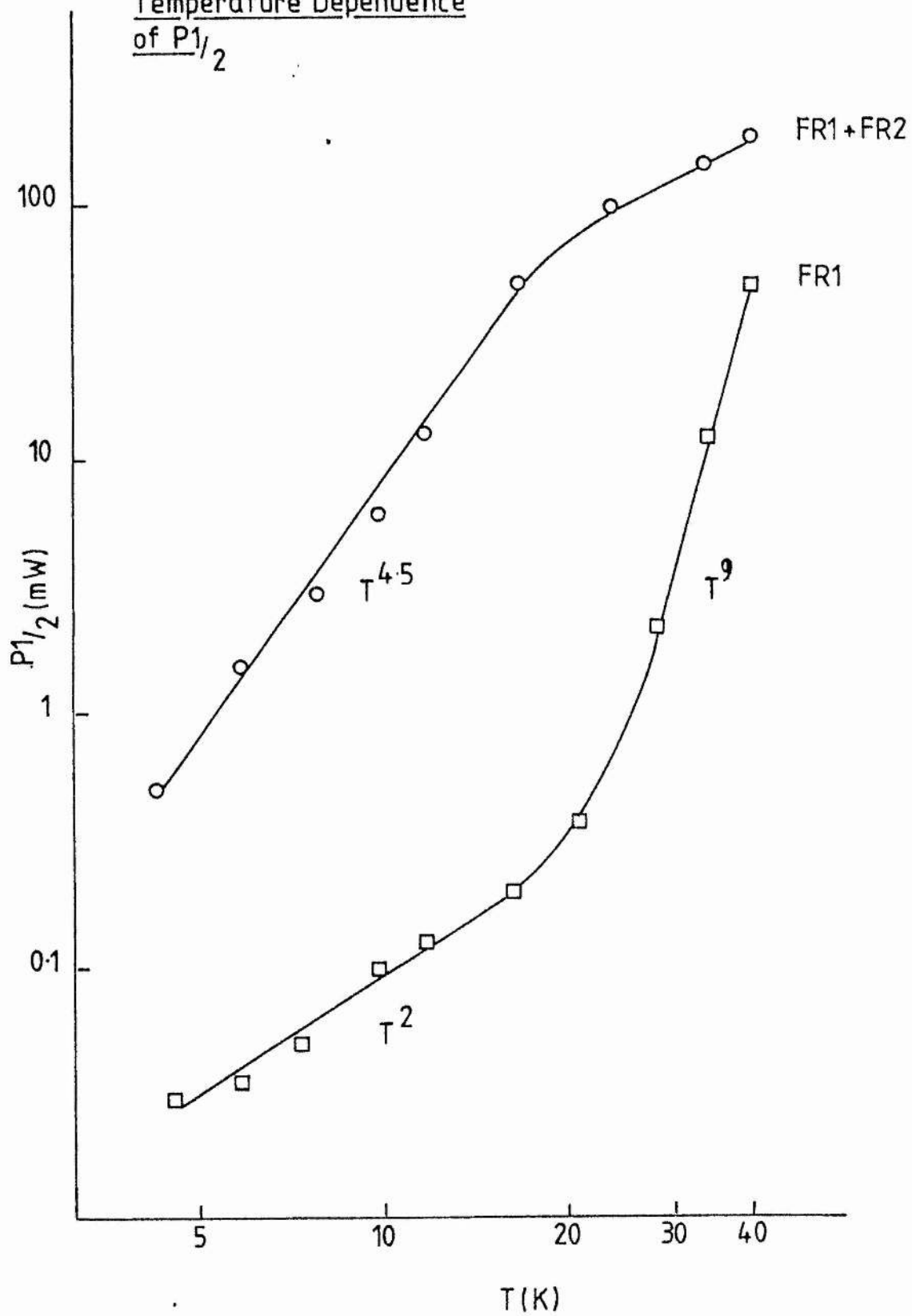
The e.p.r. spectra of the two major ferredoxins of fumarate reductase have been shown to be characterised by $g_z = 2.03$ and $g_{xy} = 1.93$ (chapter 4), one centre reducible by succinate and dithionite and the other only by dithionite. A HiPIP centre characterised by a narrow signal at $g = 2.01$ was also shown to be present. Dipolar interactions between the two ferredoxin centres and the succinate reducible centre (FR1) and the HiPIP centre (FR3), were proposed by the change in relaxation behaviour observed when two centres were paramagnetic. The enhancement of relaxation was seen as a relief of the power saturation of the centres, and was assumed to arise from the introduction of spin-spin interaction between the two centres. Interaction between paramagnetic centres results in changes in the relaxation properties of the centres by the introduction of a spin-spin relaxation time, T_2 , so it is important to know to what extent the reduction of centre FR2 (to a paramagnetic state) affects the saturation behaviour of centre FR1. The dependence of $P_{1/2}$ (defined in chapter 4), of the ferredoxin signal, on temperature is characteristic of the relaxation processes, under saturating conditions. The $P_{1/2}$ dependence on temperature, for the ferredoxin signal is shown in Fig.5.1. The two reduced

Figure 5.1.

Temperature dependence of P1/2 for the ferredoxin signal from succinate and dithionite reduced membranes

P1/2 was determined from power saturation plots and has the conditions described in the text. The log of P1/2 (mW) is shown versus the log of the temperature (K). The data obtained from succinate reduced membranes (FR1, \square) and dithionite reduced membranes (FR1 + FR2, \circ) are shown. The temperature dependencies of P1/2 are indicated adjacent to the straight-line portions of each curve. Experimental conditions were as described for fig.5.9.

Temperature Dependence
of $P_{1/2}$



states (FR1 alone and FR1 + FR2) differed markedly in their behaviour at lower temperatures: FR1 showed a T^9 dependency of $P_{1/2}$, characteristic of a second order Raman process, between 25 K to 40 K, and a T^2 dependency characteristic of a direct relaxation process (Gayda et al. 1976) below 17 K. The curve for FR1 plus FR2, however, showed a $T^{4.5}$ dependency, below 17 K, which cannot be related to any previously reported, well characterised relaxation process. This difference in the temperature dependency of $P_{1/2}$ showed that the relaxation processes differed for FR1 alone, from those of FR1 plus FR2. FR2 had an effect on the power saturation of FR1 and FR1 plus FR2 behaved as a homogeneous species.

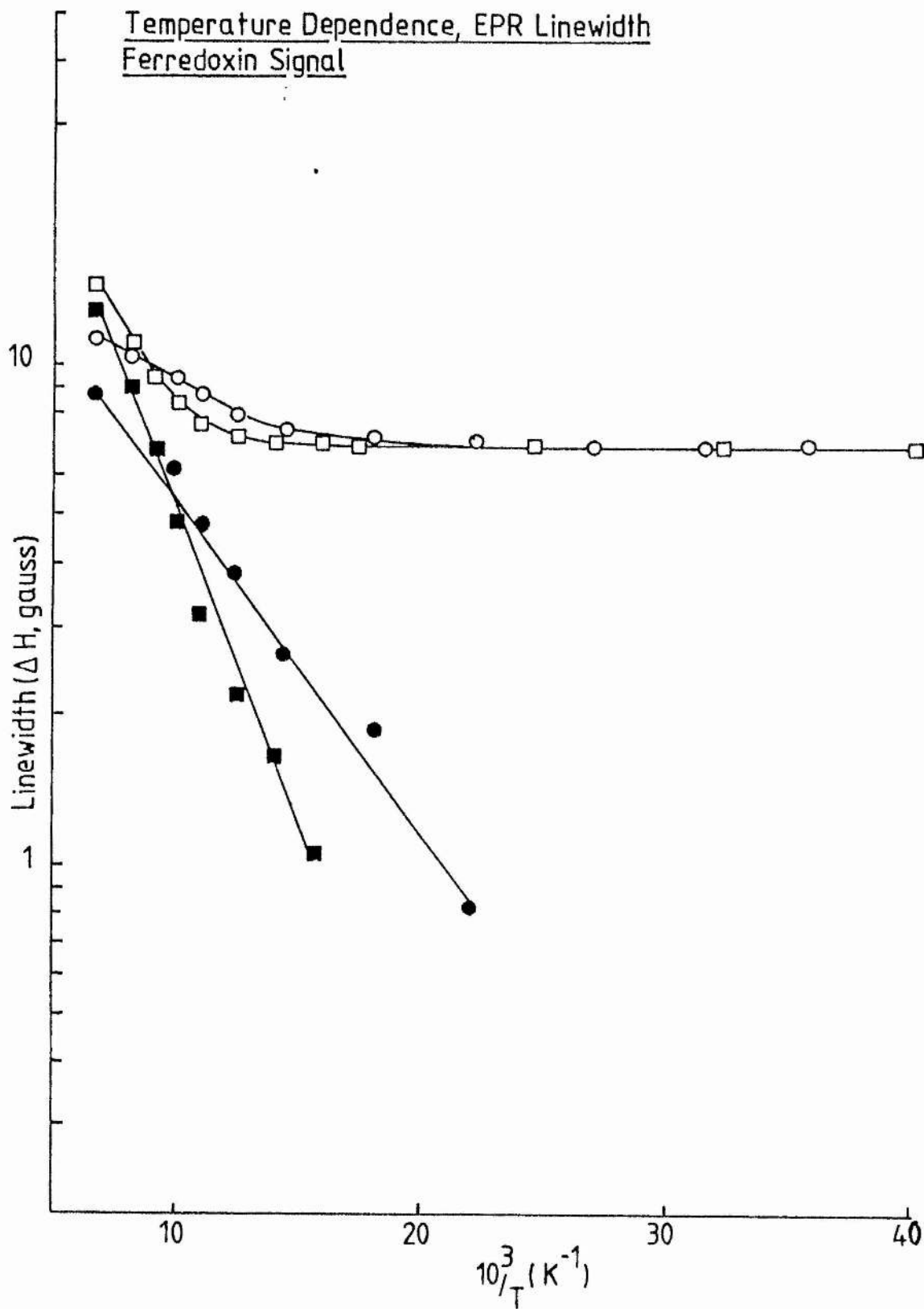
At higher temperatures the linewidth (ΔH) can be used to study the relaxation processes. A plot of linewidth (peak to peak for g_y) versus reciprocal temperature is shown in Fig.5.2. For both FR1 and FR1 plus FR2, two regions were seen: a temperature independent region and a region where ΔH was directly proportional to $\exp(\Delta/kT)$. It was seen that for FR1 plus FR2 the slope of this region was less than that of the corresponding phase for FR1 alone, again showing the enhancement of the relaxation when both ferredoxins were paramagnetic. The temperature independent regions are approximately the same for the two reduced states. This is to be expected, because the temperature independent region of the linewidth reflects the Gaussian distribution of the centres within the samples, and also corresponds to the ground states

Figure 5.2.

Temperature dependence of linewidths for succinate and dithionite reduced membranes

The linewidth (ΔH_T , peak to peak gy, open symbols) and the Lorentzian linewidth (ΔH_L , closed symbols) are shown plotted against the inverse temperature, for both succinate reduced (\square, \blacksquare) and dithionite reduced (\circ, \bullet) membranes. The Lorentzian linewidth was extracted from the total linewidth as described in the text. From the slope of ΔH_L (FR1) $J = 64.6$ and from the slope of ΔH_L (FR1 + FR2) $J = 34.9 \text{ cm}^{-1}$ respectively, as described in the text. Experimental conditions were as described for fig.5.9.

Temperature Dependence, EPR Linewidth
Ferredoxin Signal



($S=1/2$, $kT \ll 3J$) from which the e.p.r. signal arises (e.p.r. spectra were similar at lower temperatures). As the temperature is raised ($kT \geq 3J$) then the first excited state ($S=3/2$) begins to be significantly populated. $S=3/2$ is not e.p.r. detectable so we are measuring the loss of the e.p.r. signal (S is the total spin number for the e.p.r. centre, Salerno *et al.* 1977b). J is the exchange integral between the two energy levels and is related to the spin-lattice relaxation time by the following expression:

$$1/T_1 = C \exp^{-3J/kT} \quad (\text{for } \exp^{-3J/kT} \gg 1)$$

where C is a constant and k is the Boltzmann constant. The linewidth is related to the spin-lattice relaxation time by the following expression (Bertrand *et al.* 1980):

$$1/T_1 = g^\beta \Delta H_L / M$$

where β and M are constants and ΔH_L is the Lorentzian linewidth. In the temperature region under study T_2 is typically taken to be constant for a single paramagnetic species, so $T_1 = T_2$. The slope of a plot of $\log(1/T_1)$ or $\log \Delta H_L$ versus $1/T$ will thus be equal to $-1.3J$. The Lorentzian linewidth is obtained from the total linewidth by subtracting the linewidth of the temperature independent region ($\Delta H_T^2 = \Delta H_L^2 + \Delta H_{LT}^2$, Salerno *et al.* 1977), where ΔH_T is the total linewidth, ΔH_L is the Lorentzian linewidth and ΔH_{LT} is

the linewidth of the temperature independent region. This is shown in Fig.5.2. as the solid symbols. J was obtained from the slope of this plot ($\Delta = -1.3J/k$). For FR1 alone it was found that $J = 64.6 \pm 5 \text{ cm}^{-1}$ and for FR1 plus FR2, $J = 34.9 \pm 3 \text{ cm}^{-1}$. Thus FR1 plus FR2 will show faster relaxation than FR1 alone in this temperature region. This is again indicative of interaction between the two ferredoxin centres, causing this faster relaxation. Below 25 K the linewidths, in both cases, were again seen to increase (not shown), but this region is due to saturation phenomena causing depopulation of the ground state. The exchange integral can also be determined from studies of the integrated intensity of the e.p.r. signal, because this deviates from the simple Curie law temperature dependence, as the e.p.r. detectable state ($S = 1/2$) becomes depopulated (Blum *et al.* 1979, 1981). Fig.5.3. shows the data for FR1 plotted in this manner. The slope is again used to obtain the exchange integral, and the intercept can be used to obtain the multiplicity of the excited state relative to the ground state. From this method J was calculated to be $62.7 \pm 3 \text{ cm}^{-1}$ which is in good agreement with the value from linewidth studies.

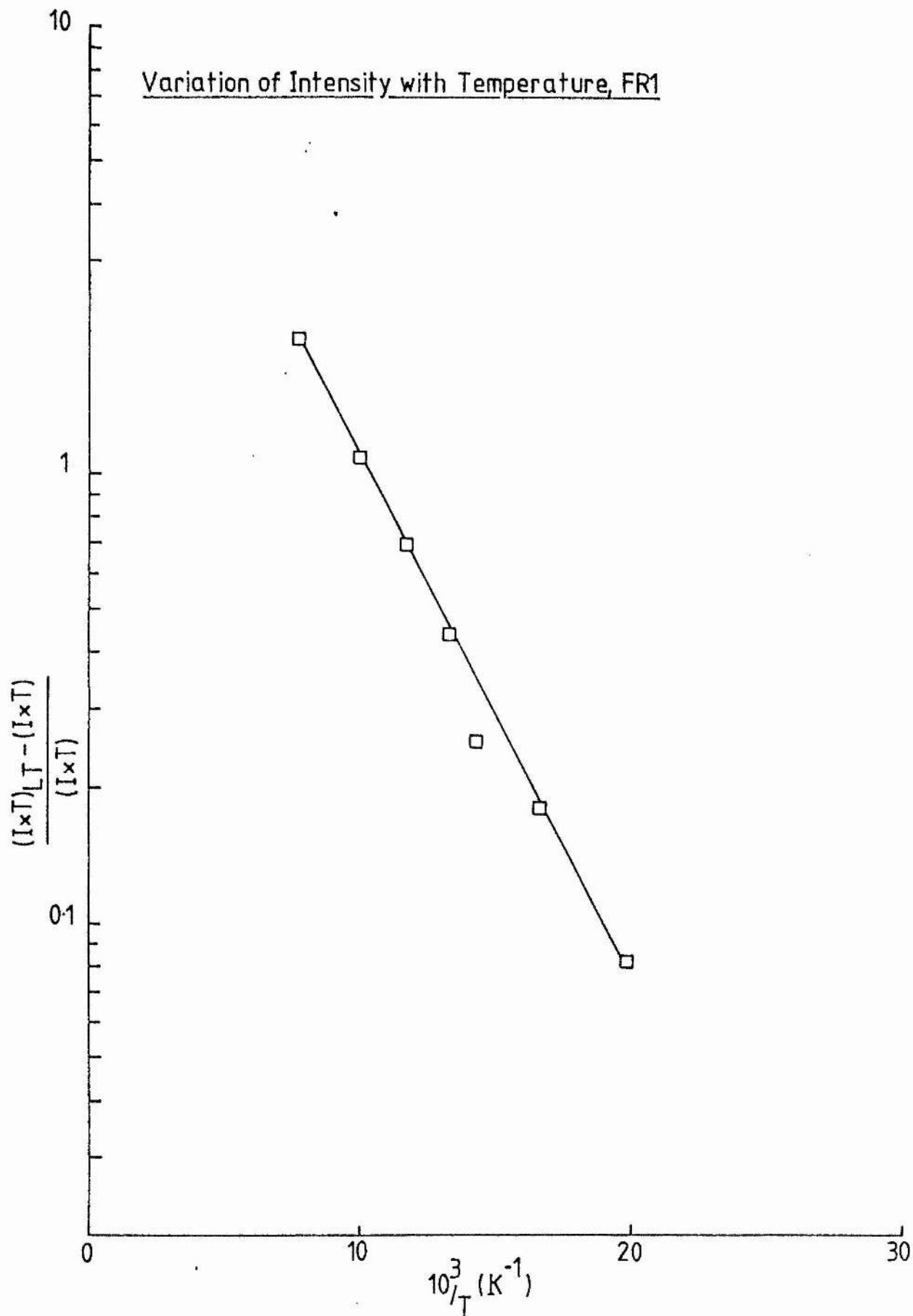
The exchange integral for FR1 of approximately 65 cm^{-1} is a reflection of the rhombicity ($g_y - g_x$) of the e.p.r. spectra obtained (Salerno *et al.* 1977, Bertrand & Gayda 1979). The spectra of FR1 alone does indeed show rhombicity over the temperature range in which the Orbach-type of relaxation mechanism is dominant, with less rhombic distortion

Figure 5.3.

Variation of intensity with temperature for succinate reduced membranes

The integrated absorption, multiplied by the temperature ($I \times T$) is plotted against the inverse temperature, after correcting for the low temperature intensity factor $(I \times T)_{LT}$, to indicate the deviation from Curie's law. From the slope $J = 62.7 \text{ cm}^{-1}$. From the intercept the multiplicity, of the ground state relative to the first excited state = 11. The experimental conditions were as described for fig.5.9.

Variation of Intensity with Temperature, FR1



as the temperature is lowered. The lower value of J for FR1 plus FR2 predicts greater rhombic distortion than for FR1 alone. However, the exchange integral also reflects changes in the environment of the iron-sulphur centres, so as the spectra were not from a single species, the value of J may reflect spin-spin interaction between FR1 and FR2; a value of J_{int} can be calculated at approximately 0.5cm^{-1} if the relaxation mechanisms are assumed to be additive (Salerno *et al.* 1977). For FR1 the spin-lattice relaxation can be summarised by the following expression:

$$1/T_1 = AT^2 + BT^9 + C\exp(\Delta/kT)$$

where each term will become dominant in turn as the temperature is raised. For FR1 plus FR2 the relaxation process can be summarised:

$$1/T_1 T_2 = B'T^{4.5} + C'\exp(\Delta'/kT)$$

where again, each term will be dominant over a given temperature range, with both spin-spin and spin-lattice relaxation processes contributing to each term.

5.2.2 The relaxation processes of the HiPIP centre

The saturation behaviour of the HiPIP centre has also been investigated. The temperature dependence of $P_{1/2}$ for HiPIP had three phases (Fig.5.4): below 7K $P_{1/2}$ is dependent on a T^2 process, between 7K and 10K a $T^{17.5}$ process. The temperature dependence of the linewidth (peak to peak for $g_{y,z}$) had two phases over the temperature range studied. A temperature independent region and a second phase where $\Delta H = Y \exp(\Delta''/kT)$, where $\Delta'' = -26.3$, (Fig.5.5.). An exchange integral of $14.3 \pm 2 \text{ cm}^{-1}$ was calculated for this centre from linewidth changes. From integrated intensity data (Fig.5.6.) An apparent J was found of $11.7 \pm 3 \text{ cm}^{-1}$, which is in fairly good agreement with the value from the linewidth plot. The relaxation mechanism for the HiPIP can be summarised:

$$1/T_1 = XT^2 + ZT^{17.5} + Y \exp(\Delta''/kT)$$

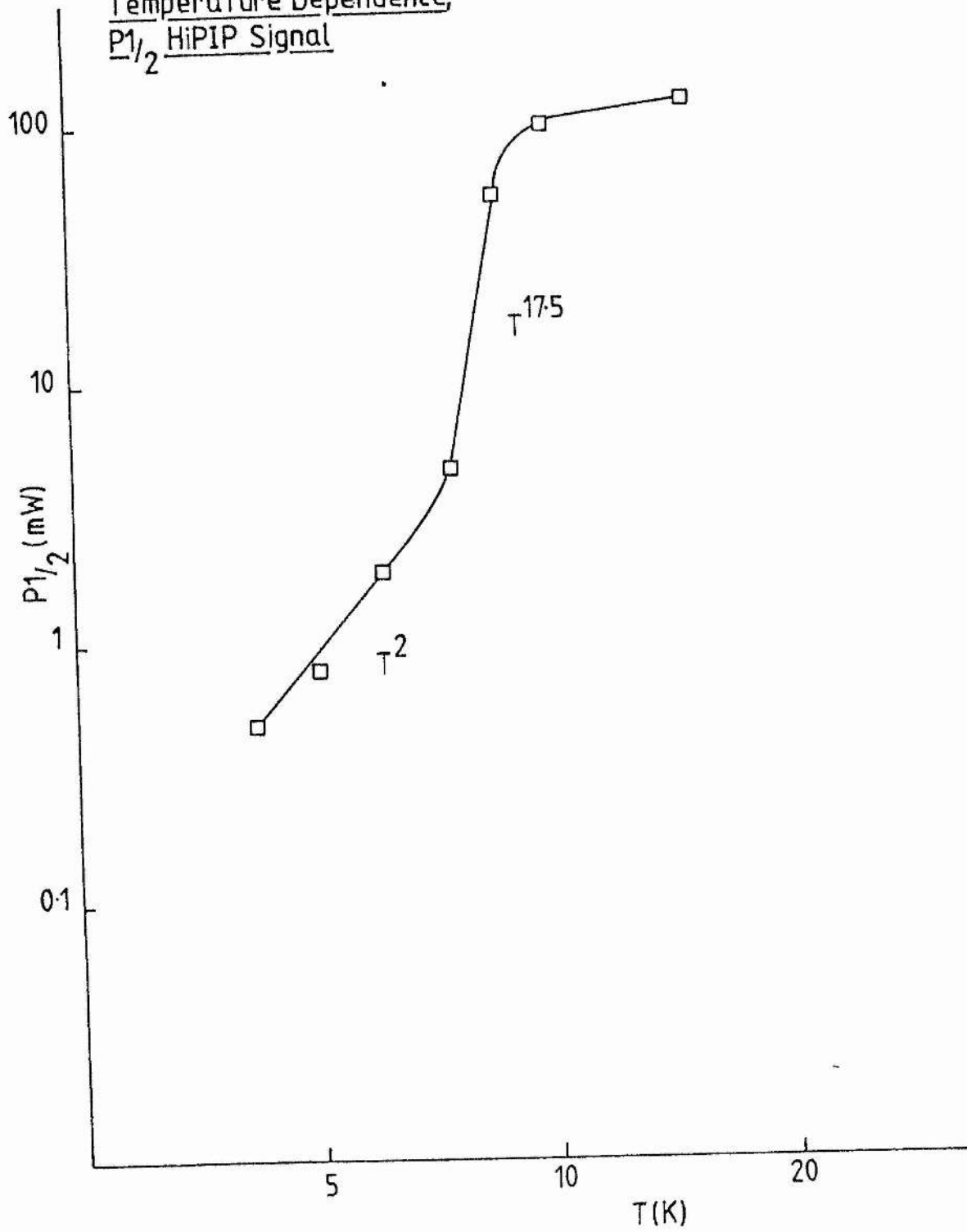
The first and last terms can be assigned to well characterised relaxation phenomena, namely, a phonon bottleneck and an Orbach process respectively. The second term may be a Raman resonance process, although it does not correspond to any well documented process. The value of the HiPIP exchange integral (14.3 cm^{-1}) is low when compared to the HiPIP of mammalian succinate dehydrogenase (44 cm^{-1} , Blum *et al.* 1979). This low value would not appear to correlate with the degree of rhombicity ($g_z - g_y$) in the e.p.r. spectrum of the HiPIP centre (Blum *et al.* 1979), with $g_z \approx g_y$, giving a narrow

Figure 5.4

Temperature dependence of P1/2 for the HiPIP signal

P1/2 was determined under the conditions described in the text. The log of P1/2 (mW) is shown plotted against the log of the temperature (K). The temperature dependencies of P1/2 are shown adjacent to the straight-line portions of the curve. Experimental conditions were as described for fig.5.10.

Temperature Dependence,
 $P_{1/2}$ HiPIP Signal



Temperature Dependence, EPR Linewidth
HiPIP Signal

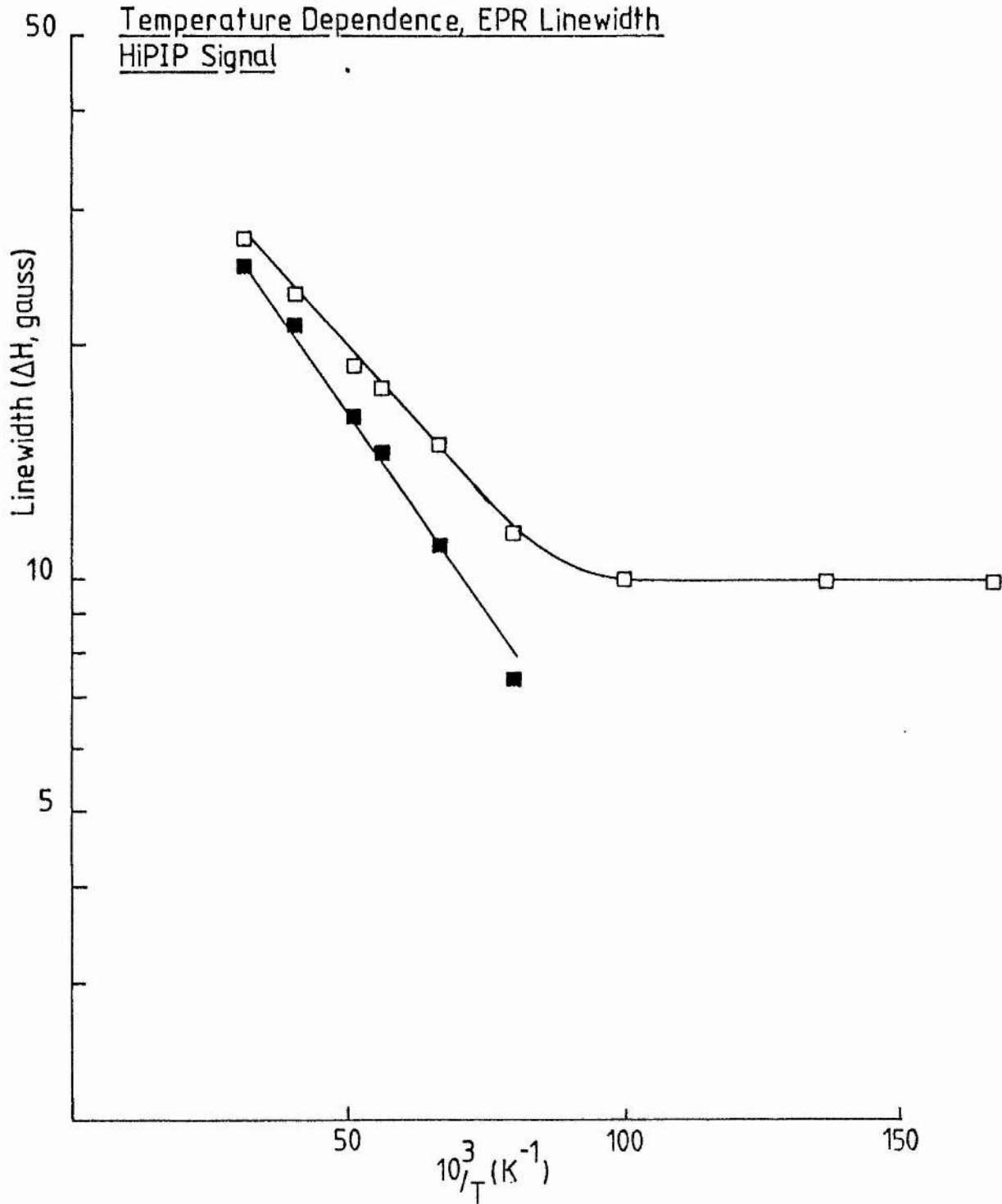
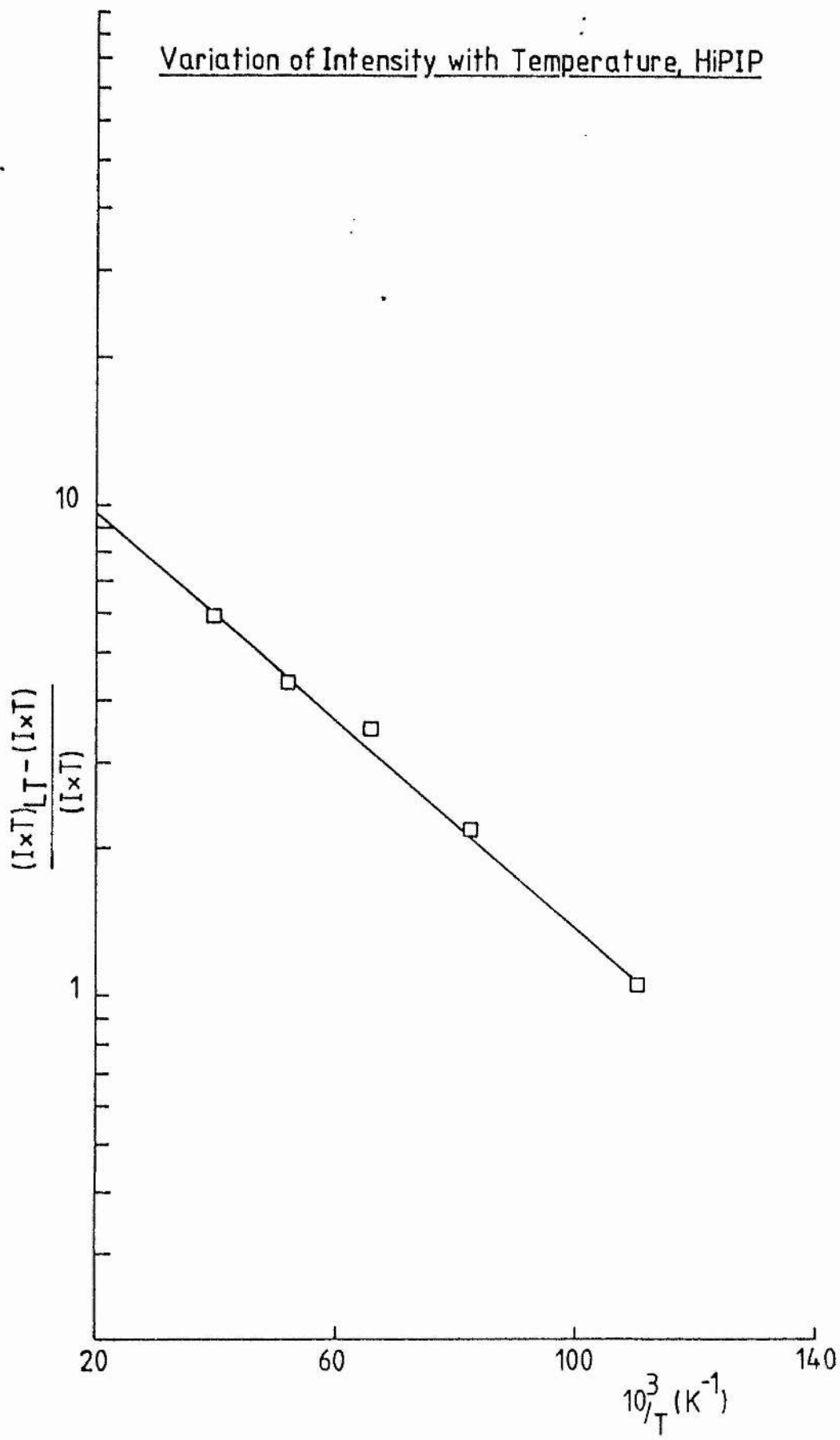


Figure 5.6.

Temperature dependence of intensity for HiPIP

The integrated absorption, multiplied by the temperature is plotted against inverse temperature, to show the deviation from Curie's law, after correction for the low temperature intensity factor. $J = 11.2 \text{ cm}^{-1}$, from the slope, as described in the text. The multiplicity of the ground state to the first excited state = 9.5. Experimental conditions were as described for fig.5.10.

Variation of Intensity with Temperature, HiPIP



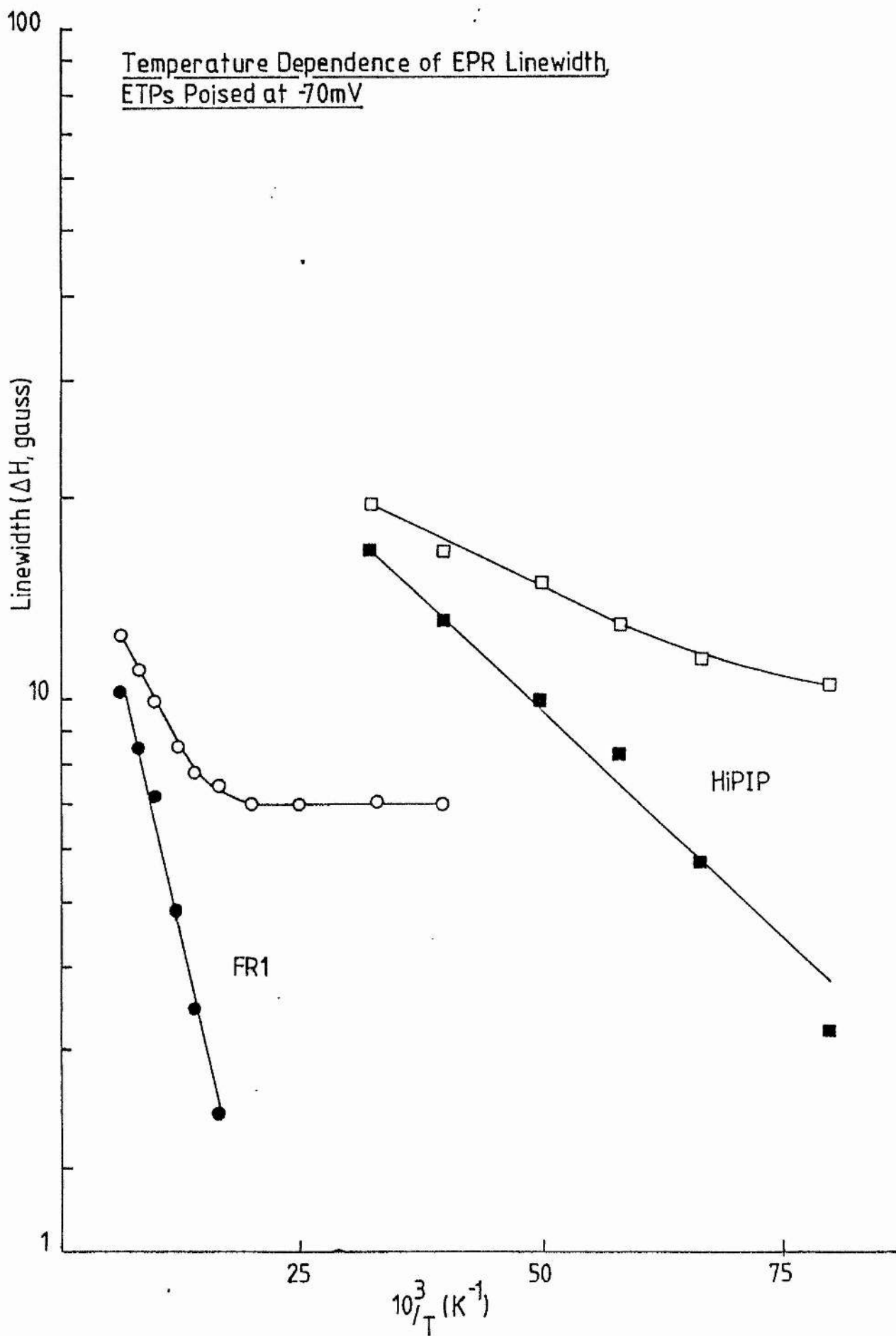
signal, which is seen in the peak at $g = 2.01$. The large linewidth for g_{xy} would, however, appear to show axially between g_x and g_y . The lack of knowledge concerning the relationship between the structure of HiPIP-type centres and their g -tensors precludes any definite conclusions, concerning the structure of the fumarate reductase HiPIP. The exchange integrals are, however, very sensitive to the inter iron distances in this centre (Salerno *et al.* 1977, Blum *et al.* 1979). The differences in the exchange integrals may also reflect differences in environmental factors such as electrostatic interactions, the nature of the surrounding amino acid residues etc.. There is however, at present, no direct evidence to link the exchange integral or spectral characteristics to the functional parameters such as mid-point potential (Bertrand & Gayda 1979). The low value obtained for the exchange integral (J) indicates that the Orbach relaxation process will start to dominate at temperatures lower than is normally seen for this type of process. Indeed this may explain the anomalous $T^{17.5}$ relaxation process which may be due to overlap with a second order Raman process. It may be that we are unable to fully evaluate this dependency because of the presence of the Orbach process at these lower temperatures.

Figure 5.7

Temperature dependence of Linewidth from membranes poised at -70 mV

The linewidths (ΔH_T) from the ferredoxin (O) and the HiPIP (\square) signals are shown plotted against inverse temperature, from a sample poised at -70 mV. The Lorentzian linewidths were obtained as described in the text, (\bullet , FR1; \blacksquare , HiPIP) and from the slopes $J = 33 \text{ cm}^{-1}$ for FR1 and $J = 7.2 \text{ cm}^{-1}$ for the HiPIP. Experimental conditions were as described for fig.5.9.

Temperature Dependence of EPR Linewidth,
ETPs Poised at -70mV



In chapter 4 it was proposed that at redox potentials at which both the HiPIP centre and FR1 were partially paramagnetic, there was interaction between these centres. Fig.5.7 shows the temperature dependence of linewidths for these two centres, from a sample poised at -70 mV (peak of change in P1/2, chapter 4). For the HiPIP centre the exchange coupling constant was found to be -7.2 cm^{-1} and for FR1 $J = -33 \text{ cm}^{-1}$. Thus it was found, as for FR1 plus FR2 that the relaxation processes of these centres are changed by their interaction, the introduction of a T_2 mechanism caused the faster relaxation of both centres. Both centres were subject to the apparent faster relaxation, because the T_2 mechanism was mutual to both centres and thus contributed to the linewidths of both.

5.2.3 Dysprosium(III) studies with membrane-bound enzyme

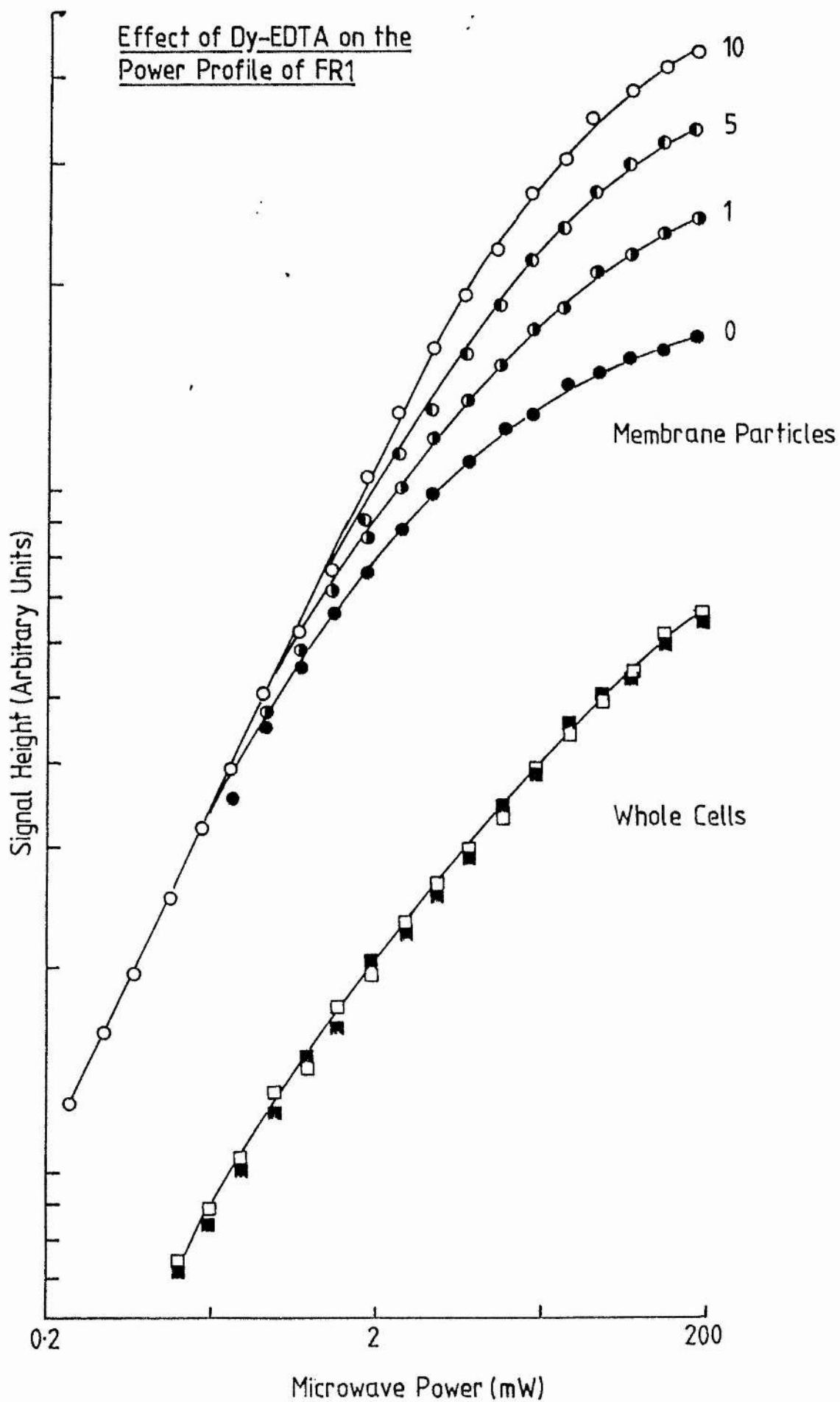
Power profiles of the ferredoxin signals from succinate reduced membranes and whole cells in the presence of various concentrations of dysprosium(III)-EDTA, are shown in Fig.5.8. The dysprosium(III) complex was shown to relieve the power saturation of the iron-sulphur centre, only in the membrane particles. Lanthanum-EDTA was included as a non-paramagnetic control and no effects were observed for this complex, in either case, indicating that changes in saturation behaviour

Figure 5.8.

Effect of Dy-EDTA on power saturation of FR1

The effect of Dy-EDTA on the power saturation profiles of membranes and whole cells is shown. The log of power is shown versus the log of signal height. For the membranes the concentration of Dy-EDTA is shown adjacent to the curves. For whole cells the data for fresh cells (open symbols) and cells in the presence of 10mM dy-EDTA (closed symbols) is shown. Experimental conditions were as described for fig.5.9; the temperature was 21 K.

Effect of Dy-EDTA on the
Power Profile of FR1



of FR1 are due to dysprosium(III)'s magnetic moment. Qualitatively similar effects were observed in all three oxidation / reduction states examined: oxidised, succinate reduced, and dithionite reduced membranes. The negative result for dysprosium(III) observed for these e.p.r. signals, when examined in whole cells indicates that the distance between the dysprosium(III) complex and the three centres in whole cells is too large for there to be any detectable interaction. As dysprosium(III)-EDTA is membrane impermeable (Ohnishi *et al.* 1982) these results indicate that all three iron-sulphur centres of fumarate reductase are located on the cytoplasmic side of the cell membrane.

The effect of dysprosium(III) on the iron-sulphur centres of fumarate reductase was studied in greater detail, to obtain information on the spatial relationship of these centres within the membrane bound and isolated protein. Spectra of FR1 and the HiPIP in the presence of varying concentrations of dysprosium(III)-EDTA are shown in Fig.5.9 & 5.10. Dysprosium(III) enhances the spin-lattice relaxation of redox centres by dipolar interaction with these centres. The enhancement of relaxation has two results, a relief of power saturation and a broadening of the e.p.r. spectrum of the intrinsic centre (Fig.5.8-5.10). The saturation parameter $P_{1/2}$ was again used as a measure of the intrinsic iron-sulphur centres' ability to relax. Fig.5.11. shows the effect of dysprosium(III)-EDTA on $P_{1/2}$, indicating that the relief of

Figure 5.9.

Epr spectra of succinate reduced membranes in the presence of Dy-EDTA

E.p.r. spectra from succinate reduced membranes in the presence of various concentrations of Dy-EDTA are shown. The concentration of Dy-EDTA is shown on the left of the spectra and the major g-values are indicated below the spectra. The gain factors are shown on the right of the spectra. Experimental conditions were: microwave power, 20mW; microwave frequency, 9.48GHz; modulation amplitude 1.0mT, modulation frequency, 100KHz; The receiver gain for the spectra in the absence of Dy-EDTA was 5.0×10^4 ; sweep rate was 0.05mT/s at a time constant of 1s. The temperature was 6 K and the protein concentration was 69mg/ml. The concentration of Dy-EDTA is shown as mM

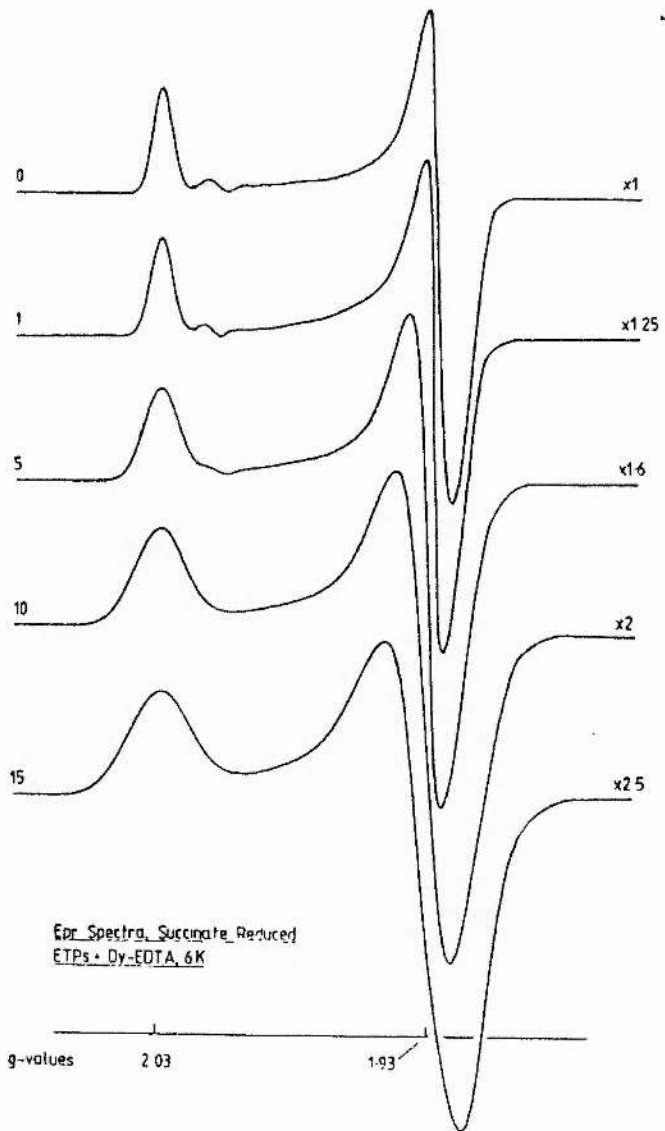


Figure 5.10.

E.p.r. spectra of oxidised membranes in the presence of Dy-EDTA

E.p.r. spectra from H_2O_2 oxidised membranes in the presence of various concentrations of Dy-EDTA are shown. The concentration of Dy-EDTA is shown on the left of the spectra and the major g-values are shown below the spectra. Experimental conditions were: microwave power, 20 mW; microwave frequency, 9.48 GHz; modulation amplitude, 1.0mT; modulation frequency, 100KHz; receiver gain 6.3×10 and the temperature was 7 K. the protein concentration was 65mg/ml.

EPR Spectra HiPIP
+Oy-EDTA, 7K

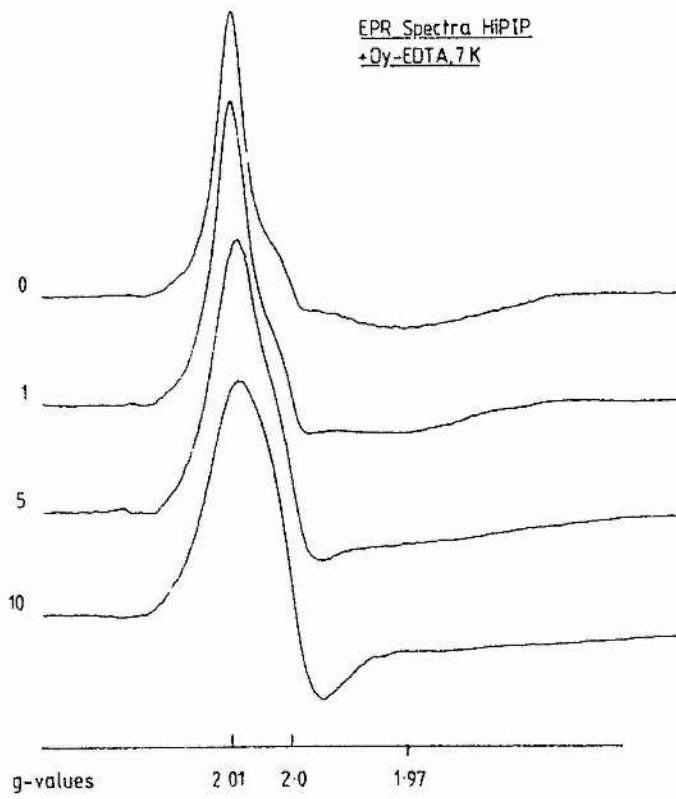


Figure 5.11.

Variation of $P_{1/2}$ with Dy-EDTA concentration

Data for the HiPIP (\square) signal and FR1 (\circ) are presented. The values of $P_{1/2}$ are shown plotted against the concentration of Dy-EDTA (mM). Values of $P_{1/2}$ (change in $P_{1/2}$ with [Dy-EDTA]) of 3.61 (HiPIP) and 1.92 (FR1) were obtained from the slopes (Table 5.1). Experimental conditions were as described for fig.5.9 except the temperatures, which were as shown in Table 5.1.

Variation of $P_{1/2}$ with Dy-EDTA Concentration

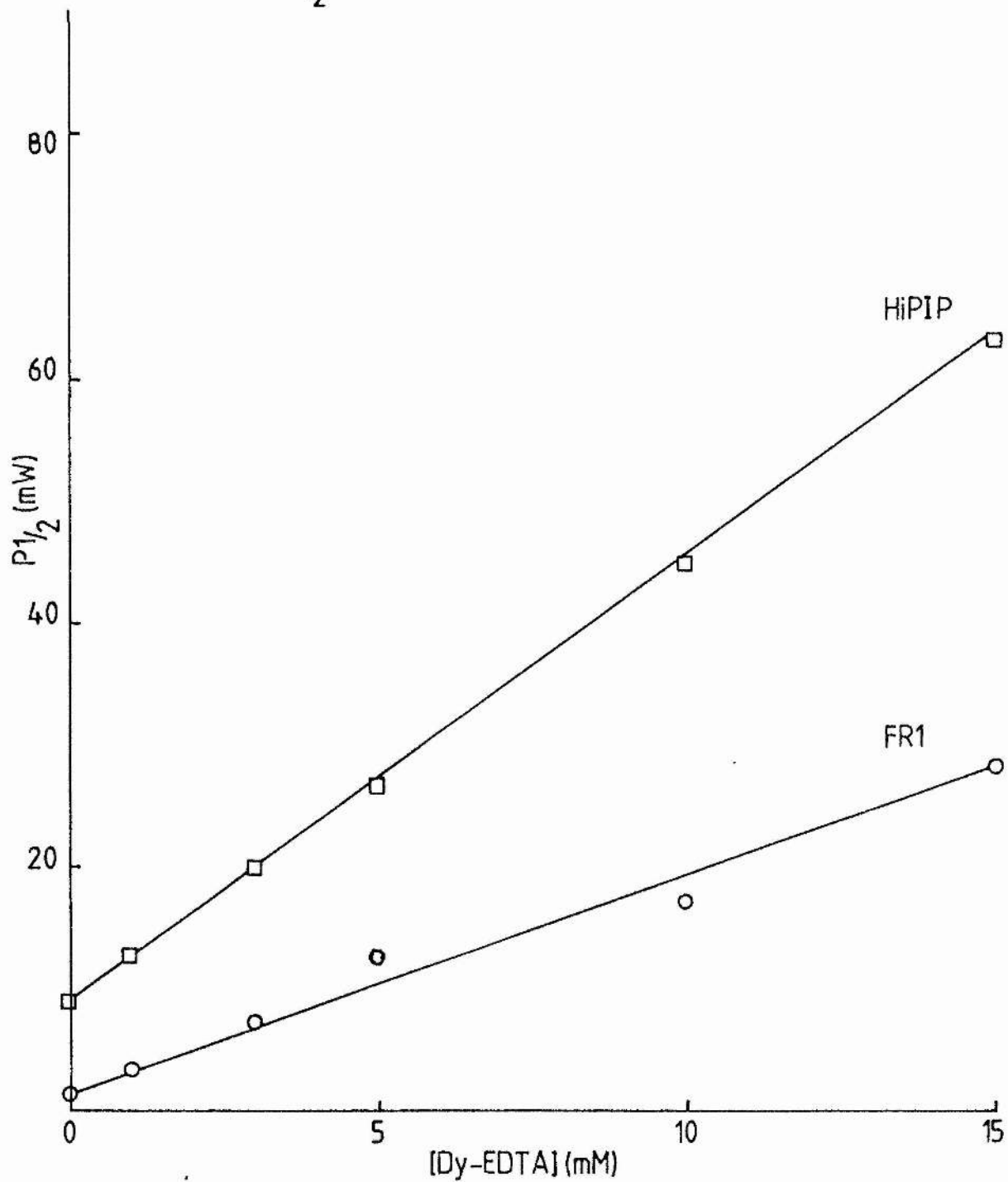
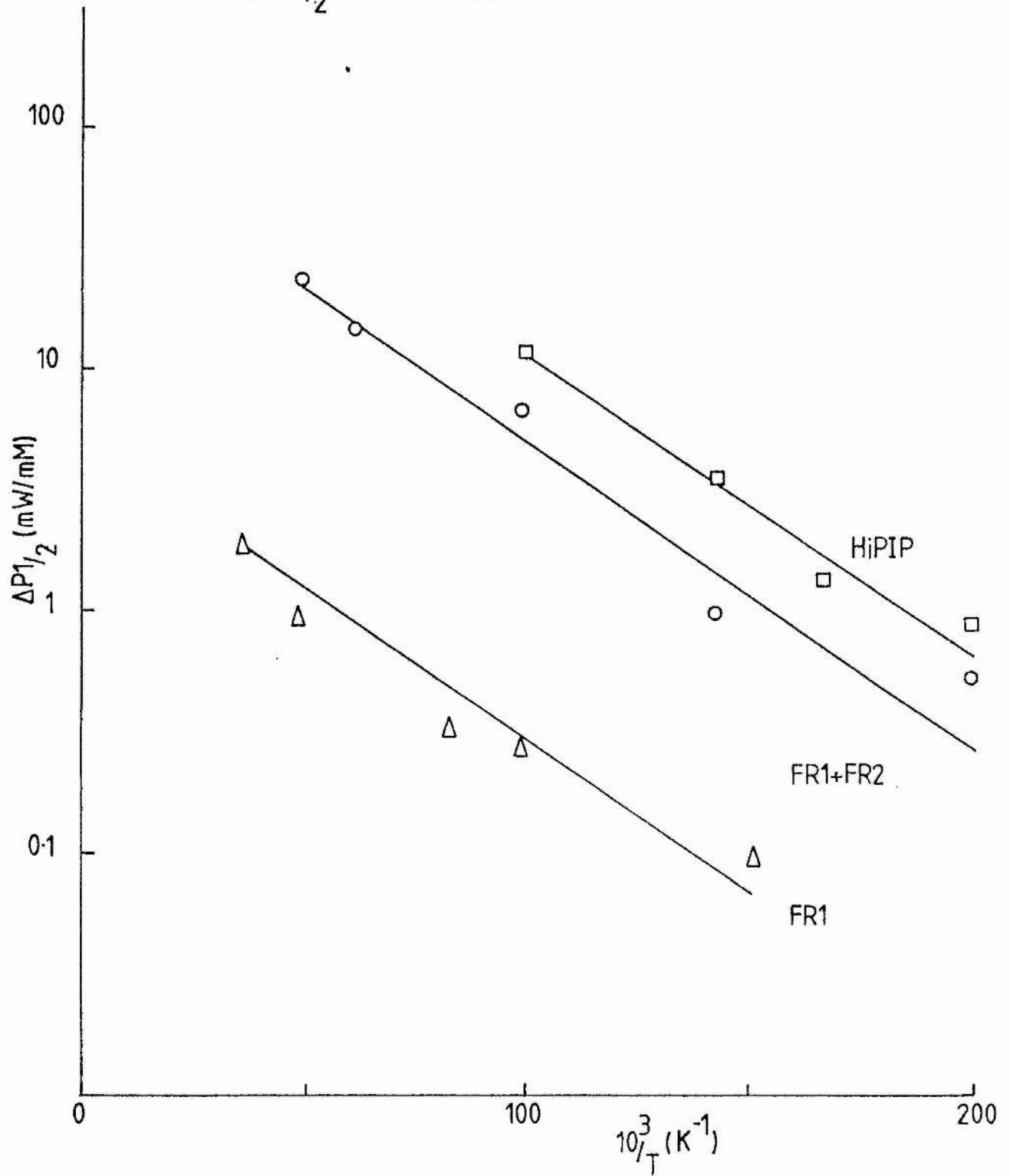


Figure 5.12.

Variation of $\delta P_{1/2}$ with temperature for the three redox states

$\delta P_{1/2}$ was obtained from the slope of $P_{1/2}$ versus Dy-EDTA concentration (fig.5.11). HiPIP (\square), succinate reduced (Δ) and dithionite reduced (O) data is presented. $\delta P_{1/2}$ is shown plotted against inverse temperature. The slope shows $\delta P_{1/2} = k \cdot \exp(-12.5/T)$ for all three redox states. The experimental conditions were as described for fig.5.9.

Variation $\Delta P_{1/2}$ with Temperature



power saturation was proportional to the concentration of dysprosium(III)-EDTA added, for FR1 and FR3. The parameter $\delta P1/2$, which is used for the distance estimates, was taken from the slope of this graph. The temperature dependence of $\delta P1/2$ (shown in Fig.5.12.) is a measure of the term $T_{1k} / (1 + \omega^2 T_{1k}^2)$, where ω is the microwave frequency of observation ($2\pi\nu$) and T_{1k} is the spin-lattice relaxation time of the dysprosium(III) complex (Hyde & Rao 1978). The variation of the $\delta P1/2$ with temperature must thus be taken into account when estimating the distance between the dysprosium(III) and the iron-sulphur centres, when using this parameter. It was seen that this term varied as $\exp(-12.5/T)$ for FR1 and FR3, which agrees with the results of Blum *et al.* (1981, 1983) for other iron-sulphur centres. Blum *et al.* (1980, 1981) indicated that the contributions to $P1/2$ were additive if T_2 was assumed to be constant in the temperature range of the system under study and developed the work of Hyde & Rao (1978), presenting an equation for the calculation of the weighted averaged distance ($|r|$) between the dysprosium(III) complex and the iron-sulphur centres:

$$\delta P1/2 = 4.12 \times 10^8 \cdot |r|^{-6} \cdot \exp(-12.5/T)$$

$\delta P1/2$ is the concentration dependence of $P1/2$ in mW / mM . A distance of 5 \AA is allowed for the size of the dysprosium(III) complex (Blum *et al.* 1981). For membrane bound proteins a correction factor of 0.7 is used to account for the

Table 5.1:

Distance measurements, from the effects of Dy³⁺ on the intrinsic e.p.r. properties of the iron-sulphur centres

	<u>FR1</u>	<u>FR1+FR2</u>	<u>HiPIP</u>
Temperature (K)	7	15	7
$\delta P_{1/2}$ (mW/mM)	1.92	15.0	3.61
$ r $ (\AA)	7.80	5.58	6.45
Temperature (K)	12	12	7
ΔH (mT/mM)	0.225	0.232	0.125
$ r $ (\AA)	5.43	5.30	4.60
ΔH_{max} (mT/mM)	0.45	0.54	0.45
$ r $ (\AA)	7.6	6.8	7.6

ΔH_{max} is the linewidth enhancement in the region of maximal broadening. $|r|$ is adjusted ($\times 0.7$) for the protein being membrane bound and 5\AA was subtracted for the size of the Dy-EDTA complex. Distances were calculated from the equations of Case et al (1976a).

dysprosium(III) only having access to one side of the protein (Ohnishi et al. 1982). This equation was used to obtain estimates of the distances of the iron-sulphur centres of fumarate reductase from the membrane surface (cytoplasmic). Table 5.1 summarises the results for the three iron-sulphur centres in membrane bound studies, indicating that they are all located close to the cytoplasmic membrane surface.

Case & Leigh (1976) derived equations for the determination of the inter-species distance from the enhancement of linewidths, caused by the addition of paramagnetic transition metal ions. The dependence of $|r|$ on the change in linewidth is either $|r|^3$ or $|r|^6$ depending on the conditions of the measurement of the interaction between the paramagnets. If the interaction is 'non-relaxing' (low temperatures) then the dependency is $|r|^3$ but $|r|^6$ if the interaction is 'relaxing' (higher temperatures, Case & Leigh 1976). Blum et al. (1981) have also presented an equation for the perturbation of linewidths by dysprosium(III), and shown its temperature dependency. Fig.5.13., shows the temperature dependency of the linewidth, of the H1PIP centre and FR1, in the presence of 5 mM dysprosium(III) to compare it to that shown by the centres studied by Blum et al. (1981). It was shown that for each centre there are two regions: at low temperatures where the linewidth enhancement was maximal, a temperature independent region (ΔH enhancement proportional

Figure 5.13.

Temperature dependence of linewidth in the presence of .5 mM Dy-EDTA

Data is presented for all three redox states; HiPIP (\square), succinate reduced (Δ) and dithionite reduced (O). The linewidths were measured as described for fig.5.2 & 5.5. The slope shows the change in $H = k \exp(15/T)$ for all three redox states. and that the linewidths reach a maximum at low temperatures (ΔH_{\max}). The experimental conditions were as described for fig.5.9 & 5.10.

Variation of Linewidth with Temperature
+5mM Dy-EDTA

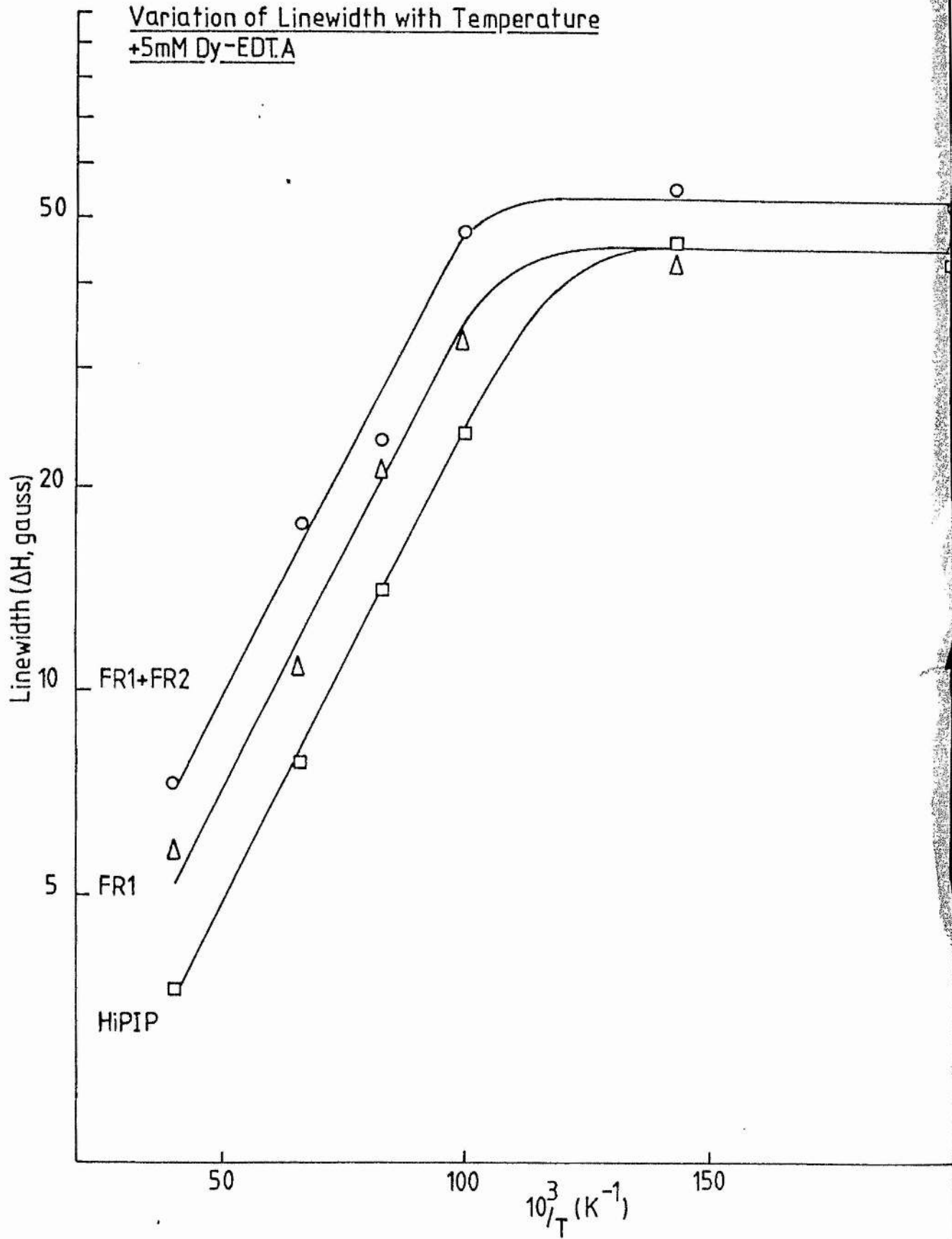
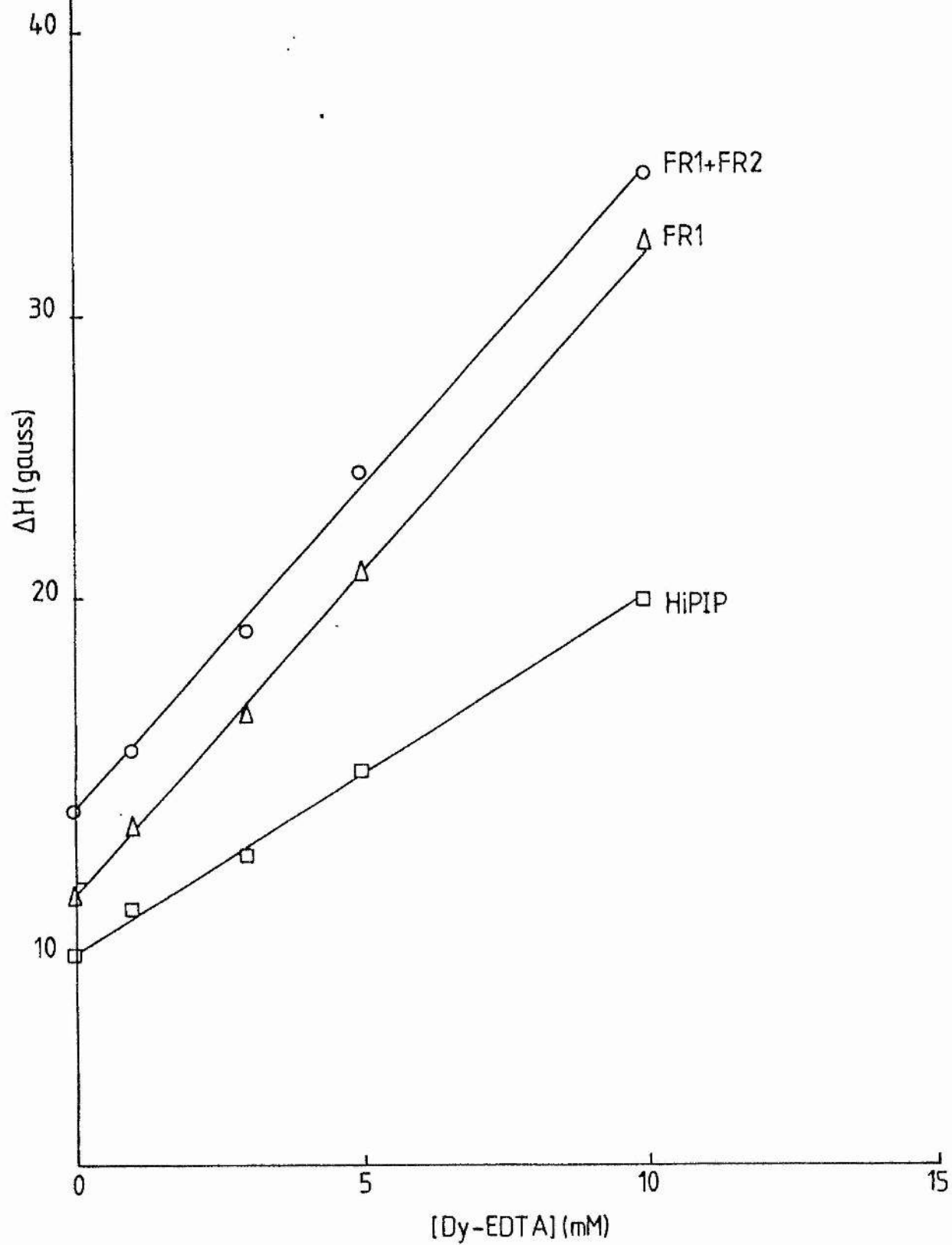


Figure 5.14.

Variation of linewidth with Dy-EDTA concentration

Data is presented for the three redox states; HiPIP (\square), succinate reduced (Δ), dithionite reduced (\circ). The linewidths are shown plotted against the concentration of Dy-EDTA. The linewidths were measured as described for fig.5.2 & 5.5. The slope shows the change in ΔH used for the distance calculations (Table 5.1). The experimental conditions were as described for fig.5.9 and 5.10.

Variation of Linewidth with
Dy-EDTA Concentration



to $|r|^3$), and as the temperature was increased, a region where the linewidth is proportional to $\exp(15/T)$ (ΔH enhancement is proportional to $|r|^6$). This is in good agreement with the data presented by Blum et al. (1981) and allows the use of their method for the estimate of distances between the dysprosium(III)-EDTA and the iron-sulphur clusters. The variation of linewidth with dysprosium(III) concentration, for each centre at 12 K and 20 mW microwave power, is shown in Fig.5.14. The results of the measurements from line broadening data are presented in Table 5.1., where distances are indicated from results obtained from both $|r|^3$ (method of Blum et al. (1981)) and $|r|^6$ regions (method of Case & Leigh (1976)). Comparison with the distances obtained from P1/2 studies shows that the results are in reasonable agreement. Distances of approximately 8 Å (13 Å - 5 Å) for the succinate reducible ferredoxin and 6 Å (11 Å - 5 Å) for the dithionite reducible ferredoxin and the HiPIP centre were obtained for the membrane-bound protein. The value from the dithionite reducible membranes can not be taken as a true estimate of the position of the second ferredoxin (FR2), because of the interaction between the two ferredoxin centres in these membranes (chapters 4 & 8) which leads to errors, as the distance obtained is that to the nearest of the interacting centres (Blum et al. 1981). However our results do indicate that all the centres are situated close to the inner membrane surface as FR2 is within 12 Å of FR1 (obtained from the strength of interaction, chapter 8).

Table 5.2

Distance measurements from isolated fumarate reductase

	<u>FR1</u>	<u>FR1+FR2</u>	<u>HIPIP</u>
Temperature (K)	5	5	5
$\delta P_{1/2}$ (mW/mM)	2.74	2.53	3.09
$ r $ (Å)	10.2	10.4	9.96
Temperature (K)	12	8	15
ΔH (mT/mM)	0.096	0.122	0.09
$ r $ (Å)	10.49	11.0	10.35
Membrane bound protein			
$ r $ (Å)	13.2	10.11	11.35

A distance of 5 Å was allowed for the size of the Dy-EDTA complex. The results from the membrane bound protein were treated in the same manner as for the isolated protein. The distance obtained was not multiplied by a correction factor (0.7) before subtracting the distance allowed for the size of the dysprosium(III) complex (Ohnishi et al 1982).

5.2.4 Dysprosium(III) studies on the isolated enzyme

Weiner et al. (1984a) and Lemire et al. (1983) have proposed a structure for the membrane bound fumarate reductase of E. coli based on electron microscopy studies. They propose that the catalytic portion of the enzyme, the flavoprotein and iron-sulphur containing subunits, protrudes from the inner membrane surface in a similar manner to the bacterial H^+ translocating ATPase. If this is the case then interactions with dysprosium(III) in membrane and isolated protein studies should yield similar results, because the dysprosium(III) complex (Dy-EDTA) would have access to the majority of binding sites on the protein surface. Thus we undertook studies on a preparation of the isolated protein to compare results with those from membrane studies, to observe any change in the interaction between the iron-sulphur centres and dysprosium(III). The studies were performed in a similar manner to those on the membrane bound protein. The distances calculated from the results are summarised in Table 5.2, which shows the distances obtained by both $P1/2$ and ΔH measurements. The results from studies on the membrane bound enzyme, treated in a similar manner are also shown. The membrane-bound estimates were not corrected for being membrane-bound ($\times 0.7$). There was a good correlation between the distances obtained for the HiPIP centre, from the two preparations (Table 5.2): distances of 9.9 (isolated) and 11.35 Å (membrane bound) were obtained. A greater distance for the membrane bound enzyme would be expected, because it is

the weighted averaged distance, the dysprosium(III) would not be able to reach all the binding sites on the membrane bound protein. FR1 does however show a large difference in the distances obtained, 10 Å (isolated) and 13.2 Å (membrane bound). This may reflect the change in binding of the dysprosium(III) to the protein in the two preparations, as there may be a specific binding site close to FR1, which would cause this large change. Weiner et al. (1984a) have proposed charged regions on the protein surface where the catalytic subunit binds the anchor polypeptides. Interaction between dysprosium(III) and these regions may account for the difference in the distance estimates, as dysprosium has a single negative charge and will thus bind more strongly to positive charged regions of the protein surface. These may be in the membrane intrinsic portion of the catalytic subunits of fumarate reductase. These results would thus appear to confirm that the iron-sulphur centres of fumarate reductase are located in a portion of the enzyme that protrudes from the membrane surface.

The catalytic portion of fumarate reductase consists of the iron-sulphur subunit and the flavoprotein subunit (69 & 27 Kdalton respectively). If we assume a partial specific volume (\bar{v}) of 0.7 and a density of 1.4 as typical values for the protein, then the radius of each subunit can be calculated. If a spherical shape is assumed then radii of 20 Å (69 000) and 14.8 Å (27 000) are obtained, which are in good agreement with those estimated by Lemire et al. (1983) from electron

microscopy studies. Alternatively the radius of each subunit can be estimated from the effect of dysprosium(III) on the iron-sulphur centres (Blum *et al.* 1983), which assumes the chromophores are in the centre of the protein. From this method, radii of 16.6 and 14.7 Å were obtained for the flavoprotein and the iron-sulphur subunits respectively. Thus using our data from the isolated protein, the HiPIP centre and FR1 were shown to be located deep within the catalytic subunit, as the values are in good agreement. Knowledge concerning the placement of the iron-sulphur centres, within the two catalytic subunits is at present limited to the knowledge of the sequences of the two polypeptides (Cole 1982, Cole *et al.* 1982). From the sequence, the cysteine residues of the iron-sulphur subunit appear to be grouped in three clusters. This would appear to indicate the presence of all three iron-sulphur clusters in that subunit, but two of the cysteine clusters only contain three residues and so would require either a cysteine residue, or the nitrogen from an amino acid as the fourth ligand, to construct a functional iron-sulphur centre. These residues may come from the flavoprotein subunit. The cysteine residues in the flavoprotein subunit are not grouped in any clusters. The clusters of the iron-sulphur subunit have been shown to be conserved between similar enzymes (Guest *et al.* 1984), confirming to a large extent the location of the clusters. If the iron-sulphur centres are all in the same subunit, then our study has placed them deep within that subunit and thus close together. The weighted averaged distance, $\langle r \rangle$, is usually an

overestimate so these distances can be taken as a maximum (Blum et al. 1981).

5.3 Conclusion

The iron-sulphur centres of the E. coli respiratory fumarate reductase have been shown to have well defined relaxation processes similar to those of other iron-sulphur centres (Blum et al. 1979, 1983, Gayda et al. 1976, Salerno et al. 1977). Namely, phonon bottle-neck, second order Raman and Resonance Raman (Orbach) mechanisms, as outlined in the Results and Discussion section. The Orbach relaxation mechanisms were used to characterise the antiferromagnetic coupling constants. The relaxation mechanisms were observed to change when more than one paramagnetic species was present. This was assumed to be due to the introduction of a T_2 mechanism between the interacting centres, because the resulting relaxation was faster than for the independent centres. In the dithionite reduced membranes the ferredoxin signal showed homogeneous relaxation. The exchange integrals indicated that the relaxation at higher temperatures was faster, when two paramagnetic species were present, because the values for J were less than those for the independent species. The relaxation processes for the interacting species will be characteristic of T_1 and T_2 .

The iron-sulphur centres of fumarate reductase were shown to be located on the cytoplasmic aspect of the cell membrane by their interaction with dysprosium(III)-EDTA. No interactions were observed in fresh whole cells, where the dysprosium(III) could not permeate the cell membrane, indicating the distance between it and the iron-sulphur centres was large ($> 25 \text{ \AA}$). A strong interaction was observed for all three iron-sulphur centres when dysprosium(III) was added to everted membrane vesicles, showing that the centres were close to the inner cell membrane surface. Distance calculations (weighted averaged distance, $|r|$) were performed in the manner of Blum et al. (1981), from the change produced in P1/2 and linewidth of the centres by the dysprosium(III) complex. FR1 was shown to be within 8 \AA of the membrane surface and the HiPIP at approximately 6 \AA from the membrane surface (Table 5.1), when the data was treated in the manner of Ohnishi et al. (1982). A reliable estimate for FR2 could not be made due to interaction between the two ferredoxin centres (Blum et al. 1981), though it was also presumed to be close to the membrane surface.

Studies on the isolated protein (catalytic dimer, Dickie et al. 1979) were performed, to determine the spatial arrangement of the centres within the protein and to investigate the structure of the protein in the membrane. When results from both isolated and membrane bound proteins were treated in the same manner (no correction for being

membrane bound), then similar distance measurements were obtained for the iron-sulphur centres from both sets of data (Table 5.2). This is a good indication that all three iron-sulphur centres are in the catalytic portion of the fumarate reductase and that this is membrane extrinsic. Comparisons of the radii for the protein obtained from the molecular weight and from the effects of dysprosium were in reasonable agreement, so the iron-sulphur clusters of fumarate reductase can be placed deep within the catalytic portion of the enzyme.

CHAPTER SIX

Characterisation of the Flavin Moiety

6.1 Introduction

Fumarate reductase has been shown to contain the same covalently bound flavin moiety as mammalian mitochondrial succinate dehydrogenase and some other flavoproteins (Weiner & Dickie 1979). This flavin moiety, 8α -[N(3)-histidyl]FAD, was located in the larger of the two catalytic sub-units of fumarate reductase, by fluorescence scanning of SDS-polyacrylamide gels from the two catalytic sub-units. The flavin coenzyme of the succinate-fumarate oxidoreductase enzymes has been proposed to function as a converter of $n = 2$ electron-transfer steps to $n = 1$ electron-transfer steps (Ohnishi *et al.* 1981). To accomplish this a stable semiquinone free radical would be required to act as an intermediate, between the fully oxidised and fully reduced forms of the flavin. Ohnishi *et al.* (1981) have shown the free radical of mammalian succinate dehydrogenase to be reasonably stable (the free radical formation constant, $K = 2.5 \times 10^{-2}$) when compared to other physiological free radicals.

Edmondson *et al.* (1981) showed that the flavin free radicals of the 8α -substituted flavins are usually in the anionic (non-protonated) form, by their narrow e.p.r. spectra. Their work was based on that of Palmer *et al.* (1971), who distinguished two ionic forms of the protein bound flavins from the e.p.r. spectral linewidths of the flavin semiquinone. This is contrary to the results of Ohnishi *et*

al. (1981), who concluded that the flavin free radical of succinate dehydrogenase was largely present in the neutral (protonated) form, from estimates of the pK values of the two protonation reactions. It was proposed that the narrow e.p.r. spectra of this flavin group arose from delocalisation of the unpaired electron within the flavin in such a way that would not be affected by protonation at N(5) of the flavin moiety. An alternative explanation for their results is that the protonation measured may not have been that of the flavin, but of a neighbouring residue that affects the flavin behaviour.

In this chapter characterisation of the flavin component of fumarate reductase is presented. The flavin was characterised by e.p.r. spectroscopy, to study its thermodynamic properties. Interaction between the flavin and the iron-sulphur clusters of fumarate reductase was studied by changes in the saturation behaviour of the flavin e.p.r. spectrum. Comparisons with the flavin moiety of succinate dehydrogenase were drawn where possible. Difficulty in observing the flavin moiety under non saturating conditions (high temperature and low power) made analysis difficult, because to obtain a sufficiently large signal the e.p.r. spectra had to be run at a higher power. The flavin semiquinone was thus saturated, but an estimate of the effects of interaction from the iron-sulphur centres was made to correct for this.

6.2 Results and discussion

6.2.1 Initial characterisation

The membranes of anaerobically grown E. coli, will contain menaquinone as an intermediate of electron-transport to fumarate (Kroger 1978, Haddock & Jones 1977). The mid-point potential (fully oxidised to fully reduced, $n = 2$) of menaquinone is -74mV at pH 7.0, this will mean that the free radical from this semiquinone moiety will give rise to an e.p.r. signal in approximately the same redox range as the flavin semiquinone moiety, assuming the two half reactions of the quinone are not widely spread. Fig.6.1 shows a potentiometric redox titration of the free radical e.p.r. signal ($g = 2.00$) from the membranes of JRG1031. It is seen that there is a broad peak from approximately -20mV to -80mV under these conditions (146K, 2mW microwave power). This was shown to arise from both the free radical of the flavin semiquinone and that of menaquinone, by the different e.p.r. spectra obtained over the redox range studied. The e.p.r. spectra of the free radical signals from JRG1031 membranes, poised at 0mV and -100mV are shown in fig.6.2. It is seen that the lineshapes and linewidths of the two spectra are different. At 0mV the e.p.r. spectrum closely resembles that of the flavin free radical from bovine-heart mitochondrial succinate dehydrogenase, indicating that at this potential the

Figure 6.1

Redox titration of the free radical signal; JRG1031 membranes

The redox titration was performed as described in the methods section, at pH 7.0. The signal amplitude of the $g = 2.00$ signal is shown plotted versus the ambient electrode potential. E.p.r. conditions were: microwave power, 2mW; microwave frequency, 9.56GHz; modulation amplitude 1.0mT; modulation frequency, 100KHz; receiver gain, 1×10^6 ; scan rate 0.05mT/s at a time constant of 1s. The temperature was 146K and the protein concentration was approximately 47mg/ml.

Redox Titration of Free Radical
JRG1031 Membranes

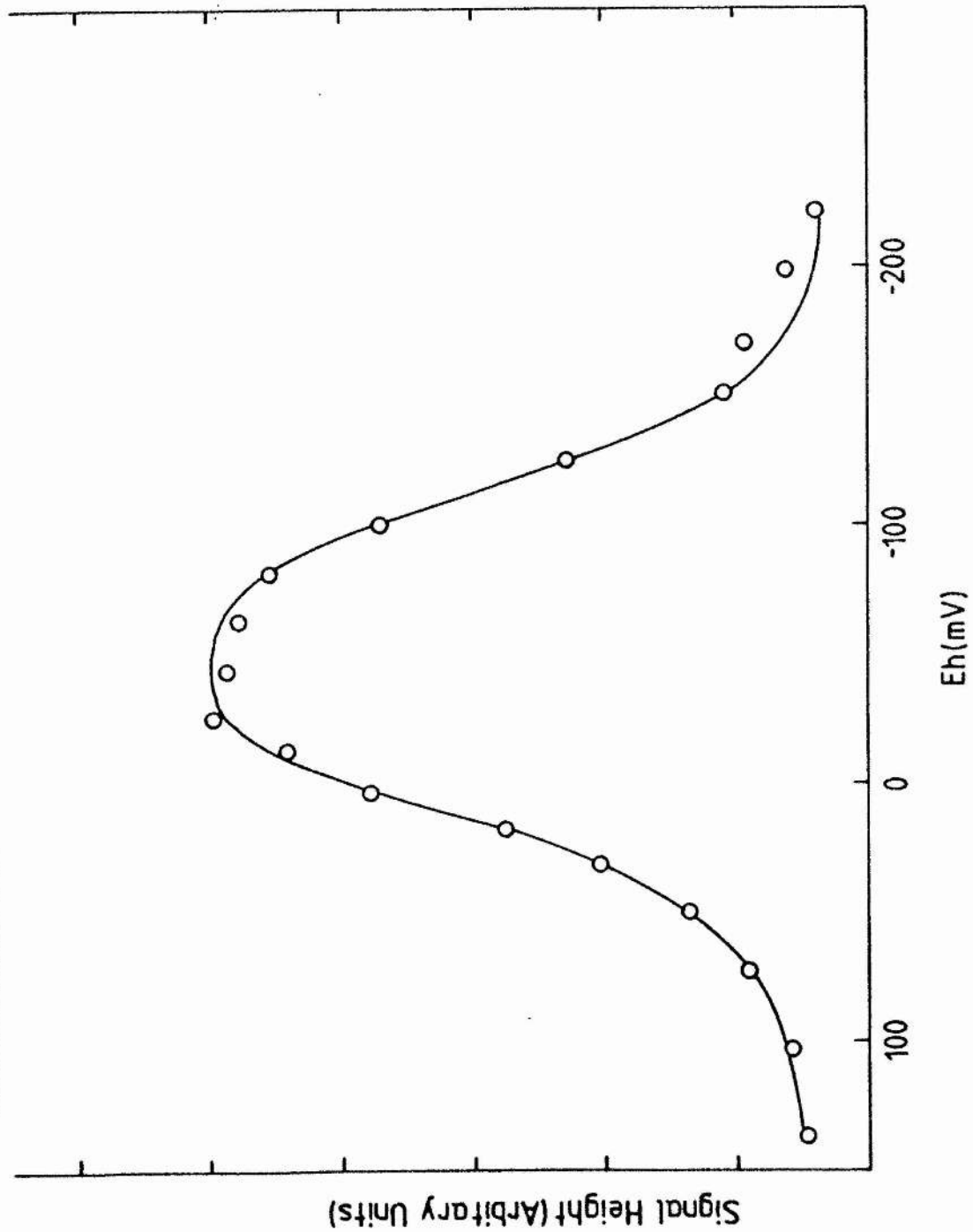
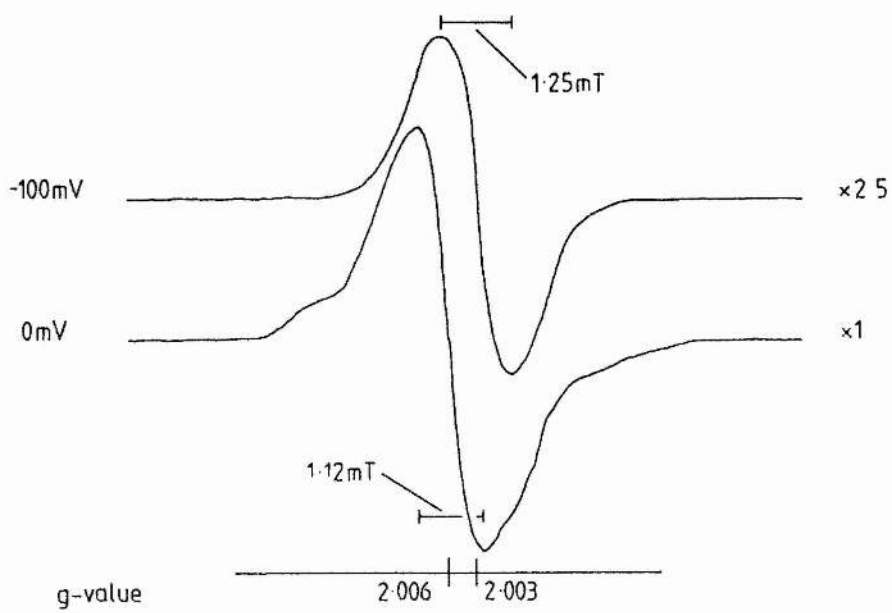


Figure 6.2

E.p.r. spectra of the free radical signals

The e.p.r. spectra from JRG1031 membranes (pH 7.0) poised at two electrode potentials are shown. The potential of the samples is indicated to the right of the spectra and the g-values are indicated below the spectra. The linewidths for the two spectra are also shown. The e.p.r. conditions were as described for fig.6.1 except: receiver gain, 2×10^6 ; scan rate, 0.025mT/s at a time constant of 2s. The temperature was 146K and the protein concentration was approximately 47mg/ml.

EPR Spectra:
Free Radical Signals,
JRG 1031 Membranes



e.p.r. signal arises mainly from the flavin semiquinone (Ohnishi *et al.* 1981, Eriksson & Ehrenberg 1973). At -100mV the e.p.r. spectrum obtained from the membranes of JRG1031 was different from that at 0mV. The 'wings' of the flavin semiquinone spectrum (due to hyperfine interaction with the flavin nitrogens) are no longer in evidence and the centre of the resonance had shifted from $g = 2.006$ to $g = 2.003$, with a broadening of the e.p.r. linewidth (peak to peak) from 1.12mT to 1.25mT. The spectrum is typical of that arising from a free radical of a quinone moiety and thus the e.p.r. signal at this potential is suggested to arise mainly from the semiquinone free radical of menaquinone. At redox potentials between that of these two samples, the e.p.r. spectrum are expected to arise from both the flavin and menaquinone semiquinone signals.

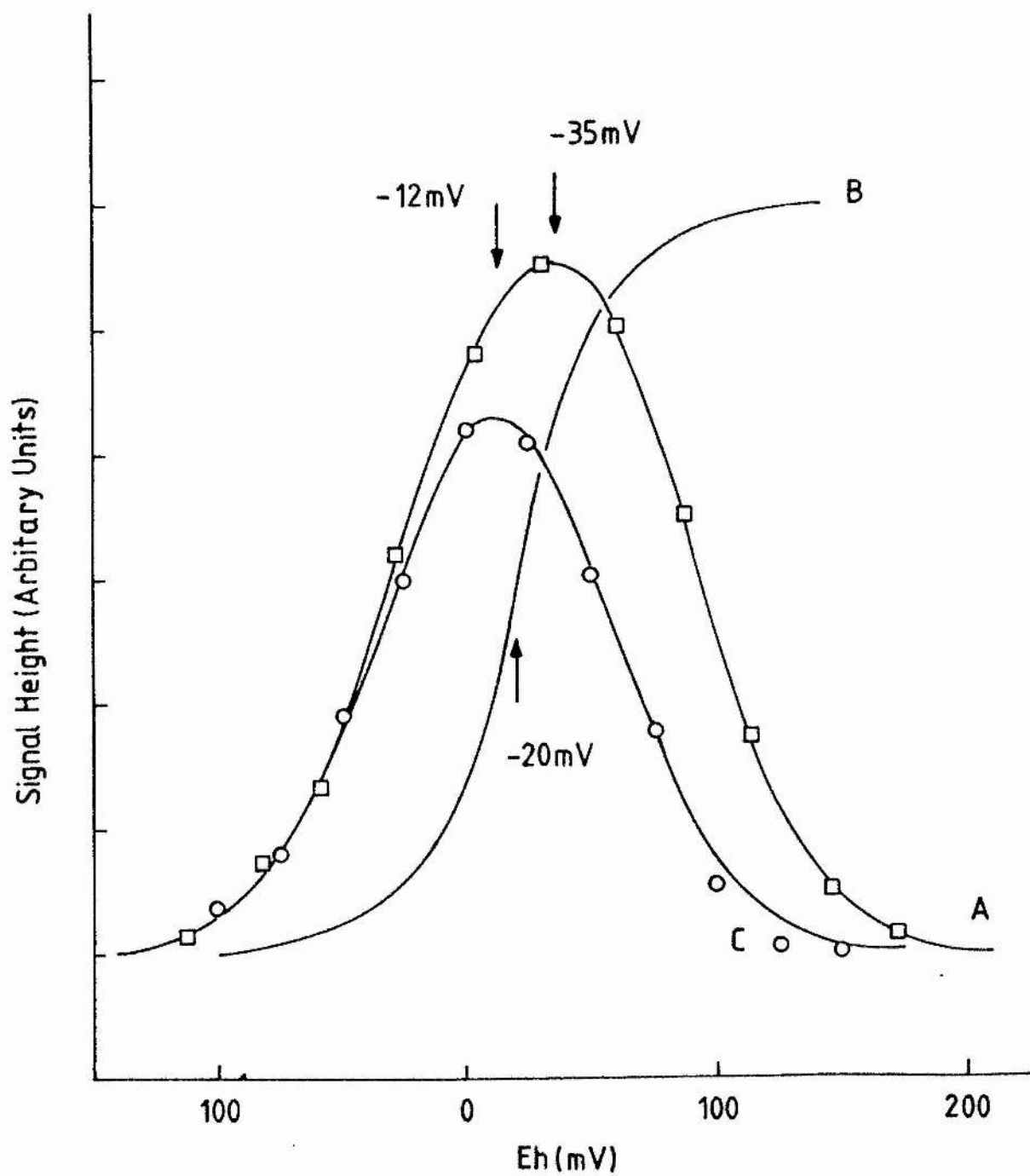
The studies to further characterise the flavin moiety of fumarate reductase were performed on the isolated enzyme (two sub-unit form), to exclude the e.p.r. signal from menaquinone. The e.p.r. signal observed from the isolated enzyme was similar to that obtained from the membranes of JRG1031 at the higher potential. A potentiometric redox titration (pH 7.0) of this signal is shown in fig.6.3(A). The peak to peak signal amplitude of the $g = 2.006$ signal of the flavin semiquinone is plotted versus the ambient electrode potential. The 'bell-shaped' titration curve gave a maximum of signal amplitude at approximately -35mV, at pH 7.0.

Figure 6.3

Redox titration of the free radical signal; isolated enzyme

A redox titration (pH 7.0) of the isolated fumarate reductase (two sub-unit form) is shown (A). The titration was performed as described in the methods section and the signal height of the $g = 2.00$ resonance is shown plotted versus the ambient electrode potential. Curve B shows the titration of FR1 and curve C the corrected titration of the flavin when interaction with FR1 is taken into consideration. The mid-point potentials of the three curves are indicated by the arrows with their values. Values of -35mV and -12mV were found for the observed and corrected titrations respectively. The value of -20mV for FR1 was used as this was the value of this centre reported by Cammack *et al.* 1984 for the isolated enzyme. The e.p.r. conditions were as described for fig.6.1 and the temperature was 148K ; the protein concentration was approximately 10mg/ml .

Redox Titration, pH7
Free Radical of Isolated Enzyme



However, under the conditions that the e.p.r. spectra were obtained (148K, 2mW microwave power) the flavin moiety is saturated, as shown by the power profile in fig.6.4(A). Thus interaction with the iron-sulphur centre FR1 would be expected under these conditions (see later section on the spatial relationships), and will therefore affect the observed titration of the flavin. An estimate of the relief of power saturation by FR1 on the flavin can be obtained from comparing samples containing FR1 paramagnetic and those lacking FR1 in a paramagnetic state (fig.6.4). It was estimated that FR1 causes a doubling of the signal height at -35mV, under these conditions. The effects of FR1 were thus subtracted from the observed redox titration of the flavin to obtain a more realistic (equally saturated) estimate of its redox behaviour (fig.6.3C). The maximum of signal amplitude for this titration was at approximately -12mV. This redox titration could be fitted by the overlap of two 1-electron redox curves, as shown in fig.6.5. The peak in signal height thus corresponds to the E_m value of the overall 2-electron transfer reaction, from the oxidised flavin to the fully reduced flavin ($Fl \leftrightarrow FlH_2$). The mid-point potentials of the two 1-electron transfer reactions are designated $E_m(I)$ and $E_m(II)$ respectively. $E_m(I)$ signifies the mid-point potential of the reaction between the oxidised flavin and the semiquinone form ($Fl \leftrightarrow FlH^*$), and $E_m(II)$ signifies the mid-point potential of the reaction between the semiquinone and the fully reduced form of the flavin ($FlH^* \leftrightarrow FlH_2$). Values for $E_m(I)$ and $E_m(II)$ of 40mV

Figure 6.4

Power profiles of the free radical, 145K

Power profiles from samples poised at -35mV and $+20\text{mV}$ are shown to compare the saturation behaviour of the flavin free radical in the presence and absence of paramagnetic FR1. The values of $P_{1/2}$ are indicated for each curve and the dashed line indicates the theoretical behaviour of the flavin in the absence of saturation. At 2mW the signal amplitude was doubled by interaction with FR1. The signal height was approximately 33% and 18% respectively of the theoretical. E.p.r. conditions were as described for fig.6.1 and the protein concentration was approximately 7mg/ml .

Power Profiles of the
Free Radical, 145K

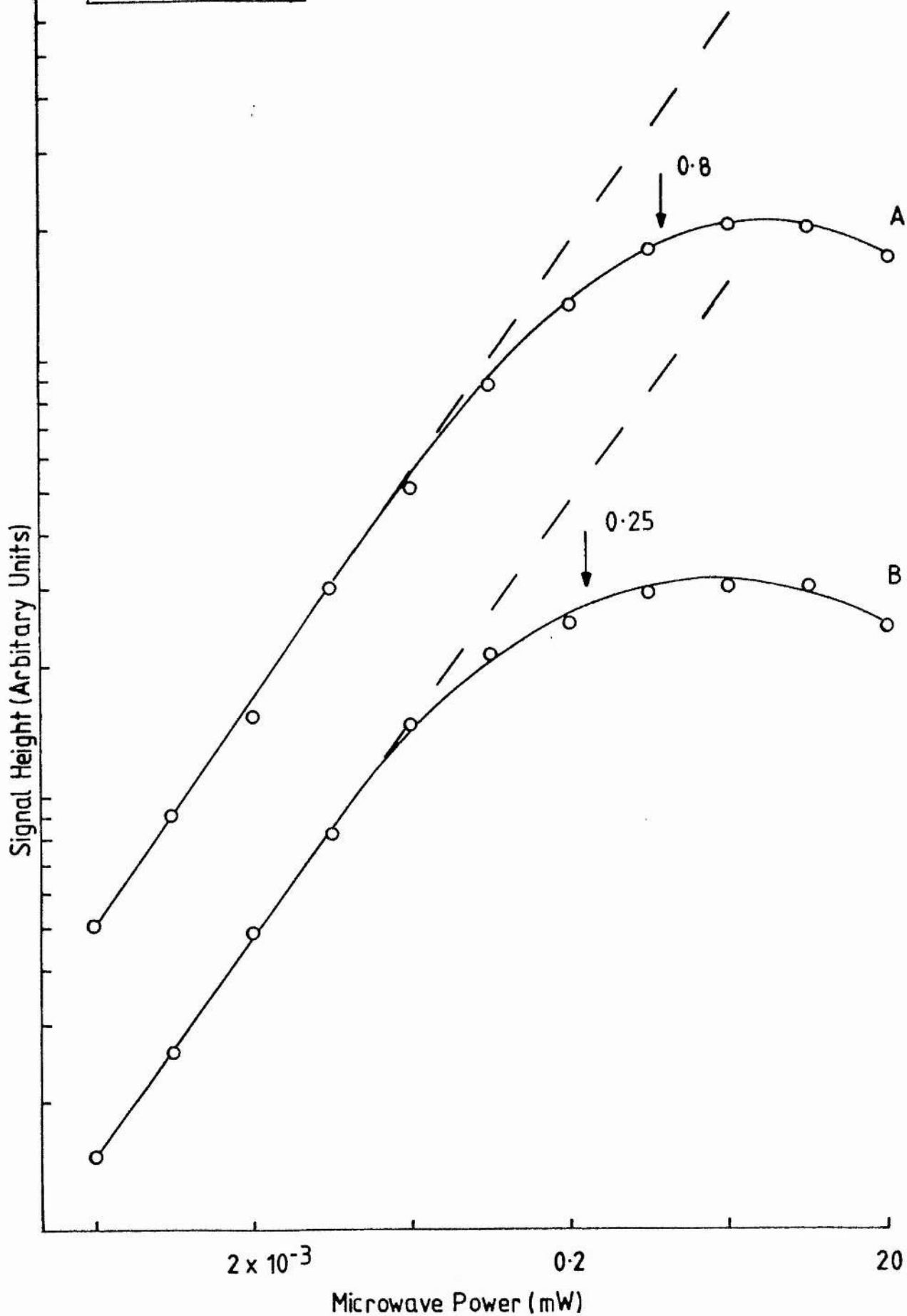
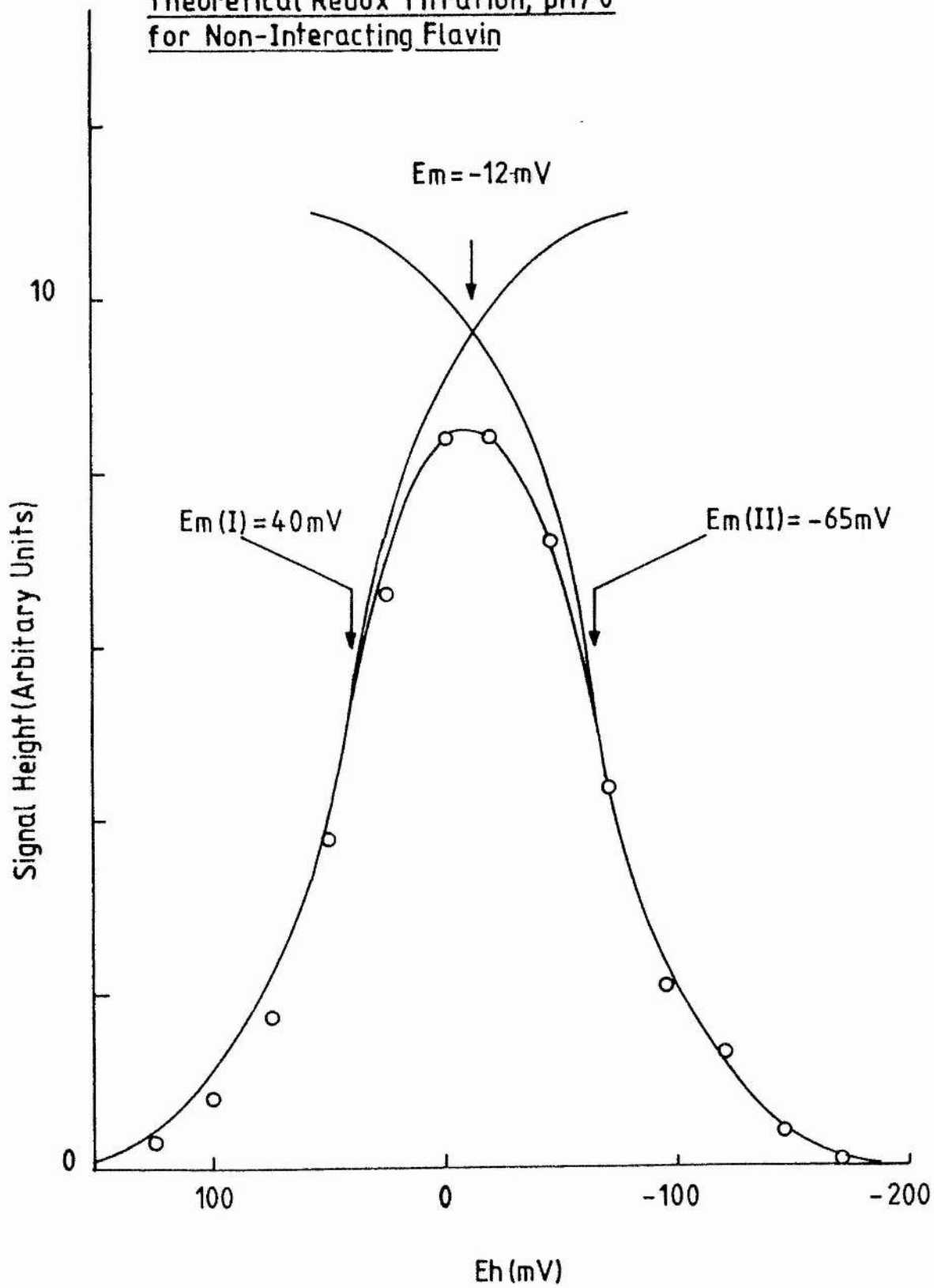


Figure 6.5

Redox titration of free radical adjusted for interaction with
FR1

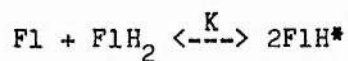
The redox titration produced from the observed titration, as described in fig.6.3, is shown with the two 1-electron titrations that fit the curve. A mid-point potential of -12mV was found for the $n = 2$ reaction and mid-point potentials of 40mV and -65mV were found for the two 1-electron reactions as shown.

Theoretical Redox Titration, pH 7.0
for Non-Interacting Flavin



and -65mV, respectively, were calculated for the pH 7.0 titration, fitting the data to the two 1-electron titrations.

The spin quantitation of the observed maximum flavin free radical signal (-35mV), by double integration of the e.p.r. signal, estimated that 8% of the total flavin was maximally present as the semiquinone species, at pH 7.0. However, this is an under estimate due to the saturation of the flavin under the observed conditions. Correction for this gave a value for the spin concentration at -12mV of approximately 12% of the total flavin present. The total flavin content was measured fluorimetrically by the method of Wilson & King (1964), as 9.3nmol./mg protein. At the peak of signal height (E_m) the concentrations of the fully oxidised and fully reduced flavins are equal, so the flavin free radical formation constant (K) can be readily estimated from the following relationships:



$$K = [F1H^*]^2 / [F1]^2 = [F1H^*]^2 / [F1H_2]^2$$

Hence as the concentration of the free radical was measured at 12%, $K = 1.9 \times 10^{-2}$. Thus the flavin semiquinone of fumarate reductase was shown to be a stable intermediate, between the fully oxidised and the fully reduced forms of the flavin. The free radical formation constant, at pH 7.0, calculated for the flavin of fumarate reductase, is similar in magnitude to that

of succinate dehydrogenase, from bovine-heart mitochondria, at the same pH (Ohnishi *et al.* 1981). It is more stable than other free radical intermediates, of redox transfer reactions, e.g. NAD^+/NADH ($K = 10^{-11}$, Blonkenhorn 1976). The flavin of fumarate reductase is thus capable of acting as a converter between 2-electron and 1-electron transfer reactions, as is the flavin from succinate dehydrogenase. The flavin of fumarate reductase acts as a converter from a 1-electron to a 2-electron transfer reaction; the flavin semiquinone is required to be stable enough to be reduced by a second electron from the iron-sulphur clusters, before passing these electrons to fumarate. In succinate dehydrogenase the flavin semiquinone accepts two electrons from succinate and donates them in sequential 1-electron steps to the iron-sulphur centres. The mechanism of electron transfer to and from the substrates is not yet fully known but presumably involves the flavin free radical of the flavin semiquinone.

6.2.2 Thermodynamic characterisation

The free radical semiquinone and fully reduced forms of the flavin can both exist in two states; protonated and non protonated. The protonated states of the reduced forms of the flavin, in the physiological pH range, can be analysed by estimating the pK values for the two protonation steps. The two pK values of interest were designated pK_S (pK semiquinone; $\text{FlH}^* \leftrightarrow \text{Fl}^{* -}$) and pK_R (pK reduced flavin; $\text{FlH}_2 \leftrightarrow \text{FlH}^-$).

The pK_R value can be estimated from the change in the mid-point potential (E_m) of the overall 2-electron transfer reaction, from the oxidised form of the flavin to the fully reduced form of the flavin (Ohnishi *et al.* 1981; fig.6.6). The E_m ($n = 2$) values were taken from the position of the signal height maxima of the redox titrations, when adjusted for the interaction with FR1 (as for fig.6.3), at different pH's. The pK_R value was estimated from the intersect of the two linear portions of the curve. Below pH 8.0 the curve had a slope of -60mV/pH and above pH 8.0 the curve had a slope of -30mV/pH , indicating the change in pH dependency either side of the pK_R . The pK_S value does not affect the pH dependency of the E_m value. A pK_R value of 8.05 was estimated from the change in the pH dependence of E_m (fig.6.6).

Fig.6.7 shows the pH dependence of the maximum free radical concentration (per cent total flavin), as determined from the peak of the observed e.p.r. redox titrations (A), together with the adjusted values, where the interaction with FR1 has been taken into account (B). The adjusted curve shows the expected behaviour, as the concentration of semiquinone becomes constant at higher pH's, where it is presumed to be in the anionic form ($\text{pH} > pK_R$ & pK_S). This plot is thus influenced by both pK_R and pK_S , and also indicates that the values for K increase with pH. Below pH 6.5 a constant free radical concentration was observed, while above pH 6.5 an increase in the maximum free radical concentration was seen, which again approached a constant value above pH 8.0. Thus the

Figure 6.6

pH dependence of E_m

The pH dependence of E_m , the mid-point potential of the overall 2-electron transfer reaction, is shown. The E_m values were taken from the peak of signal height of the e.p.r. redox titrations. The pK_R was estimated from the intersect of the two linear portion of the curve, as shown. Experimental conditions were as described for fig.6.3.

pH Dependence of E_m

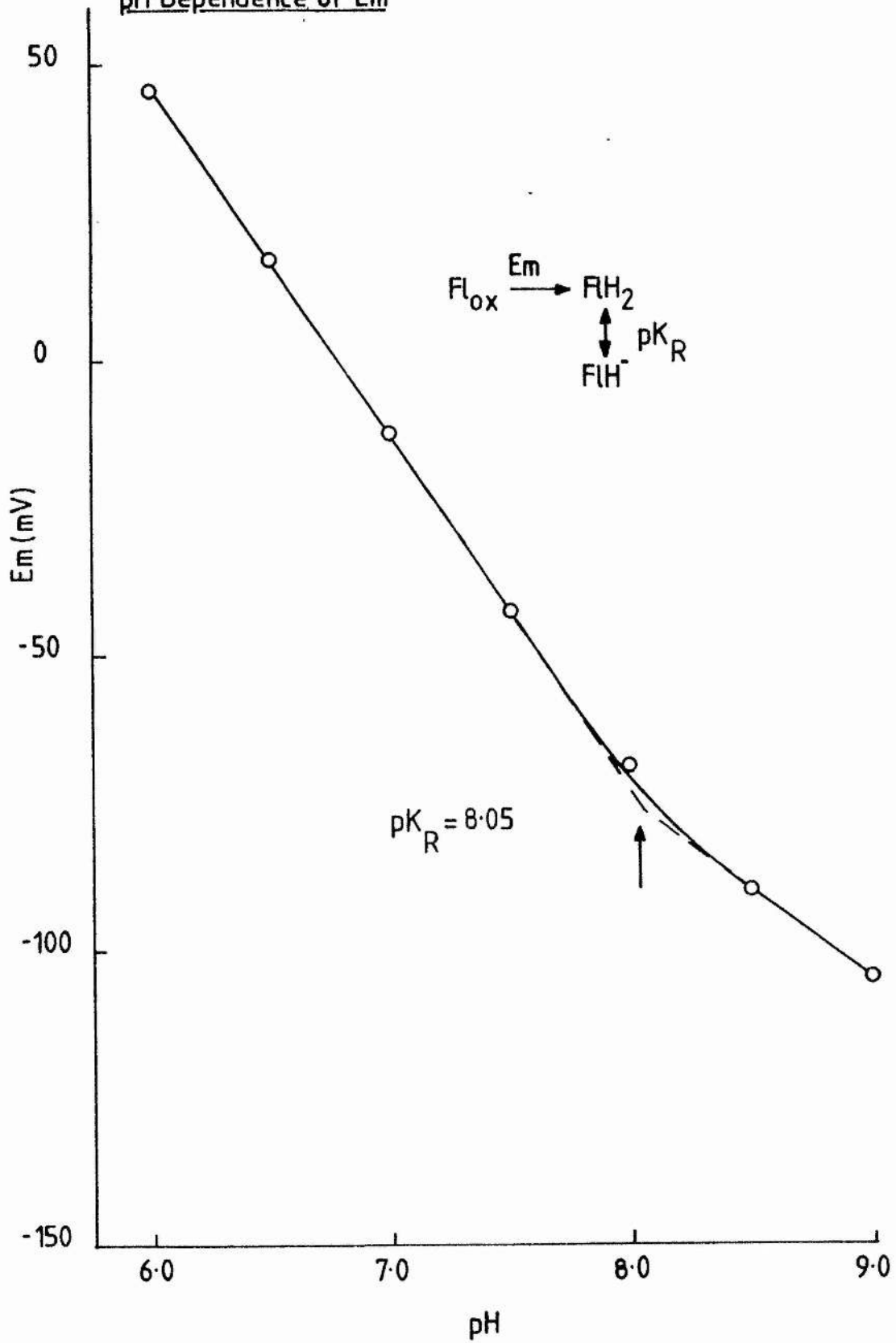
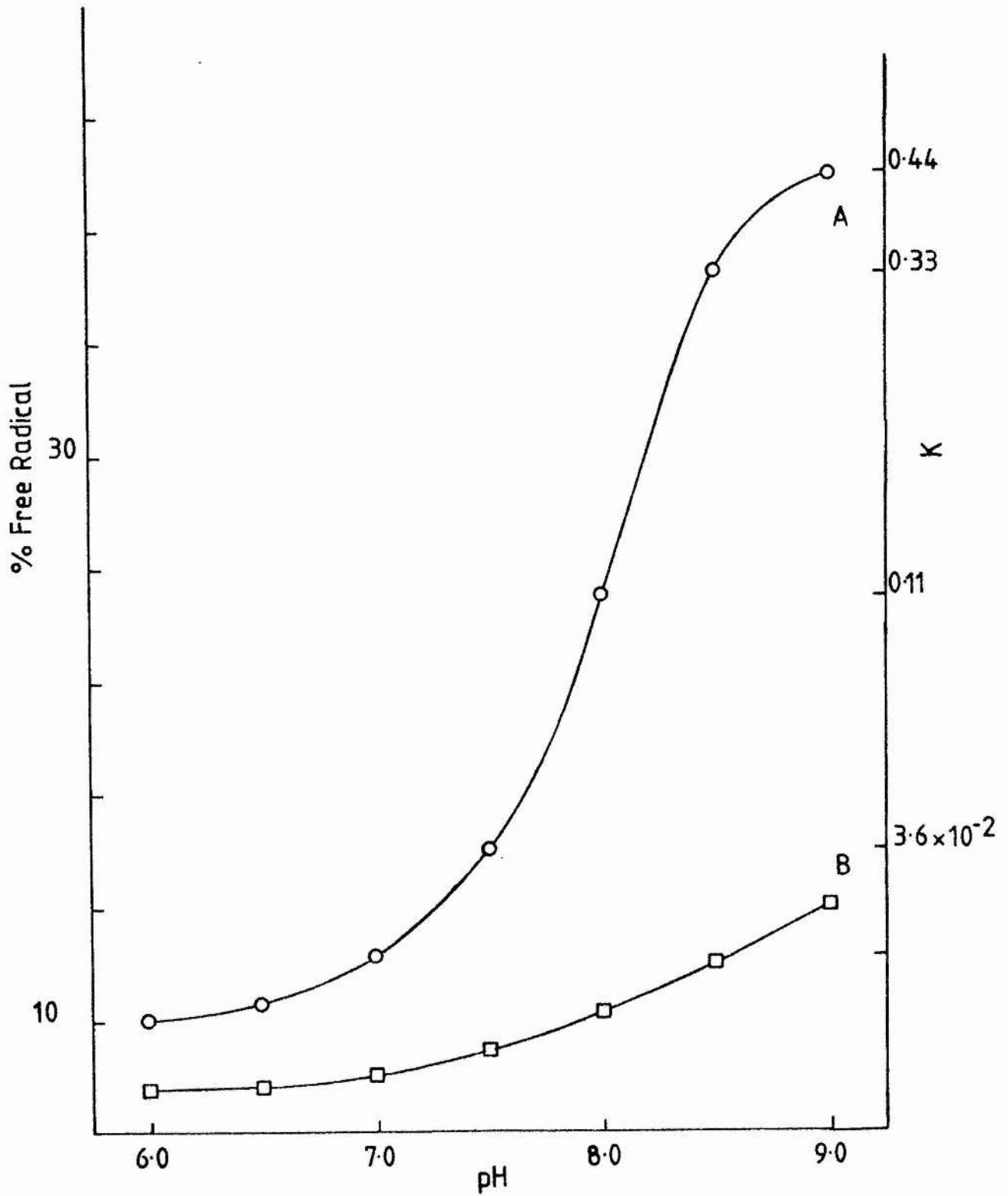


Figure 6.7

pH dependence of maximum free radical concentration

The per cent of the flavin present as the semiquinone free radical, at the peak of the titrations is shown. Spin concentrations of the $g = 2.00$ resonance were obtained by computer, double integrations of the e.p.r. spectra. Total flavin concentration was determined fluorimetrically as described in the methods section. Other experimental conditions were as described for fig.6.3.

pH Dependence of Maximum Free Radical Signal



free radical of the flavin is seen to be more stable at higher pH's. As the concentration of the flavin free radical increases, this reflects an increase in the flavin free radical formation constant (K, see later).

The values for $E_m(I)$ and $E_m(II)$ can be calculated from K (determined from the maximum per cent free radical of the non interacting titration and from E_m by the following equations:

$$E_m(I) + E_m(II) = 2E_m$$

$$E_m(I) - E_m(II) = 60 \cdot \log(K)$$

Fig.6.8 shows the pH dependence of the both the mid-point potentials of the two 1-electron reactions. At pH's below pH 7.0 the difference between $E_m(I)$ and $E_m(II)$ is constant at approximately 120mV. At higher pH's the difference between $E_m(I)$ and $E_m(II)$ is gradually diminished, as $E_m(II)$ is seen to tend towards a constant value and the pH dependence of $E_m(I)$ is seen to remain pH dependent. The mid-point potential of an oxidation-reduction reaction that involves protonation, will vary with pH as shown by the following equation:

$$E_h = E^0 + \frac{0.06 \log(\text{ox})}{n} - \frac{0.06a \cdot \text{pH}}{n}$$

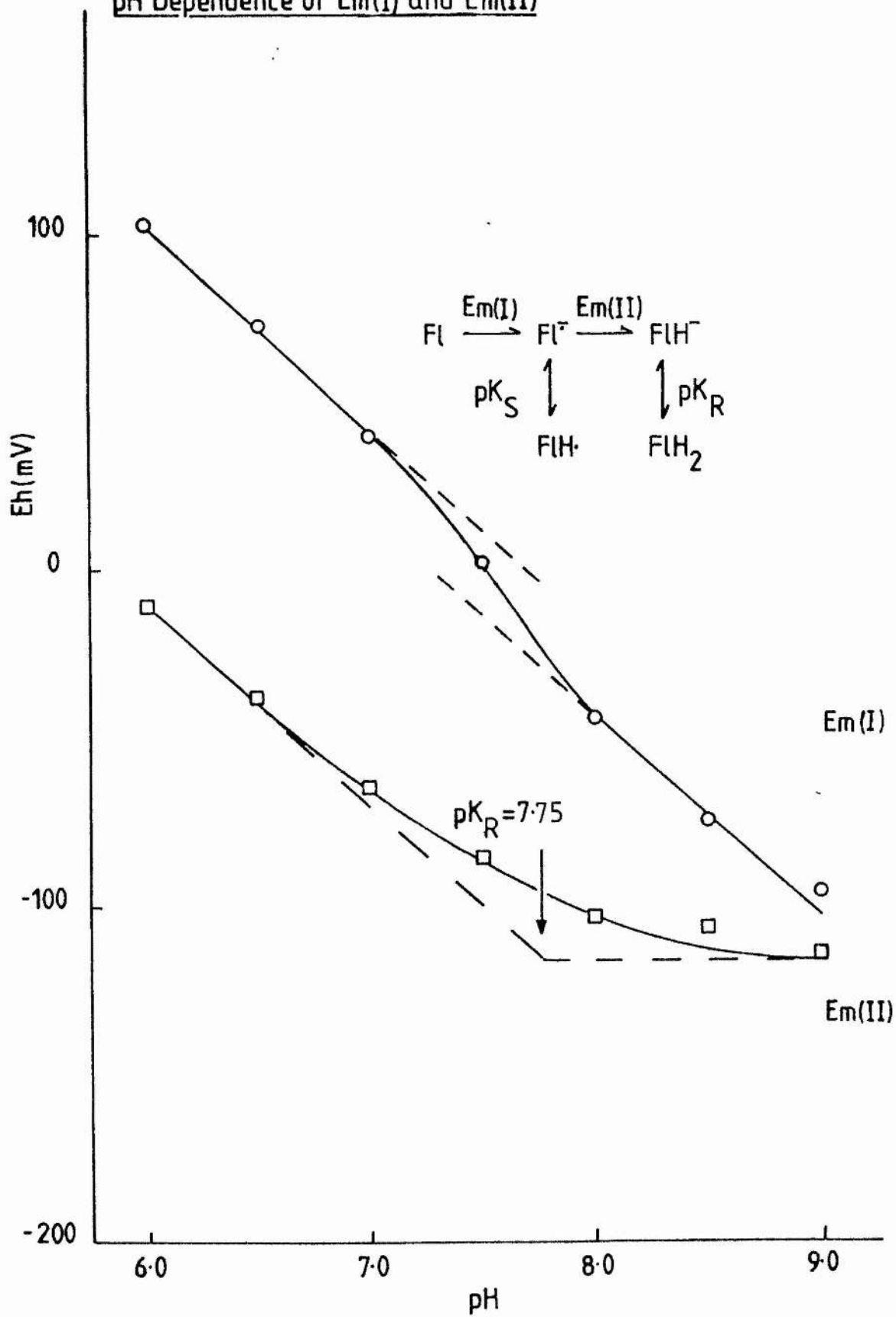
where n is the number of electrons and a is the number of protons.

Figure 6.8

pH dependence of $E_m(I)$ and $E_m(II)$

The pH dependence of $E_m(I)$ and $E_m(II)$, the mid-point potentials of the two 1-electron transfer reactions are shown. The two mid-point potentials were calculated as described in the text, from the data presented in fig.6.6 and fig.6.7 pK_R was estimated from the intersect of the two linear portions of the curve for $E_m(II)$, as shown.

pH Dependence of Em(I) and Em(II)



At the mid-point potential the first term is zero so the measurement of the mid-point potential will vary linearly with pH:

$$E_m = E^{\circ} - \frac{0.06a}{n} \cdot \text{pH}$$

For a 1-electron reaction a slope of 120mV/pH arises from a 2-proton dependent process.

The formation of the fully reduced form of the flavin, from the flavin semiquinone (as characterised by $E_m(\text{II})$), was shown to tend towards pH independence, as the pH value exceeded the value for pK_R (Ohnishi *et al.* 1981, Dawes 1980), and the fully reduced form of the flavin became predominantly un-protonated. The plot of $E_m(\text{II})$ versus pH changes from a slope of -60mV/pH to 0mV/pH, indicating the change in pH dependence associated with pK_R . An estimate of pK_R can be obtained from this plot, from the intercept of the two linear portions of the curve (fig.6.8). The pH dependence of the formation of the fully reduced form of the flavin free radical changes at pH's $> \text{pK}_R$; $\text{FlH}^{\bullet} \leftrightarrow \text{FlH}_2$ is superseded by $\text{FlH}^{\bullet} \leftrightarrow \text{FlH}^-$. A value for pK_R of 7.75 was estimated from the pH dependence of $E_m(\text{II})$. The plot of $E_m(\text{I})$ was taken to reflect neither of the pK values for the protonation of the semiquinone or the fully reduced form of the flavin. The pH dependence of $E_m(\text{I})$ was taken as an indication that the flavin semiquinone was present as the protonated (neutral) form throughout the pH range under study. Thus the pK_S of the

semiquinone was not reached in this pH range. The 1-electron step between the oxidised flavin and the semiquinone was thus $F1 \leftrightarrow F1H^*$.

The flavin semiquinone free radical from fumarate reductase has thus been shown to be reasonably, thermodynamically stable in the physiological pH range, with its stability increasing as the pH is raised. The linewidth of the flavin free radical was measured to be 1.12mT, at pH 7.0, which is narrow for the neutral form of the semiquinone. The narrow linewidth of the 8- α substituted flavin is usually associated with the anionic form of the flavins (Edmondson *et al.* 1981). Edmondson *et al.* (1981) concluded that the flavin semiquinone of succinate dehydrogenase was present as the anionic form throughout the pH range 6.1 to 9.1, because of the constant, narrow linewidth measured (1.2mT). However Ohnishi *et al.* (1981) showed that the pK value was such that at pH 7.0 the flavin would be 90% protonated (neutral) and become unprotonated (anionic) at higher pHs. It was concluded that the narrow lineshape must be due to delocalisation of the free radical electron, or that the protonation occurs on the protein rather than the flavin moiety, because the protonation does not cause any significant change in the e.p.r. linewidth. The e.p.r. linewidth of the flavin free radical resonance from fumarate reductase was observed to be constant over the pH range studied (pH 6.0 to pH 9.0). It would thus appear that the flavin moiety of fumarate reductase is similar to that of succinate

dehydrogenase in that respect. It is thus unaffected by the binding of the protons as no line broadening of the resonance, due to hyperfine interaction with the proton nuclear moment was seen.

6.2.3 Spatial relationship

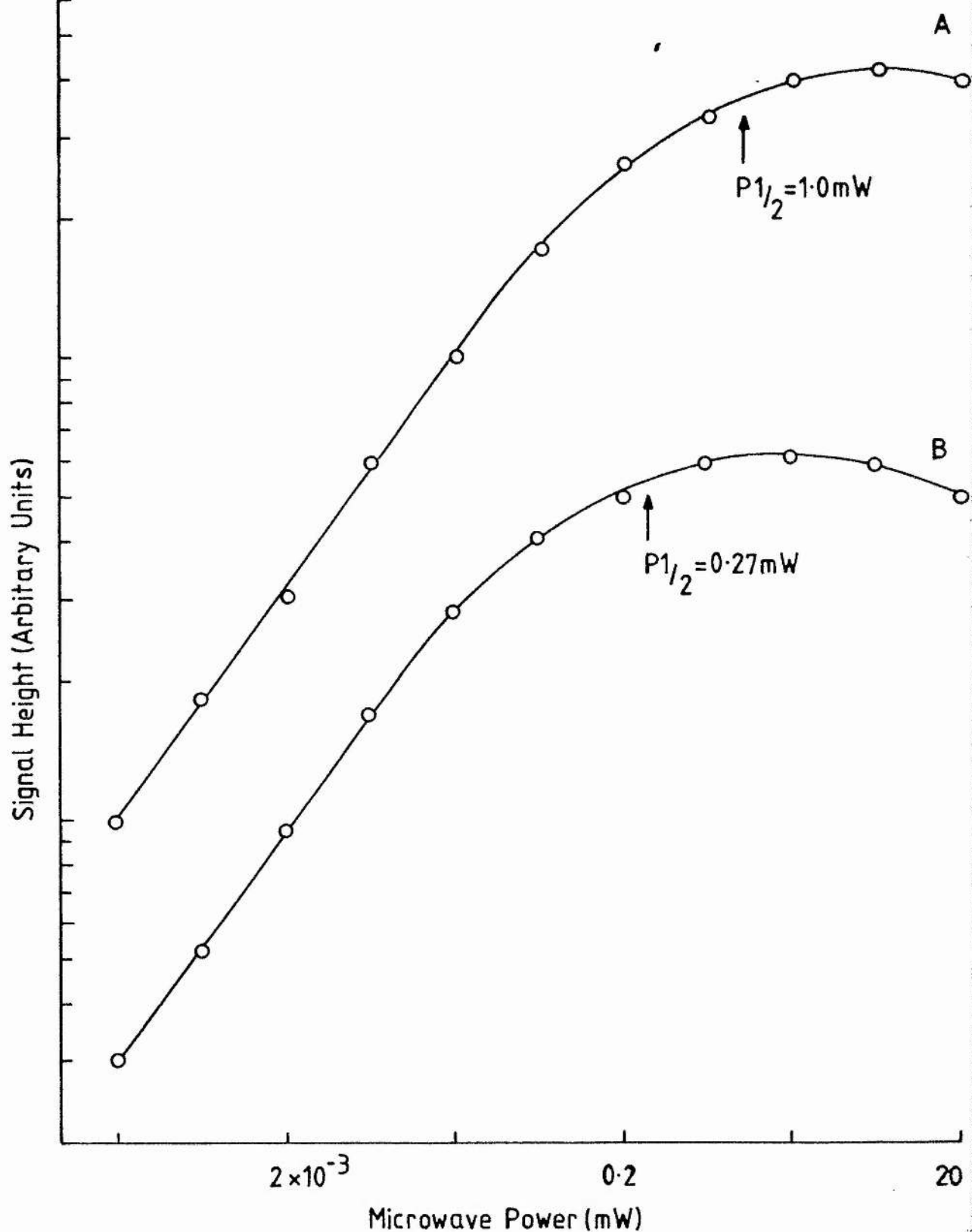
Ohnishi *et al.* (1981) showed that the flavin moiety of the bovine-heart succinate dehydrogenase was in close proximity to the iron-sulphur centre, S1 of succinate dehydrogenase. The spatial relationship of the fumarate reductase flavin moiety to the iron-sulphur centre, FR1 was studied by changes in the power saturation properties of the flavin free radical in the presence and absence of paramagnetic FR1. Fig.6.9 shows the power profiles of the flavin free radical at 180K. $P_{1/2}$, the saturation parameter (as defined in chapter 4), was measured from the power profiles and used as an indication of the saturation of the flavin. The upper curve shows the power saturation profile from the flavin free radical in isolated fumarate reductase poised at a potential of -80mV. The lower profile is from fumarate reductase that had been treated to destroy the iron-sulphur clusters, by lowering to pH 3.0 for 10 minutes. The enzyme was then brought back to pH 7.0 and the profile determined as for the untreated sample. A significant change in the $P_{1/2}$ was observed between the two preparations. However the possibility of another environmental change, other

Figure 6.9

Power profiles of the flavin free radical, 180K

Power saturation profiles of the flavin free radical from fumarate reductase are shown. Profile A: the enzyme as isolated was poised at -80mV. Profile B: acid-treated enzyme poised at -80mV. The experimental conditions were as described for fig.6.1 and the temperature was 180K. The protein concentration was approximately 7mg/ml.

Power Profiles of the
Flavin Free Radical, 180K



than the loss of FR1, induced by the low pH cannot be excluded from causing the change in P1/2. To test this the P1/2 of the flavin free radical was measured at an ambient electrode potential of 30mV, where the concentration of paramagnetic FR1 was minimal (Table 6.1). A lower value for the P1/2, as compared to the sample at -80mV, was again observed indicating that at this potential there was no relief from power saturation. The relief of power saturation at -80mV was therefore taken to be due to interaction with FR1. It was also of interest to note that there was apparently no obvious interaction with centre FR3, which is paramagnetic at the higher potential. If interaction with this centre occurred then relief of power saturation would also be expected at this higher potential. The possibility of direct interaction between the flavin and this iron-sulphur centre can thus be excluded or assumed to be very weak. Table 6.1 summarises the results obtained, and compares those obtained here for fumarate reductase, to those obtained by Ohnishi *et al.* (1981) for succinate dehydrogenase. The effect of paramagnetic FR1 was to cause relief of the power saturation of the flavin semiquinone, indicating that interaction must occur between these redox centres. The relief of saturation was observed over a range of temperatures, with concomitant increase in the value found for P1/2 of the flavin, as the temperature was raised. The interaction between FR1 and the flavin will also affect the e.p.r. properties of the iron-sulphur centre, but under the conditions of observation

Table 6.1

Saturation parameter (P1/2) for the flavin free radical

<u>Sample</u>	<u>P1/2 (mV)</u>	
	<u>F.R.</u>	<u>S.dH.</u>
Normal enzyme (-80mV)	1.0	0.78*
Acid-treated enzyme (-80mV)	0.27	0.23*
Normal enzyme (30mV)	0.30	-

Abbreviations: F.R., fumarate reductase; S.dH., succinate dehydrogenase. * Actual redox potential for these P1/2 values was -78mV, data reproduced from Ohnishi *et al.* (1981).

Experimental conditions as described for fig.6.9, temperature was 180K and the protein concentration was approximately 7mg/ml.

of the iron-sulphur centre, the flavin will be heavily saturated, so any interaction may not be observable in the e.p.r. behaviour of FR1 (chapter 4).

The strength of the interaction can be used to estimate the distance between the two interacting centres and this will provide information on the possibility of electron transfer between the two centres. Ohnishi *et al.* (1982) developed a method for the estimation of the distance between two interacting chromophores, from the enhancement of the spin-lattice relaxation time of a slow relaxing centre by interaction with a fast relaxing centre. The spin-lattice relaxation time (T_1) of the flavin was estimated from $P1/2$, and T_1 was assumed to be equal to T_2 in the absence of interaction. T_1 of the iron-sulphur centre FR1 can be estimated from the temperature dependence of the lifetime broadening of this centre (chapter 5, Gayda *et al.* 1976). T_1 of the flavin was estimated to be approximately 5×10^{-6} s and T_1 of centre FR1 was estimated at approximately 3×10^{-8} s.

δw (the difference in the resonant microwave frequency between the two centres) was estimated using the g -values of the flavin and the root-mean-square value of g ($\bar{g} = 1.959$) for FR1 (Zweier 1983). Averaging the angular term, as the samples are randomly oriented frozen solids, a distance estimate of 11.3\AA was calculated between FR1 and the flavin free radical. This distance is slightly shorter than that estimated for the distance between the flavin and S1 of succinate dehydrogenase

(Ohnishi et al 1982, 12-18Å). The limit for exchange interaction can be set at 15-16Å (Coffman & Buettner 1979a), which by definition allows electron transfer upto these distances, by orbital overlap. The dipolar coupling of the two redox centres indicates that the distance between the centres can allow other methods of electron transfer such as electron-tunnelling (Beinert 1982). The distance estimated was determined by assuming the interaction between FR1 and the flavin was largely dipolar in nature, an assumption that is valid only in the absence of a large exchange component. The distance estimate also assumes a point dipole approximation, so the distance estimate will most likely be an edge to edge approximation between the two centres and can be taken as a minimum distance between them. The contribution from exchange interaction over the distance estimated is likely to be small (J in the order of a few cm^{-1}), because exchange interactions fall off more quickly than dipolar interactions (Coffman and Buettner 1979a & b). The distance between the two redox centres can thus be estimated at to be in the region of 11Å to 17Å, if a radius of 3Å is allowed for the two redox centres, as no splitting of the flavin resonance was observed, but a strong P1/2 effect of FR1 spins on the spins of the flavin was observed. A minimum distance of 12Å was estimated by Ohnishi et al. (1981, 1982) for the distance for which no dipolar broadening/splitting can be observed between interacting chromophores, when one of the chromophores is more rapidly relaxing than the other. This approximation will hold for the interaction between FR1 and the flavin of fumarate reductase

because of the two orders of magnitude difference between their relaxation rates under the conditions of study.

6.3 Conclusion

The flavin moiety from fumarate reductase has been shown to be very similar to that of bovine-heart succinate dehydrogenase. The flavin semiquinone titrated with a mid-point potential (E_m ; $Fl_{ox} \leftrightarrow FlH_2$, $n = 2$) of approximately $-12mV$ at pH 7.0, when the interaction with FR1 was taken into account. This value is $60mV$ more positive than was found for succinate dehydrogenase (Ohnishi *et al.* 1982), this may be a function of the different directions of electron flow in the two enzymes. The flavin semiquinone was shown to be in the neutral (protonated) form at physiological pH's. Estimates of the pK value of the protonation of the fully reduced form of the flavin was found at approximately 7.75 and 8.05, which are in reasonable agreement. The pK of the semiquinone could not be estimated, in the pH range studied. The maximum concentration of the flavin semiquinone was measured at approximately 8% of the total flavin at pH7.0, but a more accurate value of 12% was estimated by adjusting for the interaction with FR1, and allowing for saturation. This value increased at higher pH's, showing the stabilisation of this free radical at these higher pH's, when the free radical was mainly in the anionic (non protonated) form. The flavin free radical formation constant (K) for the flavin semiquinone

free radical was estimated at 1.69×10^{-2} , at pH 7.0, indicating that the protonated form of the free radical can act as a stable intermediate in electron transfer from the iron-sulphur clusters to fumarate.

Interaction between the flavin free radical and FR1 was observed and the distance between the two chromophores estimated at 11 \AA to 16 \AA , assuming a largely dipolar interaction. Interaction between FR3 and the flavin free radical was excluded or shown to be weak as there was no large relief of power saturation of the flavin semiquinone in samples that contained both it and FR3 in paramagnetic states.

CHAPTER SEVEN

Studies on the Orientation of the Iron-Sulphur Clusters

7.1 Introduction

A variety of electron and hydrogen carriers have been studied in oriented membrane multilayers from bacterial, mitochondrial and other sources, using optical and e.p.r. spectroscopy (Blasie et al. 1978, Blum et al. 1978a & b, Blum & Poole 1982, Erecinska et al. 1978a & b). It has been found that the multilayers generally confer order about a single axis, upon the redox carriers (Blasie et al. 1978, Blum et al. 1978b). The iron-sulphur clusters from bovine-heart succinate dehydrogenase have been shown to be specifically oriented with respect to the membrane normal, as have several other types of chromophore (Salerno et al. 1979a, Blum et al. 1978a, Barlow & Erecinska 1979, Erecinska et al. 1978a & b).

The effect of disorder on the spectra of chromophores in oriented multilayers has been studied by computer simulations (Blum et al. 1978a & b), and these used to determine the orientation and estimate the disorder (mosaic spread). The mosaic spread was found to arise from stacking disorder of the multilayers and from the chromophore disorder. This latter term arises from non-rigid orientation of the chromophore within the protein and of the protein within the membrane. In order to relate the e.p.r. signals to the structural information, knowledge of the electronic configuration of the chromophore is required. Gibson et al. (1966) produced a model, relating g-tensors to the structure, which is generally

accepted for the binuclear ferredoxin clusters, but no such model has been proposed for the tetranuclear or trinuclear clusters.

Where there is dipolar coupling between redox carriers, it can be studied in oriented multilayers, as dipolar interactions show an angular dependency, of $(1 - 3\cos^2\theta)$, Salerno et al. 1977), where θ is the angle between the magnetic field and the inter-spin vector. Under conditions where the effects of spin coupling can be observed, the angle of the vector between the coupled chromophores can be determined for the membrane bound redox carriers (Salerno et al. 1977, 1979).

In this chapter the orientations of the intrinsic iron-sulphur centres of fumarate reductase, of E. coli are described. Strains of E. coli with amplified and non-amplified expression of fumarate reductase were used. The strain with amplified expression of this enzyme was found to produce crystal membrane multilayers, because of the high concentration of fumarate reductase in these membranes.

7.2 Results and Discussion

7.2.1 Signals Observed From Succinate Reduced Multilayers

The reduction of membrane multilayers using aqueous solutions, whilst retaining the oriented nature of the multilayers, has been a problem in their preparation (Erecinska et al. 1978a). Blum et al. (1980) overcame this problem to some extent by preparing their multilayers in the absence of oxygen. This resulted in partially reduced multilayers which could then be further reduced by addition of the reductants. A similar method was used to obtain the multilayers used in this study (see Methods), which resulted in partially reduced membranes that had both HiPIP and ferredoxin signals, as shown by e.p.r. spectroscopy (data not shown). Upon addition of sodium succinate or sodium dithionite the HiPIP signal disappeared and the size of the ferredoxin signal increased (fig.7.1 & 7.7). For studies of the HiPIP centre, multilayers were partially dehydrated in the presence of air to produce oxidised multilayers.

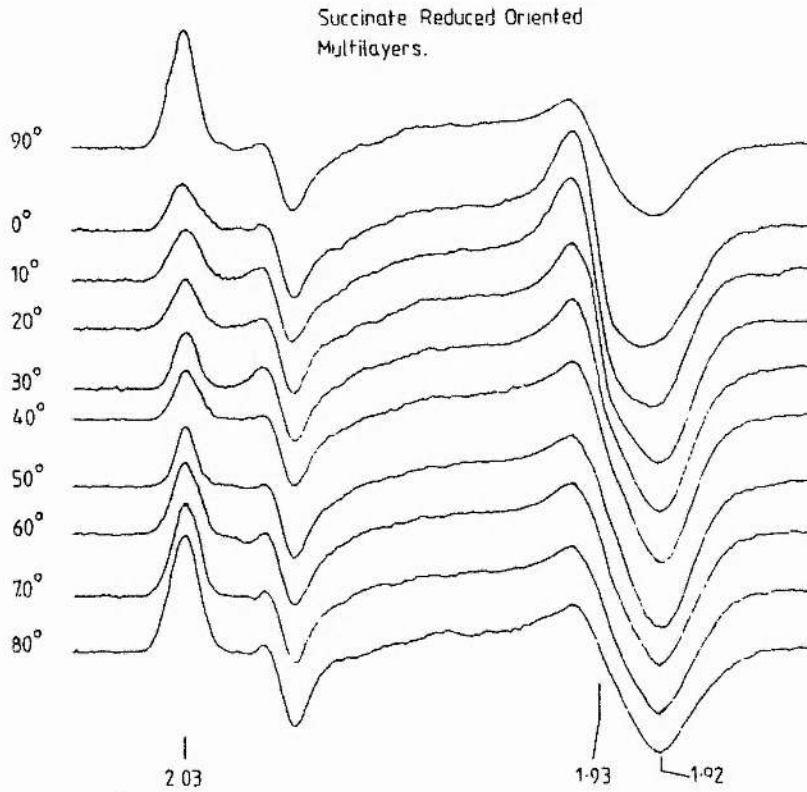
The spectra from succinate reduced multilayers, shown in fig.7.1, possessed the ferredoxin signal with principal g-values of $g = 2.03$ and $g = 1.93$, attributed to FR1. The signal amplitude of the e.p.r. spectra was clearly seen to be dependent on the angle of the multilayer to the magnetic

Figure 7.1

E.p.r. spectra of succinate reduced oriented multilayers

The e.p.r. spectra from membrane multilayers reduced anaerobically with sodium succinate, are shown at various angles of the applied magnetic field to the plane of the membrane multilayers. The angles are shown on the left of the spectra and the major g-values are indicated below the spectra. The sample temperature was 34 K. The e.p.r. conditions were: incident microwave power, 20mW; microwave frequency, 9.48GHz; modulation amplitude, 1mT; modulation frequency, 100KHz; receiver gain, 6.3×10^4 ; time constant, 500ms; scan rate 0.1mT/s.

Succinate Reduced Oriented
Multilayers.

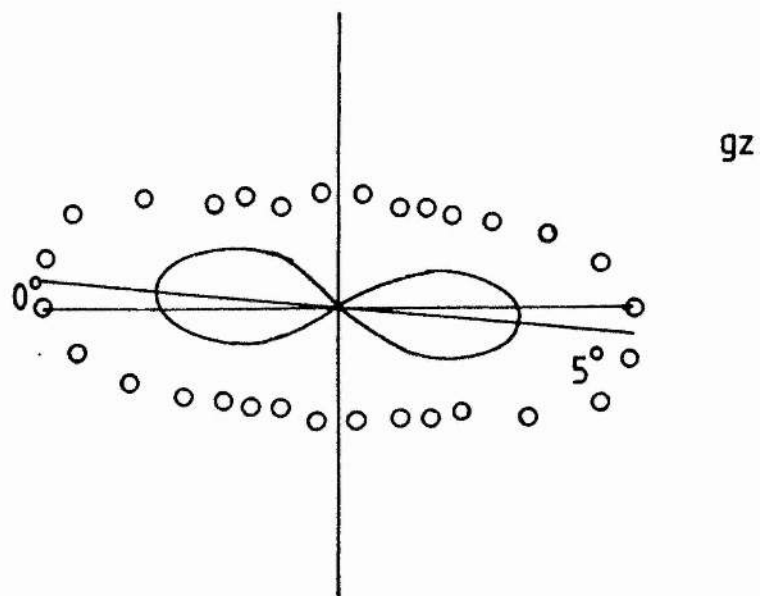
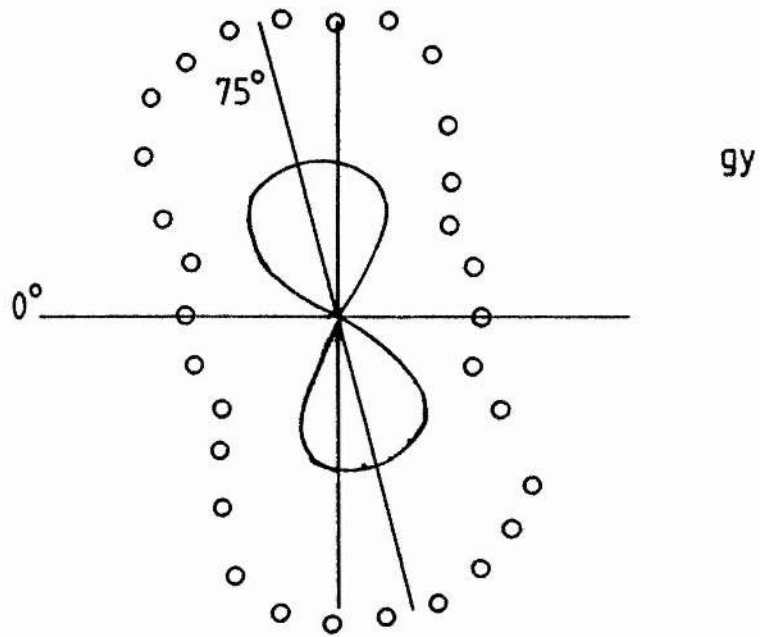
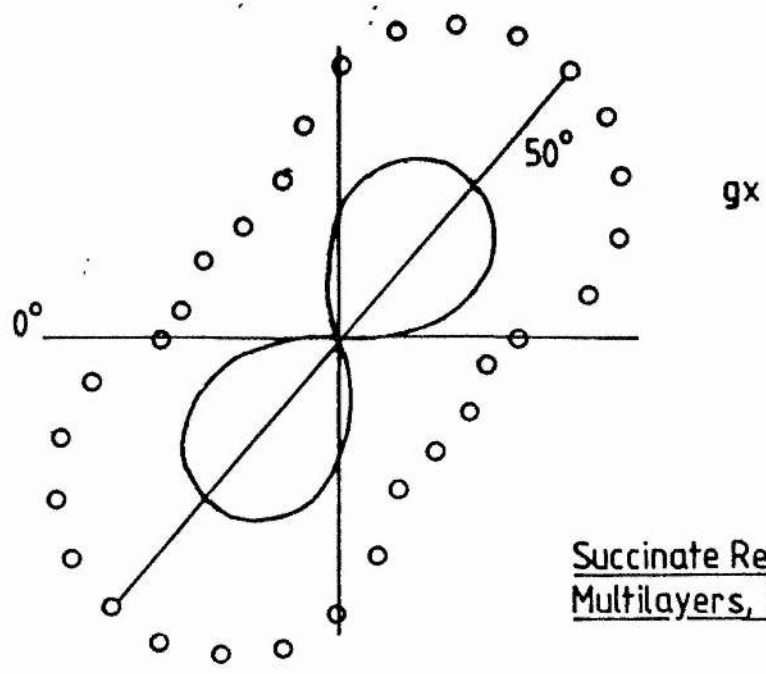


field. The signal amplitude of each g-tensor (x,y & z) is shown, replotted in fig.7.2, to indicate the angle of maximum amplitude, of the multilayer to the applied magnetic field. 0° was taken to be when the multilayer was normal to the magnetic field. The $g = 2.03$ signal (gz) was shown to be maximum when the angle between the multilayer and the magnetic field was approximately 90° (5° from the membrane normal, fig.7.2). This angle is different from that obtained for gz of S1 from either bovine-heart or E. coli succinate dehydrogenase, where the angle of maximum amplitude was in the plane of the multilayers (Salerno et al. 1979a, Blum et al. 1980). The $g = 1.93$ (gy) signal was maximal at an angle of approximately 75° to the membrane normal and the $g = 1.915$ (gx) signal was maximal at an angle of approximately 50° to the membrane normal. The equivalent g-tensors from S1 were 90° (gx) and 0° (gy) for both the E. coli and the bovine-heart enzymes. Thus FR1 from fumarate reductase is oriented differently, within these membrane, from S1 of succinate dehydrogenase (both sources). This is an important criterion for consideration of the spatial relationships of the iron-sulphur centres of these two enzymes. Interactions between paramagnetic species, that are largely dipolar in nature (over distances greater than $10 - 12 \text{ \AA}$), show an angular dependency by definition. The differing orientation of the iron-sulphur clusters of the two enzymes may affect the strengths of any interactions between them or with other paramagnetic species (flavin), and so influence the catalytic

Figure 7.2

Angular dependence of e.p.r. signal amplitude from succinate reduced multilayers

Plots for the three separate g-tensors are shown. The 1.915 signal (gx) was measured from the high field base-line to the negative peak, the 2.03 (gz) signal was measured from the low field base-line to the positive peak and the 1.93 (gy) signal was measured from the high field base-line to the positive peak, to avoid interference from the gx tensor. The experimental points are shown (o), together with the angular dependence of the signal amplitude when corrected for the membrane disorder. 0° was taken as the direction of the membrane normal. The angles of peaks of signal amplitude are indicated where they occur. Experimental conditions were as in fig.7.1.



properties of the enzymes. However, because of the crystalline nature of the membrane multilayers from the fumarate reductase amplified strain of *E. coli*, close comparisons cannot be drawn to the data presented for succinate dehydrogenase (see later).

The experimental spectra (fig.7.1) can be simulated using a computer program (Blum et al. 1978a & b), over the range 0° to 90° , to obtain the disorder inherent in the multilayer system. Fig.7.3a & b show computer simulations of the e.p.r. spectra of centre FR1. The angles used for the simulations were $\theta = 5^{\circ}$ (angle of gz to the membrane normal) and $\phi = 50^{\circ}$ (angle of gx to the membrane normal); the angles used for mosaic spread are shown with the spectra. As the experimental spectra show little or no angular variation of g-values, for FR1, the lower limit of the mosaic spread can be set at approximately 25° (Salerno et al. 1979a, Blum et al. 1978a). Comparison of the experimental and simulated spectra (fig.7.1, 7.3a & b) put the mosaic spread at between 30° and 60° . Fig.7.4 shows the results from e.p.r. spectra simulated using a mosaic spread of 35° , which gave a good fit to the experimental spectra. The mosaic spread is a measure of the amount of 'wobble' of the chromophore with respect to the magnetic field (Blum et al. 1978a & b), and arises from the unoriented areas of the multilayers, the spread of the chromophore within the protein and the spread of the protein within the membrane.

Figure 7.3

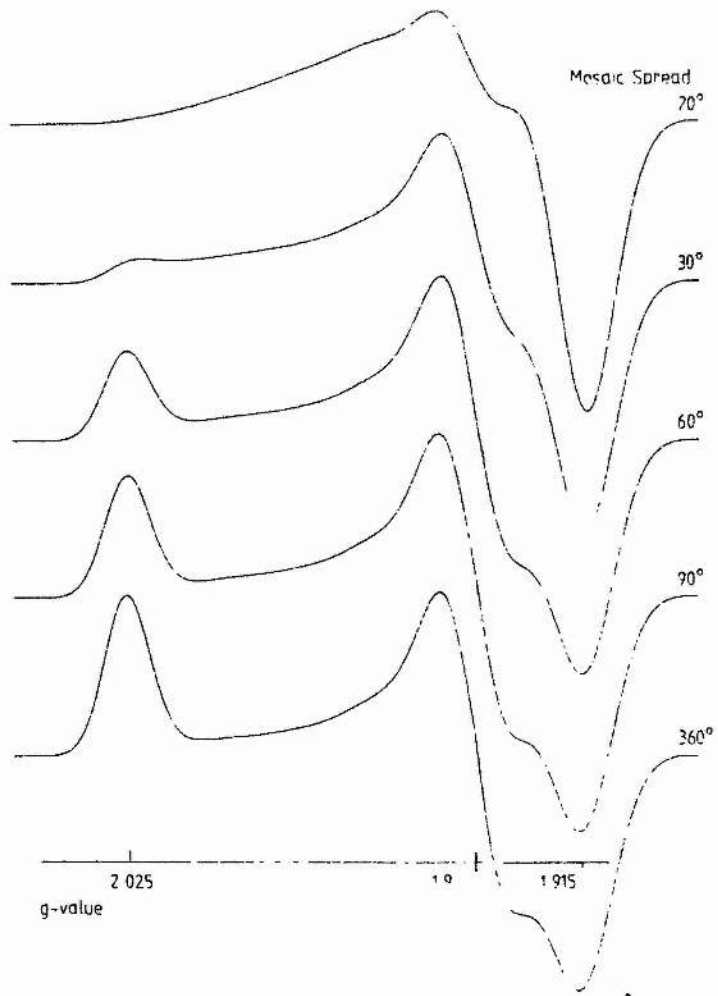
Computer simulations of e.p.r. spectra of centre FR1

The e.p.r. spectra of centre FR1 are shown simulated with different degrees of membrane disorder (mosaic spread). The principal g-values used for the simulations were $g_z = 2.025$, $g_y = 1.93$ and $g_x = 1.915$. The linewidths employed were 1.1mT (g_z), 1.25mT (g_y) and 1.5mT (g_x), and were assumed to have a Gaussian derivative lineshape. The angle of the g_z axis to the membrane normal (θ) was taken as 5° and the angle of the g_x axis to the membrane normal (ϕ) was taken as 50° . The values used for the mosaic spread are shown on the right of the spectra and the g-values are indicated below the spectra.

a) Computer simulations of centre FR1 with the angle of the applied magnetic field to the plane of the membrane multilayers taken to be 0° (parallel).

b) Computer simulations of centre FR1 with the angle of the applied magnetic field to the plane of the membrane multilayers taken to be 90° (perpendicular).

Computer Simulations, FR1
Parallel to Membrane Plane



Computer Simulations, FR1
Perpendicular to Membrane Plane

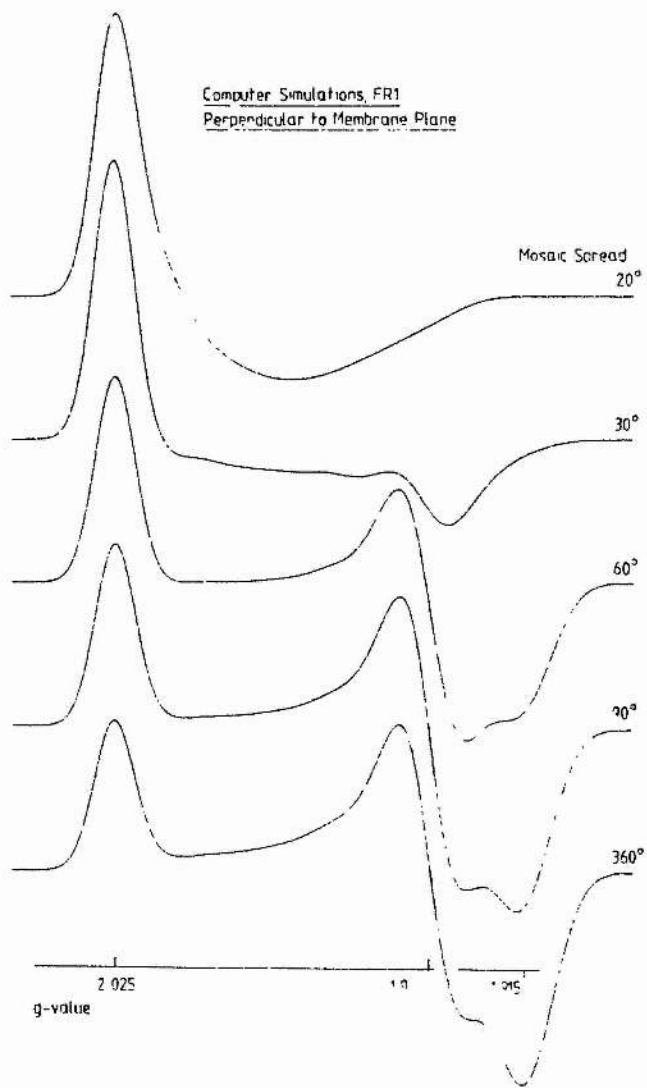
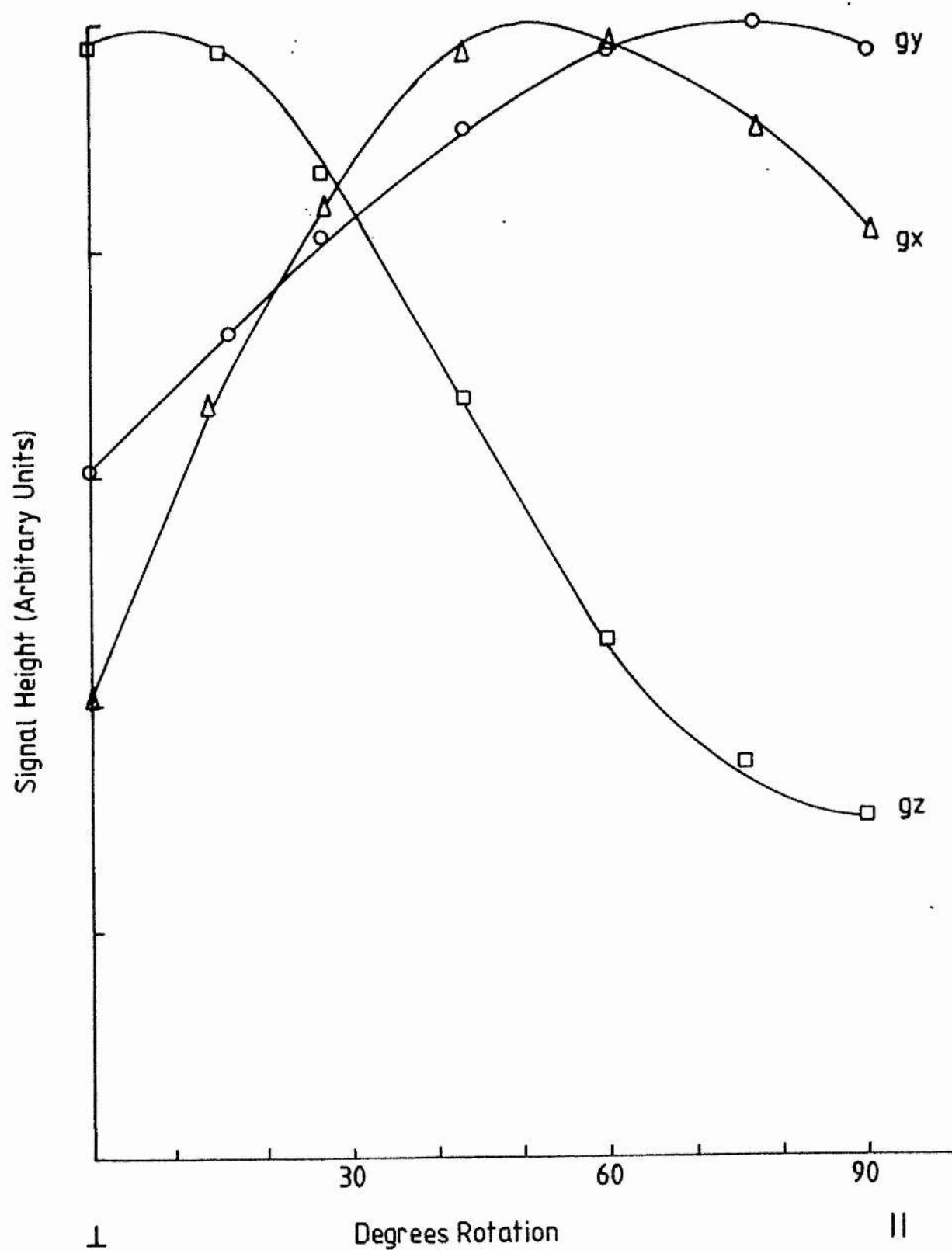


Figure 7.4

Angular dependence of e.p.r. simulations

The amplitude of the e.p.r. signals from the computer simulations are shown versus the multilayer orientation. The parameters of the computer simulation were as described in fig.7.3, and the mosaic spread was assumed to be 35° . The e.p.r. signals were measured as described for fig.7.2. 0° degrees of rotation of the multilayer, was taken as perpendicular to the plane of the membrane plane. The peak in gz signal amplitude (\square) was obtained at approx. 5° , that of gy (\circ) at approx. 75° and that of gx (Δ) at approx 50° .

Simulation of Angular Dependence of
EPR Signal, FR1



The most notable result from the oriented multilayers prepared from JRG1031, the strain of *E. coli* with amplified expression of fumarate reductase, was that the angular dependence for each g-tensor gave rise to only two peaks of signal amplitude, when the multilayers were rotated through 360° (fig.7.2). This is an unusual result for membrane multilayers derived directly from *E. coli* cells, as it indicates that the fumarate reductase in these multilayers has order within the membrane plane, as well as to the membrane normal. Fig.7.5 shows a sketch of the structure of a chromophore within normal membrane multilayers. The angular dependence of signal height should reach a maximum at four angles (θ , two either side of the membrane normal), when the magnetic field bisects the cone subtended by the g-tensor (g_z in fig.7.5). This is clearly not the case for FR1 from fumarate reductase in the membrane multilayers from strain JRG1031. Fig.7.6 shows a sketch of the structure of a chromophore within crystal membrane multilayers, where the chromophore does not have disorder within the plane of the multilayer. For this system, only two peaks of signal amplitude will occur as the vector from the g-tensor becomes parallel to the magnetic field. In the case of g-tensors that are oriented parallel to either the membrane normal or membrane plane, only two peaks of signal amplitude will be observed for either system. For the non-crystalline multilayer system the cone of disorder of the protein within

Figure 7.5

Model for a chromophore with rhombic symmetry, within oriented multilayers

The model indicates the three major g-tensors and their angles to the membrane normal (θ , ϕ). The chromophore is assumed to have order relative to the membrane normal and disorder within the membrane plane. All possible orientations about the membrane normal, describe the cone indicated for g_z . As the multilayers are rotated about the axis shown, the signal height due to g_z , produces the plot shown below the sketch. Peaks of signal height are reached at four angles, all at θ^0 either side of the membrane normal, as indicated. The signal amplitude of the other g-tensors will behave similarly.

Model for Oriented Multilayers

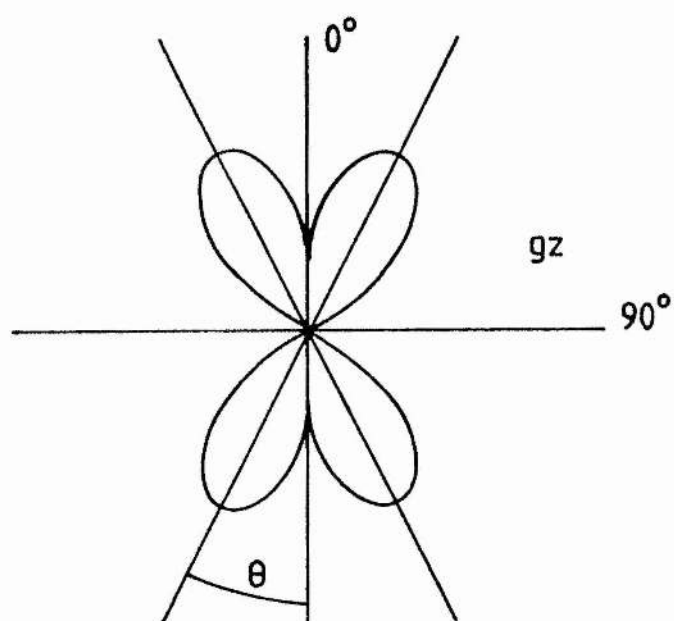
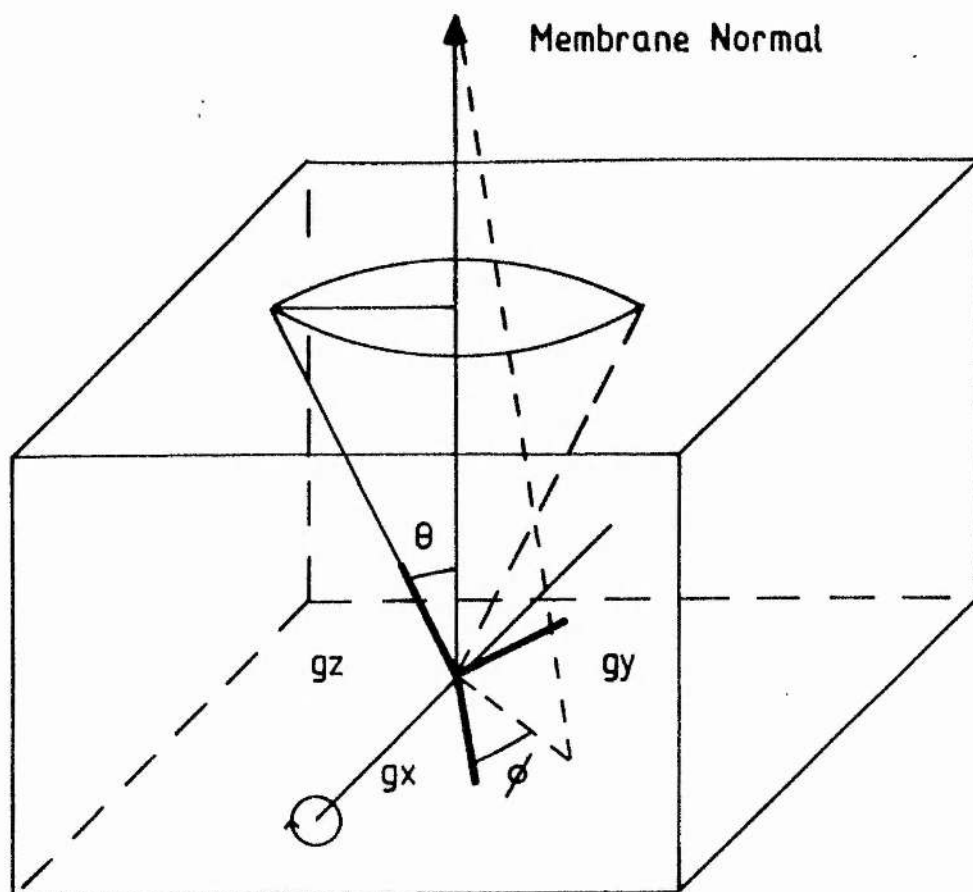
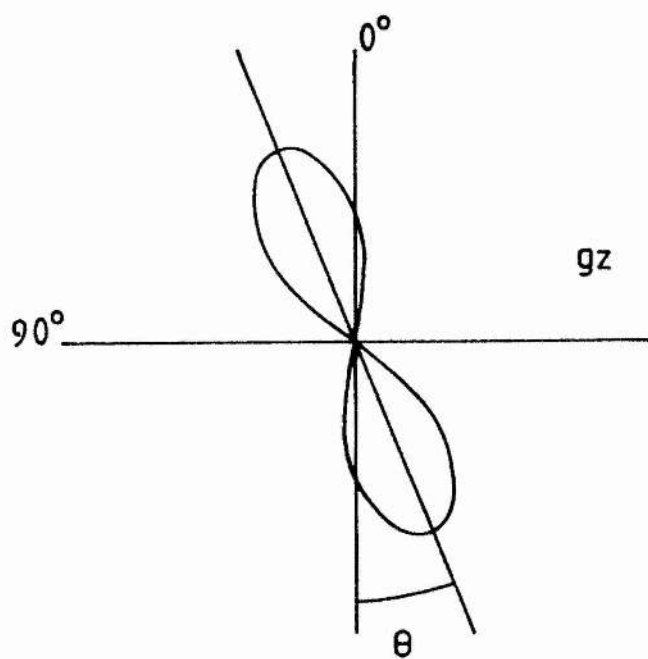
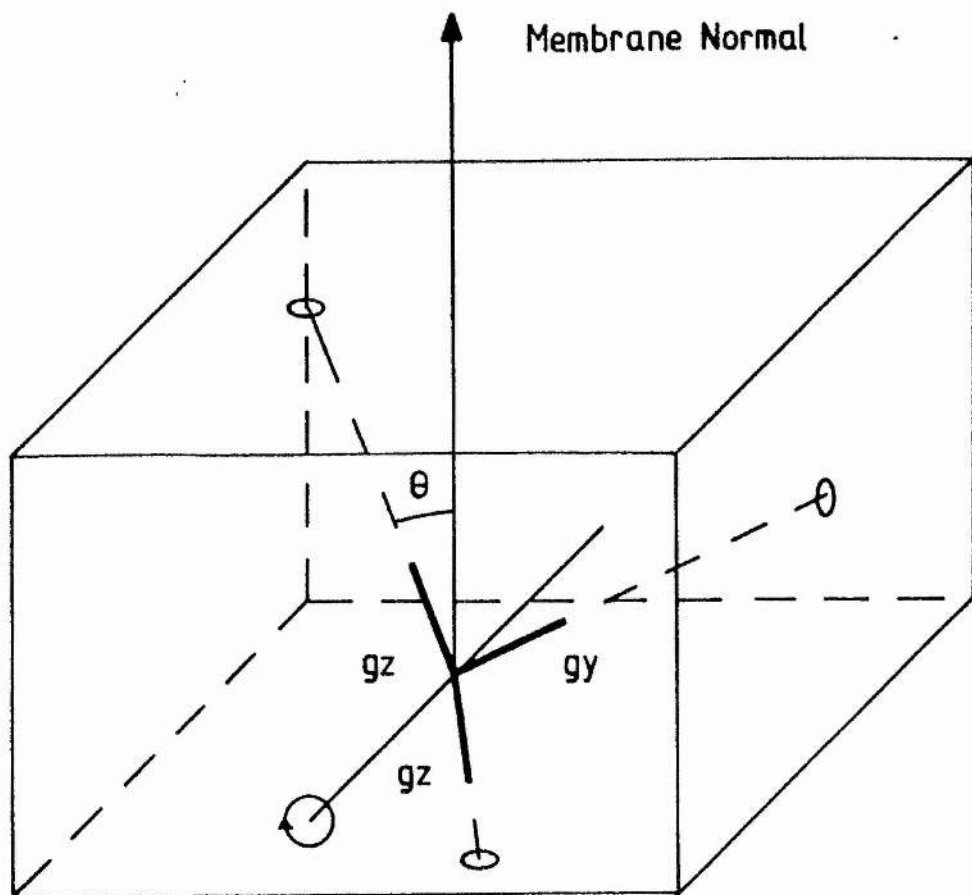


Figure 7.6

Model for a chromophore with rhombic symmetry, within crystalline multilayers

The chromophore is shown with the same angles as fig.7.5. This model assumes order in the plane of the membrane as well as to the membrane normal, for the chromophore. The g-tensors still have some degree of disorder, due to wobble of the chromophore in the protein and of the protein in the membrane, as indicated by the small circles. When rotated about the axis indicated, only two peaks of signal amplitude are observed for each g-tensor, as shown below the sketch, due to the more ordered environment of the chromophore.

Model for 'Crystal' Multilayers



the membrane reaches a minimum for these cases. The g_x of FR1 is clearly not oriented in one of these directions and thus points to the crystal nature of these membranes (as does the orientation of the other centres, see later). Further studies were performed to investigate this phenomenon (see later).

7.2.2 Signals from Dithionite Reduced Multilayers

The experimental spectra obtained from multilayers reduced with dithionite are shown in fig.7.7, and the signal height replotted against the angle of the multilayers, to the magnetic field, in fig.7.8. The angular dependence for the e.p.r. spectra, from dithionite reduced multilayers is clearly different, to those from succinate reduced multilayers. The g_z (2.03) signal reaches a maximum at approximately 25° to the membrane normal, whilst the g_y (1.93) and the g_x (1.915) show maxima in signal height at approximately 10° and 70° to the membrane normal respectively. In dithionite reduced multilayers there are probably two paramagnetic iron-sulphur centres from fumarate reductase (FR1 and FR2, chapter 4), so the signals from both of these will contribute to the e.p.r. spectra. The g_z angular dependency of signal amplitude shows small peaks at approximately 5° to the membrane normal. These can be attributed to the g_z of FR1 (fig.7.3), but the g_y and g_x results do not show these smaller peaks from FR1. Under the

Figure 7.7

E.p.r. spectra of dithionite reduced oriented multilayers

The e.p.r. spectra from membrane multilayers reduced with sodium dithionite are shown at various angles of the applied magnetic field to the plane of the membrane multilayers. The angles are shown to the left of the spectra and the major g-values are indicated below the spectra. The sample temperature was 10 K and the e.p.r. conditions were as in fig.7.1 except the receiver gain was 6.3×10^3 .

Dithionite Reduced Oriented Multilayers.

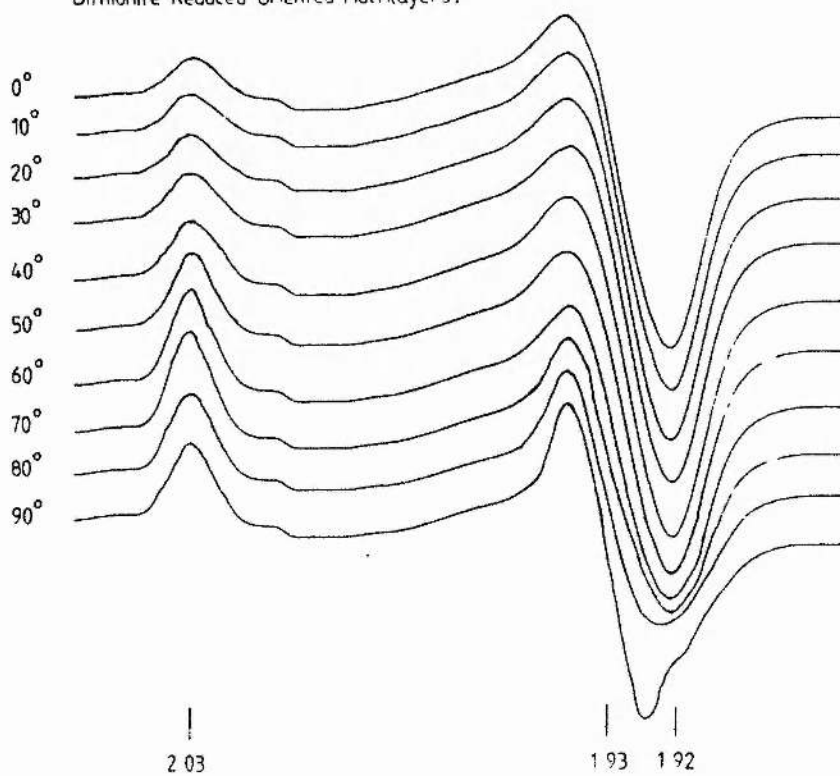
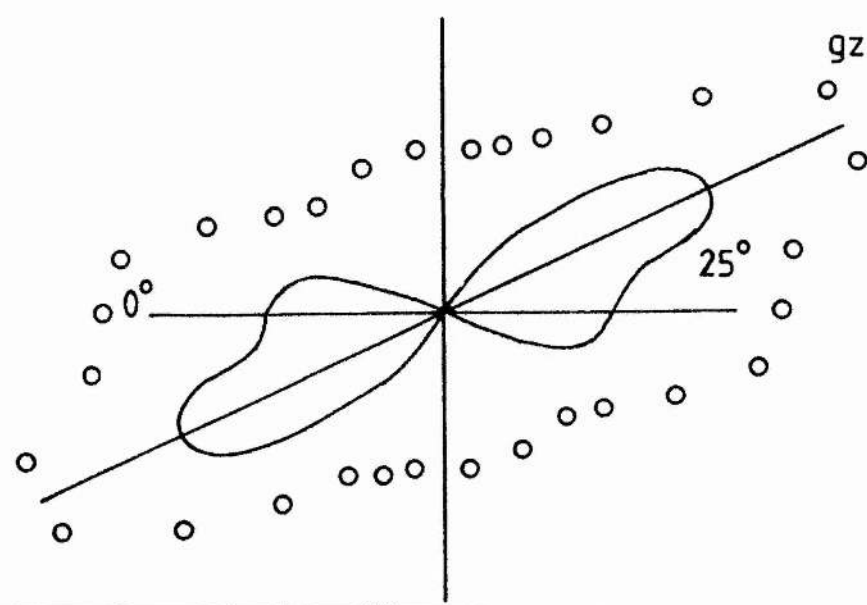
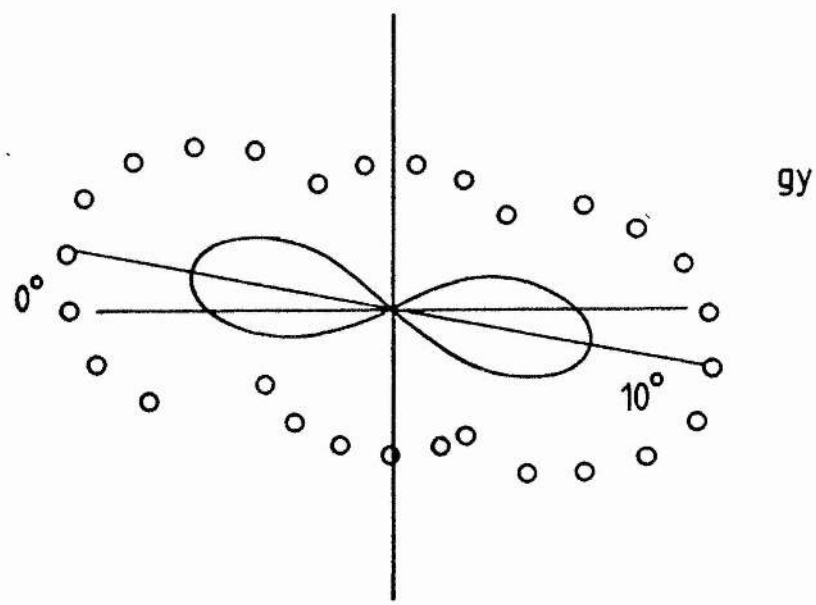
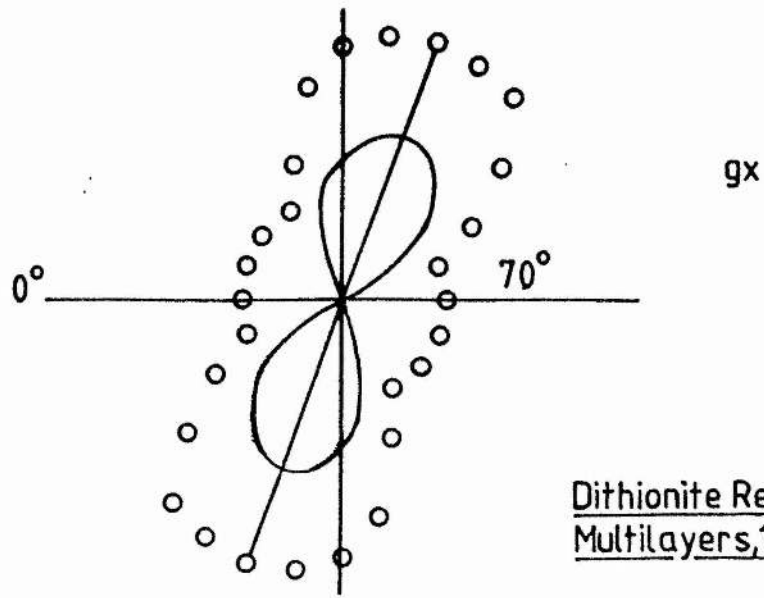


Figure 7.8

Angular dependence of e.p.r. signals from dithionite reduced multilayers

Plots for the separate g-tensors are shown. The e.p.r. signals were measured as described for fig.7.2. The experimental points are shown (o), together with the angular dependency of the signal amplitude after correction for the mosaic spread. The field angles are defined as for fig.7.3. The angles of peaks of signal amplitude are shown where they occur. Experimental conditions were as described in fig.7.7.



conditions at which the e.p.r. spectra were obtained from the dithionite reduced membranes (10 K, 20mW microwave power), the signal from FR1 would be heavily saturated if there was no interaction. It has been shown that the presence of FR2 in a paramagnetic state causes a relief of this saturation (chapter 4), by interaction with FR1. The interaction of the centres would be expected to be largely dipolar in nature (Salerno *et al.* 1979b), because of the estimate of distance from the observed effects ($>10 \text{ \AA}$, chapter 8). This interaction will show an angular dependence also, so we cannot readily interpret the results from the dithionite reduced multilayers, other than to offer tentative explanations. The simplest explanation of the observed results is that the reduction of the multilayers with dithionite causes reorientation of centre FR1 within the protein, by a conformational change, and that this then has the same orientation as centre FR2. The second possible explanation is that the angular dependence observed is for the spin-coupling of FR1 and FR2, in dithionite reduced multilayer. In the case of the first explanation (reorientation of FR1) the e.p.r. spectra would arise from both these centres FR1 and FR2 but they cannot be distinguished. The two peaks in g_z could be explained by the multilayers not all being reduced by dithionite, so leading to two enzyme populations of FR1 with different orientations. Under conditions where the e.p.r. spectrum from FR2 is non-detectable, due to extreme lifetime broadening (50 K, 2mW microwave power), the same orientation of the g -tensors was

observed from dithionite reduced multilayers (data not shown). This may therefore indicate that centre FR1 has undergone reorientation, if the signal arises from FR1 alone, the shift in angular dependence of the g-tensors (20° shift, g_x ; 65° shift, g_y ; 30° shift g_z) being caused by a conformational change induced in the protein structure. In the case of the second explanation; in the absence of paramagnetic FR2, FR1 would be heavily saturated under the conditions employed. The behaviour of FR2 cannot be determined in the absence of FR1, because of the nature of their redox chemistry. However, as the spin-coupling is mutual to both centres, it may be assumed that there is some relief of saturation of FR2, by the spin-coupling. The observed angular dependence of the g-tensors from dithionite reduced multilayers may therefore reflect the angular dependence of the spin-coupling between the two centres, because the signal from each centre will reach a maximum (due to relief of saturation) as the vector between the centres becomes parallel to the applied magnetic field. The same angular dependence of the g-tensors at 50K and 2mW microwave power, would still hold for the spin-coupling, because even though FR2 is not e.p.r. detectable it is still paramagnetic. This phenomenon was further investigated and will be reported later (chapter 8). Thus the angular dependence and hence orientation of FR2 cannot readily be determined. The smaller peak in g_z , attributable to FR1, was assumed to arise from parts of the membrane multilayers that were not fully reduced by dithionite.

7.2.3 Signals Observed from Oxidised Multilayers

The e.p.r. spectra obtained from air oxidised membrane multilayers are shown in fig.7.9, where the angles are expressed to the membrane plane. The e.p.r. spectrum typical of the HiPIP centre from this class of enzyme was seen with major g -values of 2.01 (g_z), 1.978 (g_y) and 1.955 (g_x). The spectra from multilayers showed greater rhombicity between g_y and g_z , than did the powder spectrum from unoriented samples, with g_y shifted from approximately $g = 1.99$. The value for g_x is that obtained for the temperature of observation of the spectra shown (6 K), as this g -value was temperature dependent (chapter 4). The shift in g_y may reflect the well ordered nature of the environment of the multilayer samples, from the strain of E. coli with amplification of fumarate reductase. The signal amplitude of each g -tensor is replotted in fig.7.10, versus the angle of the magnetic field to the membrane normal. It was again observed that the g -tensors for this centre gave only two maxima for the signal height, when the multilayer was rotated through 360° . The peaks in signal height were observed at approximately 33° to the membrane normal ($g = 2.01$, g_z), at approximately 70° to the membrane normal ($g = 1.978$, g_y) and at approximately 47° to the membrane normal ($g = 1.955$, g_x). The mosaic spread of the membrane multilayers was estimated as for FR1, using $\theta = 33^\circ$ and $\phi = 47^\circ$. A value of 30° for the mosaic spread gave the best fit to the experimental spectra (data not shown). The angles of orientation determined for the HiPIP centre (FR3),

Figure 7.9

E.p.r. spectra of oxidised oriented multilayers

The e.p.r. spectra from membrane multilayers dehydrated in the presence of air are shown at various angles of the magnetic field to the plane of the membrane multilayers. The angles are shown on the left of the spectra and the major g-values are indicated below the spectra. The sample temperature was 6 K and the e.p.r. conditions were as described for fig.7.1, except the receiver gain was 5×10^3 .

Oxidised Oriented Multilayers

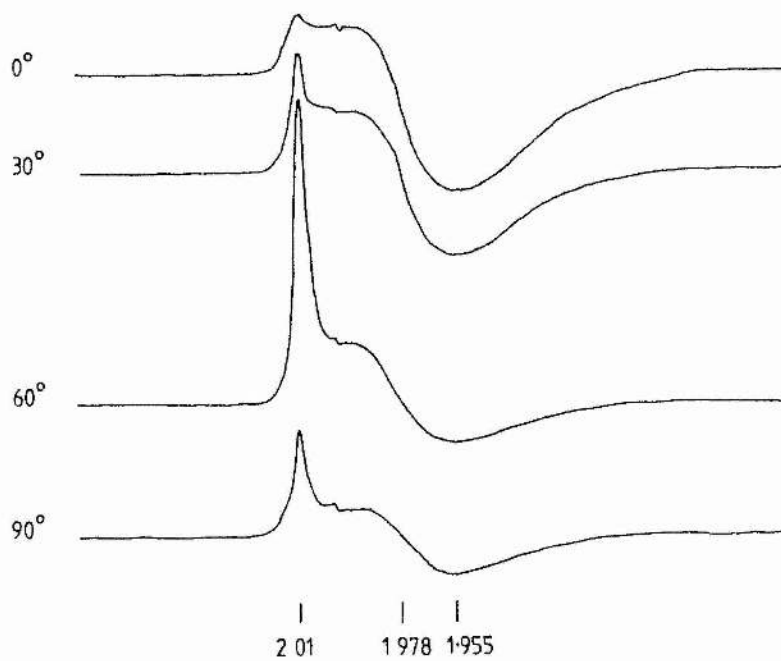
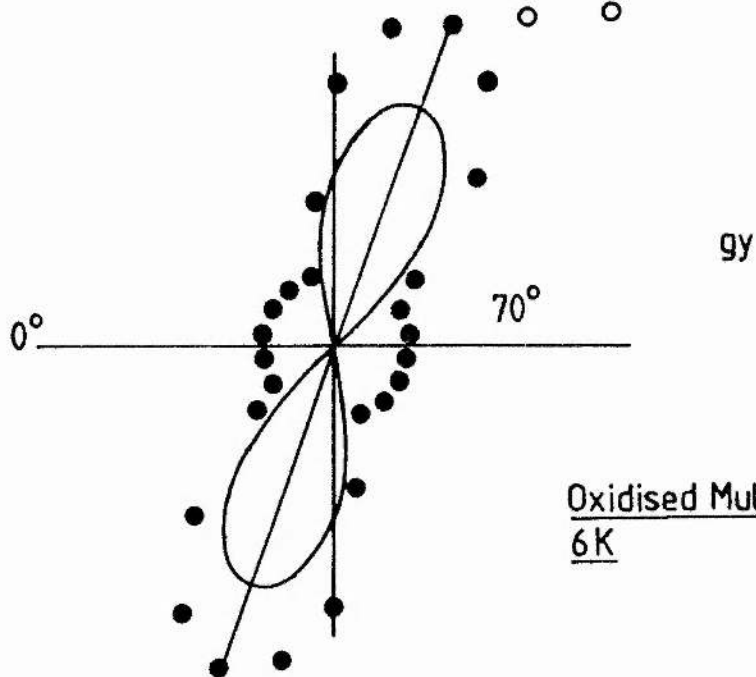
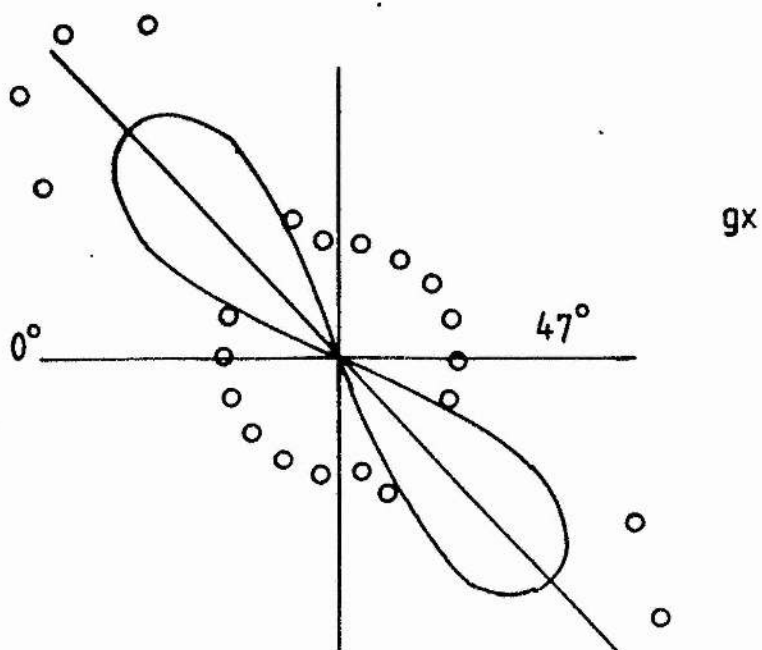


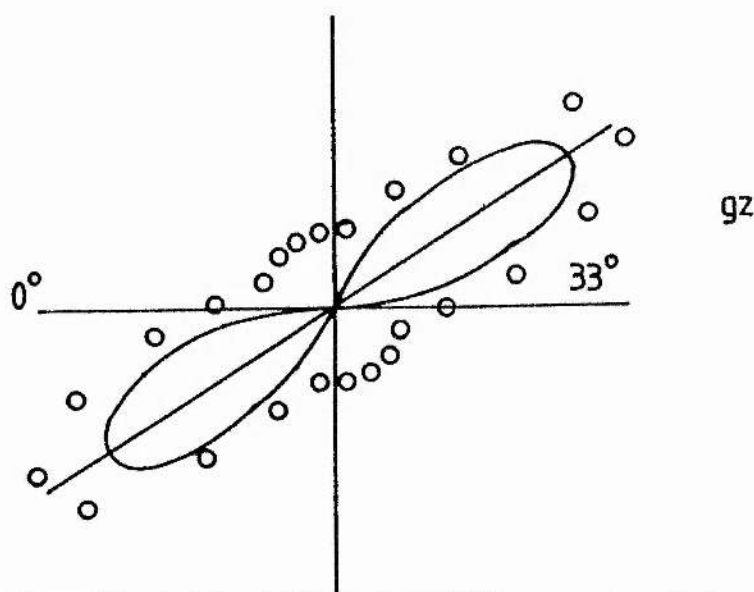
Figure 7.10

Angular dependence of e.p.r. signal amplitude from oxidised multilayers

Plots for the three major g-values are shown. The signal amplitude of the three major g-tensors was measured as described for fig.7.2. The experimental points are shown (o) together with the angular dependency of the g-tensors after correction for the mosaic spread. The field angles are as described for fig.7.2 and the peaks of signal amplitude are shown where they occur. The experimental conditions were as described for fig.7.9.



Oxidised Multilayers
6K



are again different from those of the equivalent centre from succinate dehydrogenase, where the gz axis was found to be perpendicular to the membrane plane and gx and gy to be in the plane of the membrane multilayers (bovine-heart, Salerno et al. 1979a; E. coli, Blum et al. 1980). The orientation of the g-tensors of the HiPIP centre cannot be related to any of its structural parameters, because of the lack of knowledge of the relationship between them. The different angles for the two well oriented centres (FR1 & FR3) that have been observed for fumarate reductase, compared to the equivalent centres from succinate dehydrogenase, indicate a major difference between the two enzymes. The orientation may affect the strength of the interaction between the intrinsic centres of the enzymes and thus offer a partial explanation for their differing catalytic abilities, together with the different redox chemistry of the centres. However, these results were again from the crystalline multilayers so close comparison to the results for succinate dehydrogenase cannot be drawn.

7.2.4 Studies on a Non-amplified Strain of E. coli

The observed phenomenon that indicated crystal membrane multilayers was further investigated to determine the nature of the system, and to obtain results that could be more closely compared to those of succinate dehydrogenase. Studies were performed on a wild-type strain of E. coli (EMG2), to

determine whether the crystal membranes were the result of the amplification of fumarate reductase in the E. coli membranes. The results from centres FR1 and FR3 are shown in fig.7.11 & 7.12, as plots of the signal amplitude versus the angle of the membrane multilayers to the applied magnetic field (0° parallel to the membrane normal). For both centres it was clearly seen that the g-tensors showed an angular dependence, that indicated the enzyme was in a non-crystalline environment (four maxima of signal height). The angular dependencies were however, significantly different from those obtained in the amplified membranes. The peaks of signal amplitude for FR1 were obtained at approximately 60° (gz), 60° (gy) and 30° (gx), with all angles relative to the membrane normal. These are also significantly different from those angles obtained for the equivalent centres from succinate dehydrogenase (90° , 0° & 0° to the membrane normal, Blum et al. 1980, Salerno et al. 1979a). The angular dependencies of FR3 showed maxima in signal amplitude at approximately 0° (gz), 90° (gy) and 40° (gx), which shows no greater similarity to the results published for succinate dehydrogenase (90° , 0° & 0°). The iron-sulphur centres of fumarate reductase were thus shown to be oriented at different angles to those of succinate dehydrogenase, with a 30° difference for all three g-tensors of FR1 compared to S1. The HiPIP of fumarate reductase was shown to be oriented with gz (90°), gy (90°) and gx (50°) all at different angles to those of S1. Thus a major difference between the two enzymes has been shown.

Figure 7.11

Angular dependence of e.p.r. signals of succinate reduced multilayers from a wild-type strain of E. coli

The angular dependencies of all three major g-tensors are shown. The signal amplitude was measured and the field angles are defined as described in fig.7.2. The angles of the peaks of signal height are indicated where they occur. The experimental conditions were as described in fig.7.1, except the receiver gain was 1.25×10^5 and the sample temperature was 20 K.

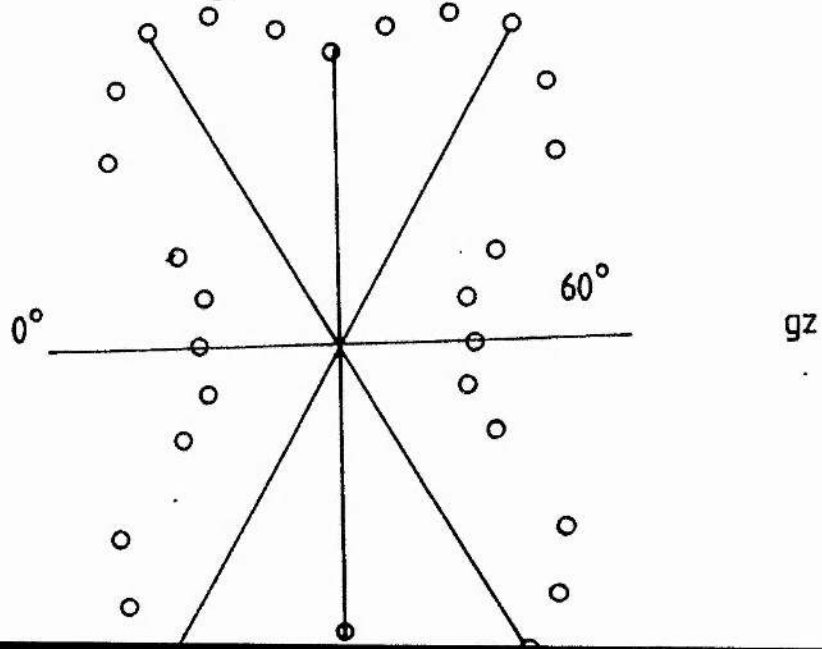
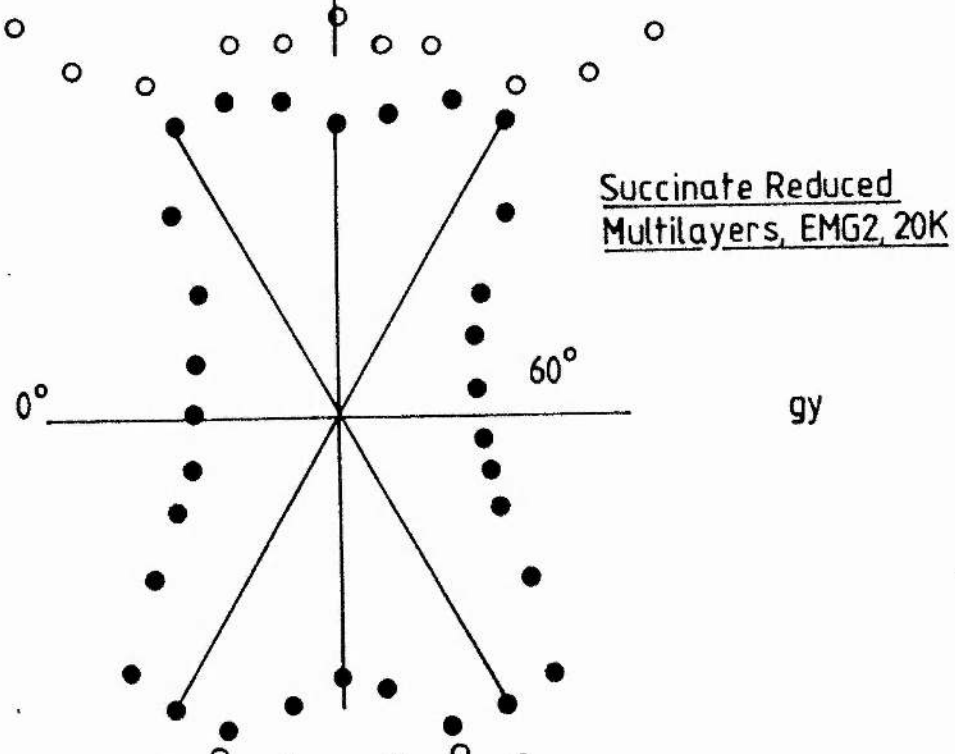
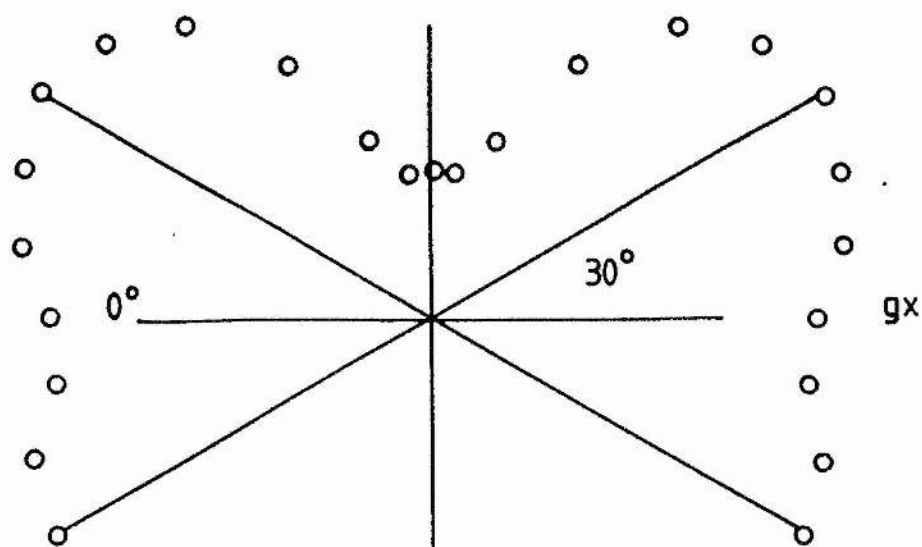
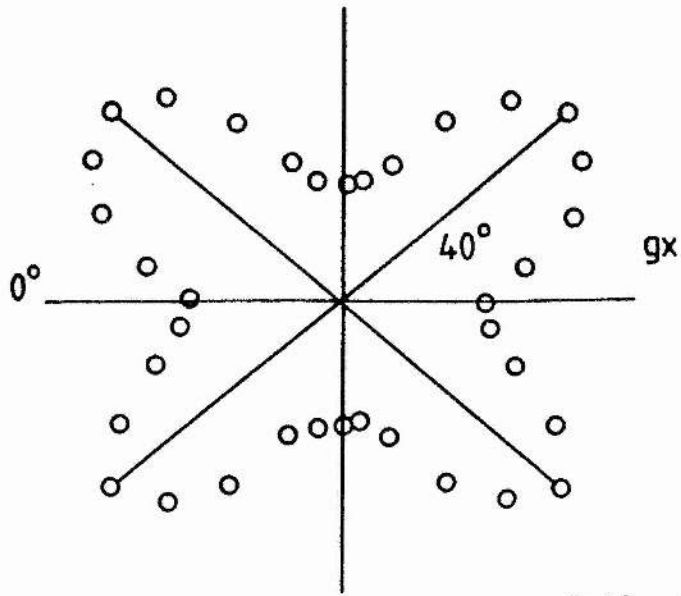


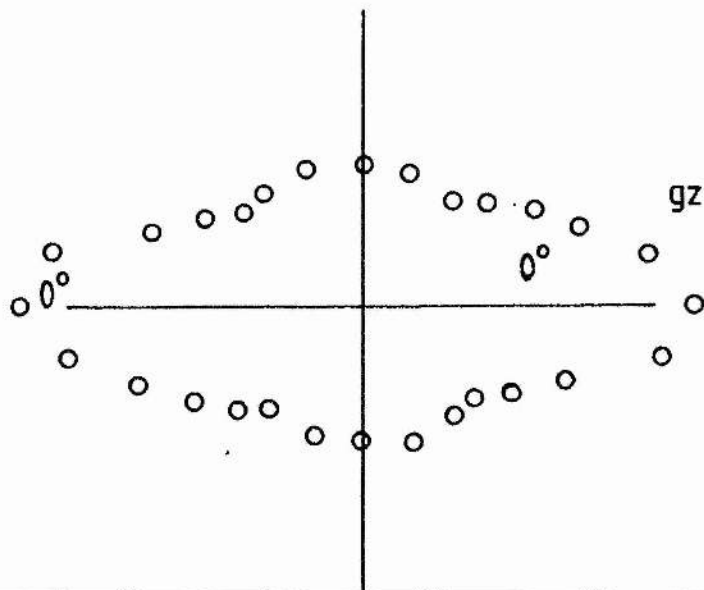
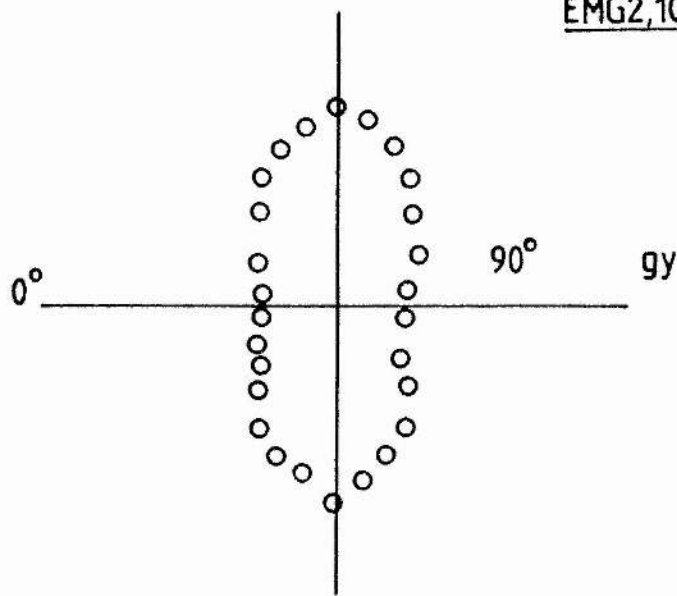
Figure 7.12

Angular dependence of e.p.r. signals of oxidised multilayers
from a wild-type strain of E. coli

Plots of the three major g-tensors are shown. The signal amplitude was measured and the field angles are defined as described in fig.7.2. The angles of peaks of signal amplitude are shown where they occur. The experimental conditions were as described in fig.7.1, except the receiver gain was 1.0×10^5 and the sample temperature was 10 K.



Oxidised Multilayers
EMG2,10 K



The production of crystal membrane multilayers was shown to be due to the amplification of fumarate reductase within the membranes of *E. coli*. The level of fumarate reductase in the membranes from JRG1031 was estimated at approximately 25% of the total membrane protein, from the concentration of acid non-extractable flavin and the spin intensity of the iron-sulphur centres (1.94 and 1.96 nmol/mg protein respectively), and assuming a molecular weight of 125 000 dalton for fumarate reductase. The feasibility of forming membrane crystals is thus apparent, though there will be interference defects from the other membrane proteins, to the crystal structure. The structure will however be similar to that found for crystals formed by vesicles from detergent solutions of proteins (Deatherage *et al.* 1982, Henderson 1981, Fuller *et al.* 1979). Fumarate reductase has been shown to form these membrane crystals in multilayers from a strain with amplified expression of the enzyme, without lengthy manipulations and so the suitability of these membranes for structural determinations has been shown. The work presented herein compliments and extends that already performed by Weiner and coworkers, who have shown two-dimensional arrays of fumarate reductase in strains amplified with the enzyme (Weiner *et al.* 1984a & b, Elmes & Weiner 1985). Their studies, by electron microscopy, have shown the fumarate reductase as knobs on the inner membrane surface and on novel membranous structures produced by their strains to

accommodate the additional fumarate reductase produced. They have shown levels of fumarate reductase in excess of 50% of the membrane bound protein (Weiner et al. 1984b).

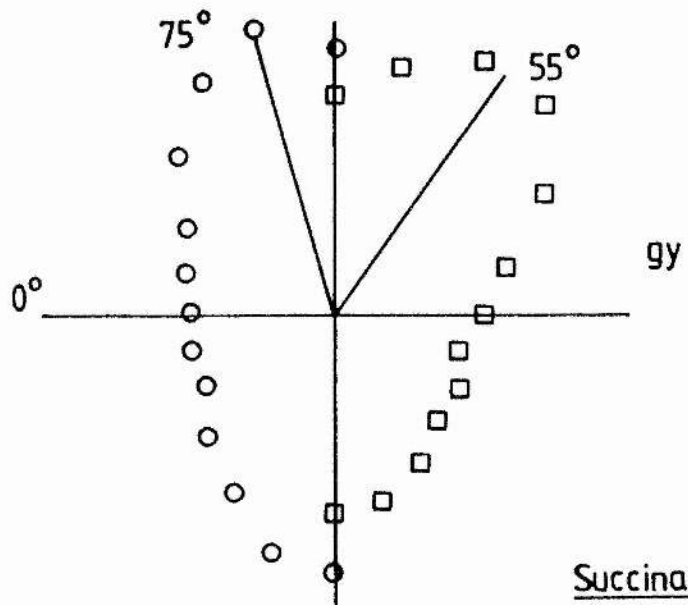
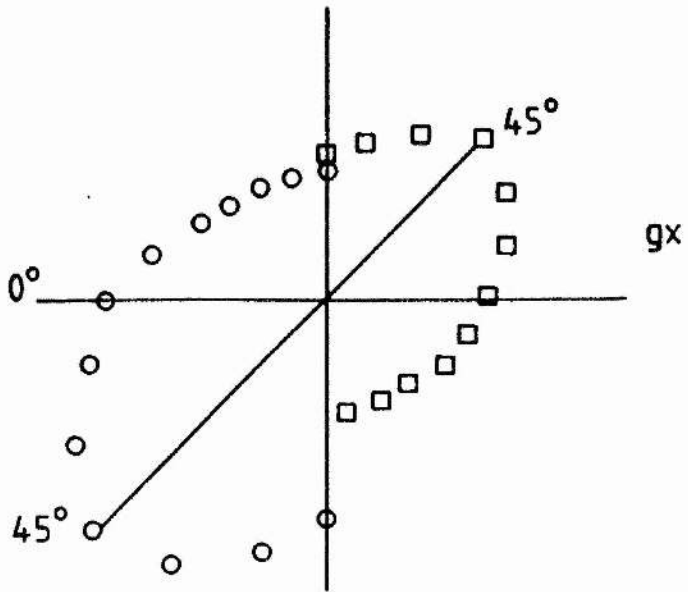
7.2.5 Studies on the Crystal Membranes

Further studies were performed to confirm the crystal nature of the membrane multilayers, produced from the strain of E. coli with amplified expression of this enzyme. If the fumarate reductase molecules are all ordered in the same manner with respect to the membrane plane, then strips cut at different angles from the multilayer sheets should show differing angular dependencies, for the g-values of the iron-sulphur centres. Each strip of membrane will contain fumarate reductase oriented at a different angle, unlike non crystalline multilayers where the enzyme can be oriented at random about the membrane normal, but still oriented at the same angle to the membrane normal. A change in the angular dependency was observed for both FR1 and FR3. Fig.7.13 & 7.14, shows the results for these clusters for strips cut at right-angles from the Mylar sheet. The angular dependencies are clearly different for each centre from the two strips. For FR1 angular dependencies of g_z with maxima at approximately 10° and 0° for the two strips were observed. Maxima at approximately 75° and 55° for g_y, and 45° for both strips for g_x were also seen. The HiPIP centre showed the following dependencies: 30° and 0° (g_z); 90° and 0° (g_y), and

Figure 7.13

Angular dependence of e.p.r. signals of succinate reduced multilayers cut at right-angles

The strips of membrane multilayers were cut at right-angles from the sheet of multilayers produced, as described in Methods. The experimental points on the left (o) of the plots were of a strip cut perpendicular to that which gave the experimental points on the right of the plots (\square). The angle for peaks of signal amplitude from each set of data is indicated. The field angles and measurement of signal amplitude were as described for fig.7.2. and the experimental conditions were as described for fig.7.2, except the temperature was 25 K.



Succinate Reduced
 Multilayers, 25K
 90° Cuts

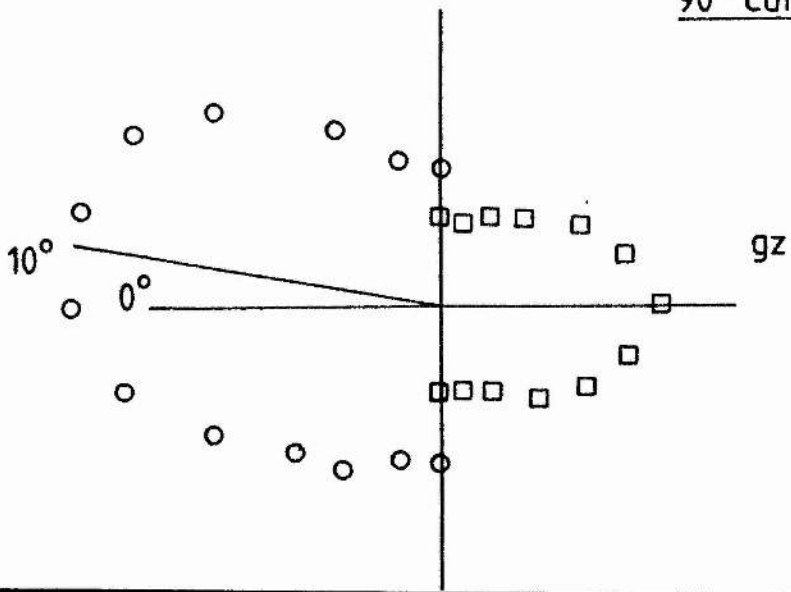
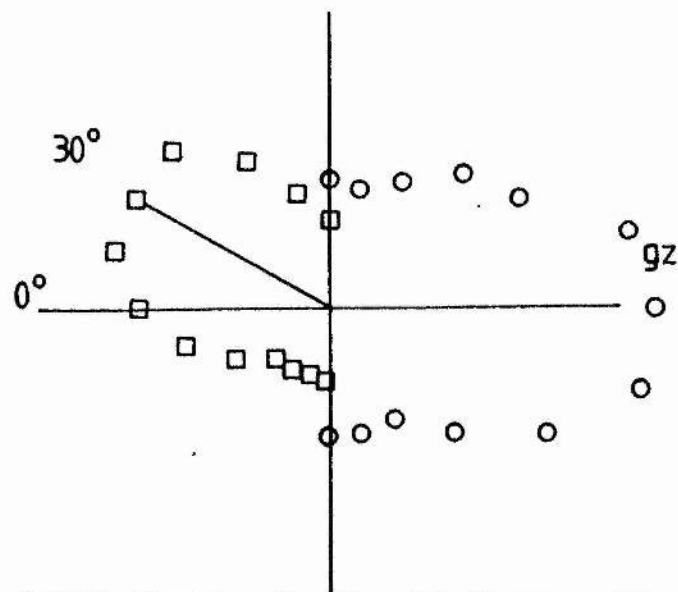
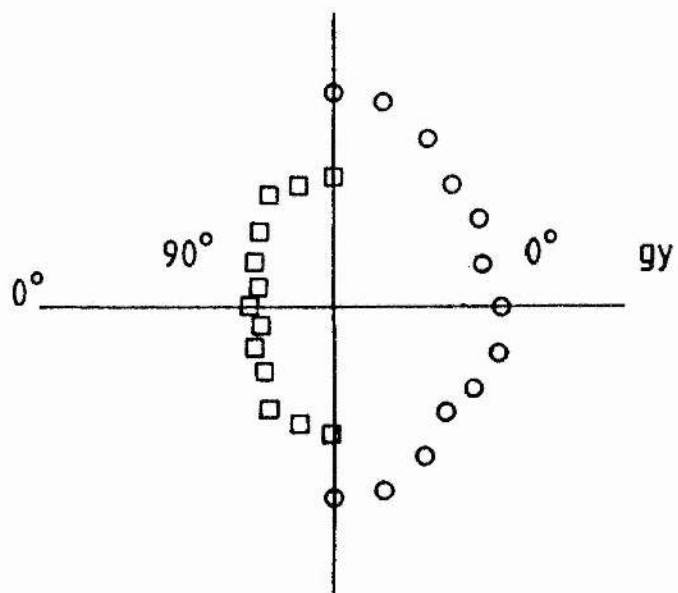
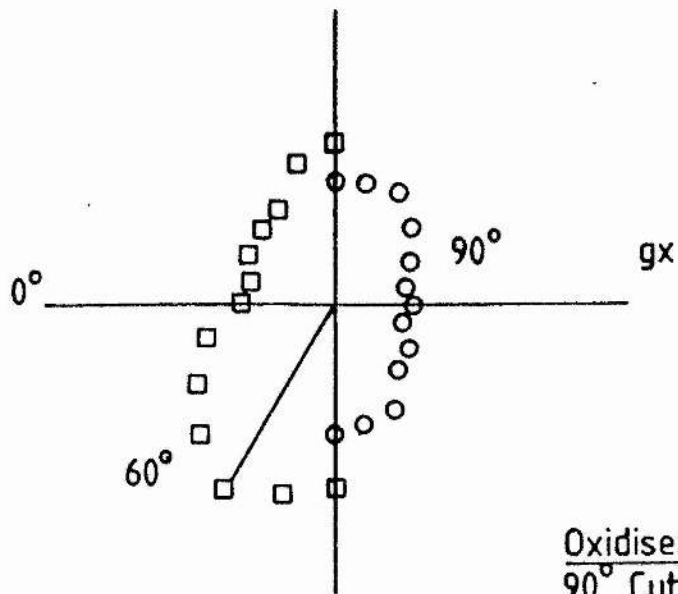


Figure 7.14

Angular dependence of e.p.r. signals from oxidised multilayers
cut at right-angles

The angular dependence of signal amplitude is shown for the three g-tensors from both samples. The experimental points on the left of the (\square) of the plots are from a sample cut at right-angles to those of the sample that gave the points on the right (o). The peaks in signal amplitude are shown for both samples where they occur. The field angles are as defined for and the signal amplitude was measured as described for fig.7.2. The experimental conditions were as described for fig.7.9.



60° and 90° (g_x). The angular dependencies of the g -tensors from each strip, could be simulated using the computer program, to obtain an estimate of the mosaic spread of the membrane multilayers (data not shown). A value of between 30° and 35° was estimated for both the oxidised and succinate reduced multilayers. In the crystal multilayers the mosaic spread has contributions from the unoriented parts of the multilayers, from the wobble of the chromophore within the protein and the wobble of the protein in the membrane (fig.7.6). Models for the angular dependencies of the g -tensors are presented in fig.7.15. For FR1 g_z must lie in the plane (a), as there was a 90° angle for the maximum of g_z signal amplitude from plane (b), cut at a right-angle to plane (a). The g_y and g_x tensors lie in the planes subtended between the two angles obtained in planes (a) and (b), as indicated. The g -tensors, by definition, are all at right-angles to each other, so the position of the g_y and g_x axes, within the arcs shown, was estimated from the relative size of the e.p.r. signals of each g -tensor in the planes (a) and (b). For the HiPIP (FR3) the g_y axis was shown to be at 90° to the membrane normal along the plane (a), whilst g_z and g_x were shown to have axes at 30° and 60° to the membrane normal respectively, in the plane (b). The angles obtained for the g -tensors of each centre will therefore be dependent on the angle at which the strip is cut from the Mylar sheet, as the angle at which the protein is oriented within the membrane, with respect to the strips, will vary.

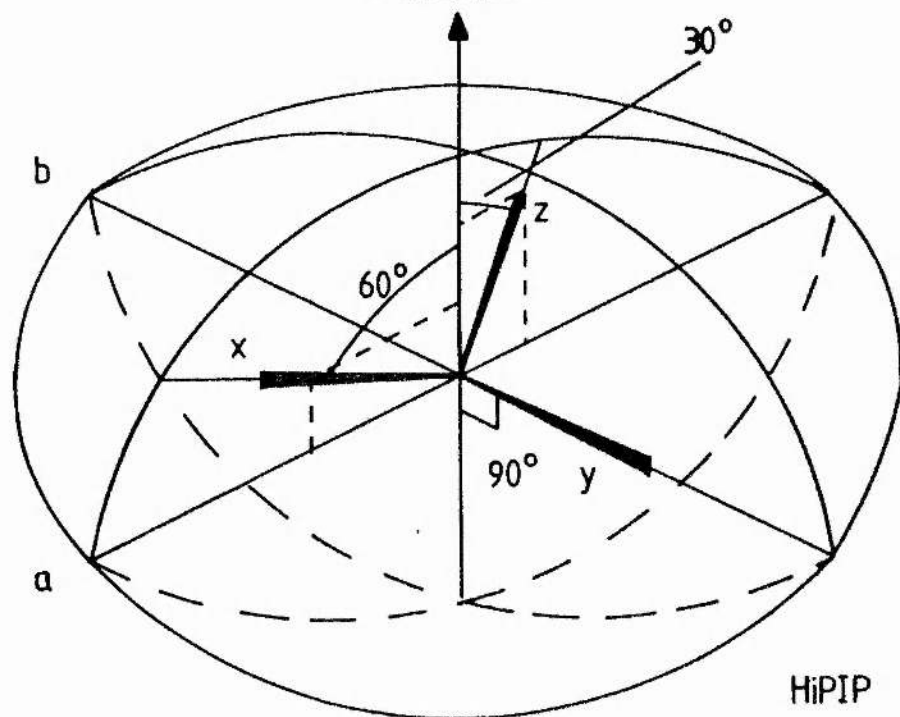
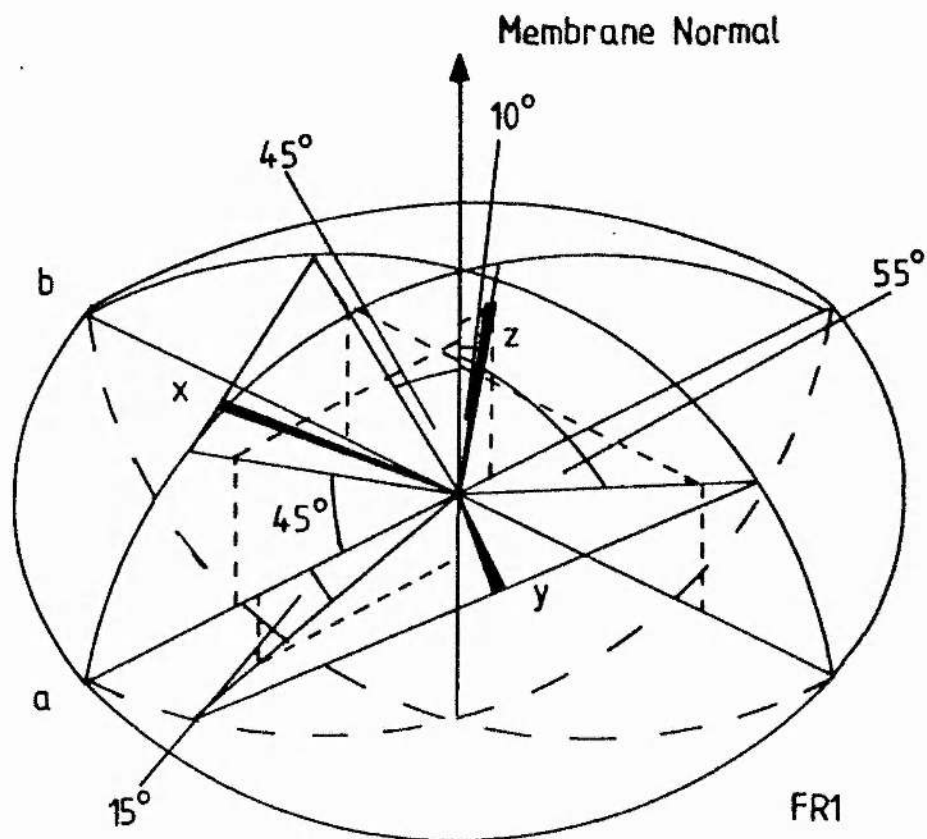
Figure 7.15

Models for the angular dependence of e.p.r. signals

The sketches show the proposed positions of the g-tensors of FR1 and FR3, relative to the membrane normal and membrane plane. The angles obtained from the multilayer samples cut at perpendicular angles are indicated: section through (a), the angles from the left-hand plots of fig.7.13 & 7.14; section through (b), the angles from the right-hand plots of fig.7.13 & 7.14. The membrane normal was taken to be 0° .

For FR1 g_z lies in the plane of (a) and g_y and g_x lie on the arcs subtended by joining the two angles obtained in planes (a) & (b). The positions within these arcs were estimated from the relative size of the e.p.r. signals for each g-tensor, in the two planes. For the HiPIP centre (FR3) g_z & g_x lie in the plane of (a), at the angles indicated to the membrane normal, and g_y lies along plane (b), parallel to the membrane plane.

Model for the Angular Dependence
of G-Tensors



7.3 Conclusions

The iron-sulphur clusters from the E. coli fumarate reductase have been studied in oriented multilayers from two strains of E. coli, one of which had amplified expression of this enzyme. The orientations of the individual g-tensors for centres FR1, the succinate reducible ferredoxin and FR3, the HiPIP centre paramagnetic in the oxidised form, could be discerned. The orientation of the second binuclear ferredoxin (dithionite reducible), could not be clearly discerned because of the presence of FR1 also. The interpretation placed on these results was not straight-forward and two possible explanations were proposed. Either the reorientation of FR1 or the interaction between the two ferredoxin centres. The orientations of centres FR1 and FR3 were found to be different to the orientations of the equivalent centres from succinate dehydrogenase, which may indicate a significant difference between the two similar enzymes.

The oriented multilayers produced from the membranes of the fumarate reductase amplified strain of E. coli, were shown to impose a crystalline array on the fumarate reductase molecules in these membranes. The angular dependence of the g-tensors was shown to change with the angle at which the multilayer strip was cut from the Mylar sheet. Crystal membranes were not observed from an E. coli strain that was unamplified in fumarate reductase expression. Schematic models were presented (fig.7.15), to account for the change in

angular dependencies observed for the g-tensors of the two centres. The results reported here indicate that the amplified strains of E. coli can provide a suitable system for the structural studies of this enzyme.

CHAPTER EIGHT

The Spatial Relationships of the Iron-sulphur Centres

8.1 Introduction

The fumarate reductase from Escherichia coli has been shown to contain three iron-sulphur centres; two [2Fe-2S] ferredoxins and a HiPIP-type centre. Interactions have been shown to occur between the succinate reducible ferredoxin and the dithionite reducible ferredoxin and also between the succinate reducible ferredoxin and the HiPIP centre (chapter 4). The effect of interaction between paramagnetic centres is to perturb the intrinsic e.p.r. properties of these centres. This can be used to study the interaction between the centres. In the case of fumarate reductase the iron-sulphur centres have redox potentials that allow the study of the interaction between the iron-sulphur centres when more than one are fully or partially paramagnetic; FR1 with FR2 and FR1 with FR3 (chapter 4). The studies on fumarate reductase have been performed on the membrane bound enzyme from a strain of E. coli with amplified expression of the enzyme. The preparations should therefore not suffer from any artifacts introduced by purification procedures, an explanation that has been put forward for the partial detection of the second ferredoxin in the isolated preparations of other enzymes of the succinate dehydrogenase (Beinert et al. 1982, Albracht 1980).

Knowledge of the spatial relationship between the e.p.r. detectable iron-sulphur centres of fumarate reductase is required for a full understanding of the type of interaction present. In this chapter the effects of interactions on the intrinsic e.p.r. properties of the iron-sulphur centres from fumarate reductase are detailed. The change in e.p.r. properties can also be used to calculate the distance between interacting centres if the type of interaction is known. Estimates of the distances between the interacting centres, both by the method of Ohnishi et al. (1982) and by studies on oriented multilayers are presented. These findings are discussed in relation to the likely contribution of the major mechanisms of spin-spin interaction to the effects observed for the iron-sulphur centres of fumarate reductase.

8.2 Results and discussion

8.2.1 Interaction between the ferredoxin centres

It was shown previously in chapter 4 that the fumarate reductase of E. coli contains three iron-sulphur centres and that interactions occur between these centres when they are paramagnetic. The interactions between paramagnetic species have two effects on the e.p.r. properties, a relief of power

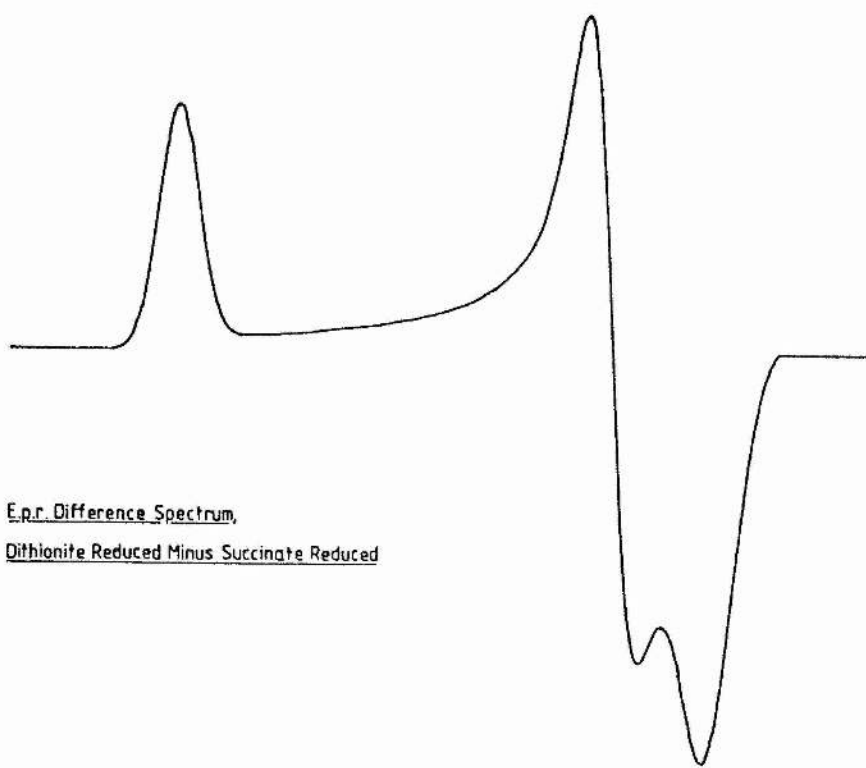
saturation and a broadening of the e.p.r. spectral linewidth. The latter effect is most pronounced at low temperatures and may be resolved into splitting of the e.p.r. signal, if the centres are close enough and at a favourable orientation. The splitting of the e.p.r. line was observed for succinate dehydrogenase spectra from mammalian heart mitochondria (Salerno et al. 1979b). Fig.8.1. shows the e.p.r. difference spectrum of the dithionite reduced spectrum minus the succinate reduced spectrum. This spectrum can only be taken as an approximation of the e.p.r. spectrum for FR2 under these conditions. This approximation assumes that FR2 has little effect on the spectrum of FR1 under these conditions (and vice versa), as both species are non-saturating (Salerno et al. 1979). This spectrum can be used to gain knowledge of the g-tensors of FR2, which can be characterised by $g_x = 1.913$, $g_y = 1.926$ and $g_z = 2.025$. The spectrum of FR2 so obtained shows a marked similarity to that of FR1 under these conditions. Quantitation of the difference spectrum gave approximately 0.9 spins/flavin.

Fig.8.2. shows the e.p.r. spectra obtained from succinate and dithionite reduced membranes under low temperature conditions. the spectrum from the dithionite reduced membranes was seen to be greatly broadened in the g_y and g_z regions, as compared to the spectrum from succinate reduced membranes. Further investigation of the dithionite reduced spectrum resolved a partial splitting of the g_y resonance, when the spectrum was recorded under conditions that were only

Figure 8.1

E.p.r. difference spectrum

The e.p.r. difference spectrum obtained by subtracting the e.p.r. spectrum from succinate reduced membranes from that obtained from dithionite reduced membranes is shown. The subtraction was performed on digitised spectra using a Comart Communicator CP100 microcomputer. The e.p.r. conditions were: microwave power, 1.1mW; microwave frequency, 9.5bGHz; modulation amplitude, 1.0mT; modulation frequency, 100KHz; scan rate, 0.1mT/s at a time constant of 500ms. The temperature was 27K for the succinate reduced sample and 17K fo the dithionite reduced sample. The protein concentration was approximately 69mg/ml.

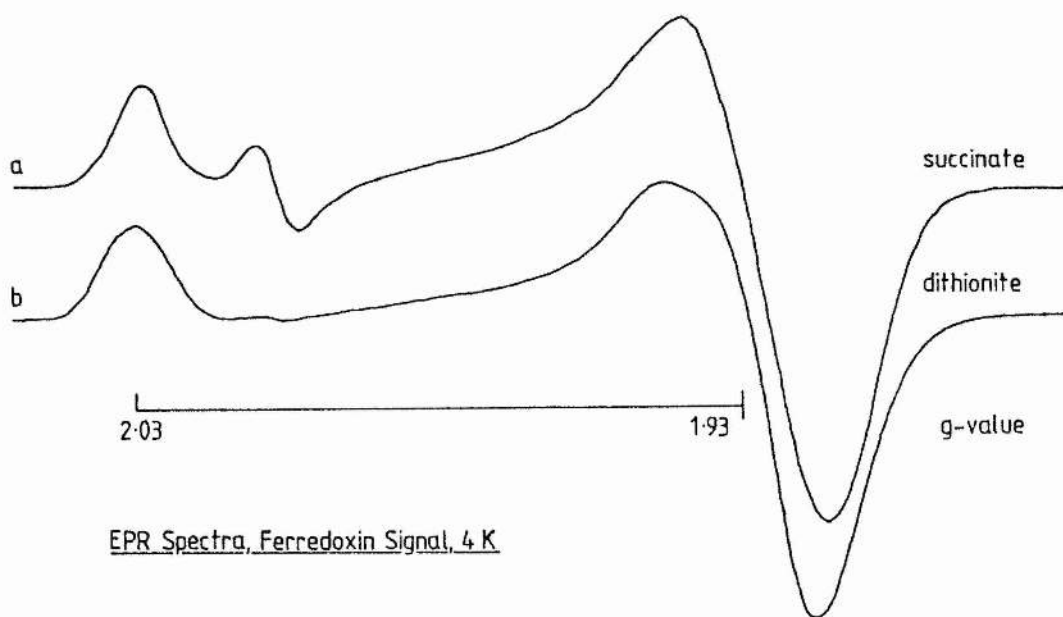


E.p.r. Difference Spectrum,
Dithionite Reduced Minus Succinate Reduced

Figure 8.2a

Low temperature e.p.r. spectra, ferredoxin signals

The e.p.r. spectra of succinate reduced (a) and dithionite reduced (b) membranes are shown, taken at 4K, to indicate the broadening of the dithionite reduced spectrum. E.p.r. conditions were as described for fig.8.1, except: microwave power, 2mW. g-values are indicated below the spectra.

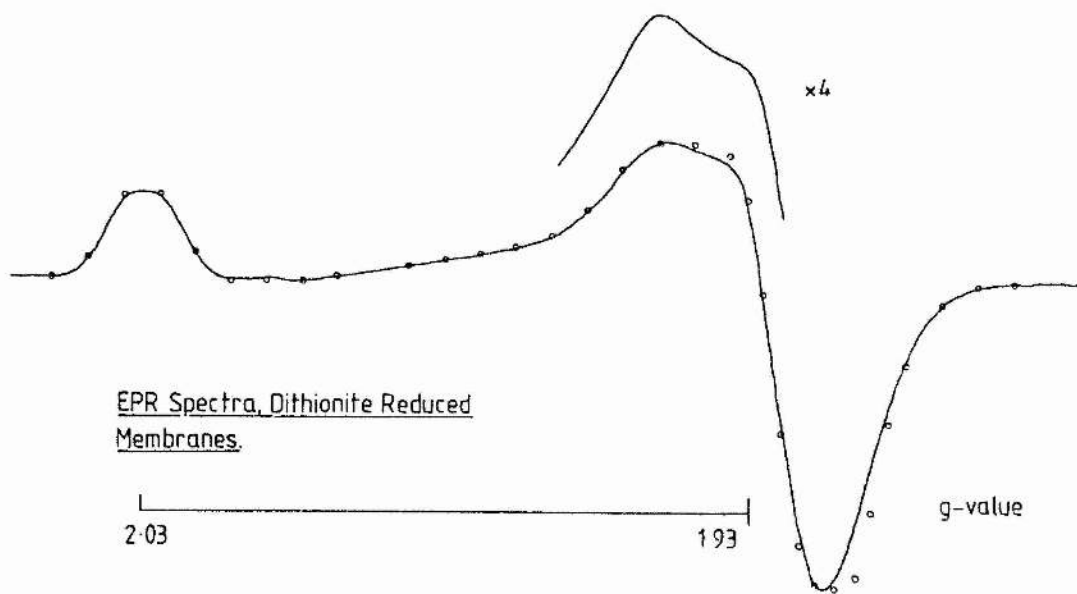


EPR Spectra, Ferredoxin Signal, 4 K

Figure 8.2b

Low temperature spectrum, dithionite reduced membranes

The spectrum from dithionite reduced membranes is shown taken at 4K and 0.07mW microwave power, to more clearly observe the broadening of the e.p.r. spectrum obtained from these membranes. E.p.r. conditions were as described for fig.8.1. Receiver gain for the main spectrum was 2.0×10^4 and 8.0×10^4 for the insert. Partial definition of a splitting of the gy resonance was observed from these conditions. g-values are indicated below the spectrum. The circles indicate the theoretical points obtained from a computer simulation of the spectrum. The g-values employed for FR1 were 2.025, 1.928 and 1.918, together with linewidths of 0.8mT, 0.95mT and 1.05mT. The g-values for FR2 were 2.025, 1.926 and 1.913, together with linewidths of 0.8mT, 1.0mT and 1.15mT. $D = 8$ for both species, $\theta = 60^\circ$ and $\phi = 45^\circ$.



EPR Spectra, Dithionite Reduced
Membranes.

2.03

1.93

g-value

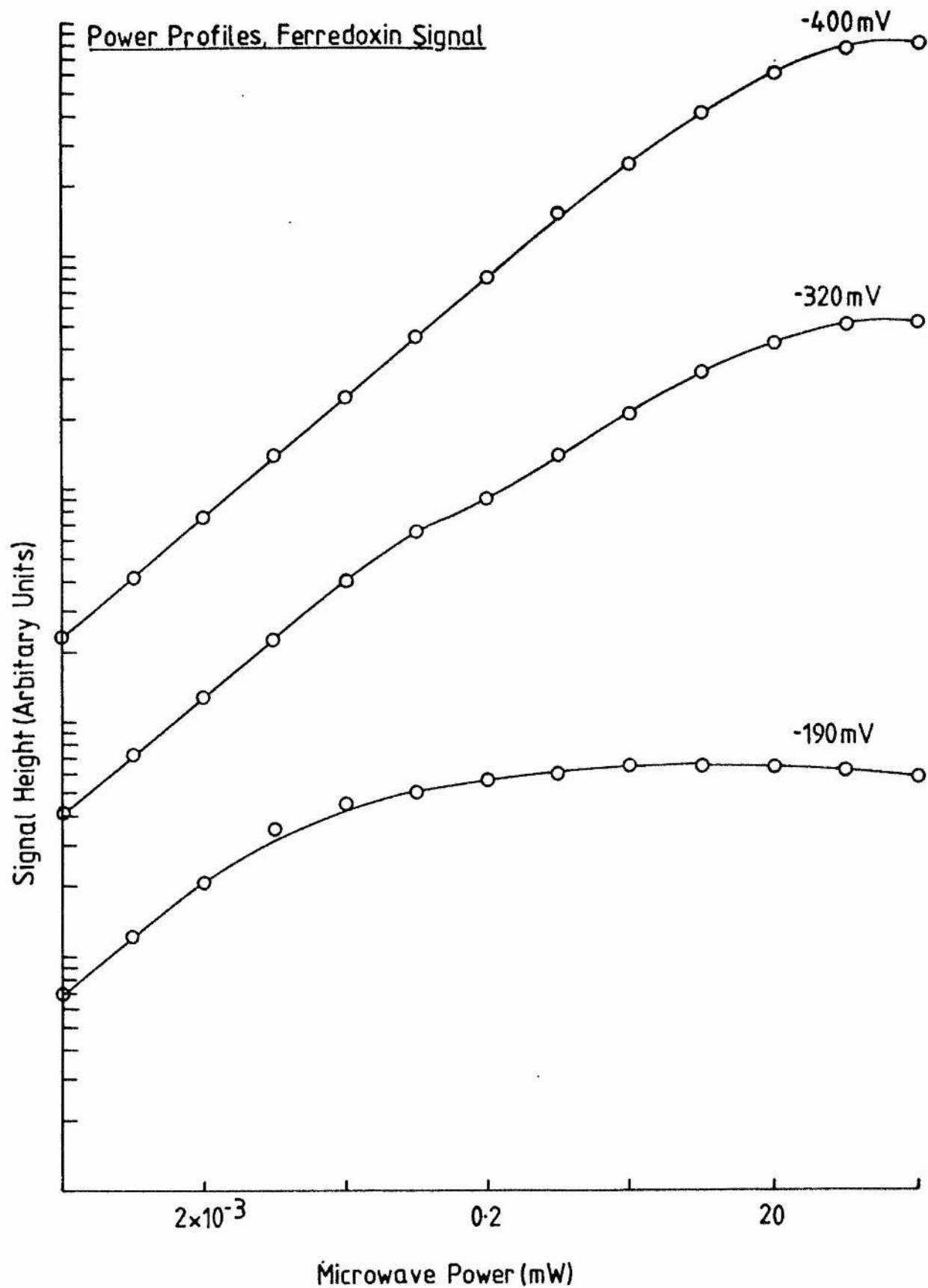
slightly saturating for the dithionite reduced signal. This splitting of the gy resonance was not as prominent as that observed for the bovine-heart succinate dehydrogenase (Salerno *et al.* 1979b), although the splitting of the gy resonance from this enzyme was dependent upon the enzyme preparation in this latter case. Environmental factors therefore may play a role in determining what degree of broadening or splitting occurs in the e.p.r. spectrum and the possibility of the centres being reasonably close cannot be excluded. The low degree of splitting may also reflect the distance between the centres and the orientation of the centres, if the splitting is due mainly to dipolar interaction. Indeed the contributions of exchange coupling and dipolar coupling to the overall interaction may well determine the degree of broadening and splitting seen (Salerno *et al.* 1979b).

The most notable observation from the interaction between the two ferredoxins is the relief of power saturation caused by the reduction of the second ferredoxin centre, which can be observed over a wide range of power and temperature settings. The power profiles of the ferredoxin signal are shown in Fig.8.3, from samples poised at various redox potentials. A monophasic profile was seen for potentials where FR1 alone was paramagnetic and where FR1 and FR2 were paramagnetic. At intermediate potentials the power profile was biphasic. The interpretation placed on this is that the two ferredoxin species had identical relaxation processes when both were

Figure 8.3

Power saturation profiles, ferredoxin signals

Power saturation profiles of the ferredoxin signals from membranes poised at various redox potentials are shown. The ambient redox potentials of the samples are shown to the right of the profiles. The profiles show the change in relaxation of the succinate reducible centre, as the dithionite reducible centre titrates. Homogeneous profiles are shown at -190mV and -400mV . E.p.r. conditions were as described for fig.8.1 and the temperature was 7K . The protein concentration was approximately 42mg/ml .



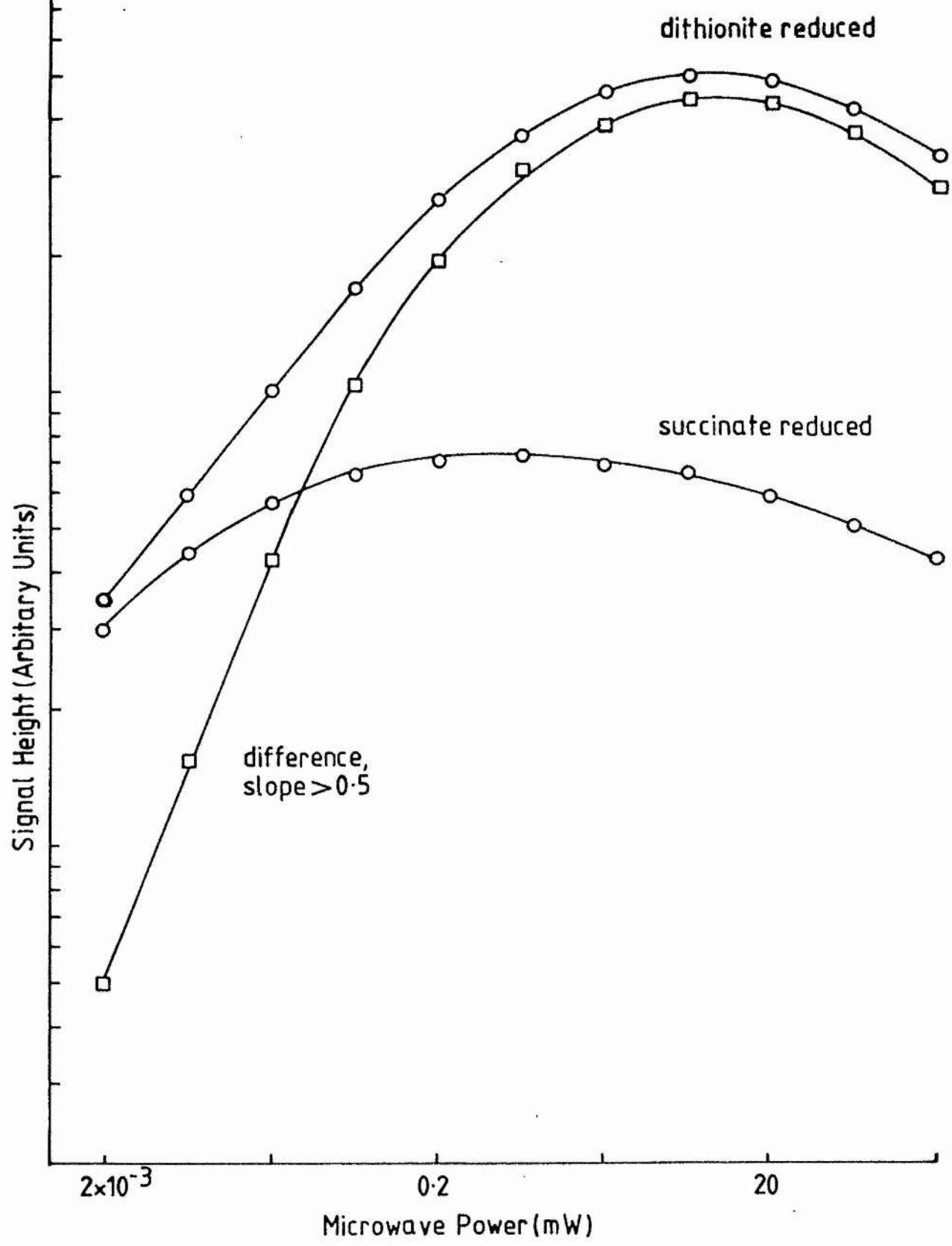
paramagnetic. As FR2 titrated some of the sample had both centres paramagnetic and some had only FR1 paramagnetic, thus a biphasic profile would result because of the two enzyme populations, the enzyme containing both centres reduced would have faster relaxation than that with just FR1 reduced. The interaction between the two centres caused the increase in relaxation of both centres, so when FR2 was fully paramagnetic only the fast relaxing species were present as a result of the interaction between the centres. Fig.8.4 shows the power profiles of the e.p.r. spectra from the two reduction states, together with a difference profile obtained by subtracting the succinate reduced profile from the dithionite reduced profile. This profile is not indicative of a separate species, but indicates interaction between the two ferredoxins. The maximum slope that should be obtainable for independent species is $1/2$, but a region of slope greater than $1/2$ is seen from the difference profile. This arises because in the dithionite reduced profile the contribution from FR1 was no longer that of the profile from succinate reduced membranes. The profile of FR1 had changed to that observed in dithionite reduced membranes, so subtraction of the original profile of FR1, from the dithionite reduced profile, at powers where FR1 alone saturates, does not remove enough signal height causing the remainder to be added to the profile of FR2, so giving the slope greater than $1/2$ (Salerno *et al.* 1979b).

Figure 8.4

Power saturation profiles of FR1 and FR2 at 4.5K

Power saturation profiles from succinate reduced (FR1) and dithionite reduced (FR1 + FR2) membranes are shown from the e.p.r. signals at 4.5K. The difference profile of the dithionite reduced profile minus the succinate reduced profile is also shown, to illustrate the interaction between FR1 and FR2. A region is seen in this profile where the slope of the profile is greater than 0.5, indicating interaction between the two ferredoxin centres (see text). E.p.r conditions were as described for fig.8.1 and the protein concentration was 69mg/ml.

Power Profiles, 4.5K



Further evidence of interaction between the ferredoxin centres of fumarate reductase was seen in the detection of a half-field signal (Steenkamp *et al.* 1978, Salerno *et al.* 1979b), from dithionite reduced samples and samples poised at low redox potentials. This signal is shown in Fig.8.5. and has a g -value ≈ 3.88 . This signal is strong evidence for the existence of spin-coupling between the two ferredoxin centres (Mathews *et al.* 1974, Salerno *et al.* 1979) and arises from the 'forbidden' transitions ($\Delta M_s = 2$) between the two centres. The signal titrated to give a mid - potential (pH 7.0) of approximately -280 mV, (Fig.8.6). This correlates well with the mid-point potential of the second ferredoxin, indicating that this signal arises from interaction between FR1 and another paramagnetic species titrating in this region. Two species are interacting, both of which are centred around approximately $g = 1.94$ and one of which has an E_m of approximately -280 mV. The homogeneous power profile and the mid-point potential of the half-field signal indicates FR2 to be this paramagnetic species.

More than one interpretation can be placed on the results obtained. The simplest interpretation is that the two ferredoxin centres have similar g -values, but different mid-point potentials and relaxation rates. The existence of both ferredoxins in a paramagnetic state causes interaction between the two centres and the change in the e.p.r.

Figure 8.5

E.p.r. half-field signals

E.p.r. spectra recorded in the half-field region are shown for membranes poised at three redox potentials. The redox potentials of the samples are shown to the left of the spectra and the g-values are indicated below the spectra. E.p.r. conditions were as described for fig.8.1, except microwave power was 20mW, the receiver gain was 1×10^6 and the temperature was 6K. The protein concentration was 42mg/ml.

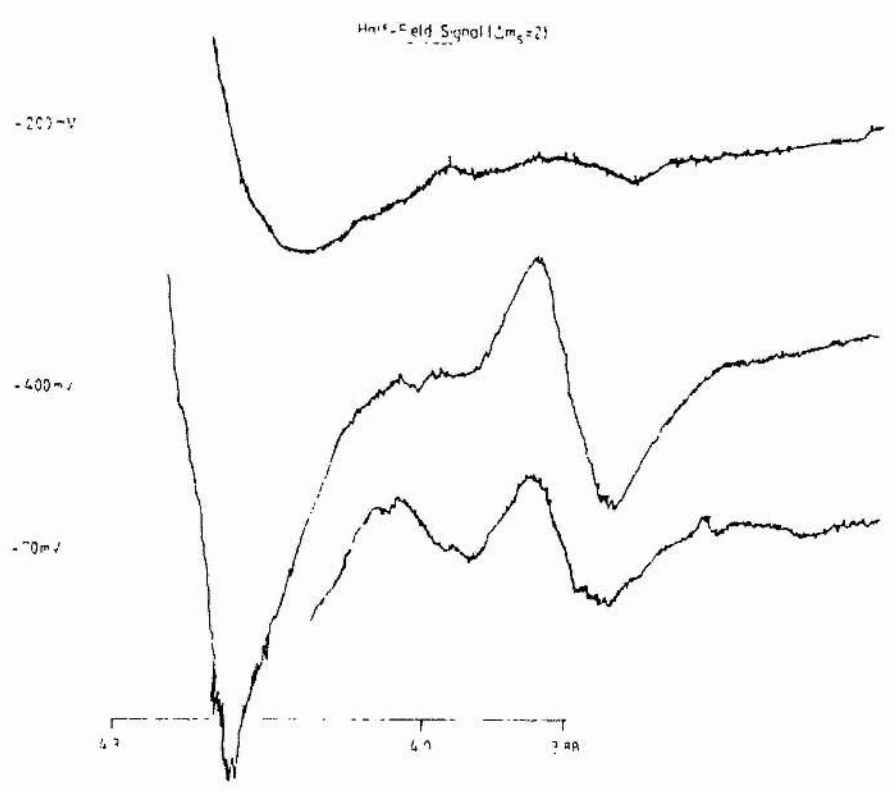
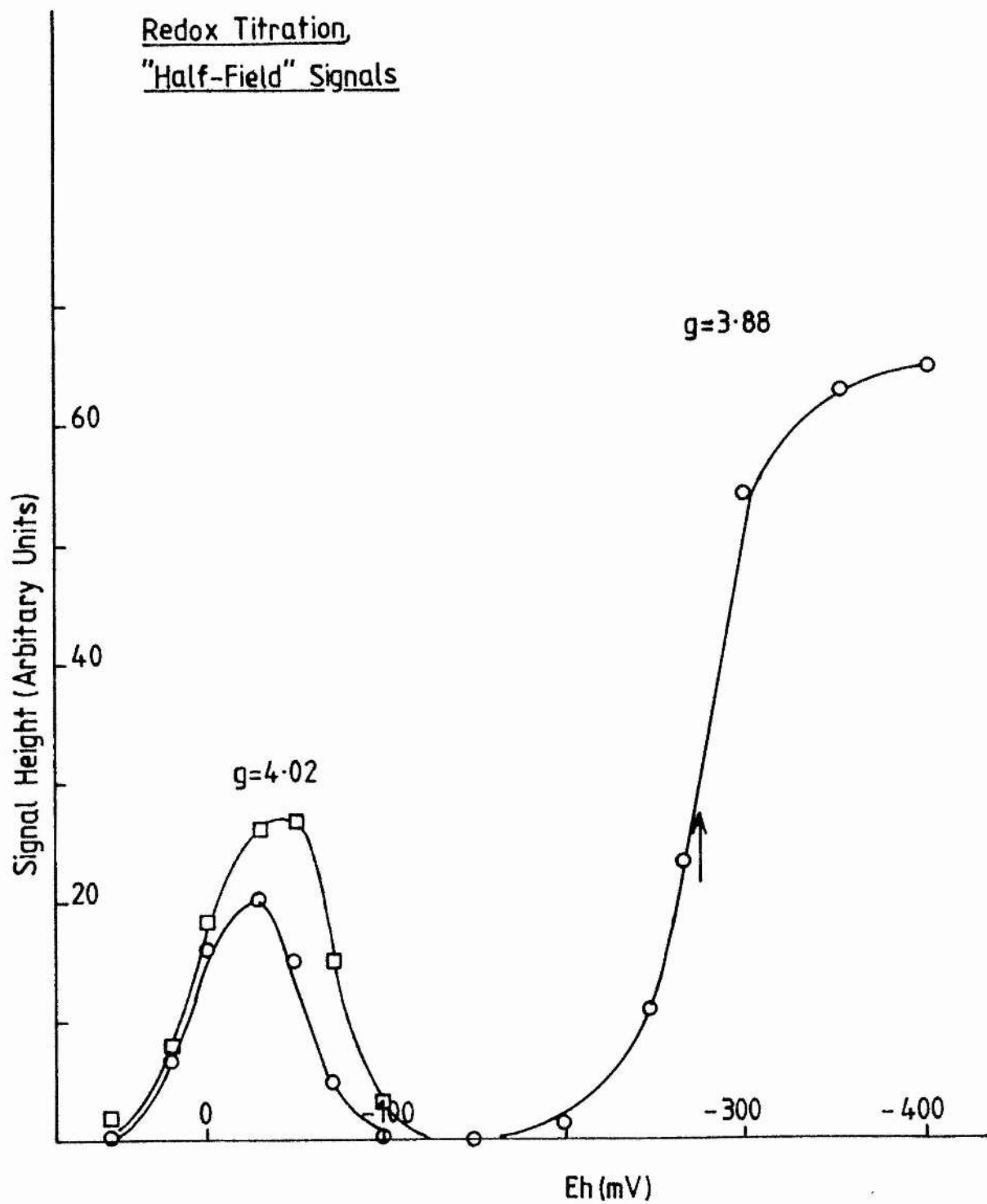


Figure 8.6

Potentometric titration of the half-field signals

A potentiometric titration of the half-field signals observed from the membranes of JRG1031 are shown. The signal height of the e.p.r. signals is shown plotted against the ambient electrode potential of the sample. The arrow indicates the mid-point potential of the $g = 3.88$ signal. E.p.r. conditions were as described fo fig.8.1 except; microwave power, 20mW; temperature, 6K and the protein concentration was 42mg/ml.

Redox Titration,
"Half-Field" Signals



properties observed. However, the explanation proposed by Salerno *et al.* (1979b) for bovine-heart succinate dehydrogenase, cannot be excluded from the results obtained. In this suggestion the iron-sulphur centres are indistinguishable, but interaction between them, causes the second electron to be accepted less readily than the first. Thus the apparent, low mid-point potential of the second ferredoxin centre is seen in the titration of the ferredoxin signal, because of the interaction. The mid-point potential of the second ferredoxin would be determined from the mid-point of the couple together with the interaction energy of the two centres. By necessity the half-reduction potential of FR2 is always measured in the presence of FR1. A mid-point potential of -120mV for FR2, together with an interaction energy of 140mV and a statistical term of 25mV would produce the measured mid-point potential ($-120 - 140 - 25 = -285\text{mV}$, Salerno *et al.* 1979b, J.C. Salerno personal communication).

The power profiles from dithionite reduced membranes showed that the relaxation of FR1 and FR2 occurred as a single species, with an increase in the relaxation rate of the FR1. The increased rate of relaxation of FR1 in the presence of paramagnetic FR2, was a result of the introduction of a spin-spin relaxation process (T_2), between the two paramagnetic species. It cannot be excluded that the relaxation rate of FR2 was enhanced in a similar manner, in the presence of FR1, as the relaxation of FR2 cannot be

measured independently. the faster relaxation of FR1 was confirmed by the difference power profile. The faster relaxation of FR1 may also be explained by reduction by dithionite causing a conformational change in the protein, which alters the environment of the iron-sulphur centre. The relaxation processes of iron-sulphur centres has been shown to be dependent on the environment of the cluster (Ohnishi et al. 1976a, Salerno et al. 1977b), so this explanation for the enhancement of the relaxation of centre FR1 cannot be excluded. The broadening of the e.p.r. spectra at low temperatures (dithionite reduced membranes) would suggest that the relaxation enhancement is due to interaction between centres, particularly in the light of the partial splitting of the gy resonance at low temperatures. Knowledge of the spatial relationships of the two ferredoxin centres would allow the assessment of the possible interaction mechanisms and help in the interpretation of the results obtained.

8.2.2 Interaction between FR1 and FR3 (HiPIP)

The fumarate reductase of E. coli presents a novel system for the succinate-fumarate oxido-reductase class of enzymes, in that the redox chemistry of the clusters is such that FR1 and FR3 can be observed in samples where both centres are partially paramagnetic (chapter 4). Interaction between these centres can thus be studied in this enzyme. Samples were thus poised at redox potentials that best allowed the interaction

to be studied by e.p.r. (typically -70mV), by titration of oxidised membranes with sodium succinate. The e.p.r. spectrum obtained at low temperatures and power (6K, 0.07mW) is shown in fig.8.7. Under these conditions a broadening of the $g = 2.01$ resonance of the HiPIP was seen, together with a broadening of the g_y and g_x of FR1. A broadening of approximately 13 gauss (g_y) was measured for the effect on both species. This phenomenon may indicate that the interaction between these two centres is large, because they are only partially in a paramagnetic state. There will be a residual e.p.r. signal from the non-interacting HiPIP and ferredoxin centres, so the observed e.p.r. spectrum will be a composite of these signals. Because the centres are only partially paramagnetic four populations of the centres will exist; that with both FR1 and FR3 paramagnetic; those with FR1 or FR3 paramagnetic and that with neither of the two centres paramagnetic. The population with only FR3 paramagnetic will give rise to the normal e.p.r. spectrum for this centre. In titrating the membranes with succinate some of the enzyme will have both centres reduced, some will have only FR1 reduced and some of the enzyme will have none of the centres reduced. The size of each population is dependent on the redox chemistry of the iron-sulphur centres. The power profiles from the redox-poised samples did indicate two populations for each centre, those interacting and those non-interacting. Fig.8.8 shows the power profiles for FR1 where this is illustrated clearly. The $P_{1/2}$ measured from the interacting population was greater than that from the non-interacting population,

Figure 8.7

E.p.r. spectrum of membranes poised at -70mV.

The e.p.r. spectrum recorded at 4K and 0.07mW microwave power, from membranes poised at -70mV is shown. The g-values are indicated below the spectra. The e.p.r conditions were as described for fig.8.1. The circles indicate theoretical points derived from a computer simulation of the spectrum. For FR1, g-values of 2.025, 1.928 and 1.918, together with linewidths of 0.8mT, 0.95mT and 1.05mT respectively were used for the simulation. For FR3, g-values of 2.01, 1.99 and 1.55, together with linewidths of 0.7mT, 2.5mT and 5.5mT respectively were used. $D = 7.5$ for both centres and $\theta = 50^\circ$ and $\phi = 65^\circ$.

EPR Spectrum:
Membrane Particles, -70mV

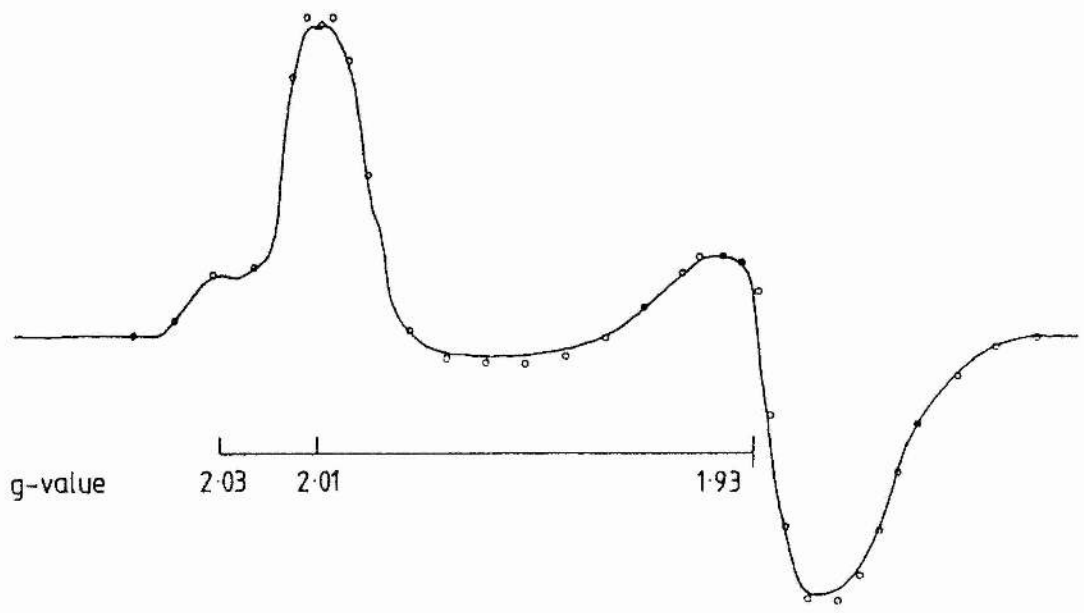
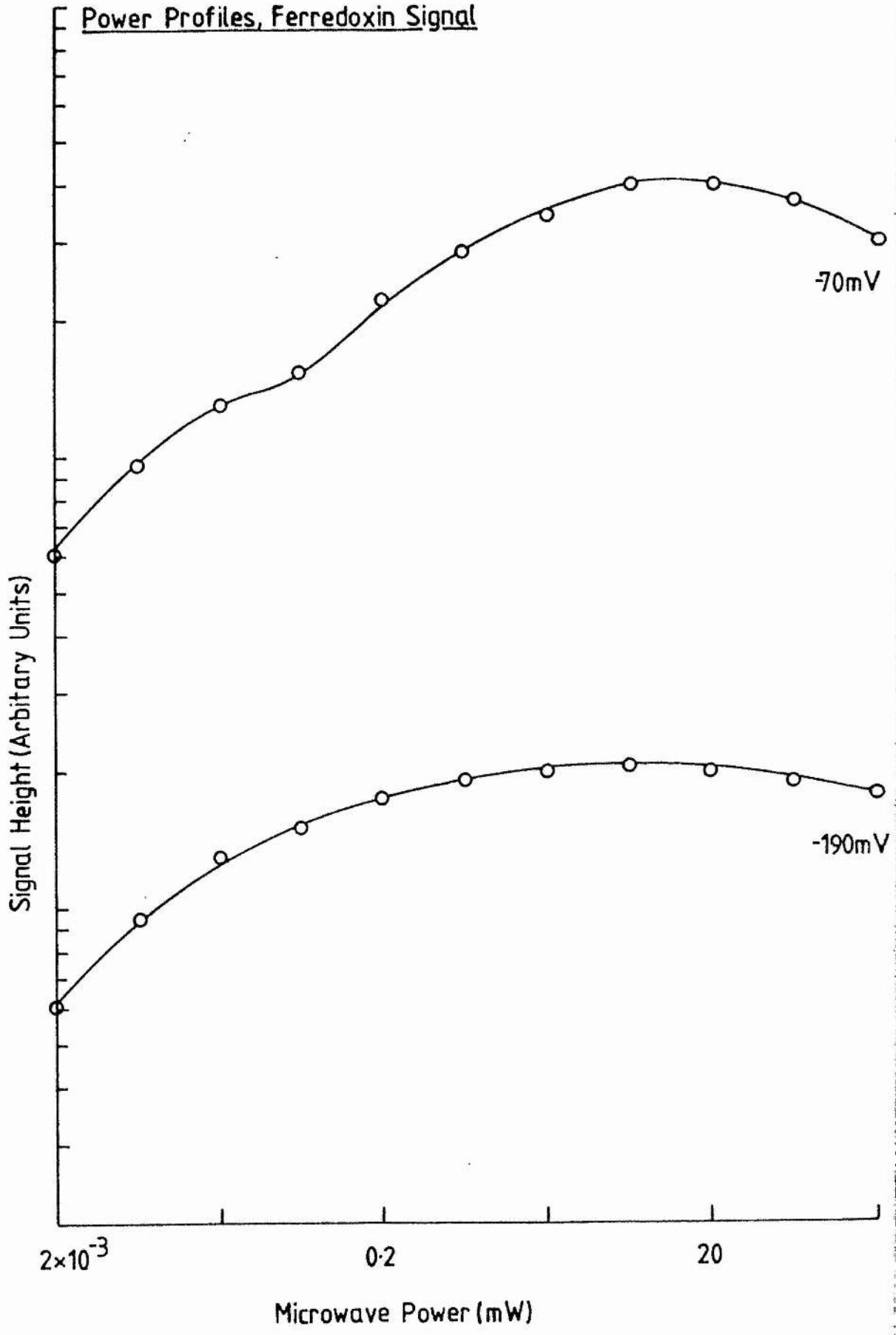


Figure 8.8

Power saturation profiles, ferredoxin signal

The power saturation profile of the ferredoxin signal are shown, from samples poised at two redox potentials, to indicate the change in relaxation behaviour of FR1 by interaction with FR3. The ambient electrode potentials of the samples are indicated to the right of the profiles. The e.p.r. conditions were as described for fig.8.1, except the temperature was 7K and the protein concentration was 42mg/ml.

Power Profiles, Ferredoxin Signal



again indicating the interaction and was dependent upon the redox potential of the sample (c.f. chapter 4).

Samples poised at the redox potentials that had both iron-sulphur centres partially paramagnetic were also examined for the presence of half-field signals. Two signals were observed in these samples with g-values of approximately 3.88 and 4.02 (fig.8.5.), similar to that observed from the dithionite reduced or low potential samples. The signals were at a lower intensity than that observed from dithionite reduced samples, but again point to the interaction between FR1 and FR3 being strong. The signals both appeared to titrate in a 'bell'-shaped manor, which fits with the hypothesis that they arise from the interaction of FR1 and FR3.

8.2.3 Contributions of exchange and dipolar coupling

Two types of interaction between paramagnetic species are likely to contribute to the interaction between the iron-sulphur centres of fumarate reductase (Coffman & Buettner 1979a & b, Salerno *et al.* 1979b). Interaction which results from the effect of the magnetic field, of each spin, on the magnetic moment of the other, is called magnetic dipole-dipole coupling. A theory was developed by Leigh (1969) to describe this phenomenon. The dipole-dipole coupling is anisotropic in

nature and an expression for the angular dependence of the splitting was presented:

$$\Delta H/2 = \mu_{\text{eff}} (1-3\cos^2\theta_r) / r^3$$

where μ_{eff} is the effective magnetic moment and θ_r is the azimuthal angle between the magnetic field and the vector connecting the two spins. If a splitting of 12-13 gauss is estimated from the low-temperature spectrum, of dithionite reduced membranes, then a maximum distance of 23\AA between centre FR1 and centre FR2 can be estimated by taking $(1-3\cos^2\theta_r)^2 = 4$, which is the maximum value for this term. At angles other than $\theta = 0$, then shorter distances will be obtained from this equation. An averaged value of the angular term, as the samples are randomly oriented frozen solids, gave an estimate of r as approximately 7\AA , when substituted in the equation for the observed splitting.

The lack of observed splitting of the HiPIP and FR1 spectra precludes the use of the previous equation for the estimation of the distance between the centres. Zweier (1983) presented an equation for the estimation of the distances between centres, from the observed broadening of the centres when both were paramagnetic:

$$r = 19.26 (\bar{g}[S(S+1)]^{1/2} / \Delta H)^{1/3}$$

where $\bar{g} = (g_x + g_y + g_z)^{1/3}$ and is the root-mean-square g-value

for spin 2. ΔH is the broadening of the e.p.r. linewidth of spin 1. Using this equation, an estimate of 10-15 \AA was obtained. This distance between FR1 and FR3 will be an overestimate because of the partial paramagnetic nature of the sample and hence the full effects of the interaction are not observed. The distance estimate for FR1 and FR3 suggests that these two centres are strongly coupled in the fumarate reductase from E. coli.

The second possible type of interaction between paramagnetic centres is an isotropic exchange interaction that occurs due to overlap of the spin orbitals of the two interacting spins. This type of interaction is only effective over short range distances and Coffman & Buettner (1979a & b) showed that there was a limit function for the range of this type of interaction. They also showed the the strength of the interaction could be used to estimate the distance between two centres, or vice versa (J the coupling constant between the two centres could be estimated). For a distance of approximately 10 \AA J could be estimated to have a value of approximately unity, whilst for a distance of 14 \AA $J \approx 10^{-4} \text{ cm}^{-1}$ using the limit function of Coffman & Buettner (1979). The interaction between the iron-sulphur centres of fumarate reductase may contain contributions from both types of interactions. If the contribution from the exchange interaction is large, then estimates of r from assuming a largely dipolar interaction will result in errors of the inter-spin distance. However, the limit of exchange

interaction (antiferromagnetic) was set at approximately 15\AA by Coffman & Buettner, and that dipolar interactions can be assumed to be the major type of interaction at distances greater than 10\AA . The strength of the dipolar interaction will depend on the relative orientations of the two centres and hence the two angles θ_r and ϕ_r (angles of the interspin vector, r to centre 1, fig.8.18) are required for the accurate estimation of the inter-spin distance.

The contribution of an exchange term to the interaction between the iron-sulphur centres would be expected to cancel the dipolar term if the value of J was large enough ($>25\text{cm}^{-1}$). If J was in the region of $5-10\text{cm}^{-1}$ then a reduction of the observed e.p.r. intensity would be expected, because of the population of the e.p.r. silent singlet ($S=3/2$). The signal would be expected to decrease more rapidly with temperature than the Curie effect predicts and could also account for the increased rate of spin relaxation observed in the fully reduced enzyme (chapter 5).

8.2.4 Estimates of the inter-spin distances

Ohnishi *et al.* (1982) presented a method for the estimation of the distance between two interacting redox centres, if the nature of the interaction was assumed to be largely dipolar in nature. The authors estimated the distance between cytochromes a and a_3 in a cytochrome c oxidase

preparation. The distance was calculated from the B term of the dipolar Hamiltonian, that arises from the enhancement of the relaxation time of the slow relaxing species, by the fast relaxing species. The B term was shown to be dominant by Hyde & Rao (1978). Progressive power saturation was used to study the interactions between FR1 and FR2 or FR3 using this method. The saturation parameter $P_{1/2}$ was used to obtain the spin-lattice relaxation times (T_1) of the two interacting species, in the absence of interaction. The value of T_1 for FR2 was estimated from the dithionite reduced membranes, as it was assumed that FR2 was faster relaxing than FR1. T_1 was assumed to be equal to T_2 in the absence of interaction. The relaxation time of the centres was estimated using the following equations:

$$\gamma^2 H_{1/2}^2 T_1 T_2 = 1 \quad : \quad k H_{1/2} = (P_{1/2})^{1/2}$$

where γ is the gyromagnetic ratio and k is a constant dependent upon the cavity loading of the e.p.r. spectrometer. Thus the shortest possible T_1 is found when $T_1 = T_2$. Whilst this assumption is not strictly valid for FR2, because of the interaction, a useful estimate of FR2's relaxation time can be obtained. T_2 for FR1 plus FR2 was estimated from the increased line width of the e.p.r. spectrum of the ferredoxin signal, in dithionite reduced membranes. T_2 was found to be, typically at least an order of magnitude less than T_1 , so a large error in the estimation of T_1 of FR2 was not likely to lead to unreasonable estimates for

this factor. The distance estimate using the equation of Ohnishi *et al.* (1982) can accommodate errors of upto 25% without producing large errors in the final estimate, because of the r^6 dependency of the inter-spin distance. The equation used for the calculation was:

$$r^6 = \gamma_f^2 \gamma_s^2 \hbar^2 / 8 \delta\omega^2 \cdot T_{1s} / T_{1f} \cdot (1-3\cos^2\theta)^2$$

where ω is the resonant e.p.r. frequency of the centres and \hbar is Planck's constant divided by 2π . $\delta\omega^2$ was calculated from the g -values of the two interacting centres. Data from the oriented multilayer studies (chapter 7) was used to estimate g -values for parallel g -tensors, using $g(\text{calc}) = g(\text{meas})\cos\theta$, where θ is the angle of the g -tensor to the membrane normal. The ratio of the spin lattice relaxation times of the slow and fast relaxing species (T_{1s}/T_{1f}) is required to obtain distance measurements. This ratio is unlikely to be less than 1 ($T_{1f} > T_{1s}$), so a lower limit of 1 was set on this value i.e. $T_{1s} = T_{1f}$. Fig.8.9 shows the variation of r with θ for FR1 plus FR2. Two curves are shown with ratios of 1 and 10 for the relaxation times of the two centres. Estimates of r for these two centres were assumed to lie below the top curve as this was produced by equal relaxation times for each centre.

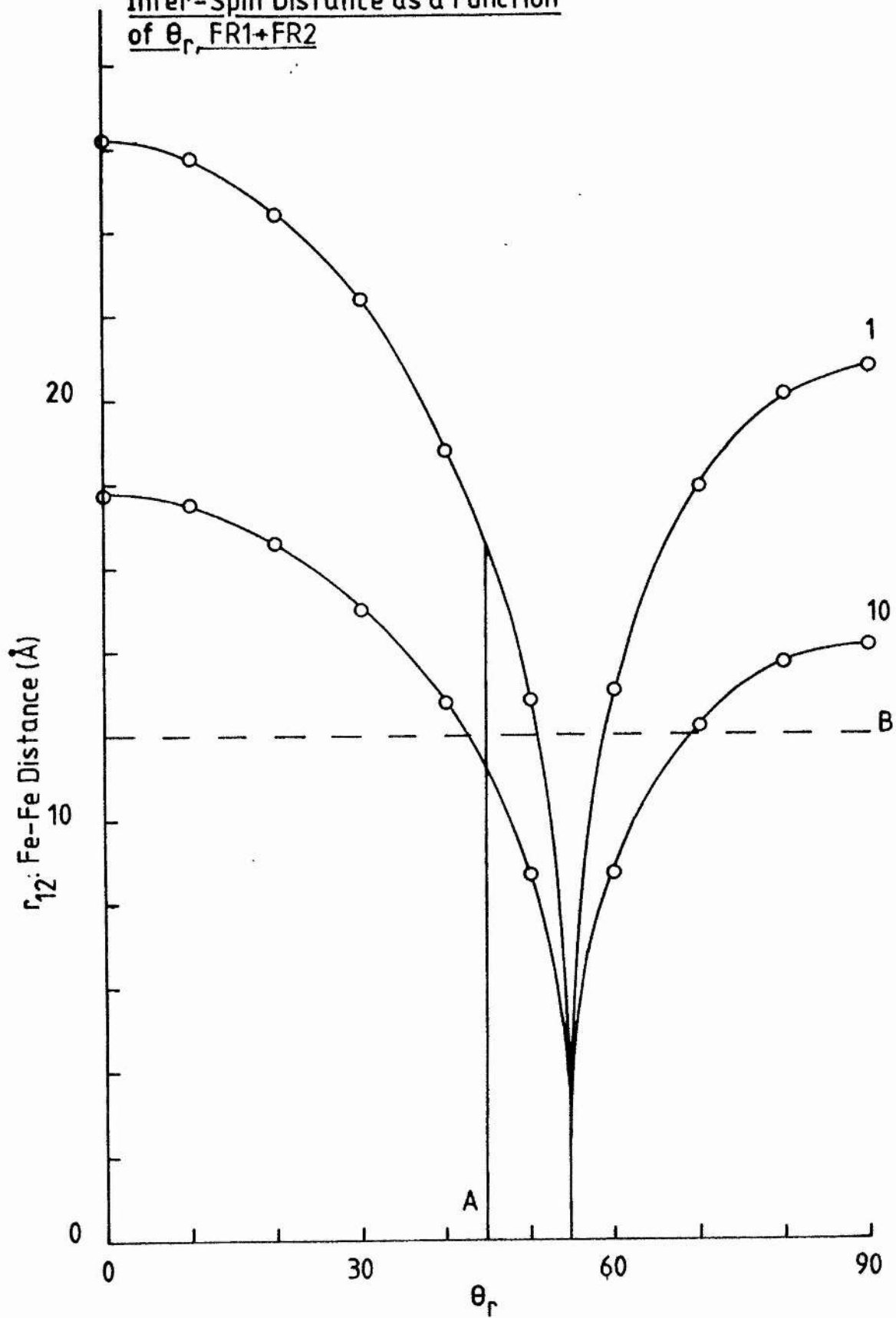
For an initial estimate the angular factor was averaged and the distances obtained from the above equation as the sample is of a randomly oriented solid. For the interaction of FR1 with FR2 a maximum distance between the two centres of

Figure 8.9

Variation of the inter-spin distance with θ_R for FR1 + FR2

The inter-spin distance r_{12} was calculated using the equation of Ohnishi et al. (1982). The top curve was calculated using a ratio of 1 for T_{1s}/T_{1f} and the bottom curve was calculated using a ratio of 10 for the same function. Line A, indicates the angle at which the peak of change in $P_{1/2}$ occurred for FR1 + FR2. Line B, indicates the minimum distance for which no dipolar spin-spin splitting will be observed.

Inter-Spin Distance as a Function
of θ_r , FR1+FR2



16\AA was found (fig.8.9), if the relaxation times were assumed to be equal. If the relaxation of FR2 was taken to be 10-fold that of FR1 then a distance of 11\AA was estimated between the centres. The lower limit for which no spin-spin splitting is observable, from dipolar interaction, was estimated at 12\AA by Ohnishi *et al.* (1982). The estimate of the inter-spin distance from the line splitting observed for the dithionite reduced membranes was somewhat smaller at 7\AA , indicating that there is also some contribution from exchange interaction in this system, assuming the error in the measurement of the linewidths was not too great. A lower limit of $9\text{-}10\text{\AA}$ can be reasonably set for the distance between FR1 and FR2, if it is assumed that J has a value in the order of a few cm^{-1} . The upper limit can be set at 12\AA , because of the small splitting of the gy resonance that was seen at low temperature.

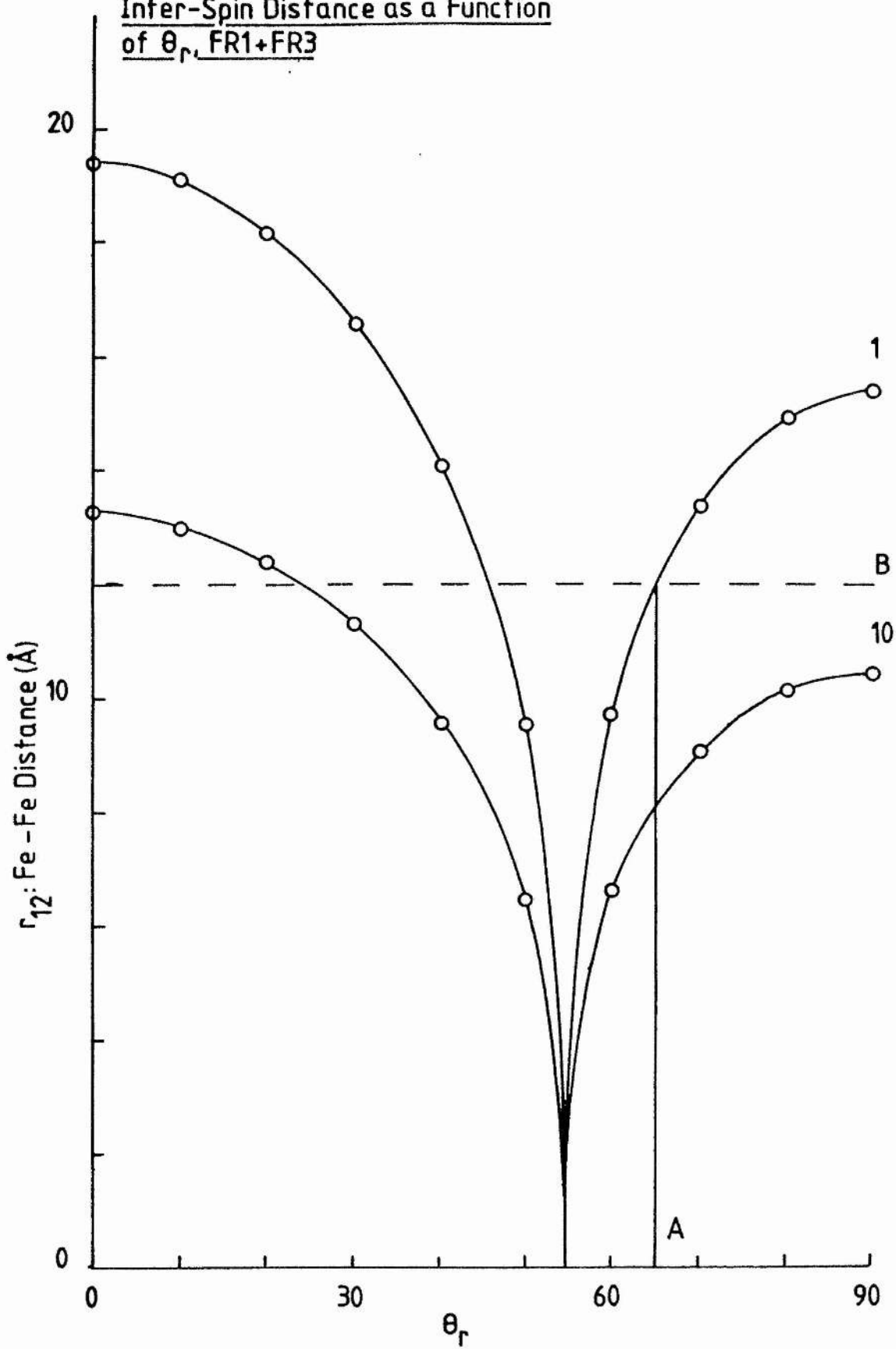
For the interaction between FR1 and FR3, averaging the angular factor and substituting in the equation gave a minimum of 12\AA for the inter-spin distance (fig.8.10), if the relaxation times are assumed to be similar. If FR3 was assumed to relax an order of magnitude faster than FR1 then a lower value for the minimum distance between the centres was obtained, at 8\AA . The value for the ratio of T_{1s}/T_{1f} was typically found to be 7.55 at 6K. This ratio allowed r to be calculated at approximately 9\AA for the distance between FR1 and FR3. This value is in reasonable agreement with that from

Figure 8.10

Variation of the inter-spin distance with θ_R for FR1 + FR3

The inter-spin distance, r_{12} , was calculated for each angle using the equation of Ohnishi *et al.* (1982). The top curve was calculated using a ratio of 1 for the T_{1s}/T_{1f} function and the bottom curve using a ratio of 10 for the same function. Line A, indicates the peak of change in P1/2 for FR1, from FR1 + FR2. Line B, indicates the minimum distance at which no dipolar spin-spin splitting will be observed.

Inter-Spin Distance as a Function
of θ_r , FR1+FR3



the observed line broadening, of the HiPIP centre and centre FR1.

The values obtained for the estimates of the inter-spin distances for the two interacting systems, using the averaged angular factor can be taken as a useful guide to the distance between the two interacting spins of each system. From the distances obtained for both systems it would appear that the dominant type of interaction was dipolar for both systems.

8.2.5 Oriented Multilayer Studies

The assumption that the interactions between the iron-sulphur centres of fumarate reductase are largely dipolar in nature, is a major criterion for the estimation of the inter-spin distances presented in the previous section. If the interactions are mainly dipolar in nature, then an angular dependency for the interaction of FR1 with FR2, or FR3 should be observed, if the interactions are studied in oriented multilayers. The multilayers obtained from the E. coli strain with amplified expression of the enzyme have been shown to exist as crystalline arrays of the enzyme (chapter 7). These membrane multilayers were used to study the interactions of the iron-sulphur centres of fumarate reductase. The interactions were studied by observing the changes in the linewidth and in $P_{1/2}$, the saturation parameter, for the two

Figure 8.11

Angular dependence of $\delta P_{1/2}$ for FR1 + FR2

The change in $P_{1/2}$ with angle, for the ferredoxin signal (g_x) from dithionite reduced membrane multilayers minus that from succinate reduced membranes multilayers, is shown plotted versus the angle of the multilayers to the magnetic field. The maximum value of $\delta P_{1/2}$ was taken to indicate the angle between the interspin vector and the magnetic field. The maximal interaction will be observed when the vector is parallel to the magnetic field ($\theta = 0$; $(1-3\cos^2\theta)^2 = 4$). The variation of the signal height is also shown. The temperature was 6K and the e.p.r. conditions were as described for fig.8.1.

Angular Dependence of $\Delta P_{1/2}$,
FR1+FR2

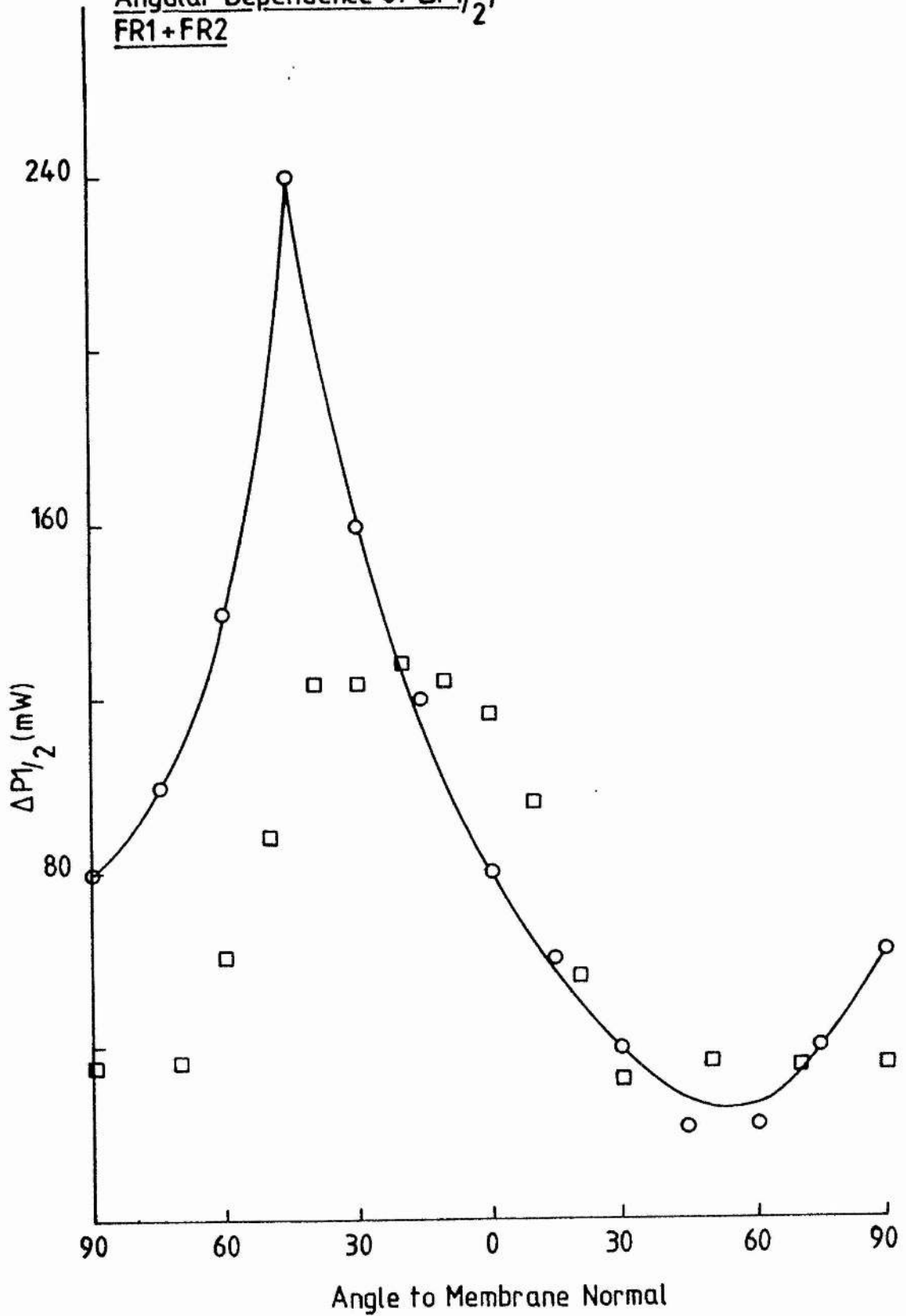
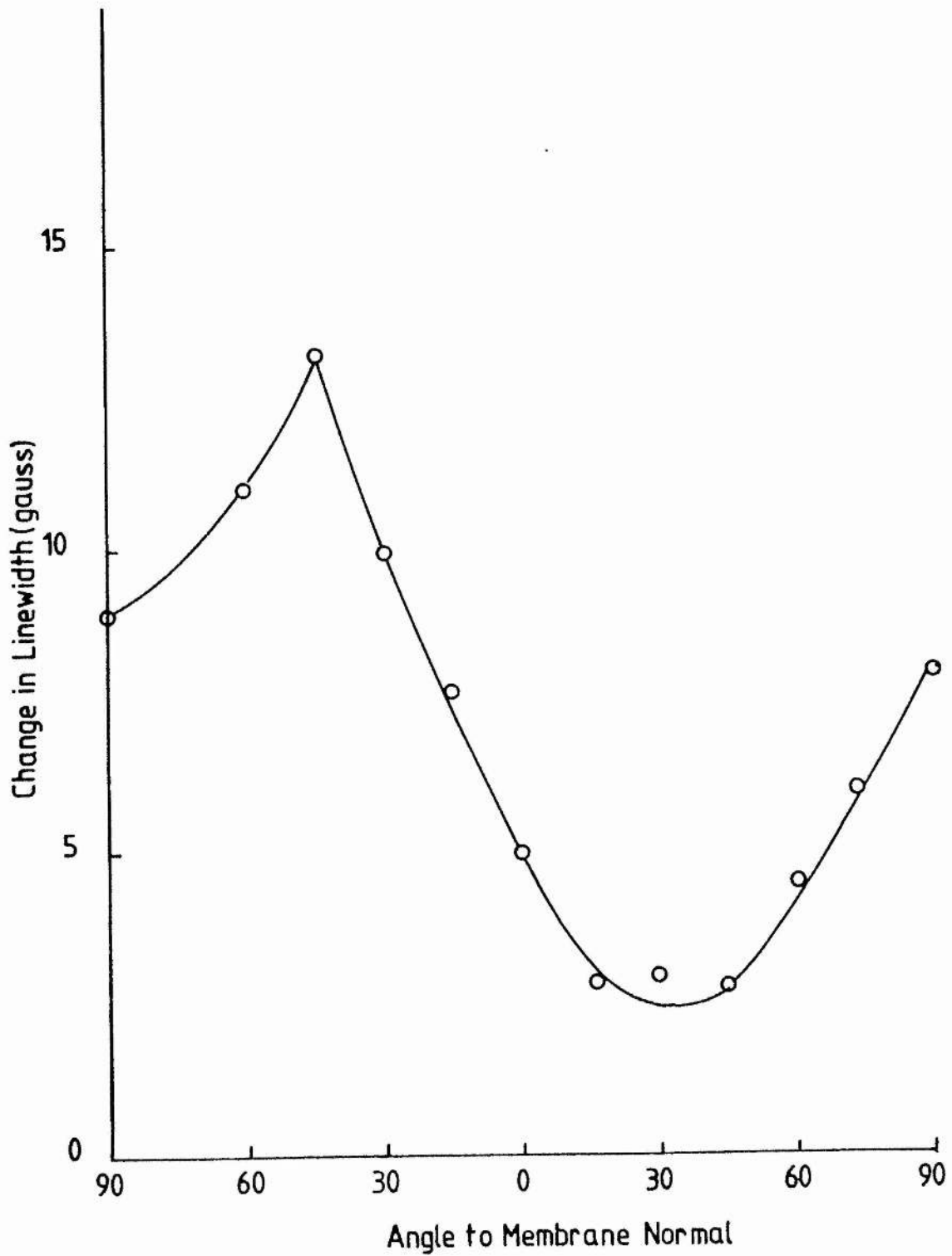


Figure 8.12

Angular dependence of linewidth for FR1 + FR2

The change in the linewidth of the ferredoxin signal (gx) from membrane multilayers reduced with dithionite, is shown plotted against the angle to the membrane normal. The peak in the value for the change in linewidth correlates with the maximum $\delta P_{1/2}$ observed from these membrane multilayers. the linewidth was measured from the peak of resonance to the half-height on the high field side. The temperature was 6K and the e.p.r. conditions were as described for fig.8.1.

Angular Dependence of Linewidth
FR1+FR2



systems. The angular dependency of the change in $P_{1/2}$ ($\delta P_{1/2}$, g_x) and linewidth (g_x) of the ferredoxin signal from dithionite reduced multilayers is shown in fig.8.11 and 8.12. An angular dependence is clearly observable for the change in $P_{1/2}$ and linewidth, confirming the dipolar nature of the interaction between these two centres. Fig.8.13 to 8.15 show that the interaction between FR1 and FR3 also shows some angular dependency. The angular dependencies of the two interacting systems did not show any 'magic-angle' properties, in that the line broadening and change in $P_{1/2}$ did not reach zero at any angle. This may indicate the contribution of exchange interaction to the two systems, as this type of interaction does not show any angular dependence (Coffman & Buettner 1979). This may, however, reflect the nature of the oriented multilayers and arise from the non-oriented regions of the multilayer system.

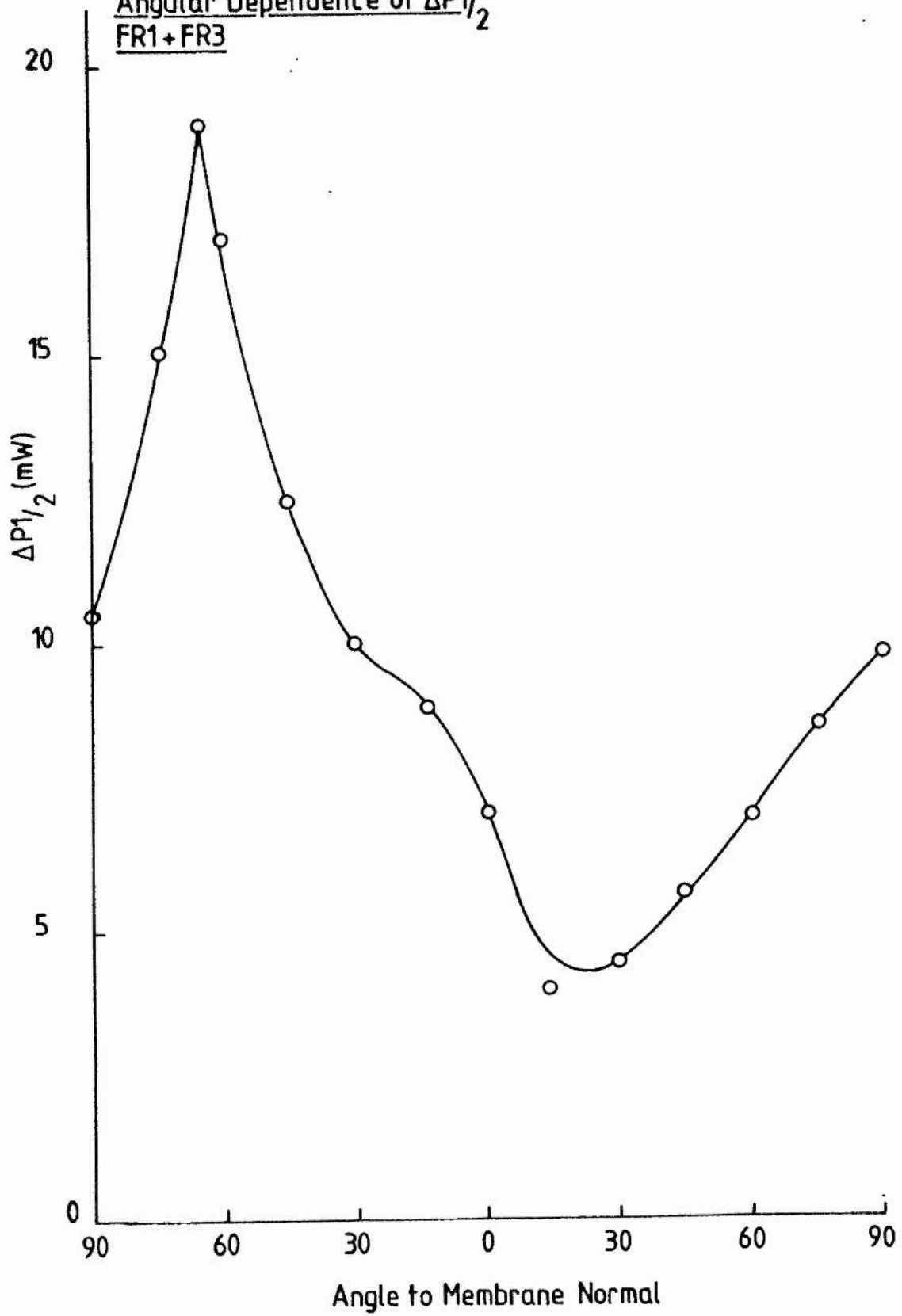
The angle of the maximum change of both $P_{1/2}$ and linewidth correlated well in both cases. A reasonable correlation was observed for signal amplitude of g_x of FR1 plus FR2 (chapter 7 & fig.8.11), which had a maximum at approximate 40° to 20° to the membrane normal. This indicates that at least part of the signal height observed in the dithionite reduced membranes, arises from the relief of saturation of FR1, by interaction with FR2. These maxima can be taken as indicating the angle between the inter-spin vector and the magnetic field. The dipolar interactions are maximum

Figure 8.13

Angular dependence of $\delta P_{1/2}$ for FR1 + FR3

The change in $P_{1/2}$ (gx) with angle for the ferredoxin signal from partially reduced oriented membrane multilayers, is shown plotted versus the angle of the magnetic field to the membrane normal. E.p.r. conditions were as described for fig.8.1 and the temperature was 6K.

Angular Dependence of $\Delta P_{1/2}$
FR1 + FR3



Figuer 8.14

The angular dependence of FR1 linewidth for FR1 + FR3

The change in linewidth (gx) of the ferredoxin signal from partially reduced membrane multilayers is shown plotted against the angle of the magnetic field to the membrane normal. E.p.r. conditions were as described for fig.8.1 and the temperature was 6K.

Angular Dependence of Linewidth of FR1,
FR1+FR3

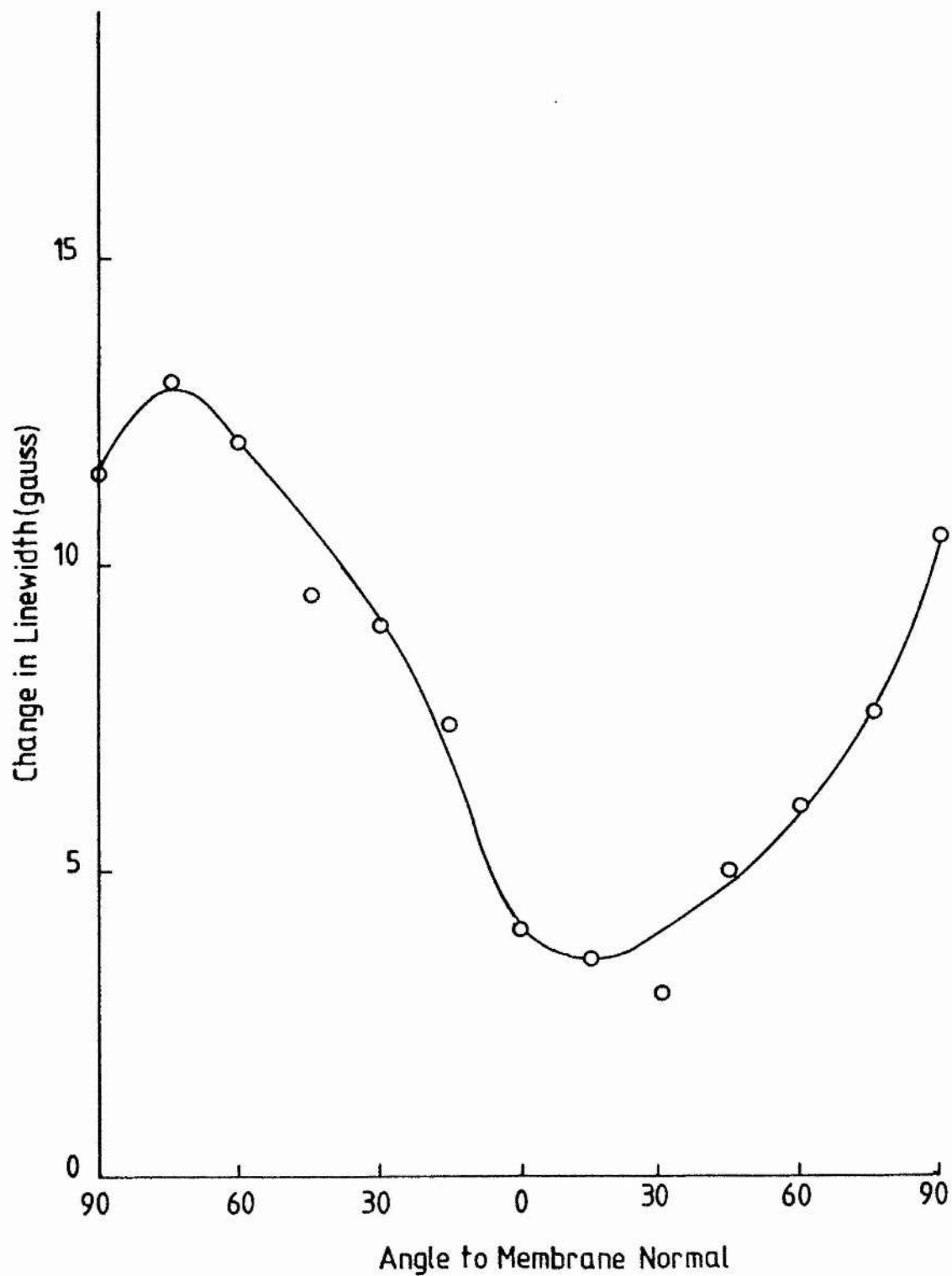


Figure 8.15

Angular dependence of FR3 linewidth

The linewidth of the $g = 2.01$ resonance of FR3, from partially reduced membrane multilayers, is shown plotted versus the angle of the magnetic field to the membrane normal. E.p.r. conditions were as described for fig.8.1 and the temperature was 5K.

Angular Dependence of FR3 Broadening

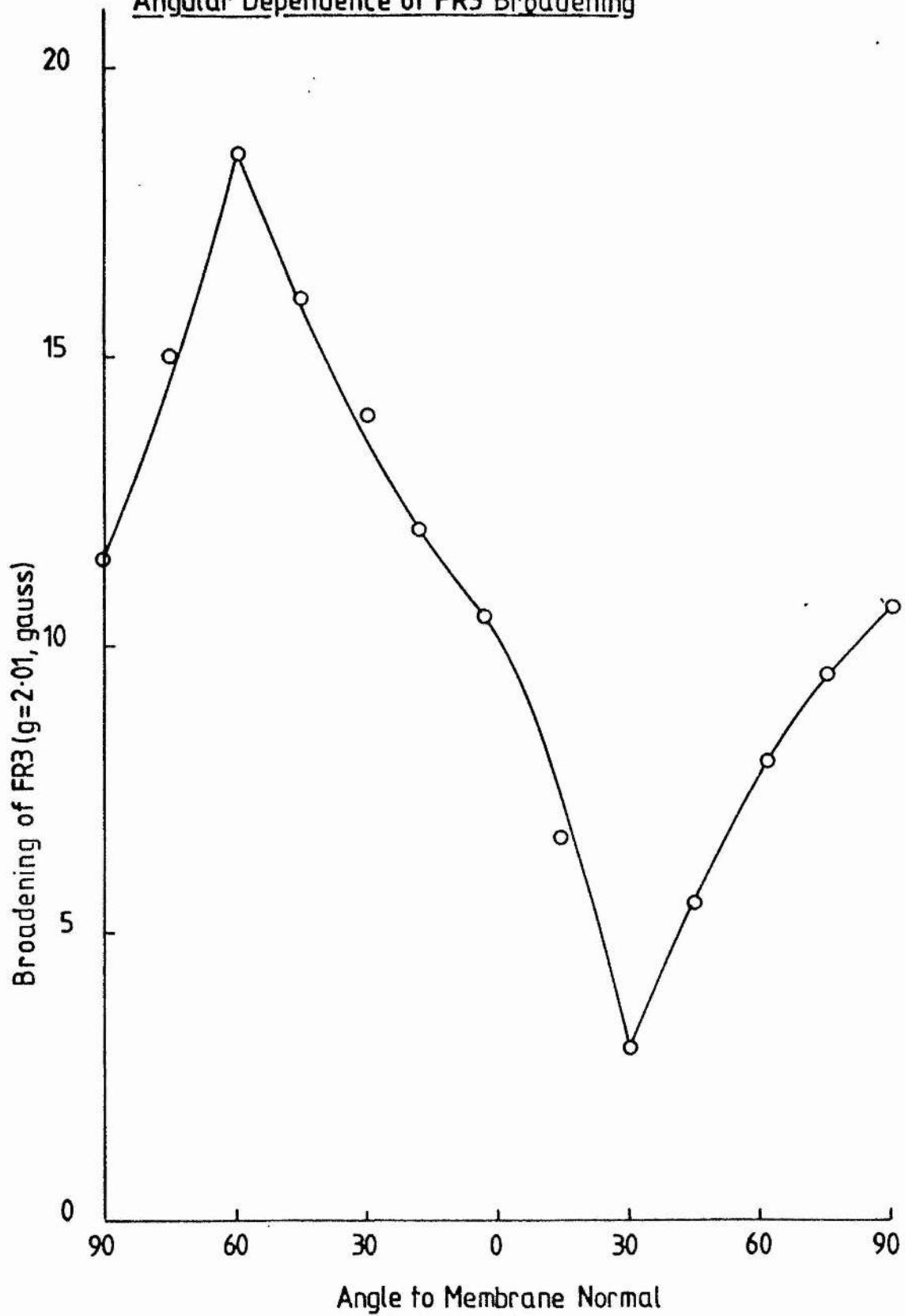
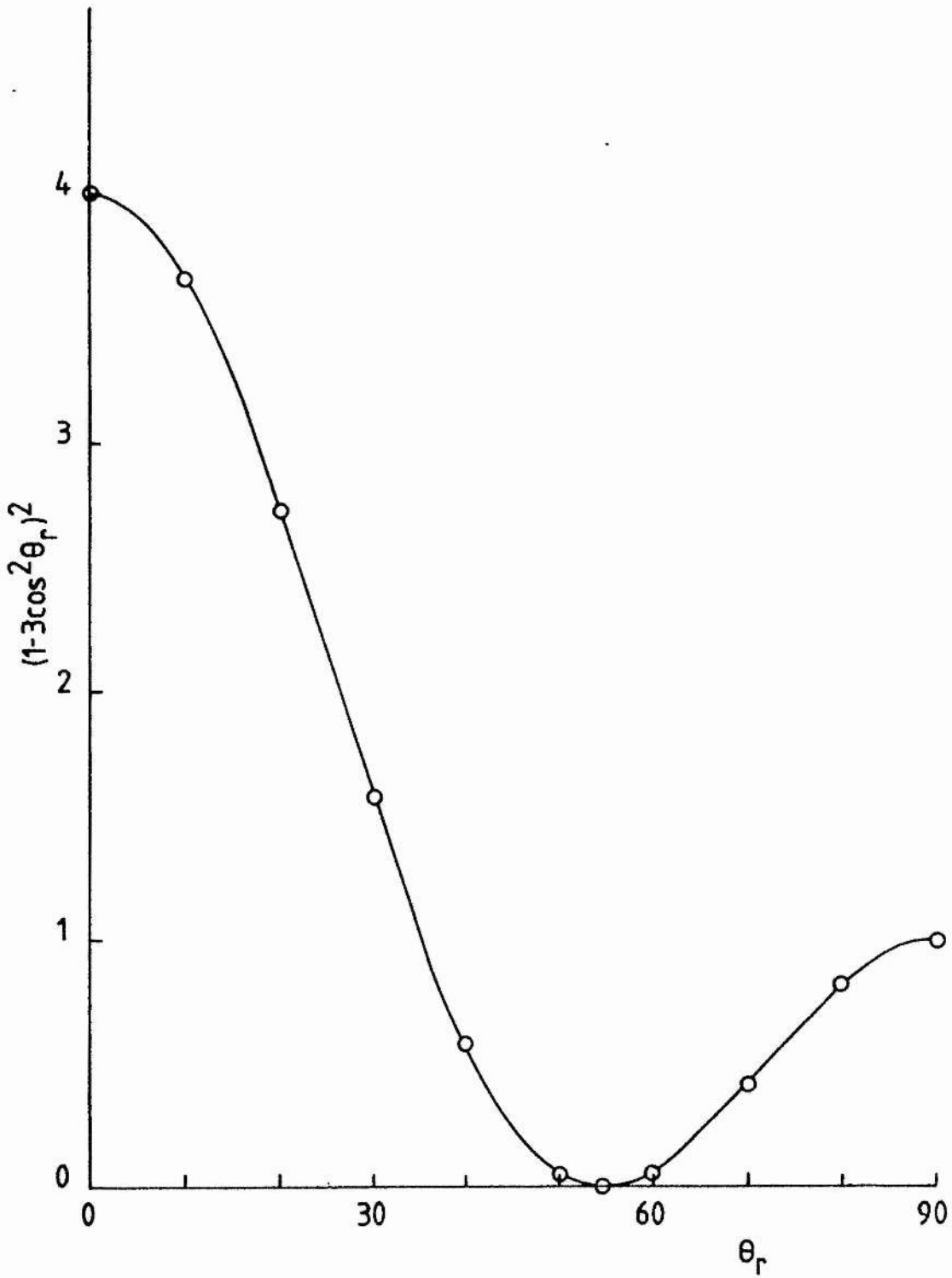


Figure 8.16

Variation of the angular function

The variation of the angular function $(1-3\cos^2\theta)^2$, is shown. The value of the function varies from 4 to 0 and this will be reflected in the strength of the dipolar interaction at each angle and also the calculation of the inter-spin distance, from the equation of Ohnishi *et al.* (1982). When the angular function is zero, the angle is said to be 'magic', as the dipolar interaction disappears at this angle ($\theta = 54.735^\circ$).

Variation of Angular Function



when $(1-3\cos^2\theta)^2 = 4$, ($\theta = 0$, fig.8.16), which is when the magnetic field lies parallel to the inter-spin vector. Thus if these angles are substituted in the equation of Ohnishi et al. (1982) a reasonable estimate for the inter-spin distance for each system should be obtained. The angle of maximal $\delta P_{1/2}$ was used as this was considered to be more accurate, due to possible errors in measurement of the linewidth. An angle of 45° , obtained from the dithionite reduced multilayers, gave an estimate of approximately 16\AA as an upper limit of the inter-spin distance for FR1 and FR2, if the relaxation times were assumed to be similar. An estimate of approximately 10\AA was obtained if FR2 was assumed to relax 10-fold faster than FR1. For the interaction between FR1 and FR3 an angle of 65° was used for the calculation, which set an upper limit of 12\AA and a value of approximately 8\AA if FR3 was assumed to relax 10-fold faster than FR1. If the value of T_{1s}/T_{1f} of 7.55 was used then an inter-spin distance of approximately 9\AA was calculated for the interaction between FR1 and FR3. The angular dependence of the two e.p.r. properties of the interacting spin systems confirms that the interactions are largely dipolar in nature and that this assumption was valid for the estimation of the distances between the interacting spins. The distances estimated by the above methods all show that the iron-sulphur centres of fumarate reductase are all located in such a manner that allows the interaction and presumably electron transfer between the centres.

A consequence of the crystal membrane structure, obtained on producing oriented multilayers from the amplified strain of E. coli, was that the orientation of the inter-spin vector could be more accurately described. By definition two angles are required to describe the position of the vector, relative to the g_z and g_y of the slower relaxing species. Estimates of these angles can be obtained by the study of the different g -tensors of the interacting spins. A different angular dependence of $\delta P_{1/2}$ was observed when the saturation function was determined using g_z (fig.8.17 & 8.18). Again good correlation with the signal height observed from dithionite reduced membrane multilayers was seen. The angles obtained from these dependencies were used as the angle of the interspin vector to the g_z of spin 1 (θ_r , fig.8.19). The angles of r to g_x of spin 1 (ϕ) were obtained from the angular dependency of the g_x functions. Fig.8.2 & 8.7 compare the e.p.r. spectra of dithionite reduced membranes and membranes poised at -70mV , to computer simulations obtained using the angles obtained from the $\delta P_{1/2}$ plots. The circles represent the theoretical points obtained from the simulations, using the parameters shown in the figure legends. It is seen that good fits of the simulations to the experimental spectra were obtained. The values of D were obtained from the following equation:

$$D = \mu_{\text{eff}} / r^3 = S(S+1)g^3 / r^3$$

Figure 8.17

Angular dependency of $\delta P_{1/2}$ (gz) of FR1 + FR2

The angular dependence of $\delta P_{1/2}$ obtained from the gz resonance of the ferredoxin signal from dithionite reduced oriented multilayers, is shown plotted against the angle between the membrane normal and the magnetic field. The peak of $\delta P_{1/2}$ occurs at a different angle to that obtained from the gy resonance. The variation of signal height is also shown. E.p.r. conditions were as described for fig.8.1 and the temperature was 6K.

Angular Dependence of $\Delta P_{1/2}$
Gz, FR1: FR1+FR2

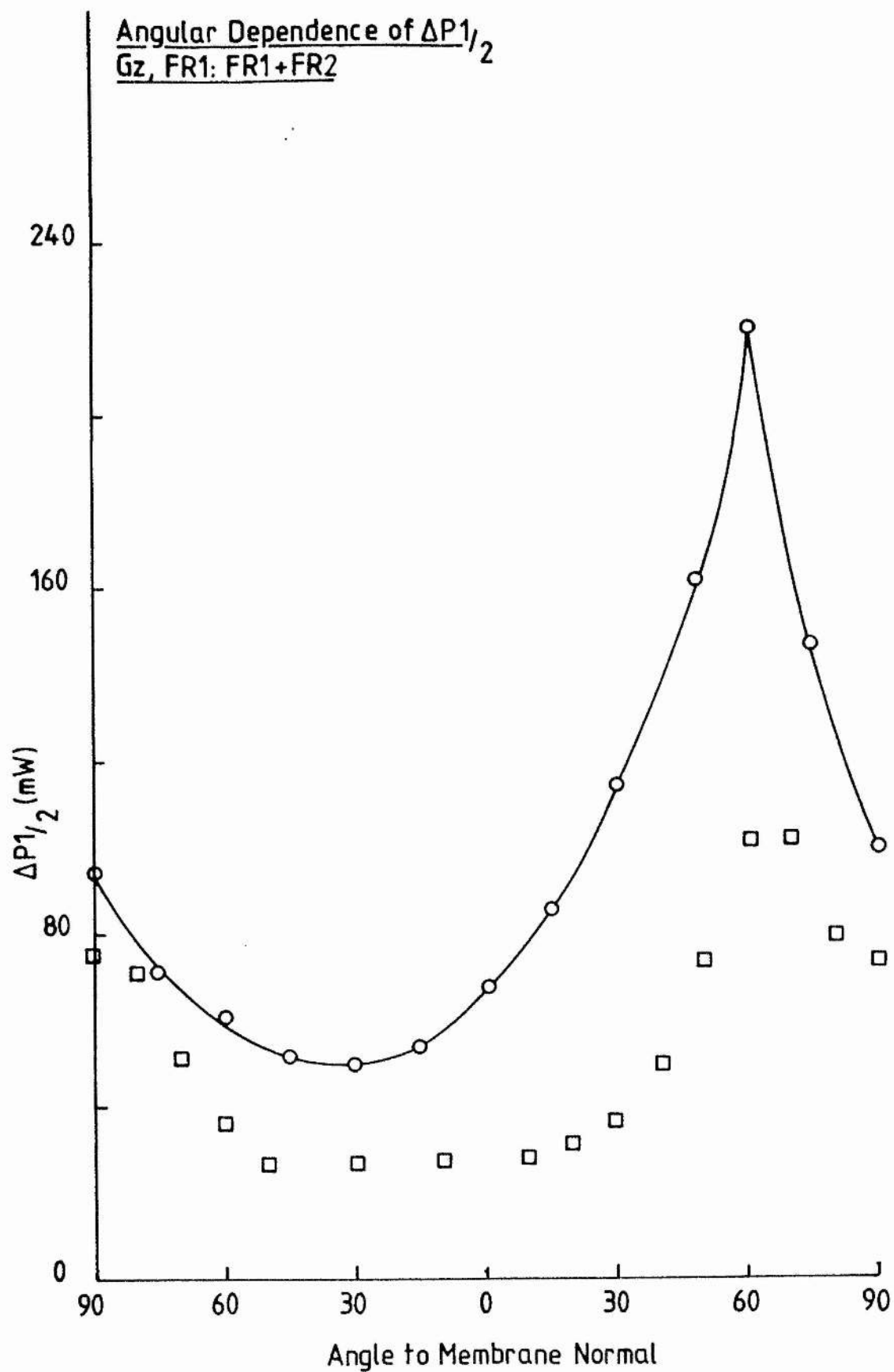


Figure 8.18

Angular dependence of $\delta P_{1/2}$ (gz) of FR1 + FR3

The angular dependence of $P_{1/2}$, obtained from the gz resonance of FR1, is shown plotted versus the angle of the normal of the membrane multilayer to the magnetic field. The peak of $\delta P_{1/2}$ occurs at a different angle to that obtained from the gx resonance. E.p.r. conditions were as described for fig.8.1 and the temperature was 5K.

Angular Dependence of $\Delta P_{1/2}$
Gz FR1+FR3

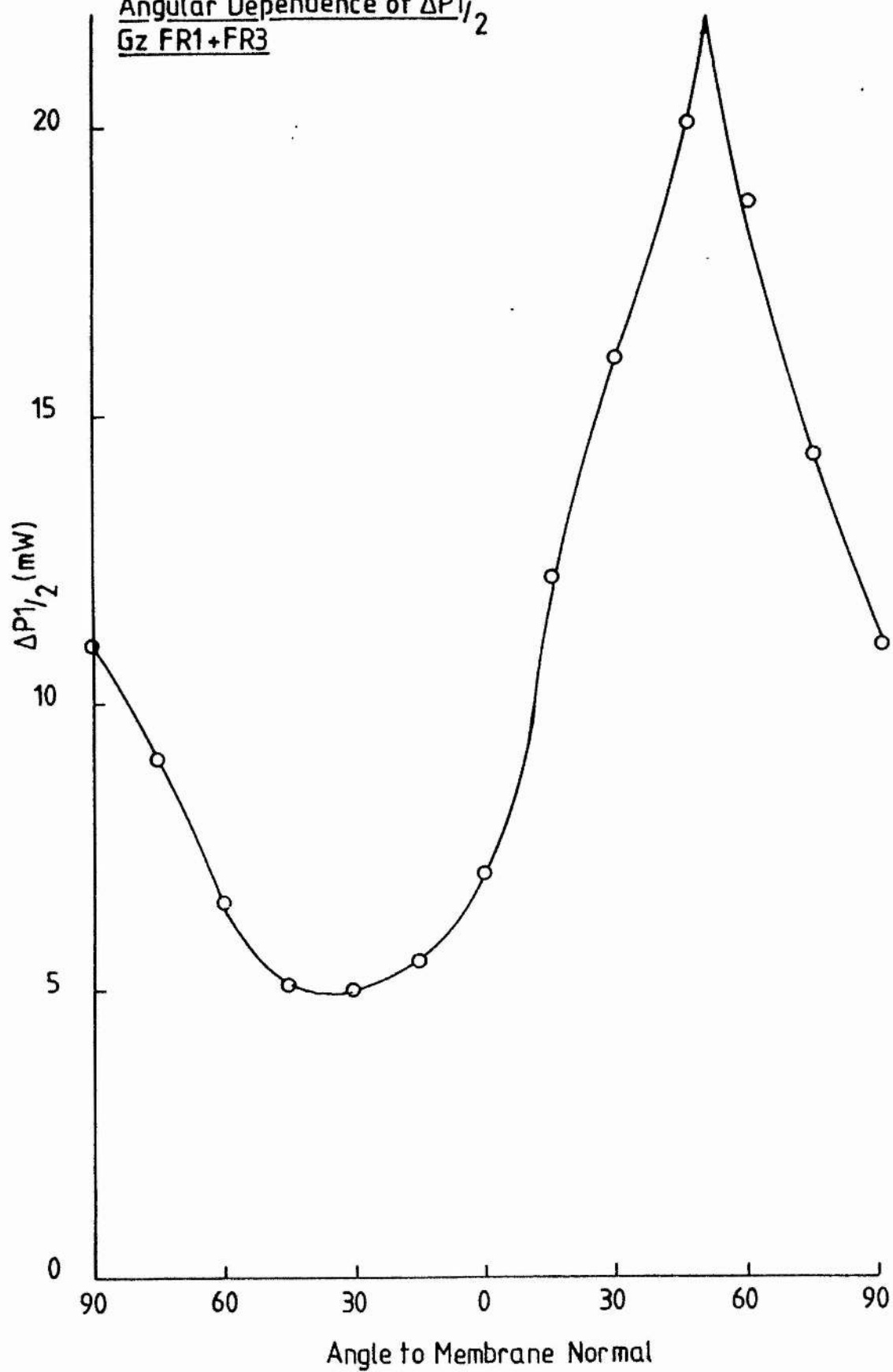
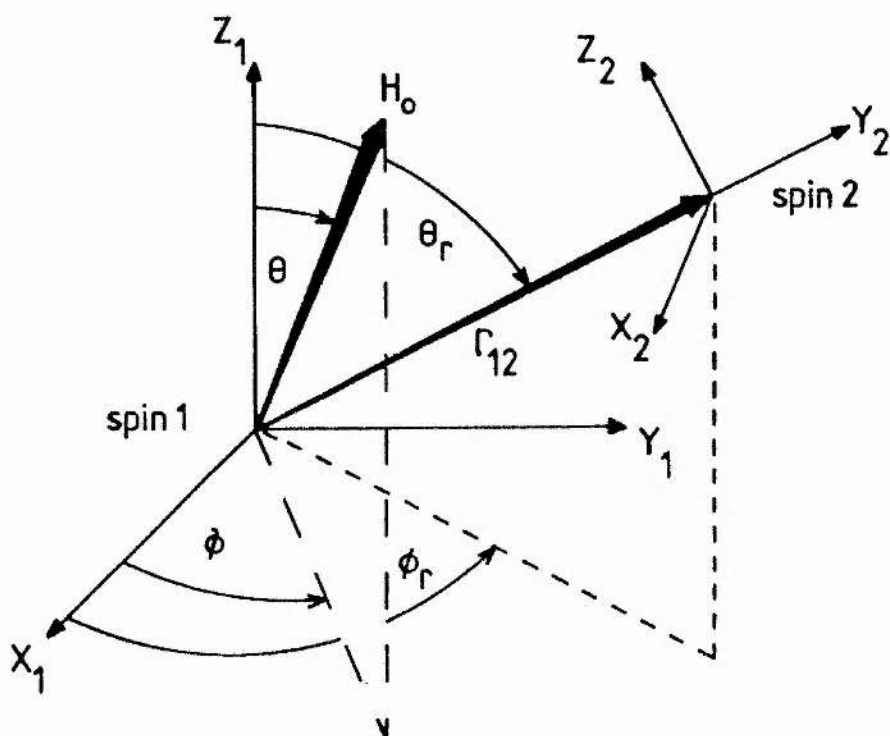


Figure 8.19

Model for the interaction of two rhombic spins

The interaction between the two spins (S_1 and S_2) is shown with the angles required to describe the spatial orientation of the spins relative to each other. The orientation of the magnetic field is given by the angles θ and ϕ ; the orientation of the inter-spin vector r_{12} , between the two spins is given by θ_R and ϕ_R .

Model for the Orientation of Two Interacting Spins



For FR1 plus FR2 the value of D was allowed to vary from 2 ($r = 16\text{\AA}$) to 12 ($r = 9\text{\AA}$). The best fit of the simulations to the experimental spectrum was obtained when D was approximately 8, which set r at 10.5\AA . Similarly for the interaction between FR1 and FR3, the spectrum could be best fit by the simulation if D had a value of 7.5, which sets r at approximately 8.5\AA . The simulations thus confirmed that the estimates obtained from the oriented multilayer studies were reasonable and that it was reasonable to assume that the interactions were largely dipolar.

A picture of the overall geometry of the iron-sulphur centres is presented in fig.8.20, showing the distances and angles estimated from this present study. The orientations of the iron-sulphur centres themselves is not shown for clarity.

8.3 Conclusions

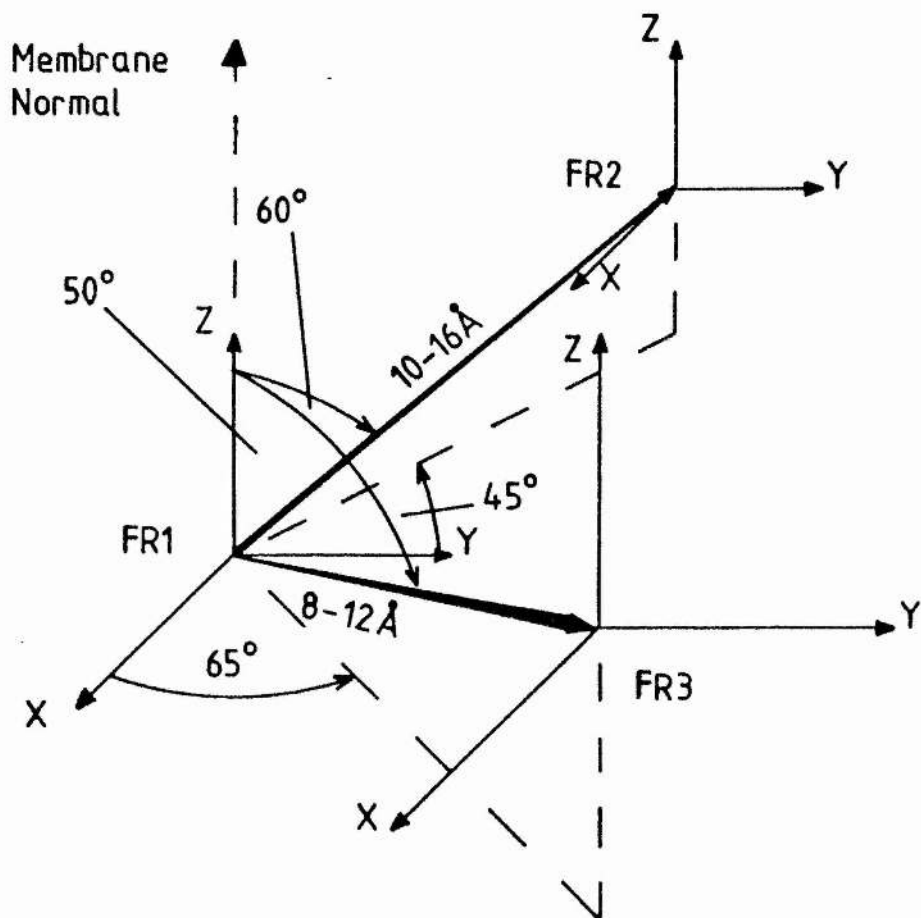
Two interacting spin systems have been demonstrated between the iron-sulphur clusters of the *E. coli* fumarate reductase. Centre FR1 has been shown to interact with both centre FR2 and FR3 (HiPIP). These interactions were observed by the changes they induced in the e.p.r. properties of the centres. The interactions were shown to be largely dipolar in both cases as an angular dependency of the change in e.p.r. properties of the centres was observed, and allowed the

Figure 8.20

Model for the interaction of the iron-sulphur centres of fumarate reductase

A sketch of the spatial relationships of the iron-sulphur clusters of fumarate reductase is shown. The angles of the inter-spin vectors to the g-tensors of FR1 are those obtained from the oriented multilayer studies. The distance estimates are the limits set by T_{1s}/T_{1f} values of 1 and 10 for the upper and lower limits respectively. The g-tensors of the centres are not shown in their orientations, to clarify the orientation of the inter-spin vectors.

Model for the Orientation of the
Iron-Sulphur Centres of Fumarate Reductase



estimation of the inter-spin distances for both systems , from these observed changes.

The observed effects of the interactions were linebroadening of the e.p.r. spectra, relief from power saturation and the observation of half-field signals. The latter phenomenon in particular indicates the presence of interacting species, and adds further evidence for the existence of the second binuclear ferredoxin centre in this enzyme. A distance of approximately 10\AA was estimated between the two ferredoxin centres, by the method of Ohnishi *et al.*, indicating that the centres were close enough for electron transfer to occur between them. The existence of only a very small degree of splitting of the e.p.r. spectrum indicates that the two centres are oriented close to the magic-angle and this was confirmed by the angles measured from the oriented multilayer studies. The small degree of splitting also indicates that the contribution of exchange interaction to the system is small as would be expected from the distance estimate.

The interaction between the HiPIP centre and FR1 was shown to be largely dipolar in nature also, and an estimate of the inter-spin distance of 9\AA was obtained. This also demonstrated the existence of possible electron flow from FR3 to FR1. The measurement of the interaction between these two centres was performed in samples that only contained part of

the centres in a paramagnetic state, i.e. not all of the population of each centre in the sample was paramagnetic. Thus the interaction between these two centres must be fairly strong and the value of the inter-spin distance can only be taken as an estimate.

CHAPTER NINE

General Conclusions

9.1 The prosthetic groups of fumarate reductase

The number and type of iron-sulphur clusters in succinate-fumarate oxido-reductases from other sources have been the subject of controversy (Albracht 1980, Beinert & Albracht 1982). The e.p.r. detectability of the cluster paramagnetic in the oxidised state, and the second 'binuclear' ferredoxin cluster is dependent upon the enzyme preparation. The results presented in this thesis, to characterise and quantitate the iron-sulphur clusters from the E. coli fumarate reductase, were largely performed on the membrane bound enzyme to minimise the loss of e.p.r. detectable centres or the introduction of artefacts by preparative procedures. A centre detectable in oxidised membranes with a mid-point potential (pH 7) of approximately -30mV was shown to be present at approximately the same concentration as the covalently bound flavin. This centre (FR3) was similar to that from succinate dehydrogenase (chapter 4), though it is detectable over a wider temperature range. This centre may be 'trinuclear' in nature, because of its similarity to S3 of succinate dehydrogenase, which may be of this type (Jonsson et al. 1985). The difference in the e.p.r. properties and relaxation rates may be due to the different environments of the two centres, as it has been proposed that the relaxation mechanisms of binuclear and tetranuclear clusters are sensitive to these changes (Bertrand & Gayda 1979, Gayda et

al. 1976, Salerno *et al.* 1977a, Blum *et al.* 1979).

The e.p.r. signals produced upon reduction by succinate, or the poisoning of membranes at approximately -200mV, indicated the presence of a 'binuclear' ferredoxin centre, as described for succinate dehydrogenase (Ohnishi *et al.* 1976). This centre had a mid-point potential (pH 7) of approximately -50mV and was present at the same concentration as the covalently bound flavin. The presence of a second 'binuclear' ferredoxin centre was shown upon reduction by dithionite and at low redox potentials, by the increased signal intensity of the ferredoxin signal under non saturating conditions. This centre was also measured at a 1 : 1 ratio to the covalently bound flavin, under specific e.p.r. conditions, and had a mid-point potential (pH 7) of approximately -280mV. The study of this second centre was complicated by the presence of FR1 and interaction with that centre.

The relaxation time of the iron-sulphur centres was characterised by the temperature dependence of their e.p.r. properties. The succinate reducible ferredoxin centre was shown to be similar to that reported for other iron-sulphur clusters, and exhibited well characterised relaxation processes, though its relaxation was somewhat faster than S1 from succinate dehydrogenase (chapter 5). Because the fumarate reductase was membrane bound, this may allow the faster relaxation of the iron-sulphur clusters by dissipation of their energy via the vibrational energy of the protein

molecule to the membrane. The relaxation of the ferredoxin signal was seen to be enhanced upon reduction of the second ferredoxin centre. The e.p.r. signal behaved as a homogeneous species, with faster relaxation than for FR1 alone. The iron-sulphur cluster paramagnetic in the oxidised state was shown to be rapidly relaxing. Enhancement of its and FR1's relaxation was observed in samples containing both centres in a paramagnetic state.

A broad e.p.r. spectrum was also observed from dithionite reduced membranes and membrane poised at low redox potentials. This centre was present at approximately 1/10th of the concentration of the other iron-sulphur centres. It was suggested that this centre may be the product of cluster conversion from the 'trinuclear' cluster (FR3), as this type of conversion has been shown to occur easily upon reduction by dithionite (Emptage *et al.* 1980, Thomson *et al.* 1981). This centre has been suggested to be FR2, but its low detectable spin concentration appears to exclude this. However, an E_{m7} of -260mV was observed for this centre.

The flavin moiety of fumarate reductase was shown to behave in a similar manner to that from succinate dehydrogenase, though a different mid-point potential (pH 7, $n = 2$) at -12mV was found for the fumarate reductase flavin. The pK value of the protonation step for the fully reduced flavin was determined, but that for the semiquinone could not be determined in the pH range studied. The flavin semiquinone

was present as the protonated (neutral) form in the pH range studied (6 to 9). The flavin semiquinone was shown to be reasonably stable and thus capable of acting as a converter from 1-electron to 2-electron transfer steps.

The reversal of electron flow in fumarate reductase, as compared to succinate dehydrogenase, can be accounted for by the redox chemistry of its prosthetic groups. Electrons are presumably donated to centre FR3 (E_{m7} , -30mV) from menaquinone (E_{m7} ($n = 2$), -74mV), by analogy with succinate dehydrogenase where electrons are passed to ubiquinone from centre S3. The electrons are then passed to centre FR1 (E_{m7} , -50mV), the flavin moiety (E_{m7} ($n = 2$), -12mV) then receives the electrons from centre FR1 and possibly centre FR2, which are then passed to fumarate (E_{m7} succinate-fumarate couple, 30mV). The possibility of the electron transfer steps has been shown by the interactions between the centres and their spatial relationships (chapter 8). The role of FR2, as that of S2 from succinate dehydrogenase, is still uncertain, as its measured mid-point potential was -280mV. However as this was measured in the presence of paramagnetic FR1, it may not be the true E_{m7} of FR2, but may reflect interaction with FR1 and thus the greater difficulty in reducing this centre (chapter 8). The possibility of FR2 receiving electrons from F3 cannot be excluded (either directly or via FR1); also the flavin may interact with this iron-sulphur centre.

9.2 Membrane location of the catalytic site and the prosthetic groups

The E. coli respiratory fumarate reductase has been studied in its membrane bound form, using a strain of E. coli that had amplified expression of the enzyme (JRG1031), as well as a wild-type strain (EMG2). The location of the fumarate reductase on the cell membranes is of prime importance in considering the energetics of respiration that utilises fumarate as the terminal electron acceptor, as the stoichiometry of proton translocation will be dependent upon its location. The weight of experimental evidence has placed major catalytic subunits of fumarate reductase on the cytoplasmic aspect of the cell membrane (Van der Plaas et al. 1983, Lemire et al. 1983). However the location of the site of reduction need not have been cytoplasmic. That the catalytic site was indeed cytoplasmic in location was shown by the requirement for the uptake of fumarate into whole cells before its reduction. The requirement for the transportation of fumarate into the cells was shown by the removal of, or interference with, the uptake causing loss of, or reduced rates of, fumarate reduction in whole cells (chapter 3).

The location of the catalytic portion of fumarate reductase on the cytoplasmic aspect of the cell membrane was shown by Lemire et al. (1983). The location of the prosthetic groups of fumarate reductase, namely the flavin moiety and the iron-sulphur centres, was thus implied to be

cytoplasmic also. The question still arose as to whether or not these prosthetic groups were located close to the membrane surface. The flavin moiety can be assumed to be located thus, because it has been shown to be bound to the 69 Kdalton subunit (Dickie & Weiner 1979), which was shown to be membrane extrinsic by Lemire *et al.* (1983). The location of the iron-sulphur subunit has been implied to be in the iron-sulphur subunit (27 Kdalton), by the primary structure of this peptide, deduced from the nucleotide sequence of the gene encoding it (Cole *et al.* 1982, Guest *et al.* 1984). It seems likely that all three clusters are located in this peptide as three groups of cysteine residues were identified from this sequence. Weiner *et al.* (1984) proposed that the flavoprotein peptide encased the iron-sulphur peptide to some extent and that both are membrane extrinsic. By using dysprosium(III)-EDTA as a paramagnetic probe to perturb the e.p.r. properties of the three iron-sulphur centres, it has been shown that they are all located close to the surface of the cytoplasmic membrane (chapter 5). The effects of dysprosium(III) were similar in membrane bound and isolated proteins, adding weight to the proposition that the iron-sulphur centres are in the membrane extrinsic portion of fumarate reductase. Centres FR1 and FR3 were shown to be located deep within the catalytic subunits, using the method of Blum *et al.* (1983), by analogy to the *Chromatium vinosum* HiPIP centre which is known to be located centrally in its protein.

9.3 Orientation and spatial relationships of the prosthetic groups

Interactions have been shown to occur between the prosthetic groups of the *E. coli* fumarate reductase (chapters 4 & 8), by the observed changes in the e.p.r. properties of the iron-sulphur centres when more than one centre was paramagnetic. Namely relief of power saturation at low temperatures and line broadening of the e.p.r. spectra. Interactions were observed between FR1 and FR2, FR1 and FR3 and FR1 and the flavin semiquinone. The distances between the interacting groups were estimated by assuming that the interactions were predominantly dipolar in nature. From the perturbations of the e.p.r. properties of the randomly oriented solid samples (frozen membrane suspensions) an averaged distance between interacting centres was estimated. The inter iron-sulphur centre distances for FR1 and FR2, and FR1 and FR3 were shown to be approximately 9-12⁰Å in both cases, by the method of Ohnishi et al. (1982). The distance between FR1 and the flavin moiety was similarly shown to be approximately 11-17⁰Å. The feasibility of electron transfer between the prosthetic groups was therefore shown (chapter 8).

The location of the succinate reducible ferredoxin centre close to the flavin moiety poses the question of which subunit it is located in. As mentioned previously it has been implied to be located in the iron-sulphur subunit, so if this is the case then it must be located in such a position that allows it to be close enough to interact with the flavin. This is possibly close to the junction of the two catalytic subunits. This location may allow the iron-sulphur cluster to utilise a cysteine residue from the flavoprotein subunit, as two of the cysteine residue clusters require a further ligand to form intact iron-sulphur clusters (Guest *et al.* 1984). An alternative source for a ligand has been proposed to be a nitrogen from one of the amino acid residues (Adman 1979). The HiPIP centre (FR3), analagous to S3 of succinate dehydrogenase, can be proposed to be located in a position close to the membrane interface that allows interaction with the menaquinone moieties in the membrane. This may account for the lability of this centre and the low values obtained for the non-haem iron and acid-labile sulphur determinations of Cole *et al.* (1982), which were performed on the catalytic dimer.

Orientation studies on the membranes derived from the fumarate reductase amplified strain showed that the protein molecules were ordered into a crystalline array upon production of the membrane multilayers. Multilayers produced from a wild-type strain of *E. coli* did not exhibit a

equivalent to FR1 and FR3 (Albracht *et al.* 1981, Uden *et al.* 1984). Both enzymes contain the same covalently bound flavin moiety which had similar mid-point potentials (E_{m7} ($n = 2$), -20mV for the *W. succinogenes* enzyme).

9.4 Future developments

The nature of the HiPIP-type centres in the succinate-fumarate oxidoreductases has become of interest since the discovery of the three-iron clusters, and the implication that the centre S3 was of this type (Johnson *et al.* 1985). The similarity of the e.p.r. signals of fumarate reductase to those of succinate dehydrogenase has implied that the iron-sulphur clusters are of the same type in the two enzymes. However, this is required to be confirmed by experimental evidence. Studies similar to those of Johnson *et al.* (1985) are required to further characterise centre FR3 and determine the nature of this cluster i.e. whether it is the degradation product of a 4Fe-centre. The nature of the second ferredoxin centre (FR2) has been further complicated by the report of the 'broad' ferredoxin signal, which titrated in the same region as that in which centre FR2 was detectable (R. Cammack, personal communication). Its low spin quantitation, in the membrane bound enzyme, appears to exclude this centre from being FR2, but it cannot be excluded that this centre is not fully e.p.r. detectable. The first excited state ($S = 3/2$) may be significantly populated. That

this centre is the result of conversion from FR3; either from a 3Fe-centre to a 4Fe-centre or between redox states of a 4Fe-centre (+1 and +3); has been proposed, but additional data is required to confirm this.

It has been assumed that FR3 receives electrons from menaquinone in a similar manner to that in which succinate dehydrogenase donates electrons to ubiquinone. However, no interaction between FR3 and the menaquinone free radical was observed in the membrane preparations used in this study. This may however be due to the titration of the flavin in the same region and its large signal masking that of the quinone. Further studies, perhaps using a mutant of *E. coli* lacking the flavin moiety, may provide additional information. It has been reported that the anchor polypeptides of fumarate reductase are required for quinone reductase activity (Cecchini *et al.* (1984), so these subunits may bind menaquinone in a similar manner as succinate dehydrogenase binds ubiquinone.

The location of the iron-sulphur clusters has been implied by the sequence of the catalytic subunits to be in the iron-sulphur subunit. However direct experimental evidence is required to confirm this location. Thus e.p.r. studies on the isolated iron-sulphur subunit, or on a mutant strain lacking *frdA* may reveal the location of the iron-sulphur centres.

The crystalline nature of the multilayers produced from the fumarate reductase amplified strain of *E. coli*, has been shown. The fumarate reductase was shown to be in a well ordered environment, within the membranes. This was distinct from the gross order observed by Weiner *et al.* (1984). These membranes thus lend themselves to use for structural studies of the enzyme, because of the ease of preparation of the samples and their high levels of the enzyme. The knowledge of the detailed structure of fumarate reductase and succinate dehydrogenase will provide evidence for many of the questions that are still unanswered or for which partial answers have been found.

BIBLIOGRAPHY

- Abou-Jaoude, A., Chippaux, M., & M.-C. Pascal (1979a).
Formate-nitrate reduction in Escherichia coli K12. 1.
Physiological study of the system. European Journal of
Biochemistry 95, 309-314.
- Abou-Jaoude, A., Pascal, M.-C., & M. Chippaux (1979b).
Formate-nitrate reduction in Escherichia coli K12. 2.
Identification of components involved in electron
transfer. European Journal of Biochemistry 95, 315-321.
- Adman, E.T. (1979). A comparison of the structures of
electron-transfer proteins. Biochimica et Biophysica Acta
549, 107-144.
- Albracht, S.P.J. (1980). The prosthetic groups in succinate
dehydrogenase. Number and stoichiometry. Biochimica et
Biophysica Acta 612, 11-28.
- Albracht, S.P.J., Uden, G., & A. Kroger (1981). Iron-sulphur
clusters in fumarate reductase from Vibrio succinogenes.
Biochimica et Biophysica Acta 661, 295-302.
- Antholine, W.S., Hyde, J.J., & H.M. Swartz (1978). Effects of
 Dy^{3+} as a free radical relaxing agent in biological
tissues. Journal of Magnetic Resonance 29, 517-522.

- Arnon, D.T., Whatley, F.R., & M.B. Allen (1957). Triphosphopyridine nucleotides as a catalyst of photosynthetic phosphorylation. Nature 180, 182-185.
- Baltscheffsky, H., & M. Baltscheffsky (1974). Electron transport phosphorylation. Annual Reviews in Biochemistry 43, 871-897.
- Barlow, C.B., & M. Erecinska (1979). Orientation of the NO ligand of cytochrome a_3 in nitrosyl cytochrome c oxidase. FEBS letters 98, 9-12.
- Beinert, H. (1982). Iron-sulphur proteins, past endeavors and present challenges. In C. Ho (Ed.), Electron transport and oxygen utilisation. Elsevier/North Holland Inc., New York. pp 345-359.
- Beinert, H., & S.P.J. Albracht (1982). New insights, ideas and unanswered questions concerning iron-sulphur clusters in mitochondria. Biochimica et Biophysica Acta 683, 245-277.
- Bertrand, P., & J.-P. Gayda (1979) A theoretical interpretation of the variations of some physical parameters within the [2Fe-2S] ferredoxin group. Biochimica et Biophysica Acta 579, 107-121

Bertrand, P., Roger, G., & J.-P. Gayda (1980). Measurement of the spin-lattice relaxation time from the broadening of EPR spectrum of a randomly oriented system with $S = 1/2$: Application to iron-sulphur proteins. Journal of Magnetic Resonance 40, 539-549.

Blasie, J.K., Erecinska, M., Sammels, S., & J.S. Leigh (1978). The structure of a cytochrome oxidase-lipid model membrane. Biochimica et Biophysica Acta 501, 33-52.

Blum, H., Harmon, H.J., Leigh, J.S., Salerno, J.C., & B. Chance (1978a). The orientation of a heme of cytochrome c oxidase in submitochondrial particles. Biochimica et Biophysica Acta 502, 1-10.

Blum, H., Salerno, J.C., & J.S. Leigh (1978b). A model for the simulation of the EPR spectra of chromophores in partially oriented membrane multilayers. Journal of Magnetic Resonance 30, 385-391.

Blum, H., Salerno, J.C., Rich, P.R., & T. Ohnishi (1979). Exchange integrals for a variety of tetranuclear ferredoxins. Biochimica et Biophysica Acta 548, 139-146.

Blum, H., Poole, R.K., & T. Ohnishi (1980). The orientation of iron-sulphur clusters in membrane multilayers prepared from aerobically grown Escherichia coli K12 and a cytochrome deficient mutant. Biochemical Journal 190, 385-393.

Blum, H., Cusanovich, M.A., Sweeney, W.V., & T. Ohnishi (1981). Magnetic interactions between dysprosium complexes and two soluble iron-sulphur proteins. Journal of Biological Chemistry 256, 2199-2206.

Blum, H., & R.K. Poole (1982). The molybdenum and iron-sulphur centres of Escherichia coli nitrate reductase are non-randomly oriented in the membrane. Biochemical and Biophysical Research Communications 291, 903-909.

Blum, H., Bowyer, J.R., Cusanovich, M.A., Waring, A.J., & T. Ohnishi (1983). Spin-lattice relaxation rates of iron-sulphur proteins and heme proteins affected by dysprosium complexes and temperature. Biophysica et Biochimica Acta 748, 418-428.

Boxer, D.H., & R.A. Clegg (1975). A transmembraneous location for the proton-translocation reduced ubiquinone \rightarrow nitrate reductase of the respiratory chain of Escherichia coli. FEBS letters 60, 54-57.

- Boyer, P.D. (1974). Conformational coupling of biological energy transductions. Biochimica et Biophysica Acta 13, 289-301.
- Brice, J.M., Law, J.F., Meyer, D.J. & C.W. Jones (1974). Energy conservation in Escherichia coli and Klebsiella pneumoniae. Biochemical Society Transactions 2, 523-526.
- Buchanan, B.B., Walasink, R.A., & P. Schurmann (1979). Thioredoxin and enzyme regulation. Trends in Biochemical Sciences 4, 93-96.
- Cammack, R., Patil, D.S., Condon, C., Owen, P., Cole, S.T., & J.H. Weiner (1984). E.s.r. spectroscopic studies of succinate dehydrogenase and fumarate reductase of Escherichia coli. In R.C. Bray et al. (Eds.) Flavins and flavoproteins, Walter de Gruyter & Co., Berlin. pp. 551-554.
- Case, G.D., & J.S. Leigh (1976). Intramitochondrial positions of cytochrome heme groups determined by dipolar interactions with paramagnetic cations. Biochemical Journal 160, 769-783.

- Case, G.D., Ohnishi, T., & J.S. Leigh (1976). Intramitochondrial positions of ubiquinone and iron-sulphur centres determined by dipolar interactions with paramagnetic ions. Biochemical Journal 160, 785-795.
- Cecchini, G., Ackerell, B.A.C., Kearney, E.B., & R.P. Gunsalus (1984). Fumarate reductase from Escherichia coli requires the frdC and frdD gene products for quinone reductase activity. In R.C. Bray et al. (Eds.) Flavins and Flavoproteins, Walter de Gruyter, Berlin. pp. 555-558.
- Coffman, R.E., & G.R. Buettner (1979a). A limit function for long-range ferromagnetic and antiferromagnetic superexchange. Journal of Physical Chemistry 83, 2387-2392.
- Coffman, R.E., & G.R. Buettner (1979b). General magnetic dipolar interaction of spin-spin coupled molecular dimers. Applications to an EPR spectrum of xanthine oxidase. Journal of Physical Chemistry 83, 2392-2400.
- Cole, S.T. (1982). Nucleotide sequence coding for the flavoprotein subunit of the fumarate reductase of Escherichia coli. European Journal of Biochemistry 122, 479-484.

- Cole, S.T., & J.R. Guest (1979a). Amplification and aerobic synthesis of fumarate reductase in ampicillin-resistant mutants of Escherichia coli K12. FEMS Microbiological letters 5, 65-67.
- Cole, S.T., & J.R. Guest (1979b). Production of a soluble form of fumarate reductase by multiple gene duplication in Escherichia coli K12. European Journal of Biochemistry 102, 65-71.
- Cole, S.T., Grundstrom, T., Jaurin, B., Robinson, J.J., & J.H. Weiner (1982). Location and nucleotide sequence of frdB, the gene coding for the iron-sulphur protein subunit of the fumarate reductase of Escherichia coli. European Journal of Biochemistry 126, 211-216.
- Condon, C., & P. Owen (1982a). The succinate dehydrogenase of Escherichia coli: resolution as a major membrane-bound immunogen possessing covalently bound flavin. FEMS Microbiological letters 14, 217-221.
- Condon, C., & P. Owen (1982b). Succinate dehydrogenase: a major cross-reacting antigen in the Enterobacteriaceae. FEMS Microbiological letters 15, 109-113.

- Condon, C., Cammack, R., Patil, D.S., & P. Owen (1985). The succinate dehydrogenase of Escherichia coli: immunochemical resolution and biophysical characterisation of a four-subunit enzyme complex. (in press).
- Davenport, H.E., Hill, R., & F.R. Whatley (1952). A natural factor catalysing reduction of methaemoglobin by isolated chloroplasts. Proceedings of the Royal Society (London) Series B 139, 346-358.
- Dawes, E.A. (1980). Oxidation-reduction potentials. In Quantitative problems in biochemistry. Sixth edition. Longman Group Ltd., London. Chapter 8, pp. 199-225.
- Deatherage, J.F., Henderson, R., & R.A. Capaldi (1982). Three dimensional structure of cytochrome c oxidase vesicles crystals in negative stain. Journal of Molecular Biology 158, 487-499.
- Dickie, P., & J.H. Weiner (1979). Purification and characterisation of membrane-bound fumarate reductase from anaerobically-grown Escherichia coli. Canadian Journal of Biochemistry 57, 813-821.

- Downie, J.A., & G.B. Cox (1978). Sequence of b cytochromes relative to ubiquinone in the electron-transport chain of Escherichia coli. Journal of Bacteriology 133, 477-484.
- Dutton, P.L. (1978). Redox potentiometry: determination of mid-point potentials of oxidation-reduction components of biological electron-transfer systems. Methods in Enzymology 54, 441-435.
- Elmes, M.L., & J.H. Weiner (1985). Fumarate reductase and membrane structure in Escherichia coli. Federal Proceedings 44, abstract 2627 p. 860.
- Emptage, M.H., Kent, T.A., Huynh, B.H., Rawlings, J., Orme-Johnson, W.H., & E. Munck (1980). On the nature of the iron-sulphur centres in a ferredoxin from Azobacter vinelandii. Journal of Biological Chemistry 255, 1793-1796.
- Fujita, T., & R. Sato (1966a). Studies on soluble cytochromes in Enterobacteriaceae. III. Location of cytochrome c₅₅₂ in the surface layer of cells. Journal of Biochemistry (Tokyo) 60, 568-577.

Fujita, T., & R. Sato (1966b). Studies on soluble cytochromes in Enterobacteriaceae. IV. Possible involvement of cytochrome c₅₅₂ in anaerobic nitrite metabolism. Journal of Biochemistry (Tokyo) 60, 691-700.

Fujita, T., & R. Sato (1967). Studies on soluble cytochromes in Enterobacteriaceae. V. Nitrite dependent gas evolution in cells containing cytochrome c₅₅₂. Journal of Biochemistry (Tokyo) 60, 230-238.

Fuller, S.D., Capaldi, R.A., & R. Henderson (1979). Structure of cytochrome c oxidase in deoxycholate-derived two-dimensional crystals. Journal of Molecular Biology 134, 305-327.

Garland, P.B., Downie, J.A., & B.A. Haddock (1975). Proton translocation and the respiratory nitrate reductase of Escherichia coli. Biochemical Journal 152, 547-559.

Gayda, J.-P., Gibson, J.F., Cammack, R., Hall, D.O., & R. Mullinger (1976). Spin-lattice relaxation and exchange interaction in a 2-iron, 2-sulphur protein. Biochimica et Biophysica Acta 434, 154-163.

Gayda, J.-P., Bertrand, P., Deville, A., More, C., Roger, G., Gibson, J.F., & R. Cammack (1979). Temperature dependence of the electronic spin-lattice relaxation time in a 2-iron, 2-sulphur protein. Biochimica et Biophysica Acta 581, 15-26.

Gibson, J.F., Hall, D.O., Thornley, J.H.M. & F.R. Whatley (1966). The iron complex in spinach ferredoxin. Proceedings of the National Academy of Sciences of the U.S.A 56, 987-990.

Graham, A., & D.H. Boxer (1978). Immunochemical localisation of the nitrate reductase in Escherichia coli. Biochemical Society Transactions 6, 1210-1211.

Graham, A., & D.H. Boxer (1980a). Membrane location of the α -subunit of nitrate reductase from Escherichia coli. Biochemical Society Transactions 8, 331.

Graham, A., & D.H. Boxer (1980b). Arrangement of respiratory nitrate reductase in the cytoplasmic membrane of Escherichia coli: localtion of α -subunit. FEBS letters 113, 15-20.

Graham, A., Tucker, A.D., & N.H. Smith (1981). The formate-nitrate respiratory chain of Escherichia coli: localisation of proteins by immunoadsorption studies. FEMS Microbiological Letters 11, 141-147.

Green, D.E. (1974). The electromechanochemical model for energy coupling in mitochondria. Biochimica et Biophysica Acta 346, 27-78.

Greville, G.D. (1969). A scrutiny of Mitchell's chemiosmotic hypothesis. Current Topics in Bioenergetics 30, 1-78.

Guest, J.R., Darlison, M.G., Wilde, R.J., & D. Wood (1984). Structural comparison of the succinate dehydrogenase and fumarate reductase of Escherichia coli. In R.C. Bray et al. (Eds.) Flavins and Flavoproteins, Walter de Gruyter & Co., Berlin. pp. 225-228.

Gutowski, S.J., & H. Rosenberg (1976). Effects of dicyclohexylcarbodiimide on proton translocation coupled to fumarate reduction in anaerobically grown Escherichia coli K12. Biochemical Journal 164, 265-267.

Gutowski, S.J., & H. Rosenberg (1977). Proton translocation coupled to electron flow from endogenous substrates to fumarate in anaerobically grown Escherichia coli K12. Biochemical Journal 164, 265-267.

Hackett, N.R., & P.D. Bragg (1983). Membrane cytochromes of Escherichia coli grown aerobically and anaerobically with nitrate. Journal of Bacteriology 154, 708-718.

Hackett, N.R., & P.D. Bragg (1983). Membrane cytochromes of Escherichia coli chl mutants. Journal of Bacteriology 154, 719-727.

Haddock, B.A. (1980). Microbial Energetics. Philosophical Transactions of the Royal Society of London. Series B. 2901, 329-339.

Haddock, B.A., & M.W. Kendall-Tobias (1975). Functional anaerobic electron transport linked to the reduction of nitrate and fumarate in membranes from Escherichia coli as demonstrated by quenching of atebrin fluorescence. Biochemical Journal 152, 655-659.

Haddock, B.A., & C.W. Jones (1977). Bacterial Respiration. Bacteriological Reviews 41, 47-99.

Harold, F.M. (1972). Conservation and transformation by bacterial membranes. Bacteriological Reviews 36, 172-230.

- Harold, F.M. (1977). Membranes and energy transduction in bacteria. Current Topics in Bioenergetics 6, 83-149.
- Hellingwerf, K.J., Bolscher, J.G.H., & W.N. Konings (1981). The electrochemical proton gradient generated by the fumarate reductase system in Escherichia coli and its bioenergetic implications. European Journal of Biochemistry 113, 369-374.
- Henderson, R. (1981). Membrane protein structure. In R. Balion et al. (Eds.), Membranes and Intercellular Communication, North Holland Co., London, pp. 232-249.
- Henderstedt, L., & L. Rutberg (1981). Succinate dehydrogenase - a comparative review. Microbiological Reviews 45, 542-555.
- Hirsch, C.A., Rasminsky, M., Davis, B.D., & E.C.C. Lin (1963). A fumarate reductase in Escherichia coli distinct from succinate dehydrogenase. Journal of Biological Chemistry 238, 3770-3774.
- Hyde, J.S., & K.V.S. Rao (1978). Dipolar-induced electron-spin-lattice relaxation in unordered solids. Journal of Magnetic Resonance 29, 509-516.

Ingledeu, W.J. (1983). The electron transport chain of Escherichia coli grown anaerobically with fumarate as terminal electron acceptor: an electron paramagnetic resonance study. Journal of General Microbiology 129, 1651-1659.

Ingledeu, W.J., Salerno, J.C., & T. Ohnishi (1976). Studies on electron paramagnetic resonance spectra manifested by a respiratory chain hydrogen carrier. Archives of Biochemistry and Biophysics 177, 176-184.

Ingledeu, W.J., Cox, J.C., Jones, R.W., & P.B. Garland (1978). Vectoral oxidoreductions: the ferrous iron oxidase complex of Thiobacillus ferrooxidans and the nitrate reductase complex of Escherichia coli. In P.L. Dutton et al. (Eds.), Frontiers of Biological Energetics. Vol. 1, Academic Press Inc., New York, pp. 334-341.

Ingledeu, W.J., & R.K. Poole (1984). The respiratory chains of Escherichia coli. Microbiological Reviews 48, 222-271.

Johnson, I.L. (1980). The molybdenum cofactor common to nitrate reductase, xanthine dehydrogenase and sulphite oxidase. In M. Coughlan (Ed.), Molybdenum and Molybdenum Containing Enzymes. Pergamon Press, Oxford, pp. 345-384.

- Johnson, M.K., Morningstar, J.E., Bennett, D.E., Ackrell, A.C., & E.B. Kearney (1985). Magnetic circular dichroism studies of succinate dehydrogenase. (In press).
- Jones, R.W., & P.B. Garland (1977). Sites and specificity of the reaction of bi-pyridylum compounds with anaerobic respiratory enzymes in Escherichia coli. Effects of permeability barriers imposed by the cytoplasmic membrane. Biochemical Journal 164, 199-211.
- Jones, R.W., Ingledew, W.J., Graham, A., & P.B. Garland (1978). Topography of nitrate reductase of the cytoplasmic membrane of Escherichia coli. The nitrate-reducing site. Biochemical Society Transactions 6, 1287-1289.
- Kay, W.W., & H.L. Kornberg (1971). The uptake of C4-dicarboxylic acids by Escherichia coli. European Journal of Biochemistry 18, 274-281.
- Kent, T.A., Dreyer, J.L., Emptage, M.H., Moura, I., Moura, J.J., Huynh, B.H., Xavier, A.V., LeGall, J., Beinert, H., Orme-Johnson, W.H., & E. Munk (1982). Evidence for a novel three-iron centre in two ferredoxins and aconitase. In C. Ho (Ed.), Electron Transport and Oxygen Utilisation. Macmillan Press Ltd., London, pp.372-374.

- King, T.E., Nickel, K.S., & D.R. Jensen (1964). Iron, copper, cytochrome and lipid contents of heart muscle preparation and heart mitochondria. Journal of Biological Chemistry 239, 1989-1994.
- Kita, K., & Y. Anraku (1981). Composition and sequence of b cytochromes in the respiratory chain of aerobically grown Escherichia coli K12 in the early exponential phase. Biochemistry International 2, 105-112.
- Konings, W.W., & H.R. Kaback (1973). Anaerobic transport in Escherichia coli membrane vesicles. Proceedings of the National Academy of Sciences of the U.S.A. 70, 3376-3381.
- Kroger, A. (1978). Fumarate as terminal electron acceptor of phosphorylative electron transport. Biochimica et Biophysica Acta 505, 129-145.
- Leigh, J.S. (1969). ESR rigid-lattice line shape in a system of two interacting spins. Journal of Chemical Physics 52, 2608-2612.
- Lemire, B.D., Robinson, J.J., & J.H. Weiner (1982). Identification of membrane anchor polypeptides of Escherichia coli fumarate reductase. Journal of Bacteriology 152, 1126-1131.

- Lemire, B.D., Robinson, J.J., Bradley, R.D., Scraba, B.D., & J.H. Weiner (1983). Structure of fumarate reductase on the cytoplasmic membrane of Escherichia coli. Journal of Bacteriology 155, 391-397.
- Lo, T.C.Y., Rayman, M.K., & B.D. Sanwal (1972). Transport of succinate in Escherichia coli. Journal of Biological Chemistry 247, 6323-6331.
- Lowe, D.J., Lynden-Bell, R.M., & R.C. Bray (1970). Spin-spin interaction between molybdenum and one of the iron-sulphur systems of xanthine oxidase and its relevance to the enzymatic mechanism. Biochemical Journal 130, 239-249.
- Lowry, O.H., Rosenbrough, N.J., Farr, A.L., & R.T. Randall (1951). Protein measurement with the folin phenol reagent. Journal of Biological Chemistry 193, 265-275.
- MacGregor, C.H., & A.R. Christopher (1978). Asymmetric distribution of nitrate reductase subunits in the cytoplasmic membrane of Escherichia coli: evidence derived from surface labelling studies and transglutaminase. Archives of Biochemistry and Biophysics 185, 204-213.

- Mathews, R., Charlton, S., Sands, R.H., & G. Palmer (1974). On the nature of the spin-coupling between the iron-sulphur clusters in the eight-iron ferredoxins. Journal of Biological Chemistry 249, 4326-4328.
- Miki, K., & E.C.C. Lin (1973). Enzyme complex which couples glycerol-3-phosphate dehydrogenase to fumarate reductase in Escherichia coli. Journal of Bacteriology 144, 767-771.
- Miki, K., & E.C.C. Lin (1975). Anaerobic energy yielding reaction associated with transhydrogenation from glycerol-3-phosphate to fumarate by Escherichia coli. Journal of Bacteriology 124, 1288-1294.
- Mitchell, P. (1966). Chemiosmotic coupling in oxidative and photosynthetic phosphorylation. Biological Reviews of the Cambridge Philosophical Society 41, 445-502.
- Mitchell, P. (1968). Chemiosmotic coupling and energy transduction. Glynn Research Ltd, Bodmin, Cornwall, U.K..
- Motteram, P.A.S., McCarthy, J.E.G., Ferguson, S.J., Jackson, J.B., & J.A. Cole (1981). Energy conservation during the formate dependent reduction of nitrite by Escherichia coli. FEMS Microbiological Letters 12, 317-320.

- Ohnishi, T. (1979). Mitochondrial iron-sulphur flavo-dehydrogenases. In R.A. Capaldi (Ed.) Membrane Proteins in Energy Transduction. Marcel Dekker, New York, pp. 1-87.
- Ohnishi, T., Salerno, J.C., Winter, D.B., Lim, J., Yu, C.-A., Yu, L., & T.E. King (1976a). Thermodynamic and EPR characteristics of two ferredoxin-type iron-sulphur centres in the succinate-ubiquinone reductase segment of the respiratory chain. Journal of Biological Chemistry 251, 2094-2104.
- Ohnishi, T., Lim, J., Winter, D.B., & T.E. King (1976b). Thermodynamic and EPR characteristics of a HiPIP-type iron-sulphur centre in the succinate dehydrogenase of the respiratory chain. Journal of Biological Chemistry 251, 2105-2109.
- Ohnishi, T., King, T.E., Salerno, J.C., Blum, H., Bower, J.R., & T. Maida (1981). Thermodynamic and electron paramagnetic resonance characterisation of flavin in succinate dehydrogenase. Journal of Biological Chemistry 256, 5577-5582.

Ohnishi, T., LoBrutto, R., Salerno, J.C., Bruckner, R.C., & T.G. Frey (1982). Spatial relationship between cytochrome a and a₃. Journal of Biological Chemistry 257, 14821-14825.

Ohnishi, T., Blum, H., Harmon, H.J., & T. Hompo (1982). Location of the Rieske iron-sulphur centre in the mitochondrial membrane. In C. Ho (Ed.), Electron Transport and Oxygen Utilisation. Elsevier North Holland Inc., New York, pp. 387-393.

Owen, P., & C. Condon (1982). The succinate dehydrogenase of Escherichia coli: subunit composition of the triton X-100 solubilised antigen. FEMS Microbiological Letters 14, 213-227.

Palmer, G. (1973). Current insights into the active centre of spinach ferredoxin and other iron-sulphur proteins. In W. Lovenberg (Ed.), Iron-Sulphur Proteins. Vol. II., Academic Press Inc., New York, pp. 286-325.

Palmer, G., & R.H. Sands (1966). On the magnetic resonance of spinach ferredoxin. Journal of Biological Chemistry 241, 253-254.

- Palmer, G., Sands, R.H., & L.E. Mortenson (1966). Electron paramagnetic resonance studies on the ferredoxin from Clostridium pasteurianum. Biochemical and Biophysical Research Communications 23, 357-362.
- Poole, R.K. (1982). The oxygen reactions of bacterial cytochrome oxidases. Trends in Biochemical Sciences 7, 32-34.
- Poole, R.K. (1983). Bacterial cytochrome oxidases. A structurally and functionally diverse group of electron-transfer proteins. Biochimica et Biophysica Acta 726, 205-243.
- Pundek, M.R., & P.D. Bragg (1976). Redox potentials of the cytochromes in the respiratory chain of aerobically-grown Escherichia coli. Archives of Biochemistry and Biophysics 174, 546-552.
- Rabinowitz, J.C. (1978). Analysis of acid-labile sulphur and sulphhydryl groups. Methods in Enzymology 53, 275-277.
- Reid, G.A., & W.J. Ingledew (1979). Characterisation and phenotypic control of the cytochrome content of Escherichia coli. Biochemical Journal 182, 465-472.

Ruiz-Herrera, J., & J.A. DeMoss (1969). Nitrate reductase complex of Escherichia coli K12: participation of specific formate dehydrogenase and cytochrome b₁ components in nitrate reduction. Journal of Bacteriology 99, 720-729.

Ruiz-Herrera, J., & L.G. Garcia (1972). Regulation of succinate dehydrogenase in Escherichia coli. Journal of General Microbiology 7, 29-35.

Rupp, H., Rao, K.K., Hall, D.O., & R. Cammack (1978). Electron spin relaxation of iron-sulphur proteins studied by microwave power saturation. Biochimica et Biophysica Acta 537, 255-269.

Ruzicka, F.J., Beinert, H., Schepler, K.L., Dunham, W.R., & R.H. Sands (1975). Interaction of ubisemiquinone with a paramagnetic component in heart tissue. Proceedings of the National Academy of Sciences of the U.S.A. 72, 2886-2890.

Salerno, J.C., Harmon, H.J., Blum, H., Leigh, J.S., & T. Ohnishi (1977a). A transmembraneous quinone pair in the succinate dehydrogenase-cytochrome b region. FEBS Letters 82, 179-182.

- Salerno, J.C., Ohnishi, T., Blum, H., & J.S. Leigh (1977b).
Determination of the exchange integral in binuclear
iron-sulphur clusters in proteins of varying complexity.
Biochimica et Biophysica Acta 494, 191-197.
- Salerno, J.C., Blum, H., & T. Ohnishi (1979a). The orientation
of iron-sulphur clusters and a spin-coupled ubiquinone
pair in the mitochondrial membrane. Biochimica et
Biophysica Acta 547, 270-281.
- Salerno, J.C., Lim, J., King, T.E., Blum, H., & T. Ohnishi
(1979b). The spatial relationships and structure of the
binuclear iron-sulphur clusters in succinate
dehydrogenase. Journal of Biological Chemistry 254,
4828-4835.
- Salerno, J.C., & T. Ohnishi (1980). Studies on the stabilized
ubisemiquinone species of the succinate-cytochrome c
reductase segment of the intact mitochondrial membrane
system. Biochemical Journal 192, 769-781.
- San Pietro, A., & H.M. Lang (1958). Photosynthetic pyridine
nucleotide reductase. I. Partial purification and
properties of the enzyme from spinach. Journal of
Biological Chemistry 231, 211-229.

- Shipp, W.S. (1972). Cytochromes of Escherichia coli. Archives of Biochemistry and Biophysics 150, 459-472.
- Slater, E.C. (1974). Electron transfer and energy conservation. Biochimica et Biophysica Acta 13, 1-20.
- Smith, M.W., & F.C. Neidhardt (1983a). Proteins induced by anaerobiosis in Escherichia coli. Journal of Bacteriology 154, 336-343.
- Smith, M.W. & F.C. Neidhardt (1983b). Proteins induced by aerobiosis in Escherichia coli. Journal of Bacteriology 154, 344-350.
- Spencer, M.F., & J.R. Guest (1973). Isolation and properties of fumarate reductase mutants of Escherichia coli. Journal of Bacteriology 114, 563-570.
- Steenkamp, D.J., Singer, T.P., & H. Beinert (1978). Participation of the iron-sulphur cluster and of the covalently bound coenzyme of trimethylamine dehydrogenase in catalysis. Biochemical Journal 169, 361-369.
- Subramanian, V., Lui, T.N., Yeh, W.K., & D.T. Gibson (1979). Toluene dioxygenase: purification of an iron-sulphur protein by affinity chromatography. Biochemical and Biophysical Research Communications 91, 1131-1139.

Takagi, M., Tsuchiyu, T., & M. Ishimoto (1981). Proton translocation coupled to trimethylamine N-oxide reduction in anaerobically grown Escherichia coli. Journal of Bacteriology 148, 762-768.

Thomson, A.J., Robinson, A.E., Johnson, M.K., Cammack, R., Rao, K.K., & D.O. Hall (1981). Low-temperature magnetic circular dichroism evidence for the conversion of four-iron-sulphur clusters in a ferredoxin from Clostridium pasteurianum, into a three-iron-sulphur cluster. Biochimica et Biophysica Acta 639, 423-432.

Uden, G., Hackenberg, H., & A. Kroger (1980). Isolation and functional aspects of the fumarate reductase involved in the phosphorylative electron transport of Vibrio succinogenes. Biochimica et Biophysica Acta 591, 275-288.

Uden, G., & A. Kroger (1982). Reconstitution in liposomes of the electron-transport chain catalysing fumarate reduction by formate. Biochimica et Biophysica Acta 682, 258-263.

Uden, G., Albracht, S.P.J., & A. Kroger (1984). Redox potentials and kinetic properties of fumarate reductase complex from Vibrio succinogenes. Biochimica et Biophysica Acta 767, 460-469.

- Van der Plaas, J., Hellingwerf, K.J., Seigen, H.G., Guest, J.R., Weiner, J.H., & W.N. Konings (1983). Identification and localisation of enzymes of fumarate reductase and nitrate respiration systems of Escherichia coli, by crossed immunoelectrophoresis. Journal of Bacteriology 153, 1027-1037.
- Wallace, B.J., & I.G. Young (1977). Role of quinones in electron transport to oxygen and nitrate in Escherichia coli. Studies with a ubiA⁻ menA⁻ double quinone mutant. Biochimica et Biophysica Acta 461, 84-100.
- Weiner, J.H., & P. Dickie (1979). Fumarate reductase of Escherichia coli. Elucidation of the covalent flavin component. Journal of Biological Chemistry 254, 8590-8593.
- Weiner, J.H., Lemire, B.D., Jones, R.W., Anderson, W.F., & D.G. Scraba (1984a). A model for the structure of fumarate reductase in the cytoplasmic membrane of Escherichia coli. Journal of Cellular Biochemistry 24, 207-216.
- Weiner, J.H., Lemire, B.D., Elmes, M.L., Bradley, R.D., & D.G. Scraba (1984b). Overproduction of fumarate reductase in Escherichia coli induces a novel intracellular lipid-protein organelle. Journal of Bacteriology 158, 590-596.

Wilson, D.F., & T.E. King (1964). The determination of acid nonextractable flavin in mitochondrial preparations from heart muscle. Journal of Biological Chemistry 239, 2683-2690.

Zweier, J.L. (1983). Electron paramagnetic resonance measurement of the distance between the metal binding sites of transferrin. Journal of Biological Chemistry 258, 13759-13760.